5-18-2007

Simulation of Combustion and Thermal-flow Inside a Petroleum Coke Rotary Calcining Kiln

Zexuan Zhang
University of New Orleans

Simulation of Combustion and Thermal-flow Inside a Petroleum Coke Rotary Calcining Kiln

A Thesis

Submitted to the Graduate Faculty of the
University of New Orleans
in partial fulfillment of the
requirements for the degree of

Master of Science
in
Mechanical Engineering

by

Zexuan Zhang

B.S. University of New Orleans, 2003

May, 2007

ACKNOWLEDGMENT

I would like to express my sincere appreciation and gratitude to my advisor Dr. Ting Wang for his support, guidance, and assistance that helped me accomplish this thesis. The coordination, valuable suggestions, instructions via classes, and productive discussions with Dr. Wang inspired me toward the successful completion of this task.

I would like to show appreciation to CII Carbon, L.L.C. for their support and funding on this research. Part of the support from Louisiana Board of Regents' Industrial Ties Research Subprogram (BOR-ITRS) is also greatly appreciated.

I would also like to take this opportunity to thank Drs. Paul Herrington and Martin J. Guillot for serving on my thesis committee.

I extend special thanks to my family, ECCC staff, and friends for their encouragement and moral support in this regard.

TABLE OF CONTENTS

LIST OF FIGURES

LIST OF TABLES

NOMENCLATURE

a	Local speed of sound (m/s, ft/s)
c	Concentration (mass/volume, moles/volume)
c_p, c_v	Specific heat at constant pressure, volume (J/kg-K, Btu/lbm-°F)
Dij	Mass diffusion coefficient (m^2/s, ft^2/s)
E	Total energy, activation energy (J, Btu)
f	Mixture fraction (dimensionless)
g	Gravitational acceleration (m/s^2 , ft/s^2)
H	Total enthalpy (energy/mass, energy/mole)
h	Heat transfer coefficient (W/m^2-K, Btu/ft^2-hr-°F)
h	Species enthalpy (energy/mass, energy/mole)
h_0	Standard state enthalpy of formation (energy/mass, energy/mole)
I	Radiation intensity (energy per area of emitting surface per unit solid angle)
J	Mass flux; diffusion flux (kg/m^2-s, lbm/ft^2-s)
K	Equilibrium constant = forward rate constant/backward rate constant (units vary)
k	Kinetic energy per unit mass (J/kg, Btu/lbm)
k	Reaction rate constant, e.g., k1, k-1, $k_{f;r}$, $k_{b;r}$ (units vary)
k	Thermal conductivity (W/m-K, Btu/ft-hr-°F)
k_B	Boltzmann constant ($1.38x10^{-23}$ J/mole-K, $7.27x10^{-27}$ Btu/mole-°R)
k,kc	Mass transfer coefficient (units vary)
l, L	Length scale (m, cm, ft, in)
m	Mass (kg, lbm)
$\dot{m}$	Mass flow rate (kg/s, lbm/s, metric ton/hr)
M_w	Molecular weight (kg/kgmol)
M	Mach number = ratio of fluid velocity magnitude to local speed of sound
Nu	Nusselt number ≡ hL/k (dimensionless)
P	Pressure (Pa, atm, mm Hg, lbf/ft^2)
Pr	Prandtl number = α/ν (dimensionless)
Q	Flow rate of enthalpy (W, Btu/hr)
q"	Heat flux (W/m^2 , Btu/ft^2-hr)
R	Gas-law constant ($8.31447x10^3$ J/kgmol-K, 1.98588 Btu/lbmol-°F)
r	Radius (m, ft)
R	Reaction rate (units vary)
Re	Reynolds number ≡ UL/ν (dimensionless)
S	Total entropy (J/K, J/kgmol-K, Btu/lbmol-°F)
s	Specific entropy
s_0	standard state entropy (J/kgmol-K, Btu/lbmol-°F)
Sc	Schmidt number = ν/D (dimensionless)
S_{ij}	Mean rate-of-strain tensor (s^{-1})
T	Temperature (K, °C, °R, °F)
t	Time (s)
t	thickness (m, ft)
U	Free-stream velocity (m/s, ft/s)

u; v; w Velocity components (m/s, ft/s); also written with directional sub-scripts (e.g., vx, vy, vz, vr)

V Volume (m^3, ft^3)

$\vec{v}$ Overall velocity vector (m/s, ft/s)

X Mole fraction (dimensionless)

Y Mass fraction (dimensionless)

α Permeability, or flux per unit pressure difference (L/m^2-hr-atm, ft^3/ft^2-hr-(lbf/ft^2))

α Thermal diffusivity (m^2/s, ft^2/s)

α Volume fraction (dimensionless)

β Coefficient of thermal expansion (K-1)

γ Specific heat ratio, c_p/c_v (dimensionless)

Δ Change in variable, final – initial (e.g., .p, .t, .H, .S, .T)

δ Delta function (units vary)

ε Emissivity (dimensionless)

ε Turbulent dissipation rate (m^2/s^3, ft^2/s^3)

η',η'' Rate exponents for reactants, products (dimensionless)

θ_r Radiation temperature (K)

ν Dynamic viscosity (cP, Pa-s, lbm/ft-s)

μ Kinematic viscosity (m^2/s, ft^2/s)

ν',ν'' Stoichiometric coefficients for reactants, products (dimensionless)

ρ Density (kg/m^3, lbm/ft^3)

σ Stefan-Boltzmann constant (5.67×10^{-8} W/m^2-K^4, 1.71×10^{-9} Btu/hr-ft^2-°R^4)

σ_s Scattering coefficient (m^{-1})

$\bar{\bar{\tau}}$ Stress tensor (Pa, lbf/ft^2)

τ Shear stress (Pa, lbf/ft^2)

τ Time scale, e.g., τ_c, τ_p (s)

Φ Equivalence ratio (dimensionless)

Φ Diameter (m, ft)

ABSTRACT

Calcined coke is the best material for making carbon anodes for smelting of alumina to aluminum. Calcining is an energy intensive industry and a significant amount of heat is wasted in the calcining process. Efficiently managing this energy resource is tied to the profit margin and survivability of a calcining plant.

3-D computational models are developed using FLUENT to simulate the calcining process inside the long slender kiln. Simplified models are employed to simulate the moving petocke bed with a uniform distribution of moisture evaporation, devolatilization, and coke fines entrainment rate with a conjugate radiation-convection-conduction calculation. The results show the 3-D behavior of the flow, the reaction inside the kiln, heat transfer and the effect of the tertiary air on coke bed heat transfer. The ultimate goals are to reduce energy consumption, recover waste-heat, increase thermal efficiency, and increase the product yield.

Keywords: Petroleum coke, Calcination, Rotary kiln, Combustion, Conjugate Heat transfer, CFD

CHAPTER ONE

INTRODUCTION

1.1 Background

Petroleum coke (often abbreviated petcoke) is a carbonaceous solid derived from petroleum refinery cracking process. Calcination is the process of heating a substance to a high temperature, but below its melting or fusing point, to bring about thermal decomposition or a phase transition in its physical or chemical constitution. Petroleum coke is usually calcined in a gas-fired rotary kiln or rotary hearth at high temperatures, around 1,200 to 1,350 °C, to remove moisture, drive off volatile matters, increase the density of the coke structure, increase physical strength, and increase the electrical conductivity of the material (Figure 1.1). The product is hard, dense carbon (calcined petroleum coke) with low hydrogen content and good electrical conductivity. These properties along with the low metals and ash contents make calcined petroleum coke the best material currently available for making carbon anodes for smelting of alumina to aluminum [Bagdoyan and Gootzait, 1985].

Calcination is an energy intensive process. During the petroleum coke calcination, energy input is needed to heat up the petroleum coke and maintain the required calcining kiln temperature to produce the desired calcined petroleum coke quality. Meanwhile, volatile matters, producer gas, and a significant amount of waste heat are generated from the calcining process. Efficiently managing these energy resources is necessary for increasing the profit margin and survivability of a calcining plant.

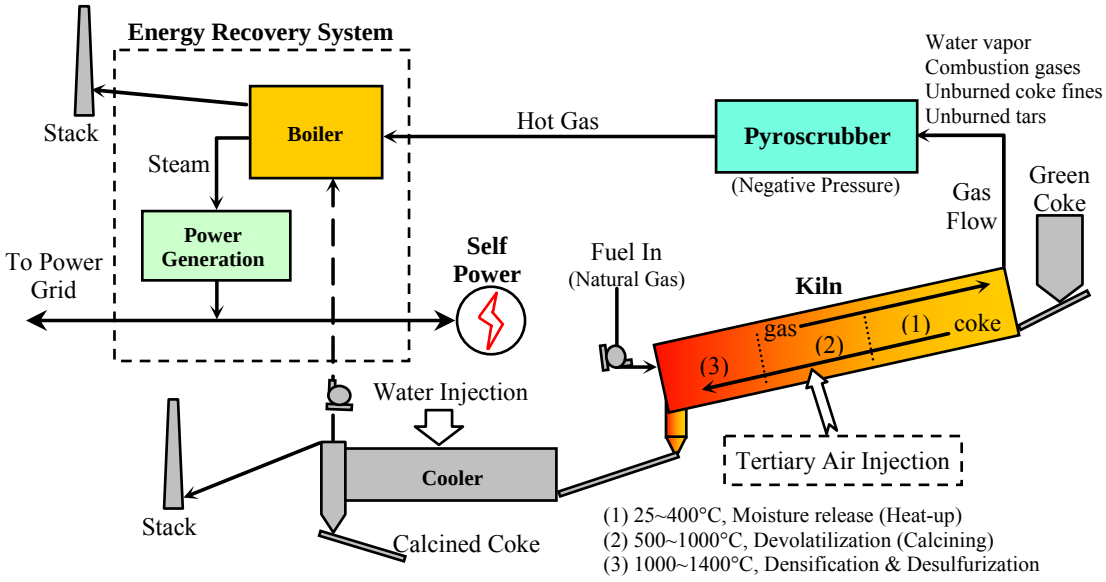

Figure 1.1 Schematic of calcining process for petroleum coke

Currently, natural gas is used for the kiln's primary combustion. In fact, the calcining process produces more energy from the volatiles in the petroleum coke than the theoretical energy needed for the calcining process. The ideal system would, except for start up, not need burning natural gas because the energy from the petroleum coke could be utilized instead. In view of the continuously rising natural gas price, minimizing natural gas consumption is essential to reducing production cost as well as avoiding unsteady impact on profit margin exerted by fluctuating natural gas price.

To minimize or remove natural gas consumption, a thorough 3-D modeling and analysis of the calcining process in the kiln are essential. The detailed dynamic simulation in the kiln will gain insights into the thermal-flow and chemical reaction process in the kiln, including 3-D flow pattern, the turbulence structure, the combustion process, the local heat release rate, heat transfer process, temperature distribution, and species concentration distributions. With the established detailed simulation, various means can be quickly simulated by the computer to effectively use the producer gases (volatile matters, CO and H_2), control the combustion rate, and manipulate

heat distribution. This study employs the Computational Fluid Dynamics (CFD) simulation to show what happens at any location inside the kiln and help engineers make decisions on how to utilize the volatiles derived from the petroleum coke, and ultimately, eliminate the use of natural gas.

Fluid velocity, pressure, temperature, and chemical reactions can be analyzed by using CFD scheme and appropriate models throughout the computational domain with complicated geometries and boundary conditions. During the analysis, modifications of geometries or boundary conditions can be easily applied to view their impact on the thermal flow patterns or species concentration distributions.

Currently, the calcined coke is the best material for making carbon anodes for smelting alumina to aluminum. In addition, calcined coke is used in many other industries such as the manufacturing of graphite electrodes, titanium dioxide, and steel (to increase the carbon levels). The largest consumer of the calcined coke is the aluminum industry, at more than 70 % of the world's total.

As the modernization progress accelerates, China has become the world biggest aluminum consumer and thus significantly elevating the demand for aluminum. Aluminum is widely used for construction of homes and furniture. Aluminum also makes noted contributions to fuel-efficient engines in cars and trucks as well as high-speed rail and sea travel. It replaces inefficient, wasteful, non-recyclable packaging. Without aluminum there would be no affordable commercial air travel. Aluminum is becoming the cornerstone metal of today's modern society.

Aluminum is the most common metallic element in the earth's crust but metallic aluminum does not exist in a natural state. It has to be extracted from an ore most commonly bauxite. Bauxite is converted to alumina using the Bayer process. Bauxite is combined with

caustic soda, lime, and steam to produce sodium aluminate liquor. Impurities are filtered or settled out of the liquor and alumina hydrate is precipitated out of the mixture. The alumina hydrate is calcined to remove moisture and drive off the bounded moisture. The resulting alumina is ready for smelting into aluminum.

Alumina is electrolytically reduced into molted aluminum. This reaction occurs in Hall-Heroult reduction cells (called pots) where the bounded oxygen in the alumina reacts with carbon electrodes to form carbon dioxide gas and aluminum (Eq.1.1).

$$2Al_2O_3 + 3C + \text{Power} \rightarrow 4Al + 3CO_2 + \text{Heat} \qquad \text{(Eq.1.1)}$$

The molten aluminum is then either cast into ingots, bars, rolled into sheets, plates or foils, or drawn into rods. These intermediate shapes are then shipped to processing plants where the aluminum is shaped into consumer products. Each ton of aluminum requires 0.4 to 0.5 tons of carbon anodes. The U.S. production of aluminum in 2004 totaled 2.52 million tons, which required 1.26 million tons of carbon anodes.

The Soderberg process and the pre-bake method are the two methods used to make carbon anodes for using in the reduction cells. The Soderberg process bakes the carbon into anodes in the Hall-Heroult reduction cell. The heat released from the alumina reduction process slowly bakes the carbon anodes as it moves down the cell. Carbon anode paste is continuously replenished at the top of the cell. The pre-bake method forms the carbon anodes in ovens outside the reduction cell. The fully formed anodes are inserted into the molten aluminum in the smelting pot to reduce the alumina into aluminum. Anode baking is typically carried out in gas-fired ovens.

Since the 1950's, petroleum and natural gas have become the most important energy resources. The demand for petroleum and natural gas continuously increases; however, with the

current consumption rate, the known global petroleum and natural gas reserves can only supply the world for about another 40 years. Energy resources and security have become a top issue in many countries including the United States. With the continued increase of oil and natural gas prices, implementation of energy efficiency and conservation have become more important than ever to reduce energy cost of a production plant. There is no exception from the petcoke calcining industry. This study will investigate the potential means to reduce energy cost of the calcining process using a rotary kiln. The elimination of natural gas can result in a savings of one million dollars per year per kiln.

1.2 Objectives

To reach the ultimate goal of cutting the energy costs of the calcining process, it is necessary to understand in greater detail the thermal-flow and combustion process inside the kiln. To this end, the objective of this study is modeling and simulating the thermal-flow and combustion behavior of an industry petroleum coke calcining rotary kiln. The kiln information is provided by CII Carbon, L.L.C. The gas flow, reactions, and temperature are simulated with the commercial CFD package FLUENT. FLUENT is a finite volume CFD code for solving transport equations of mass, momentum, and energy conservation including chemical reactions. The specific goals are

1. To develop a numerical model to simulate the combustion, gas phase and solid phase motion in the kiln
2. To investigate the flow pattern and temperature distribution inside the kiln
3. To study the flow behavior and combustion inside the kiln
4. To study the effect of different tertiary air injection angle
5. To study the moving bed and conjugate situation

6. To identify the means that can help reduce natural gas consumption and increase kiln energy efficiency

CHAPTER TWO

LITERATURE SEARCH

The literature search focuses on introducing the classifications, fundamental functions, and requirements of calcination, calcining kiln, combustion, and calcined coke quality.

2.1 Calcination

For continuous calcinations of petroleum coke (petcoke), the rotary kiln and the rotary hearth furnace are the two primary methods commonly used in the calcining industry all over the world [Ellis and Paul, 2000].

Rotary Kiln

Kiln: Most petroleum coke is calcined in a rotary kiln. A rotary kiln is a slightly tilted horizontal cylinder rotating at a controlled slow rate. An industrial rotary kiln is typically of 2.5 to 5 meters in diameter, 50 to 80 meters in length, and insulated with 0.23 meter thick high-temperature refractory bricks inside the kiln. The kiln shell is made of 25 mm thick steel with sections under the kiln tires being 50 to 70 mm thick. The kiln shell is supported by tires, which ride on two wheels or trunions. The kiln is rotated via a large bull gear that is larger than the diameter of the kiln shell and is driven by one or two spur gears. The spur gears are driven through a gearbox by either a direct electrical drive or by hydraulic motors.

Calcining Process Flow: Raw petroleum coke is sized to 50 to 100 mm lump and fed to raw feed silos, then to the feed end of the rotary kiln (at the high end) through a side feed scoop or through a feed pipe (in older units). The kiln is sloped downward towards the discharge end at a slope of 4.16 to 6.23 cm per meter (½ to ¾ inch per foot). After entering the rotary kiln,

moisture is driven off the petroleum coke in the “Heat-up Zone”. Devolatilization occurs mostly at 500 to 1,000 °C in the “Calcining Zone”. Further dehydrogenation and some desulfurization take place in the “Calcined Coke Zone” at 1,200 to 1,400 °C. In this zone, the petroleum coke structure densifies and shrinks. As the petroleum coke progresses down the rotary kiln countercurrent to the hot combustion gases, the temperature increases to a maximum temperature of around 13 to 20 meters before the discharge end of the rotary kiln. The petroleum coke moves through the rotary kiln in about 40 to 60 minutes. It then drops off at the discharge end of the rotary kiln through a refractory-lined chute and into a rotary cooler.

Cooler: The cooler is a bare steel cylinder similar to the rotary kiln, but it is usually smaller in diameter, shorter, and rotated at higher rpm’s than a rotary kiln with water sprays in the front end. Water is sprayed and contacts with the hot calcined petroleum coke, using the latent heat of vaporization of the water for cooling. In places where water quality is poor and not suitable for direct cooling, indirect water-cooled rotary cylinder coolers are used. The calcined petroleum coke stays about 20 minutes in the cooler and is then discharged onto high temperature conveyor belts or into screw feeders. Computer controls and adjusts the water sprays to maintain the temperature of the calcined petroleum coke at around 120 to 180 °C at the cooler exit, to keep the calcined product dry.

Firing Crown and Heat Transfer: At the discharge end of the rotary kiln, a burner is installed in the firing crown (a hood that fits over the discharge end of the rotary kiln) to preheat the refractory before startup and to supply heat for maintaining the coke bed at certain temperatures in most applications. Most kiln burners are natural gas fired, but some older model kilns have oil-fired burners. Primary combustion air is also injected through the firing crown. Some kiln use oxygen instead of air to reduce combustion gas flows and to decrease or eliminate

the need for natural gas firing. The temperature of the discharging calcined petroleum coke is monitored by an optical pyrometer. The temperature is controlled by the amount of natural gas, excess combustion air, rotary kiln rotation speed, and raw petroleum coke feed rate. As illustrated in Figure 2.1 [Bagdoyan and Gootzait, 1985], almost all of the heat transfer to the coke bed is by radiation and convection from the gases inside the rotary kiln and exposed portions of the refractory wall. A recent transient analysis [Zhao and Wang, 2007] showed that only a small amount of heat is transferred by conduction from the refractory brick layer to the material. Analysis of either the real density or the electrical resistivity of the calcined coke measures the degree and quality of calcination process.

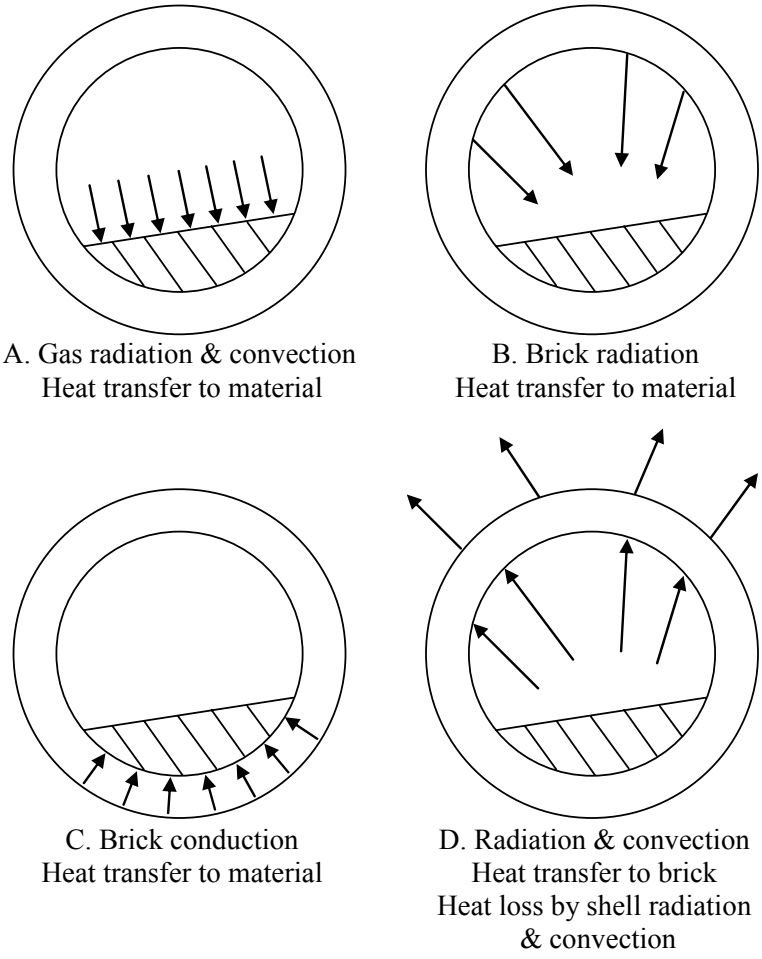

Figure 2.1 Modes of heat transfer in a rotary kiln

Tertiary Air Injection: Since the volatiles coming off the coke during calcination contain approximately 1.5 to 2 times of the fuel value (1,343 kJ/kg) [See Appendix B] required for the calcining process, these volatile matters are ideal to be utilized for the calcining process. Tertiary air is injected into the calcining zone through the side of the kiln from shell mounted blowers to burn the volatile matters and forms a second hot zone extending upward to the feed end of the kiln (Figure 2.2). Many rotary kilns use tertiary air for the advantage of increasing production rates and decreasing the natural gas consumption. The major disadvantage of using tertiary air is a faster up-heat rate in the critical range of 500 to 700 °C [Brooks 1989] may result in poorer coke quality than without tertiary air.

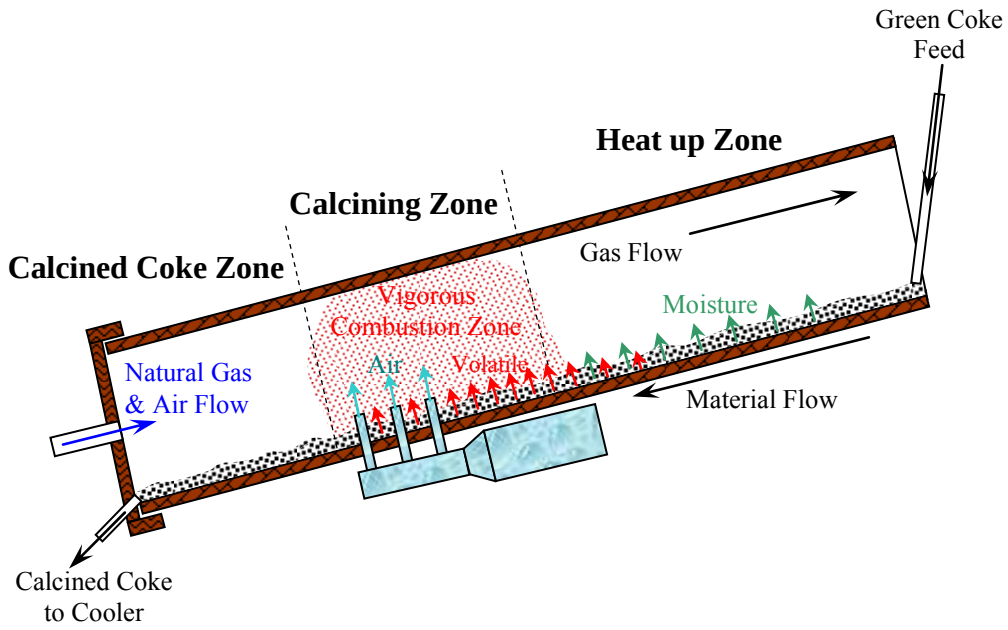

Figure 2.2 Petroleum coke calcination with tertiary air

Rotary Kiln Operation: Some of the key control parameters for operating a rotary kiln and producing good quality calcined coke include sizing of the petcoke, the control of the up-heat rate of the raw petroleum coke, and the feed consistency of raw petroleum coke.

Slow up-heat rate is critical to the calcining process**.** The primary objective in calcining petroleum coke for the aluminum industry is to slowly heat the petroleum coke, around 500 to

600 °C, during the initial devolatilization, so the mesophase or liquid crystal part of the petroleum coke does not bloat or distort (like pop-corn) during the devolatilization process. Petroleum coke with anisotropic (needle) structure and high volatile matters must be calcined with slow up-heat rates to produce good calcined densities and low porosity.

Some attempts have been made to stir the coke bed using "tumblers," also called "lifters," in kilns to increase production and keep the coke up-heat rate down [Kaiser Aluminum 1983]. Tumblers are castable refractory or refractory bricks that stand above the surrounding bricks. The use of a tumbler has successfully resulted in increased production; however, the optimum location for installing a tumbler is not yet known. There is a problem with keeping tumblers in a rotary kiln. Refractory bricks and the steel shell of a rotary kiln both expand. Bricks must expand enough as not to be too loose in the kiln to prevent excess migrating, yet not so tight, as to exceed the hot crushing strength of the brick. Tumblers get hotter at their tips, have a pinch point at the interface of the surrounding bricks, and are subject to breaking at the interface. Several complete rings of taller bricks seem to hold together, but the adjacent bricks on the upside (the side facing the rotating direction) wear out earlier due to a stagnant layer of coke that grinds down the bricks. Tumblers can also cause the other problem when a coke bed is stirred too much: The coke fines are entrained into combustion gases and reduce the calcined coke production rate.

The degree of petroleum coke calcinations depends mostly on variations in the raw petroleum coke such as differences in structure, volatile matters, and particle sizing. In rotary kilns, it has been documented that coarse particles travel faster through the rotary kiln than the finer particles. Some calciners have stated that coarser coke with lower quantities of fines can increase the production rate in a rotary kiln. Without proper sizing and feeding of a rotary kiln, slides can occur and will dump most of the incomplete product rapidly out of the rotary kiln.

Rapid devolatilization in the calcining zone tends to fluidize the petroleum coke. Excessive fluidization causes the slides.

Rotary Hearth

The other commercial method of calcining petroleum coke employs rotary hearth calciners. Marathon Oil and Wise Coal and Coke Company jointly developed the rotating hearth furnace for calcining coal and adapted the technology for calcining petroleum coke [Merrill, Jr. 1978]. The first rotary hearth petroleum coke calciners were located in Europe. A simplified process flow sheet for a rotary hearth calciner operation and an elevation view are shown in Figures 2.3.

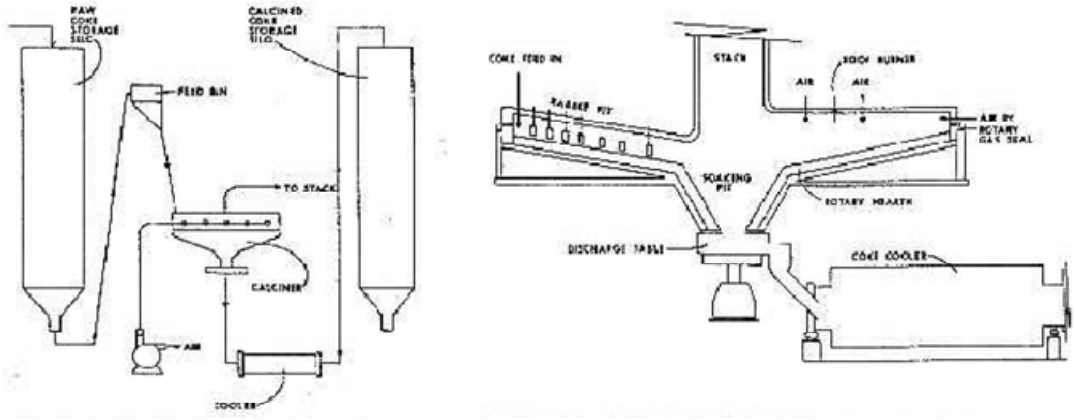

(a) (b)

Figure 2.3 (a) Simplified process flow sheet for rotary hearth calciner operation
(b) Elevation view of rotary hearth calciner

The rotary hearth consists of a large rotating disk-type furnace that slopes from the outside toward the center. Raw coke is fed into the outer edge of the rotary hearth and is plowed inward with water-cooled plows called rabbles that push the coke toward the center (Figure 2.4a). The rabbles can be adjusted to control the coke bed depth leaving enough stagnant coke to prevent wear of the refractory. Coke fines usually deposit onto the coke bed thus eliminating any entrainment with the combustion gases above the coke bed. The stirring of the coke bed is

critical for good heat transfer so that all coke can reach calcinations temperature. After passing through a center-soaking pit, the hot coke falls through a rotating discharge table into a cooler.

Burners and combustion air nozzles are located on a stationary, suspended roof (Figure 2.4b) that is connected to the rotating hearth with a seal between the two. After start-up, the rotary hearth calciner makes use of the complete combustion of the volatile matters of the raw coke feed. Little or no excess fuel is required for heating. The hot combustion gases coming off the top center of the roof are used to preheat the combustion air in some hearths to further improve combustion efficiencies. The small amount of coke fines and the volatile matters from the coke are completely consumed in the roof of the hearth, so no external incinerator is required. A schematic of the combustion process in a rotary hearth calciner is shown in Figure 2.4c [Allred 1971; Merrill, Jr. 1978].

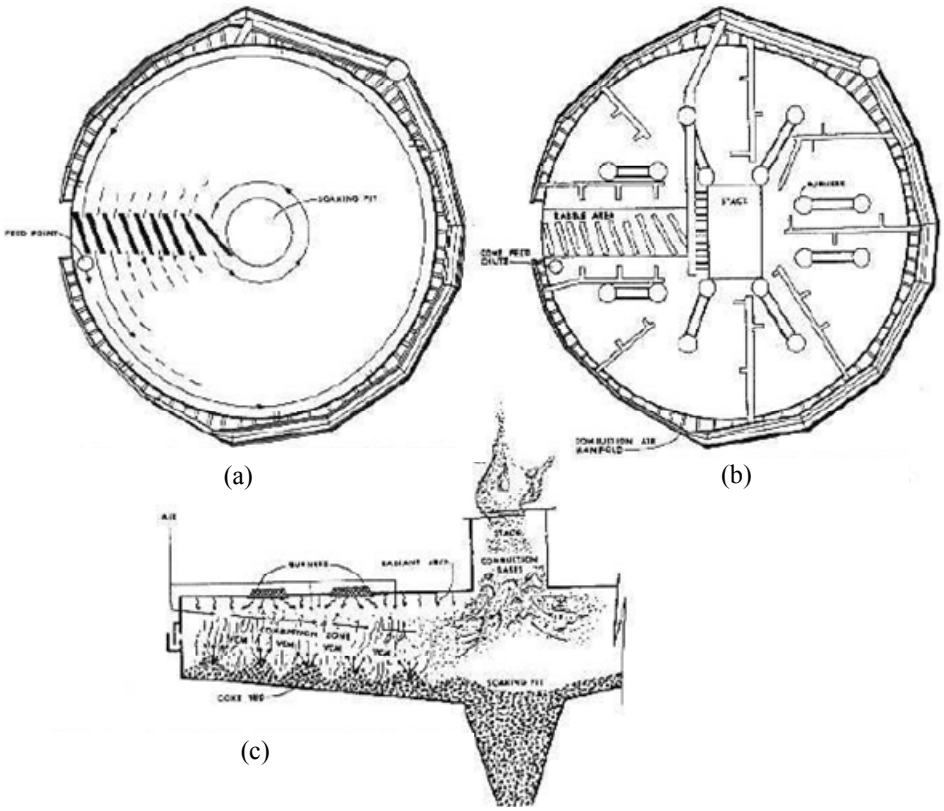

Figure 2.4 (a) Coke movement across rotary hearth (b) Plane view of rotary hearth claciner (c) Schematic of combustion process for rotary hearth clacining

2.2 Combustion

Combustion or burning is a complicated sequence of chemical reactions between a fuel and an oxidant accompanied by the production of heat or both heat and light in the form of either a glow or flames. In a complete combustion reaction, a compound reacts with an oxidizing element at the maximum percentage, and the products are compounds of each element in the fuel with the oxidizing element. The complete combustion reaction of carbon with oxygen is:

$$C + O_2 \rightarrow CO_2 + \text{Heat} \qquad \text{(Eq.2.1)}$$

In reality, combustion processes are never perfect or complete. In flue gases from combustion of carbon (Eq.2.2) or carbon compounds (as in combustion of hydrocarbons, wood etc.) both unburned carbon (known as soot) and carbon compounds (CO (Eq.2.3) and others) will be present.

$$C + \tfrac{1}{2}O_2 \rightarrow CO + \text{Heat} \qquad \text{(Eq.2.2)}$$

$$CO + \tfrac{1}{2}O_2 \rightarrow CO_2 + \text{Heat} \qquad \text{(Eq.2.3)}$$

Also, when air is the oxidant, some nitrogen will be oxidized to various, mostly harmful, nitrogen oxides (NO_x). The effectiveness of combustion can be determined by analyzing the flue gas and the amount of soot.

There are three types of fuel present in the calcining process, methane (as natural gas), carbon (as petroleum coke), and volatile matters (as hydrocarbons).

The complete combustion of methane and volatile matters can be presented as:

$$CH_4 + 2O_2 \rightarrow CO_2 + 2H_2O + \text{Heat} \qquad \text{(Eq.2.4)}$$

$$C_xH_yO_z + \left(x + \tfrac{y}{4} - \tfrac{z}{2}\right)O_2 \rightarrow xCO_2 + \tfrac{y}{2}H_2O + \text{Heat} \qquad \text{(Eq.2.5)}$$

2.3 Calcined Petroleum Coke Properties

The calcined petroleum coke properties need to meet the specifications for anode grade coke for aluminum smelting industries. The physical properties include real density, electrical resistivity, Hg apparent density, vibrated bulk density, hardgrove grindability index, pulverization factor, grain stability, crystallite thickness, interlayer spacing, shot coke content, screen sizing, air and CO_2 reactivities. The chemical properties include volatile matters, hydrogen, moisture, ash, sulfur, metals, and nitrogen. Table 2.1 [Bagdoyan and Gootzait, 1985] shows the general specification comparison between petroleum coke and calcined petroleum coke.

Table 2.1 General specifications for raw and calcined petroleum coke

Properties	**Raw**	**Calcined**
Moisture, wt%	8-10	<0.30
Ash, wt%	<0.40	<0.40
Sulfur, wt%	<3.5	<3.0
V, wppm	<300	<250
Ni, wppm	<200	<200
Si, wppm	<250	<200
Vibrated Bulk Density (VBD), g/cc	----	>0.84
Hydrogen, wt%	----	<0.10
VM, wt%	<11.5	<0.40
Shot Coke Content, %	0	0
Na, wppm	<100	<100
Fe, wppm	<300	<300
Ca, wppm	<200	<150
AD (Hg), g/cc	----	>1.70
Real Density, g/cc	----	2.050-2.080
Air Reactivity @600C (Fast), %/min	----	<0.25
CO2 Reactivity, %	----	<12.0
Pulverization Factor	----	0.9-1.1
Electrical Resistivity, ohm-in	----	<0.042
Air Reactivity @525C (Slow), %/min	----	<0.30
Grain Stability, %	----	>75
HGI	75-85	32-40
Sizing, Cumulative%		
+30 mm	----	0
+8 mm	----	>8.0
+4 mm	----	30-40
+2 mm	----	>45
-1 mm	----	<30
-0.25 mm	----	<15

CHAPTER THREE

PROBLEM SETUP AND MODELING

The overall design of the studied rotary calcining kiln is shown in Figure 3.1. The model is developed and meshed using GAMBIT, which is an intelligent toolkit to construct 3D geometries and meshes. The studied domain basically consists of three sections: the calcined coke zone (Figure 3.2), the calcining zone (Figure 3.3), and the heat-up zone (Figure 3.5). The fresh green petcoke is fed from the entrance of the heat-up zone (right upper end in Figure 3.1) and discharged at the end of the calcined coke zone (left lower end in Figure 3.1). The primary injection of air and fuel (natural gas) is located at the firing crown at the end of the calcined coke zone. In the calcining zone, six tertiary injectors are aligned along the kiln wall in a form of two longitudinal arrays located diametrically opposite to each other as shown in Figures 3.3 and 3.4. The downstream tertiary injectors are labeled as D1, D2, and D3, while the upstream injectors are labeled as U1, U2, and U3. Those injectors provide the necessary air to combust the volatile matters in the calcining and heat-up zones. The fuel used in the primary injection is methane, CH_4. It is burned in the calcined coke zone to control the temperature and hence the quality of the calcined coke product.

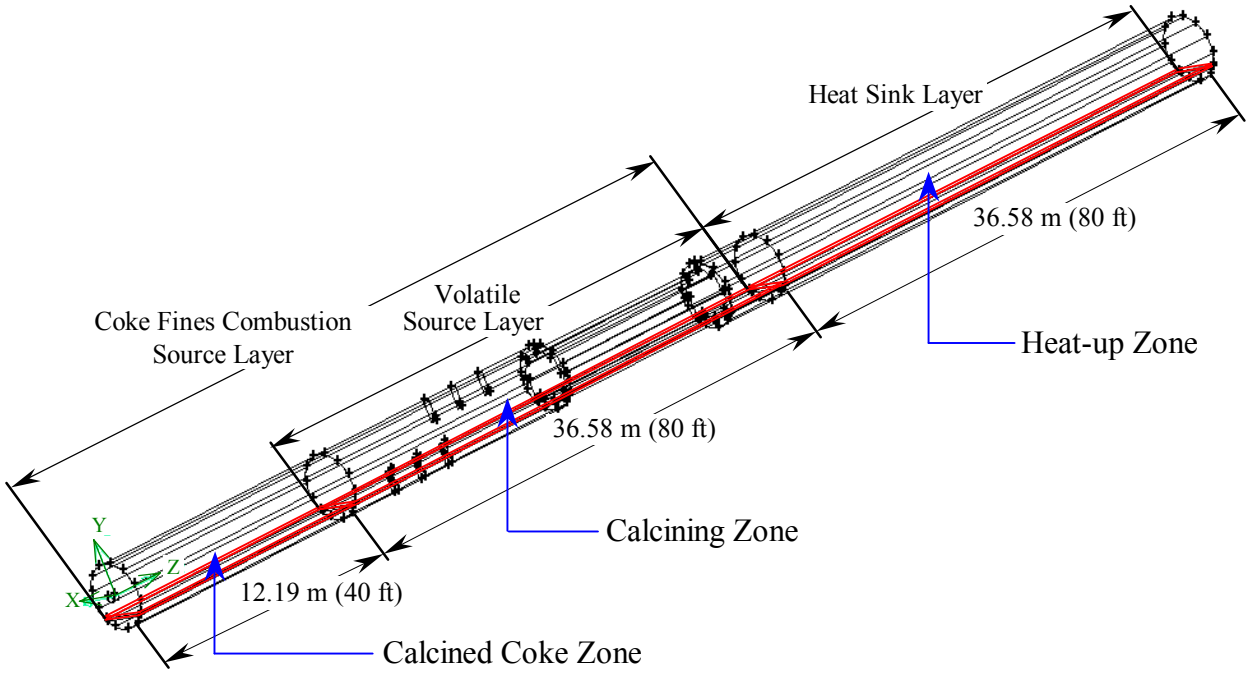

Figure 3.1 A 3-D view of the simulated calcining rotary kiln

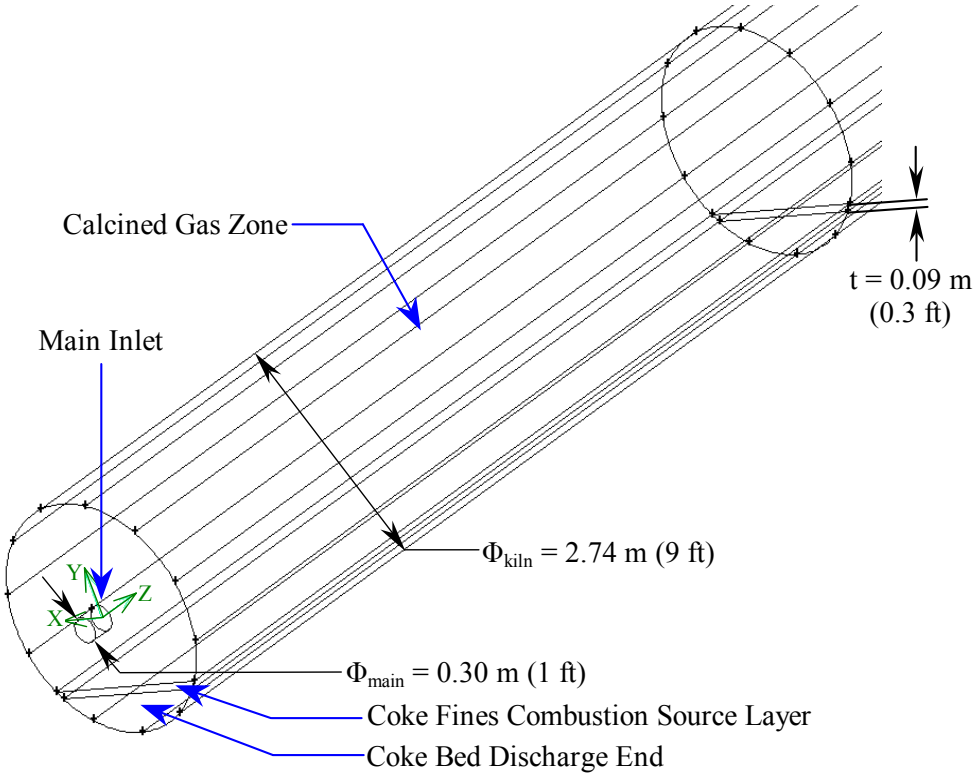

Figure 3.2 Detailed calcined coke zone near the discharge end

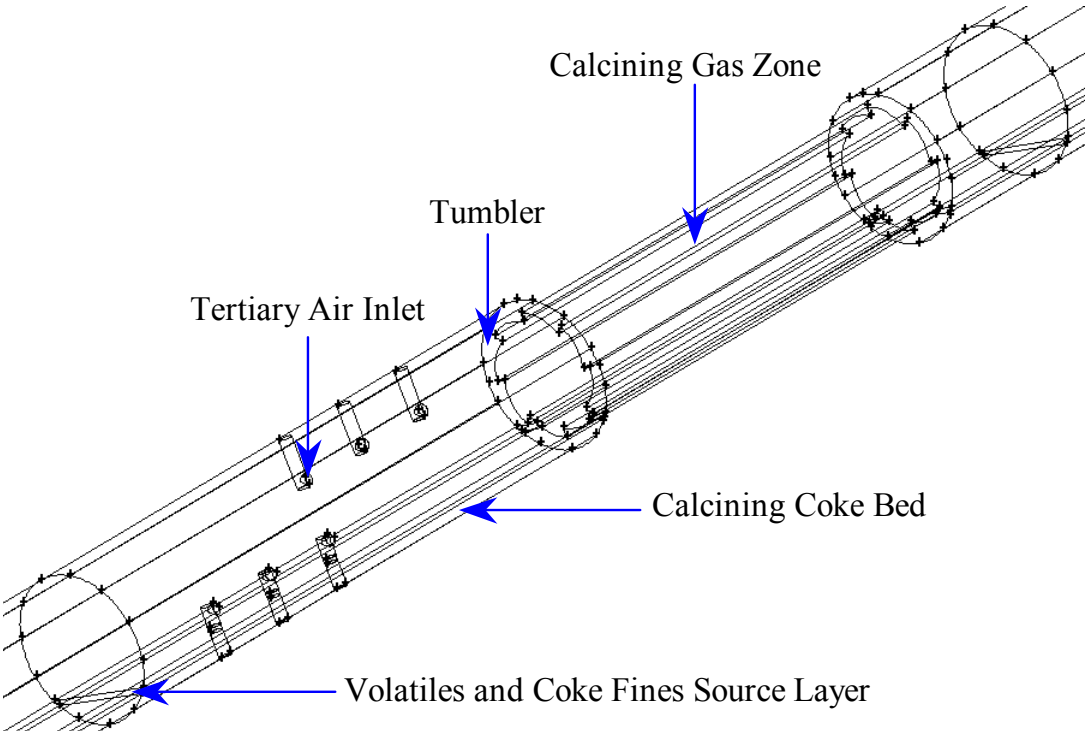

Figure 3.3 Detailed calcining coke zone including tertiary air injectors and tumblers

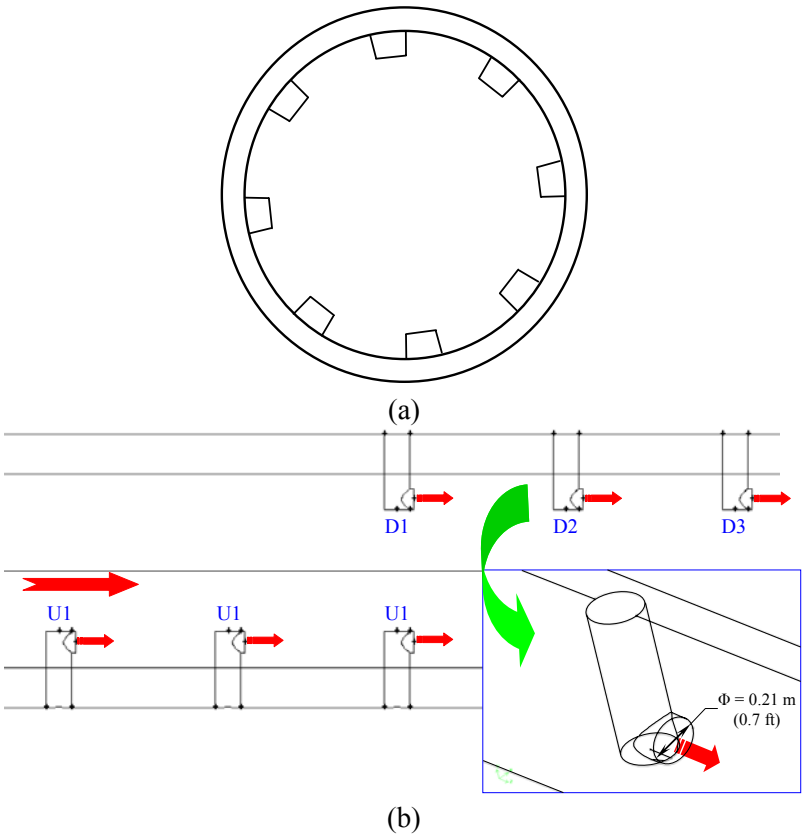

Figure 3.4 (a) The Cross-sectional view of the tumbler (b) Tertiary air injector arrangement

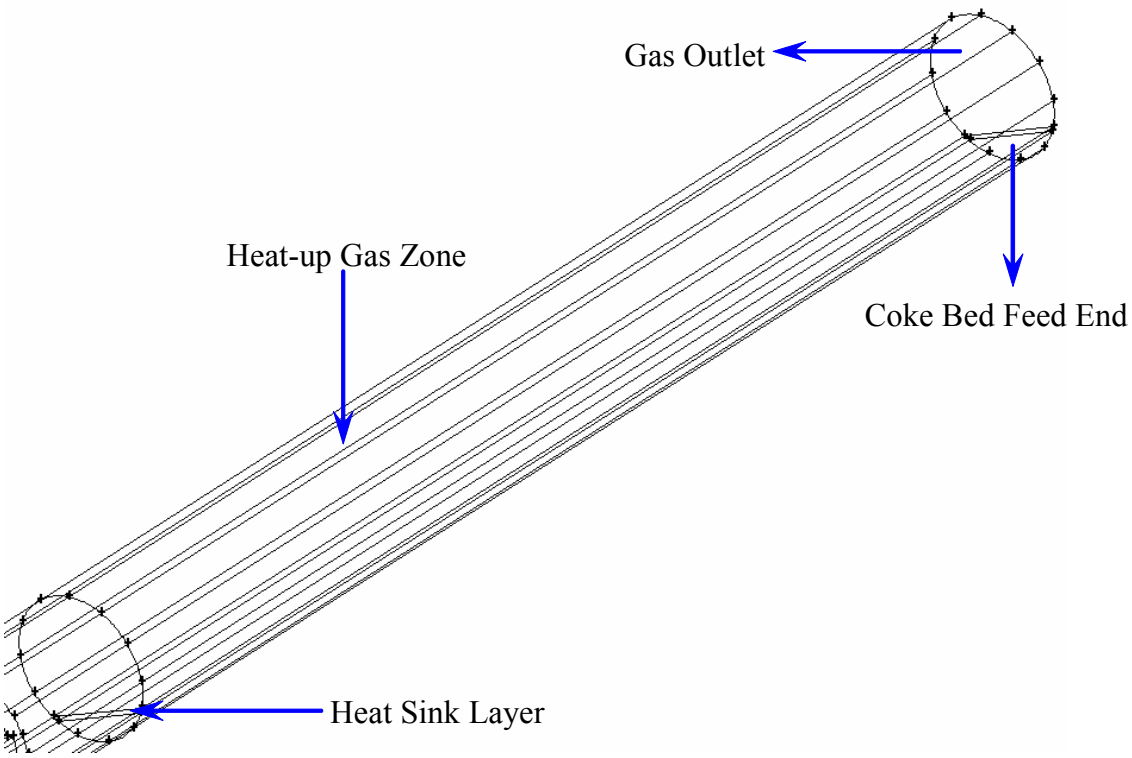

Figure 3.5 Close-up view of the heat-up zone

The problem is modeled with the following general assumptions:

1. Three dimensional
2. Steady and incompressible flow
3. Constant material properties for the coke bed
4. Variable material properties for air and reacted gases
5. Buoyancy force neglected
6. No-slip condition (zero velocity) on wall surfaces
7. Turbulent flow
8. Chemical reactions are faster than the time scale of the turbulence eddies.

3.1 Governing Equations

The conservation equations for mass, momentum and energy conservation in general form are shown below.

$$\frac{\partial \rho}{\partial t} + \nabla \bullet (\rho \vec{v}) = 0 \qquad \text{(Eq.3.1)}$$

$$\frac{\partial}{\partial t}(\rho \vec{v}) + \nabla \bullet (\rho \vec{v}\vec{v}) = -\nabla p + \nabla \bullet \left(\bar{\bar{\tau}}\right) + \rho \vec{g} + \vec{F} \qquad \text{(Eq.3.2)}$$

$$\frac{\partial}{\partial t}(\rho E) + \nabla \bullet \left(\vec{V}(\rho E + p)\right) = \nabla \bullet \left(k_{eff} \nabla T - \sum_j h_j \vec{J}_j + \left(\bar{\bar{\tau}}_{eff} \bullet \vec{v} \right) \right) + S_h \qquad \text{(Eq.3.3)}$$

The momentum equations are solved with the complete three-dimensional Navier-Stokes equations, so, $\bar{\bar{\tau}}$, the stress tensor is given by

$$\bar{\bar{\tau}} = \mu \left[\left(\nabla \vec{v} + \nabla \vec{v}^{\,T} \right) - \frac{2}{3} \nabla \bullet \vec{v} \bullet I \right] \qquad \text{(Eq.3.4)}$$

where I is the unit tensor.

In the energy equation E is given as

$$E = h - \frac{p}{\rho} + \frac{v^2}{2} \qquad \text{(Eq.3.5)}$$

"h" is the sensible enthalpy and for incompressible flow it is given as

$$h = \sum_j Y_j h_j + \frac{p}{\rho} \qquad \text{(Eq.3.6)}$$

$$h_j = \int_{T_{ref}}^{T} c_{p,j} dT \qquad \text{(Eq.3.7)}$$

T_{ref} is the reference temperture, taken as 298.15 K

S_h in the energy equation is the source term and is provided by the net enthalpy formation rates from the species transport reactions.

The flow and thermal variables are defined by the boundary conditions. The boundary conditions on the model surfaces are assigned below:

1. Velocity inlet -- All the inlets are defined as velocity inlet with a uniform velocity distribution. Velocity, temperature of the mixture, and mass fraction of all species in the mixture are assigned according to the values given below:
    a. Main inlet:
        i. Velocity inlet condition:
            1) $v_{main\ inlet}$ = 20 m/s (65.62 ft/s)
            2) Air volume flow rate = 2,505.12 SCFM
            3) CH_4 feed rate = 230.37 kg/hr (507.87 lbm/hr)
        ii. Temperature condition, $T_{main\ inlet}$ = 300 K (80.33 °F)
        iii. Mass fraction:
            1) O_2 = 0.22
            2) CH_4 = 0.043 (lean)
            3) N_2 = 0.737 (If no other species are included, these mass fractions should add up to 1.)
    b. Tertiary air inlet:
        i. Velocity inlet condition:
            1) $v_{main\ inlet}$ = 50 m/s (164.04 ft/s)
            2) Air volume flow rate = 18,279.43 SCFM
        ii. Temperature condition, $T_{main\ inlet}$ = 300 K (80.33 °F)
        iii. Mass fraction:
            1) O_2 = 0.23

2) $N_2 = 0.77$

2. Pressure outlet -- The outlet surfaces are defined as pressure outlet. The pressure, temperature, and species mass fraction of the mixture of the reverse flow are specified as follows:
    a. Gas outlet: Constant pressure outlet condition, P = 1 atm
    b. Temperature condition, T_{outlet} = 300 K (80.33 °F)
    c. Mass fraction:
        i. $O_2 = 0.23$
        ii. $N_2 = 0.77$
3. Source layers are assigned as follows:
    a. Coke fines combustion source layer from Z = 0 to 12.19 m - Releasing rate = 0.0505 kg/m^3-s (0.8089 lbm/ft^3-s). (This is to simulate the coke fines entrainment effect and provide a carbon source for combustion.)
    b. Volatiles and coke fines source layer from Z = 12.19 to 36.58 m. (This is to simulate both the volatiles releasing and the coke fines entrainment effect as the source of combustion.):
        i. Carbon releasing rate = 0.0505 kg/m^3-s (0.8089 lbm/ft^3-s)
        ii. Volatiles releasing rate = 0.1534 kg/m^3-s (2.4572 lbm/ft^3-s)
    c. Heat sink layer - Energy absorption rate = 346,989.3 W/m^3 (3,591,339.26 Btu/hr-ft^3) (This is to simulate the moisture evaporation absorbing energy from the gas flow.)
4. Wall -- The outer rims of the geometry are defined as a wall boundary. The walls are treated as adiabatic with no-slip velocity condition:

a. Adiabatic wall condition, heat flux = 0

b. No slip condition at the walls, u = 0, v = 0, w = 0

The step by step procedure of setting the baseline case is provided in Appendix A.

3.2 Computational Domain

The simulations are conducted in the following stages.

1. Thermal-flow behavior with different tertiary air injector positions related to the coke bed (Figure 3.6 a)
2. Thermal-flow behavior with different tertiary air injection angles (Figure 3.6 b)
3. Thermal-flow behavior with moving petroleum coke bed (i.e. conjugate situation)

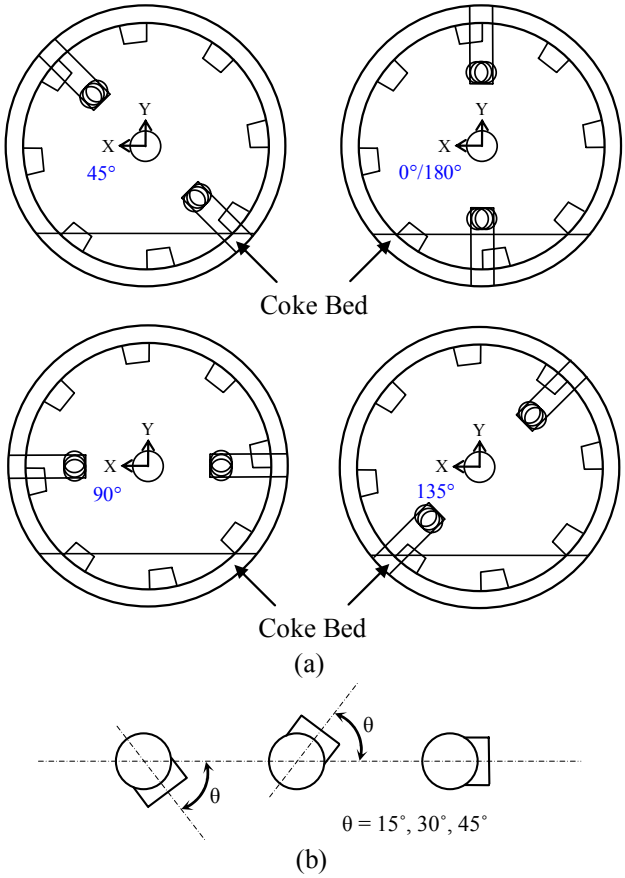

Figure 3.6 (a) Relative coke bed and tertiary air inlet position (rotational angles) (b) Three different tertiary air injection angles; note: In a real situation, the coke bed tilts at an angle approximately 15°. Since the injector's location is cited relative to the coke bed, it is more convenient to show the figures without tilting the coke bed.

3.3 Turbulence Model

Turbulent flows are characterized by spectrally broad-band randomly fluctuate within the velocity fields. These fluctuations advected transported quantities such as momentum, energy, and species concentration and cause the transported quantities to fluctuate as well. Since these fluctuations can be of small scale and high frequency, they are too computationally intensive to simulate directly in practical engineering calculations. Instead, the instantaneous governing equations can be time averaged, ensemble-averaged, or otherwise manipulated to remove the small scales, resulting in a modified set of equations that are computationally less expensive to solve. However, the modified equations contain additional unknown variables, and turbulence models are needed to determine these variables in terms of known quantities.

The following turbulence models are available in public literature:

1. Spalart-Allmaras model
2. k - ε models
    a. Standard k - ε model
    b. Renormalization-group (RNG) k - ε model
    c. Realizable k - ε model
3. k - ω models
    a. Standard k - ω model
    b. Shear-stress transport (SST) k - ω model
4. v^2 - f model
5. Reynolds stress model (RSM)
6. Large eddy simulation (LES) model

This study selects the standard k - ε model due to its suitability for a wide range of wall-bounded and free-shear flows. The standard k - ε model is the simplest of turbulence two-equation model in which the solution of two separate transport equation allows the turbulent velocity and length scales to be independently determined. The k - ε model is a semi-empirical model with several constants obtained from experiments.

All the three k - ε models have similar forms with major differences in the method of calculating the turbulent viscosity, the turbulent Prandtl numbers, and the generation and destruction terms in the k - ε equations.

The standard k - ε model is a semi-empirical model based on model transport equations for the turbulence kinetic energy (k) and its dissipation rate (ε). The model transport equation for (k) is derived from the exact equation, while the model transport equation for (ε) is obtained using physical reasoning and bears little resemblance to its mathematically exact counterpart.

The turbulence kinetic energy, (k), and its rate of dissipation, (ε), are obtained from the following transport equations:

$$\frac{\partial}{\partial t}(\rho k)+\frac{\partial}{\partial x_i}(\rho k u_i)=\frac{\partial}{\partial x_j}\left[\left(\mu+\frac{\mu_t}{\sigma_k}\right)\frac{\partial k}{\partial x_j}\right]+G_k+G_b-\rho\varepsilon-Y_M+S_k \qquad \text{(Eq.3.8)}$$

$$\frac{\partial}{\partial t}(\rho \varepsilon)+\frac{\partial}{\partial x_i}(\rho \varepsilon u_i)=\frac{\partial}{\partial x_j}\left[\left(\mu+\frac{\mu_t}{\sigma_\varepsilon}\right)\frac{\partial \varepsilon}{\partial x_j}\right]+C_{1\varepsilon}\frac{\varepsilon}{k}(G_k+C_{3\varepsilon}G_b)-C_{2\varepsilon}\rho\frac{\varepsilon^2}{k}+S_\varepsilon \qquad \text{(Eq.3.9)}$$

In these equations, G_k represents the generation of turbulence kinetic energy due to the mean velocity gradients and the Reynolds stress, calculated as

$$G_k=-\overline{\rho u_i' u_j'}\frac{\partial u_j}{\partial x_i} \qquad \text{(Eq.3.10)}$$

G_b represents the generation of turbulence kinetic energy due to buoyancy, calculated as

$$G_b = \beta g_i \frac{\mu_t}{Pr_t} \frac{\partial T}{\partial x_i} \quad \text{(Eq.3.11)}$$

where Pr_t is the turbulent Prandtl number and g_i is the component of the gravitational vector in the i-th direction. For standard k - ε model the value for Pr_t is set to be 0.85 in this study.

β is the coefficient of thermal expansion and is given as

$$\beta = -\frac{1}{\rho}\left(\frac{\partial \rho}{\partial T}\right)_P \quad \text{(Eq.3.12)}$$

Y_M represents the contribution of the fluctuating dilatation in compressible turbulence to the overall dissipation rate, and is given as

$$Y_M = 2\rho\varepsilon M_t^2 \quad \text{(Eq.3.13)}$$

where M_t is the turbulent Mach number, given as

$$M_t = \sqrt{\frac{k}{a^2}} \quad \text{(Eq.3.14)}$$

where $a = (\gamma RT)^{0.5}$ is the speed of sound.

The turbulent (or eddy) viscosity, μ_t, is computed by combining k and ε as

$$\mu_t = \rho C_\mu \frac{k^2}{\varepsilon} \quad \text{(Eq.3.15)}$$

$C_{1\varepsilon}$, $C_{2\varepsilon}$, C_μ, σ_k and σ_t are constants and have the following values

$C_{1\varepsilon} = 1.44$, $C_{2\varepsilon} = 1.92$, $C_\mu = 0.09$, $\sigma_k = 1.0$, and $\sigma_t = 1.3$

These constant values have been determined from experiments with air and water for fundamental turbulent shear flows including homogeneous shear flows and decaying isotropic grid turbulence. They have been found to work fairly well for a wide range of wall- bounded and free-shear flows. The initial value for k and ε at the inlets and outlets are set as 1 m^2/s^2 and 1 m^2/s^3 respectively.

In general, turbulent flows are significantly affected by the presence of walls. Very close to the wall, viscous damping reduces the tangential velocity fluctuations. While kinematic blocking reduces the normal fluctuations, away from the wall, the turbulence is increased by the production of turbulence kinetic energy. In the near-wall region, the solution variables have large gradients, and the momentum and other scalar transports occur strongly. Therefore, accurate representation of the flow in the near-wall region is required for successful predictions of wall-bounded turbulent flows.

The k - ε turbulence model used in this study is primarily valid for turbulent core flows (i.e., the flow in the regions somewhat far from walls). Wall functions are used to make this turbulence model suitable for wall-bounded flows. Wall functions are a collection of semi-empirical formulas and functions that link the solution variables at the near-wall cells and the corresponding quantities on the wall. The wall functions consist of the following:

1. Laws of the wall for mean velocity and temperature and other scalars
2. Equations for near-wall turbulent quantities.

The law-of-the-wall for mean velocity gives

$$U^+ = \frac{1}{\kappa}\ln\left(Ey^+\right) \qquad \text{(Eq.3.16)}$$

$$\text{where} \quad U^+ \equiv \frac{U_P C_\mu^{0.25} k_P^{0.5}}{\frac{\tau_w}{\rho}} \qquad \text{(Eq.3.17)}$$

$$y^+ \equiv \frac{\rho C_\mu^{0.25} k_P^{0.5} y_P}{\mu} \qquad \text{(Eq.3.18)}$$

κ = Von Karman constant (= 0.42)

E = empirical constant (= 9.793)

U_P = mean velocity of the fluid at point P

k_P = turbulence kinetic energy at point P

y_P = distance from point P to the wall

μ= dynamic viscosity of the fluid

The logarithmic law for mean velocity is valid for y^+ > about 30 to 60

The law-of-the-wall for temperature is given

$$T^+ \equiv \frac{(T_w - T_P)\rho c_P C_\mu^{0.25} k_P^{0.5}}{q''} = Pry^+ + 0.5\rho.5 \frac{C_\mu^{0.25} k_P^{0.5}}{q''} U_P^2 \qquad \left(y^+ < y_T^+\right) \qquad \text{(Eq.3.19)}$$

$$= Pr_t\left[\frac{1}{\kappa}\ln\left(Ey^+\right) + P\right] + 0.5\rho\frac{C_\mu^{0.25} k_P^{0.5}}{q''}\left[Pr_t U_P^2 + (Pr - Pr_t)U_c^2\right] \qquad \left(y^+ > y_T^+\right) \qquad \text{(Eq.3.20)}$$

where P is computed using the formula

$$P = 9.24\left[\left(\frac{Pr}{Pr_t}\right)^{3/4} - 1\right]\left[1 + 0.28e^{-0.007 Pr/Pr_t}\right] \qquad \text{(Eq.3.21)}$$

k_f = thermal conductivity of the fluid

ρ = density of fluid

c_P = specific heat of fluid

q" = wall heat flux

T_P = temperature at the cell adjacent to the wall

T_w = temperature at the wall

Pr = molecular Prandtl number ($\mu c_P / k_f$)

Pr_t = turbulent Prandtl number (= 0.85 at the wall)

A = 26 (Van Driest constant)

κ = 0.4187 (Von Karman constant)

E = 9.793 (wall function constant)

U_c = mean velocity magnitude at $y^+ = y^+_T$

For k - ε turbulence model, wall adjacent cells are considered to solve the k-equation. The boundary condition for k imposed at the wall is $\partial k/\partial n = 0$, where "n" is the local coordinate normal to the wall. The production of kinetic energy, G_k, and its dissipation rate, ε, at the wall-adjacent cells, which are the source terms in k-equation, are computed on the basis of equilibrium hypothesis with the assumption that the production of k and its dissipation rate assumed to be equal in the wall-adjacent control volume. The production of k and ε is computed as

$$G_k \approx \tau_w \frac{\partial U}{\partial y} = \tau_w \frac{\tau_w}{\kappa \rho C_\mu^{0.25} k_P^{0.5} y_P} \quad \text{(Eq.3.22)}$$

$$\varepsilon_P = \frac{C_\mu^{0.75} k_P^{1.5}}{\kappa y_P} \quad \text{(Eq.3.23)}$$

3.4 Radiation Model

The P-1 radiation model is used to calculate the flux of the radiation at the inside walls of the rotary kiln. The P-1 radiation model is the simplest case of the more general PN radiation model that is based on the expansion of the radiation intensity I. The P-1 model requires only a little CPU demand and can easily be applied to various complicated geometries. It is suitable for applications where the optical thickness aL is large where a is the absorption coefficient and L is the length scale of the domain.

The heat sources or sinks due to radiation is calculated using the equation

$$-\nabla q_r = aG - 4aG\sigma T^4 \quad \text{(Eq.3.24)}$$

where

$$q_r = -\frac{1}{3(a+\sigma_s) - C\sigma_s} \nabla G \quad \text{(Eq.3.25)}$$

and q_r is the radiation heat flux, a is the absorption coefficient, σ_s is the scattering coefficient, G is the incident radiation, C is the linear-anisotropic phase function coefficient, and σ is the Stefan-Boltzmann constant.

The flux of the radiation, $q_{r,w}$, at walls caused by incident radiation G_w is given as

$$q_{r,w} = -\frac{4\pi\varepsilon_w \frac{\sigma T_w^4}{\pi} - (1-\rho_w)G_w}{2(1+\rho_w)} \quad \text{(Eq.3.26)}$$

where ε_w is the emissivity and is defined as

$$\varepsilon_w = 1 - \rho_w \quad \text{(Eq.3.27)}$$

and ρ_w is the wall reflectivity.

3.5 Combustion Model

Modeling for combustion ranges from nonreacting to multiple reactions with multiple species at instant rate or finite rate kinetics. In this study, combustion of methane is modeled by a single-step reaction. The mixing and transport of chemical species is modeled by solving the conservation equations describing convection, diffusion, and reaction sources for each component species. The species transport equations are solved by predicting the local mass fraction of each species, Y_i, through the solution of a convection-diffusion equation for the i-th species. The species transport equation in general form is given as:

$$\frac{\partial}{\partial t}(\rho Y_i) + \nabla \bullet (\rho \vec{v} Y_i) = -\nabla \bullet \vec{J}_i + R_i + S_i \quad \text{(Eq.3.28)}$$

where R_i is the net rate of production of species i by chemical reaction. S_i is the rate of creation by addition from the dispersed phase plus any user-defined sources. $\vec{J}_i$ is the diffusion flux of species i, which arises due to concentration gradients. Mass diffusion for laminar flows is given as

$$\vec{J}_i = -\rho D_{i,m} \nabla Y_i \qquad \text{(Eq.3.29)}$$

For turbulent flows, mass diffusion flux is given as

$$\vec{J}_i = -\left(\rho D_{i,m} + \frac{\mu_t}{Sc_t} \right) \nabla Y_i \qquad \text{(Eq.3.30)}$$

where Sc_t is the turbulent Schmidt number given as $\mu_t / \rho D_t$, where μ_t is the turbulent viscosity and D_t is the turbulent diffusivity.

In this study, the reaction rate that appears as source term in (Eq.3.28) is given by the turbulence-chemistry interaction model called the eddy-dissipation model. The overall rate of reaction for most fast burning fuels is controlled by turbulent mixing. The net rate of production of species i due to reaction r, $R_{i,r}$, is given by the smaller of the two given expressions below:

$$R_{i.r} = \nu'_{i,r} M_{w,i} A \rho \frac{\varepsilon}{\kappa} \min_R \left(\frac{Y_R}{\nu'_{R,r} M_{w,R}} \right) \qquad \text{(Eq.3.31)}$$

$$R_{i.r} = \nu'_{i,r} M_{w,i} AB \rho \frac{\varepsilon}{\kappa} \frac{\sum_P Y_P}{\sum_j^N \nu''_{j,r} M_{w,j}} \qquad \text{(Eq.3.32)}$$

where Y_P is the mass fraction of any product species, P

Y_R is the mass fraction of a particular reactant, R

A is an empirical constant equal to 4.0

B is an empirical constant equal to 0.5

$\nu'_{i,r}$ is the stoichiometric coefficient for reactant i in reaction r

$\nu''_{j,r}$ is the stoichiometric coefficient for product j in reaction r

In the above equation (Eq.3.31) and (Eq.3.32), the chemical reaction rate is governed by the large-eddy mixing time scale, κ/ε, and an ignition source is not required. This is based on the

assumption that the chemical reaction is much faster than the turbulence mixing time scale, so the actual chemical reaction is not important.

In this study, methane (CH_4) is used as fuel, a FLUENT build-in coal_mv_volatiles ($CH_{3.086}O_{0.131}$) is used as volatile matters, and carbon (C) is used for coke combustion. The complete stoichiometric combustion equations are given below:

$$CH_4 + 2O_2 \rightarrow CO_2 + 2H_2O \quad \text{(Eq.3.33)}$$

$$CH_{3.086}O_{0.131} + 1.706O_2 \rightarrow CO_2 + 1.543H_2O \quad \text{(Eq.3.34)}$$

$$C + O_2 \rightarrow CO_2 \quad \text{(Eq.3.35)}$$

CHAPTER FOUR

COMPUTATIONAL METHOD

4.1 The CFD Code Background

The commercial computational fluid dynamics (CFD) code, FLUENT, is used in this study. FLUENT is one of the most widely-used commercial CFD software. CFD can turn a computer into a virtual laboratory allowing engineers and designers to simulate fluid flow, heat and mass transfer, and a host of related phenomena involving turbulence, reaction, and multiphase flow. CFD can also provide insight of thermal-fluid physics to guide experimental process or design selections. Significant time reduction, cost savings and return on investment can be realized.

4.2 Solution Methodology

In typical CFD simulations, the following stages are taken to solve fluid flow and heat transfer fields:

1. Pre-processing:

The pre-processing stage includes geometry generation, mesh generation, medium properties specifications, physical model selections, and boundary condition specifications.

2. Processing:

In the processing stage, appropriate solution parameters are chosen to allow the simulation for the equations and models set up in the pre-processing stage to reach convergence as the calculation progresses.

3. Post-processing:

After the converged solutions are obtained from the simulation, the results can be analyzed and interpreted in the post-processing stage in forms of, for examples, X-Y plots, contour plots, velocity vector plots, streamline plots, and animations.

In this study, GAMBIT version 2.3.16 is used as the pre-processing tool, and the CFD solver used is FLUENT version 6.2.13, which is a finite volume CFD solver written in C language. The basic program structure of FLUENT is shown in Figure 4.1.

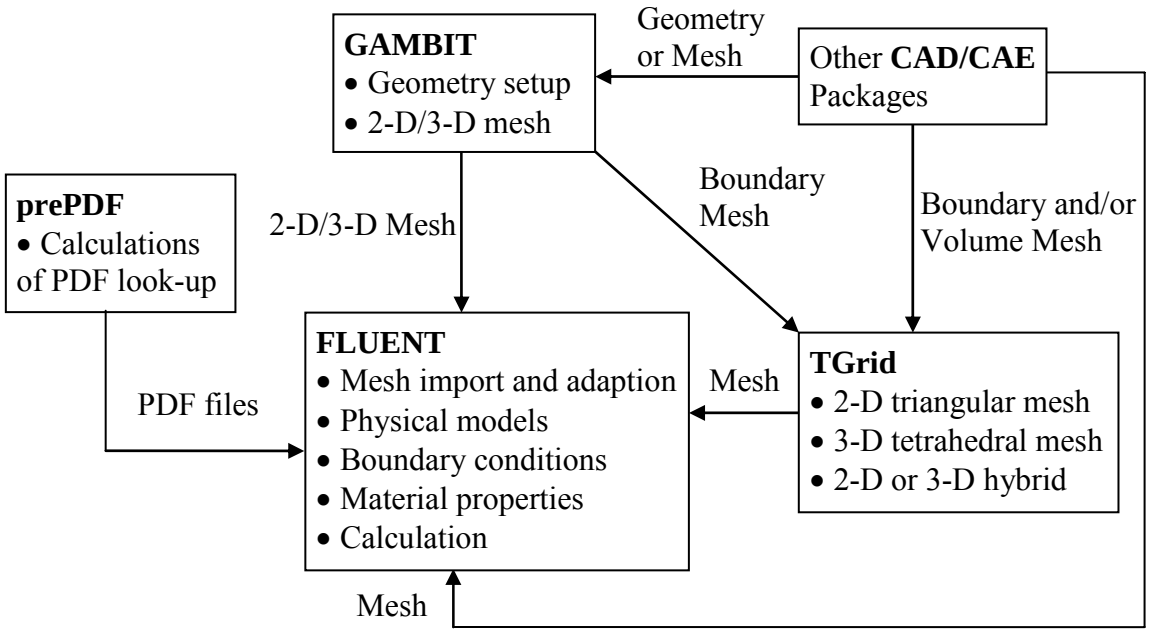

Figure 4.1 Basic program structure for FLUENT

4.3 Computational Grid

The computational geometry is constructed and meshed in GAMBIT. The three-dimensional geometry is modeled after the calcinations kiln in CII Carbon, L.L.C. Chalmette plant with some simplifications. Three-dimensional tetrahedral mesh is used for meshing the entire rotary kiln. Figure 4.2 illustrates the model geometry with computational grids used in the baseline case study. A total of 1,331,654 cells are employed. The computational domain is a long and slender cylinder; the length-diameter ratio is 200:9. To properly mesh the geometry and

avoid grid aspect ratio problem, this domain is divided into nine sub domains as shown in Figure 3.2, 3.3, and 3.5. In the diametric direction, the kiln is separated into three horizontal zones based on the property of the media as: coke bed, coke-fines/volatiles/moisture source layer, and the gas zone. In the axial direction (z-direction) from the feed end to the discharge end and based on the function of kiln, the kiln is separated into three sections: heat-up, calcining, and calcined zones. The mesh number of each subdomain is shown in Table 4.1.

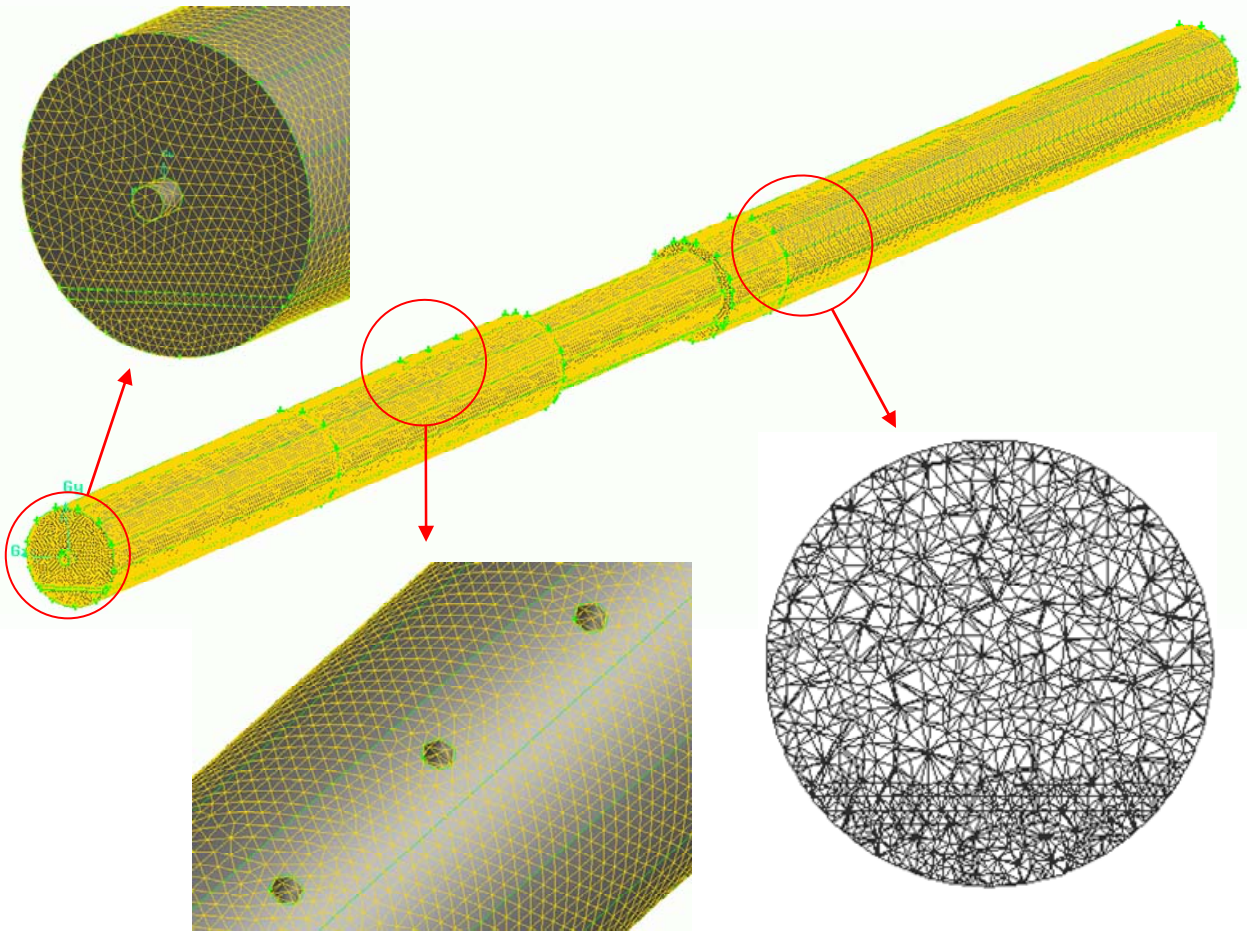

Figure 4.2 Meshed geometry for the rotary calcining kiln

Table 4.1 Mesh numbers in the nine sub domains

Axial Sections / Horizontal Zones	Calcined Coke Zone	Calcining Zone	Heat-up Zone
Gas Zone	251,621	282,985	356,819
Source Layer	22,036	38,173	43,353
Coke Bed	77,997	101,014	157,656

The heat-up coke bed (157,656 cells) is connected to calcining coke bed (101,014 cells) and then connected to the calcined coke bed (77,997 cells). On top of the coke bed, there is a special function layer. This layer is also separated into three portions from the feed end to the discharge end. They are heat sink layer (43,353 cells) connecting with the volatiles/coke-fines source layer (38,173 cells) and then connected to the coke fines combustion source layer (22,036 cells). The gas zone is formed by three zones, heat-up zone (356,819 cells), calcining zone (282,985 cells), and calcined zone (251,621 cells) respectively. All zones are meshed with tetrahedral mesh elements to avoid potential large aspect ratio problem, which is often seen in long and slender geometry meshed with hexahedral mesh elements. Along the cylinder wall, extra lines are created to achieve better mesh quality. The model is then exported to FLUENT after being meshed.

4.4 Numerical Procedure

The numerical simulation is carried out with the following procedure:

1. Create and mesh the computational model using GAMBIT
2. Import the model to FLUENT
3. Define solver model
4. Define viscous model
5. Define species model
6. Define materials and chemical reactions

7. Define boundary and initial conditions
8. Iterate until convergence is achieved
9. Post-process the results

FLUENT offers two different solvers: segregated and coupled. Segregated solver only has implicit formulation while coupled solver has implicit and explicit formulations. Segregated method solves the governing equations sequentially. On the contrary, coupled method solves the governing equations simultaneously. In this study, segregated solver is employed to solve the governing equations of the conservation of mass, momentum, energy, turbulence and the species transports. The segregated method proceeds with following steps:

1. Fluid properties are first updated based on the current solution or the initial conditions.
2. Momentum equations are solved with the current values of pressure and face mass fluxes to update the velocity field.
3. Equation for the pressure correction is calculated from the continuity equation and the linearized momentum equations since the velocity field obtained from step 2 may not satisfy the continuity equation.
4. The pressure correction equation obtained from step 3 is solved to acquire necessary corrections for the pressure, velocity field, and face mass fluxes such that the continuity equation is satisfied.
5. The transport equations for scalars such as turbulence, and energy are solved using the updated values of the other variables.
6. The reactions are solved with the input of the stochiometeric coefficients and adoption of the eddy dissipation model for reaction rate.

7. The species transport equations are solved with the velocity filed, species concentration, and the species source term obtained from step 6.
8. The equation is checked for convergence.

These steps are repeated until the convergence criteria are met. Figure 4.3 shows the flow chart of the segregated method proceeding steps.

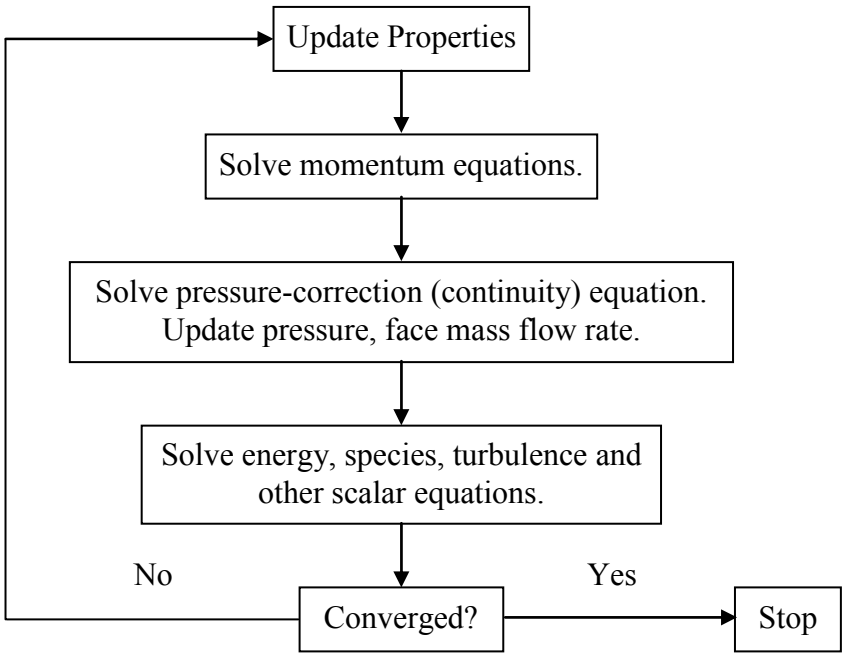

Figure 4.3 Flow chart for segregated solver

In this simulation, the SIMPLE algorithm [Patankar, 1980] is used to couple the pressure and velocity. The momentum, energy, turbulence and species equations are discretized using the finite volume second order upwind scheme. The standard k - ε turbulence model is used with the model constants as,

$C_\mu = 0.09$, $C_{1\varepsilon} = 1.44$, $C_{2\varepsilon} = 1.92$, $C_\varepsilon = 1.3$.

The species transport model with volumetric reaction and the eddy-dissipation model are chosen to simulate the chemical reactions. The chemical reaction rates are assumed to be faster than the mixing rates and are controlled by the turbulence time scale.

In this study, methane-air, volatile-air, and coke (carbon)-air combustions are simulated. The mixture consists of seven species (C, O_2, CH_4, mv_vol, CO_2, H_2O, and N_2). All the species in the mixture are defined as fluid species and are assumed to mix at the molecular level. The property values in the gas vary with temperature and pressure. The densities of the species obey incompressible ideal gas law, and the specific heat of the species follows the mixing law. The chemical reactions (Eq.3.31 to Eq.3.33) are defined in the reaction windows.

For the baseline case, the solution convergence is obtained by monitoring the residuals of the continuity, momentum, energy, turbulence and species equations separately:

- Continuity (mass conservation) < 2×10^{-3}
- X-velocity < 9×10^{-5}
- Y-velocity < 8×10^{-5}
- Z-velocity < 2×10^{-5}
- Energy < 5×10^{-5}
- k (turbulence energy) < 3×10^{-4}
- ε (turbulence dissipation) < 2×10^{-3}
- Volatiles < 3×10^{-4}
- O_2 < 3×10^{-4}
- CO_2 < 6×10^{-5}
- H_2O < 6×10^{-5}
- C < 3×10^{-4}
- CH_4 < 5×10^{-3}
- P-1 < 4×10^{-5}

Physical iteration time of 5000 iterations for baseline case using different computer equipments is listed below:

- 1 × Pentium 4 3.2GHz with 2GB RAM computer requires approximate 68 hours.
- 4 × Pentium 4 3.2GHz with 2GB RAM computers parallel processing requires approximate 20 hours.

4.5 Grid Sensitivity Study

Due to the limitation of the computer power with eight desktop personal computers in parallel processing, the results have not reached grid independency. Instead, a grid sensitivity study is carried out by comparing the change of results from two different mesh sizes. The baseline case has a higher number of cells (1,331,654 cells) and the other lower mesh number case has 384,111 cells. Figure 4.4 shows the variation of gas zone centerline static temperature of these two cases. In the important calcining and calcined coke zone, the difference of centerline temperatures of two mesh sizes is within 50 to 200 K (3 to 12%). In the heat-up zone, which is not critical for the calcining process, the temperature difference is less than 50 K (3%). Based on this grid-sensitivity study, it is felt that the temperature differences will reduce when the mesh number are than 1.4 million meshes. For the purpose of current study, 10 % of computational uncertainty is acceptable.

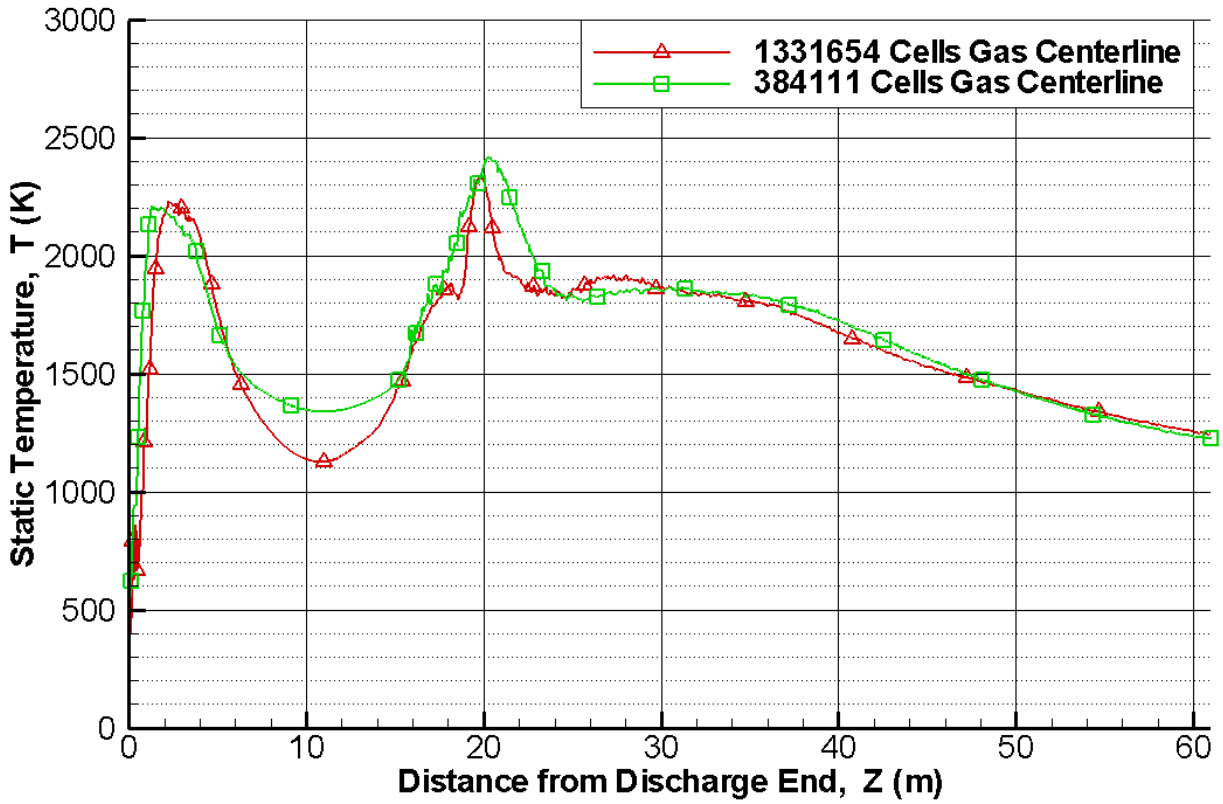

Figure 4.4 Gas centerline static temperature for various cell numbers

CHAPTER FIVE

RESULTS AND DISCUSSIONS

Total thirteen 3-D cases and six 2-D cases are conducted. For reference of comparison, the normal (reference) operating conditions are recapped here:

- Natural gas supplying rate = 0.0640 kg/s (507.74 lbm/hr)
- Petcoke feed rate = 9.3 kg/s (33.48 metric ton/hr)
- Petcoke combustion rate = 0.3456 kg/s (0.7619 lbm/s)
- Volatiles source rate = 0.6994 kg/s (1.5419 lbm/s)
- Heat sink for latent heat absorption during moisture evaporation = 346,989.3 W/m^3 (3,591,339.26 $Btu/hr\text{-}ft^3$)
- Main air inlet injection velocity and flow rate = 20 m/s (65.62 ft/s), 2,504.49 SCFM
- Tertiary air inlet injection velocity and total flow rate = 50 m/s (164.04 ft/s), 18,279.26 SCFM
- Adiabatic wall condition
- Kiln wall rotational velocity = 0.133 rad/s (1.27 rpm)
- Coke bed sliding velocity = 0.01 m/s (0.0328 ft/s), resident time = 1.69 hr

The results will be analyzed and discussed with the following different operating conditions:

- Various rotational angles (Cases 5, 6, 9, 10, and 11)
- Various tertiary air injection angles (Cases 6, 7, and 8)
- Discharge end flow control (Cases 1, 2, and 3)

- Discharge end flow extraction and return (Cases 5 and 13)
- Various coke bed devolatilization conditions (Cases 5, 6, and 12)
- Various coke bed properties (Cases A, B, C, D, E, and F)

The corresponding 3-D case numbers, simulation conditions, and number of cells are listed in Table 5.1. The locations and labeling of the tertiary air injectors are shown in Figure 5.1.

Table 5.1 3-D case number and descriptions (major variations are noted in bold font)

3D Case Number	Case Descriptions	Mesh Numbers
Case 1	0 degree tertiary inlet position, 15 degree injection angle, with coke bed, normal operation condition **(Baseline)**	1,331,654
Case 2	0 degree tertiary inlet position, 15 degree injection angle, with coke bed, normal operation condition with **10kPa suction at main inlet, and no natural gas**	1,331,654
Case 3	0 degree tertiary inlet position, 15 degree injection angle, with coke bed, normal operation condition **with 10kPa suction at main inlet and 2 upstream tertiary air injections,** and no natural gas	1,331,452
Case 4	0 degree tertiary inlet position, 15 degree injection angle, **no coke bed**, normal operation condition	751,226
Case 5	0 degree tertiary inlet position, 15 degree injection angle, no coke bed, normal operation condition **without coke fines combustion**	763,538
Case 6	**45 degree** tertiary inlet position, **15 degree injection angle,** no coke bed, normal operation condition without coke fines combustion	762,687
Case 7	45 degree tertiary inlet position, **30 degree injection angl**e, no coke bed, normal operation condition without coke fines combustion	764,546
Case 8	45 degree tertiary inlet position, **45 degree injection angl**e, no coke bed, normal operation condition without coke fines combustion	763,040
Case 9	**90 degree tertiary inlet position**, **15 degree injection angle,** no coke bed, normal operation condition without coke fines combustion	760,579
Case 10	**135 degree tertiary inlet position**, 15 degree injection angle, no coke bed, normal operation condition without coke fines combustion	764,451
Case 11	**180 degree tertiary inlet positio**n, 15 degree injection angle, no coke bed, normal operation condition without coke fines combustion	763,579
Case 12	0 degree tertiary inlet position, 15 degree injection angle, no coke bed, normal operation condition without coke fines combustion, and **shortened devolatile zone**	747,420
Case 13	0 degree tertiary inlet position, 15 degree injection angle, no coke bed, without coke fines combustion**,** no natural gas, 10kPa suction at main inlet, and **extracted hot combustion gas returned at Z = 35.052 m**	763,505

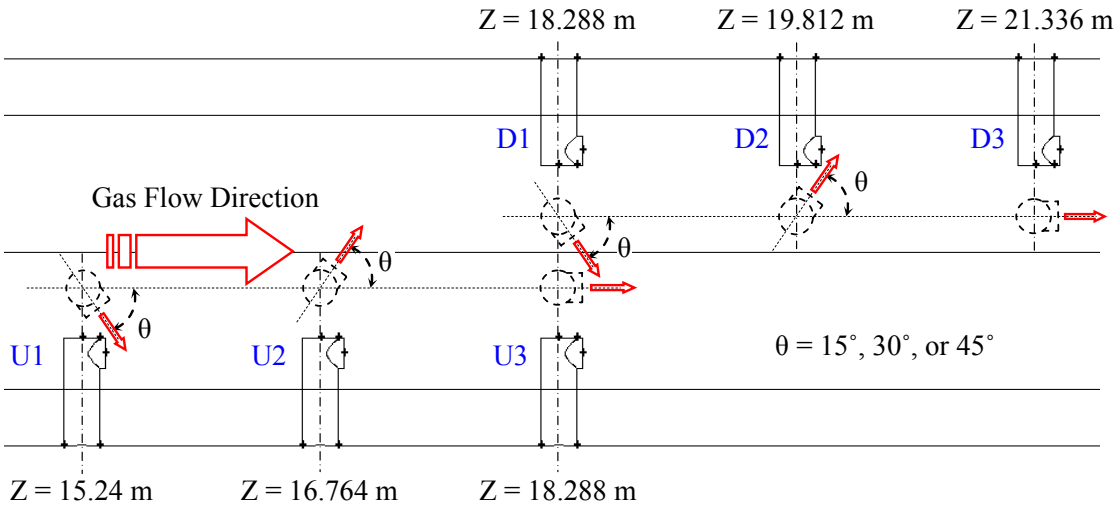

Figure 5.1 Tertiary air injector locations and labeling

5.1 Baseline Case (Case 1)

In the baseline case, the tertiary inlet is at 0 degree position (see Figure 3.6a), and the tertiary air injection angles of D1, D2, U1 and U2 are ±15 degrees (See Figure 5.1). The entire kiln wall is set as the adiabatic wall condition. The combustion consists of all three types of reactions, natural gas with air, volatiles with air, and coke fines with air. The air is supplied with 0.23% oxygen and 0.76% nitrogen. In the heat-up zone, a thin layer is added above the coke bed acting as a heat sink that absorbs latent heat (347 kW/m^3) and simulates a moisture evaporation process. The simulation is carried out under a steady-state condition.

Figure 5.2a is a vertical plane view cutting through the middle of the kiln at X = 0. In this figure, the natural gas and the main air are supplied at the coke discharge end (left end of Figure 5.2a), the combusted gas moves from left to right, and the coke moves from right to left at the bottom. Moving in the gas direction (from left to right) is assigned as **downstream** direction and moving against the gas direction (from right to left) is assigned as **upstream** direction. The natural gas combustion flame can be seen near the main air inlet with a flame temperature above 2,500 K. Downstream (toward right) of this natural gas combustion region, a relatively cooler

region with a temperature of around 1,000 K exists due to depletion of natural gas and oxygen. In this relatively cooler zone, the coke bed surface temperature is calculated between 1,200 and 1,400 K (see Figure 5.2c), which is actually higher than the gas temperature. This region is where the heat is lost from the coke bed to the gas. Moreover, this region is also where the quality of the calcined coke is critically dependent on the coke bed temperature. The current practice is adding natural gas combustion near the discharge end to maintain the required coke bed temperature and produce quality carbon products. However, as the natural gas price continues to be volatile and climbing, finding a means to reduce the natural gas consumption is an important operating goal in reducing production cost. This search for viable alternatives to natural gas consumption is the motivation for Section 5.4, which is exploring utilization of gas extraction at the discharge end to increase the local gas temperature.

In the tertiary air zone, volatiles that devolatilized from the coke bed are combusting with the fresh injected air resulting in another high temperature region. At this region and in this figure, there are two groups of combustion flames present. The top flame is a result of the combustion of volatiles and coke fines (dusts) emitted from the coke bed with the air supplied from D1, D2, U1 and U2 tertiary air injectors. The bottom flame is created by the combustion of volatiles and coke fines with the air supplied solely by the U3 tertiary air injector. The cold air from the D3 tertiary air injector actually reduces the temperature in the tertiary air zone. This effect is clearly shown downstream of the D3 tertiary injector in Figure 5.2a. In the heat-up zone, the heat sink embedded on the coke bed surface (between Z = 36.576 and 60.96 m) continuously absorbs latent heat from the main flow to vaporize moisture. This heat-sink effect can be observed by the reduced temperature at the layer right above the coke bed in Figure 5.2a.

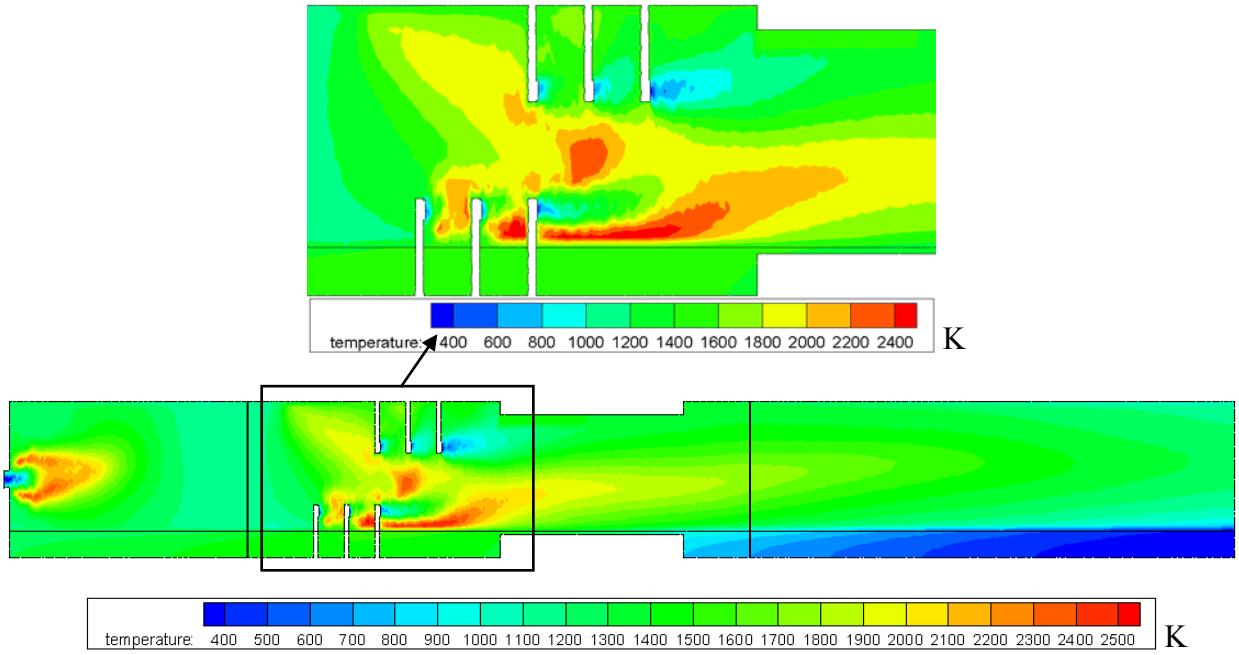

(a) Vertical mid-plane at X = 0

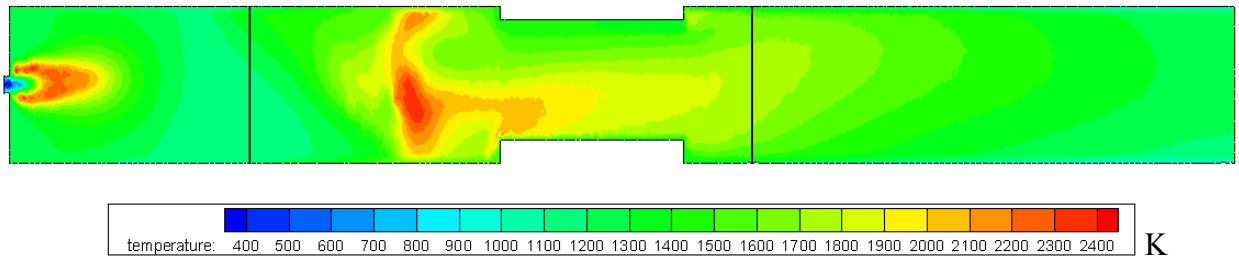

(b) Horizontal mid-plane at Y = 0

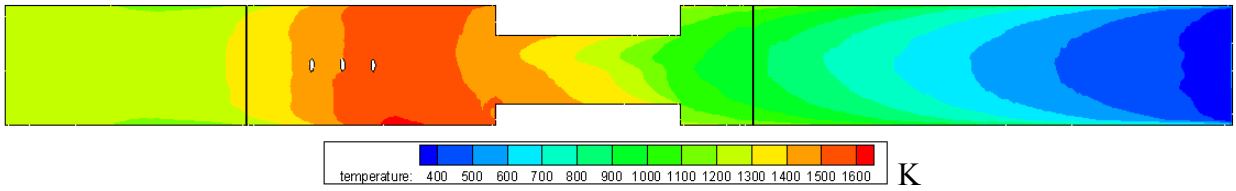

(c) Horizontal plane of the coke bed surface at Y = – 0.9144

Figure 5.2 Temperature contours inside the kiln for different planes for Case 1

The temperature contours in Figures 5.2 a & b show an interesting combustion pattern; the combustion takes places near the coke bed in the tertiary air injection region, but it lifts over to the center of the flow passage. Examination of the species concentration in Figure 5.3 reveals this phenomenon is caused by a depletion of oxygen near the coke bed surface and a growing layer of unburned volatiles released from the coke bed. The oxygen concentration in Figure 5.3 a

shows plenty of oxygen existing in the upper part of the kiln but is depleted in the lower part of the flow passage. The oxygen rich air stream is somehow partitioned from the fuel (volatiles) rich gas by the combusted gas. Mass weighted mass fraction distributions in Figure 5.4 also show about 14% (or 1% of the total gas mass) of the volatiles are not burned at gas exit (feed end) of the kiln. This simulated result provides an important insight into the combustion phenomenon, and hence, by increasing downstream mixing provides an opportunity for implementing a means to manipulate the flow to achieve a more effective combustion near the coke bed. This will be a worthwhile task for future study.

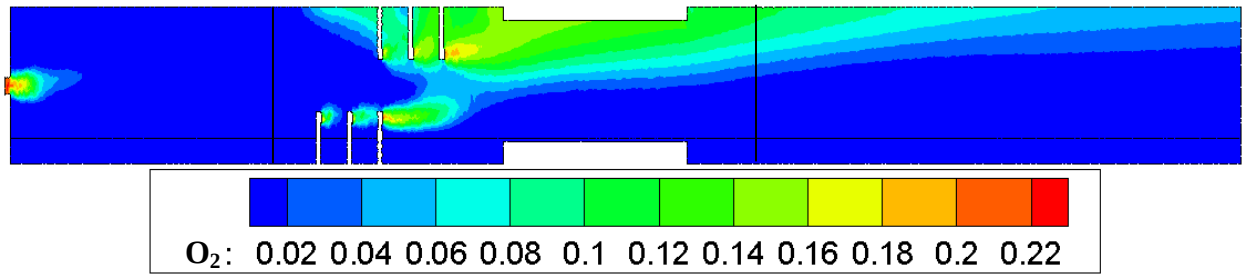

(a) Mass fraction of O_2

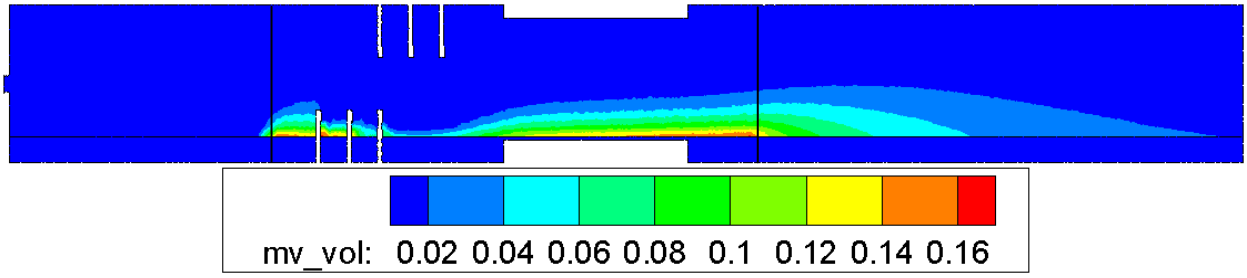

(b) Mass fraction of volatile matters

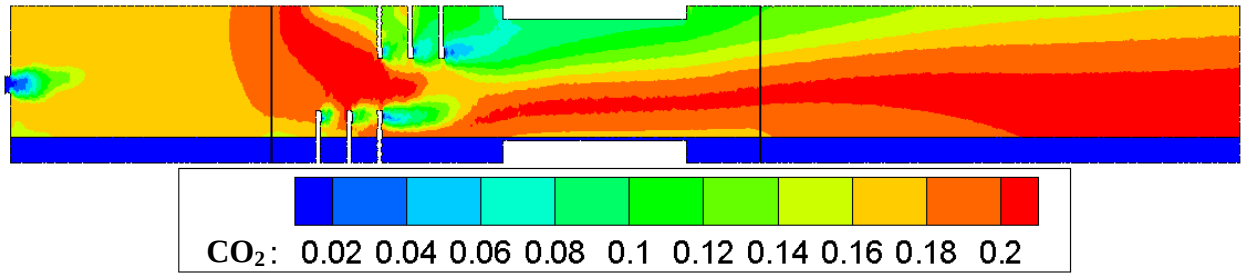

(c) Mass fraction of CO_2

Figure 5.3 Species mass fraction inside the kiln for vertical mid-plane at X = 0 for Case 1

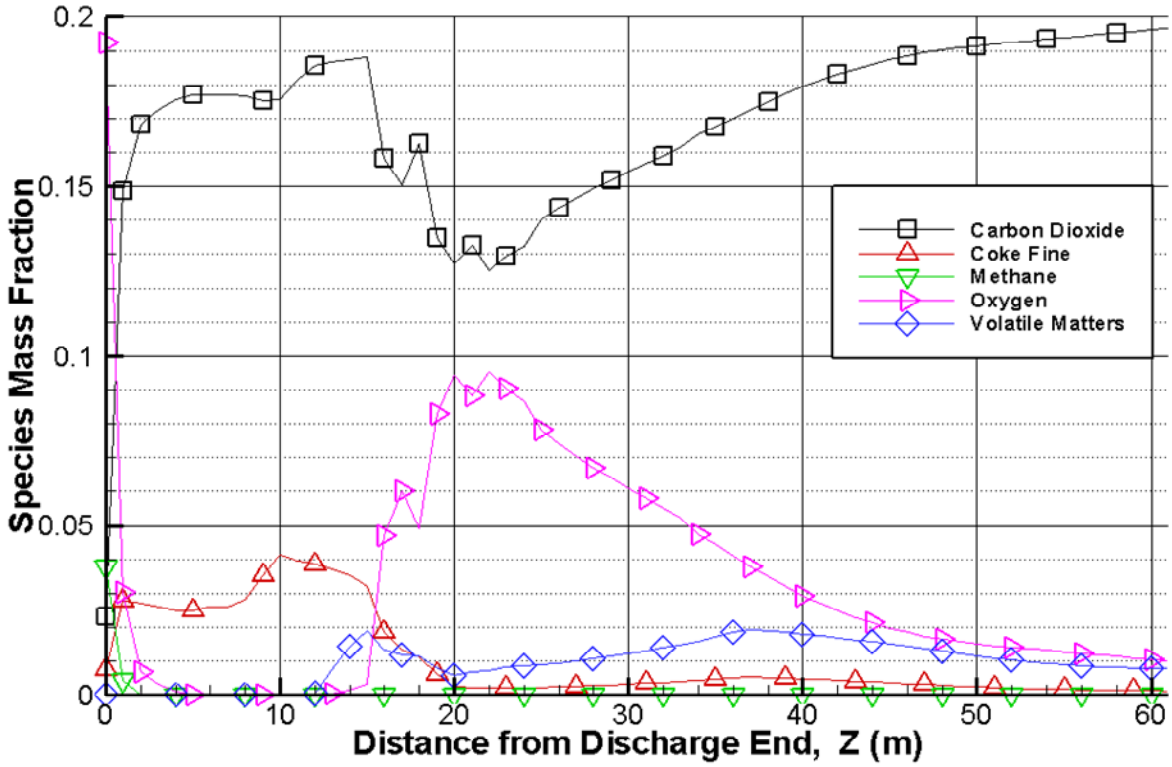

Figure 5.4 Mass weighted species mass fraction distributions inside the kiln for Case 1

Some effects of the tertiary injection angle and arrangement can be observed in the horizontal mid-plane view of Y = 0 (Figure 5.2b). In the calcining zone, the U1 tertiary air injector creates a combustion flame that goes up and the U2 tertiary air injector creates a relatively hot zone that moves down. Figure 5.2c is plane view for Y = – 0.9144, which is the coke bed surface plane. Figure 5.2c shows the coke bed surface temperature gradually increases from the feed end (300 K) to as high as 1,600 K at the calcining zone and finalizes at 1,200 K at the discharge end.

Figure 5.5 shows temperature contours of ten cross-sections cutting through the six tertiary inlet piping and downstream of the injectors. The cold air injected from the U1 tertiary air inlet reduces the temperature in its cross-sectional view. In the U2 cross-sectional view, the air from the U1 tertiary air inlet combusts with volatiles and coke fines right above the coke bed. The core of that air stream is still cold. In U3 cross-sectional view, the combustion is stronger,

but it seems the combustion takes place on the shear layer surrounding the cold core of air stream. Stronger combustion is taking place in the D2 cross-sectional view, and again, cold air streams from the U3 and D1 tertiary air injections create relatively cold regions. The signature of the cold air stream core persists throughout the tertiary air injection region as can be seen in Figure 5.2a and Figure 5.5.

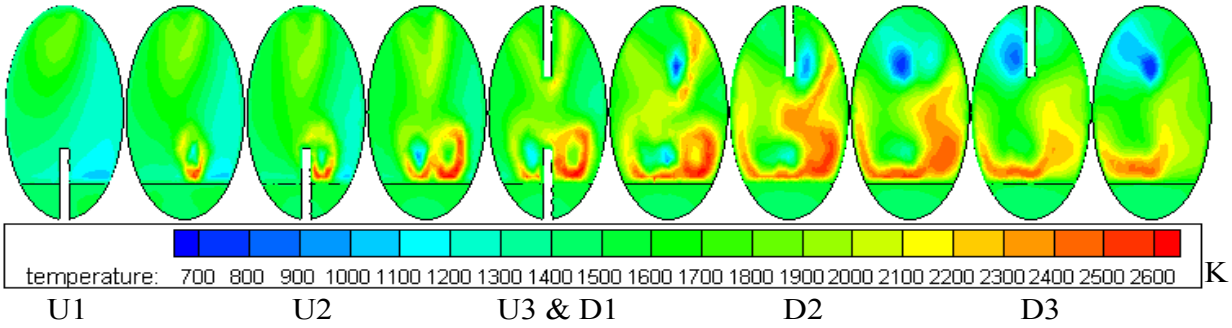

Figure 5.5 Temperature contours at each tertiary air inlet location for Case 1

The temperature distribution along the centerlines (X = 0) of the gas region as well as three different depths in the coke bed (coke bed surface, in the mid-depth, and at the bottom) are shown respectively in Figure 5.6. The centerline gas temperature shows that the peak temperature of the main inlet combustion is about 2,200 K at less than 5 m from the discharge end, and in the tertiary air inlet zone, the combustion peak temperature rises up to 2,300 K at Z = 20 m. Between these two peaks, the temperature drops below 1,150 K at the end of natural gas combustion zone at Z = 10 m. In this region of relatively cool gas temperature (Z = 7 ~ 15 m), the coke bed temperature is actually higher than the gas temperature, so heat is lost from the coke bed to the gas. Heat lost from the coke bed can be further supported by comparing the centerline temperature at three different depths: the temperature at the coke bed bottom is higher than in the mid-depth, which in turn has the temperature higher than on the coke bed surface, and the mass weighted average static temperature reaches around 1,800 K for natural gas combustion and volatiles combustion.

Coke bed surface temperature starts cold at the feeding end (Z = 60.96 m) and reaches the maximum value of 1,500 K at around Z = 15 m; at the discharge end, the coke bed temperature becomes uniform and is discharged at about 1,300 K. Starting from the feeding end, the coke bed surface always receives the heat from the hot gas and maintains at the hottest in the coke bed until the coke moves to the relatively cool gas region at Z = 15 m. Reversal of temperature gradient from receiving heat to losing heat is clearly shown at Z = 16 m in Figure 5.6, where the coke bed surface temperature drops becoming the coolest in the coke bed.

Representative flow fields are shown in Figure 5.7. From the flow field shown in the vertical mid-plant (X = 0) in Figure 5.7a, a stagnant flow induced by recirculation can be seen between the discharge end and the tertiary air injection region. This recirculation flow is caused by the entrainment induced by the strong main flow entering momentum. This entrainment is so strong that even the air flow injected from the D1 tertiary injector is reversed (see Figure 5.7c) and moves toward the discharge end. The combustion produced by the reversed tertiary flow can be seen in Figure 5.2a upstream of the D1 tertiary air injector. The reversed flow is stopped by the main flow entering from the discharge end and forms a high-pressure stagnant region between Z = 5 and 15 m. It is here no combustion occurs, and the gas temperature reduces to below 1,150 K, as discussed earlier in Figure 5.6, due to entrained cold tertiary air. A study has been undertaken to investigate the options of removing this stagnant region by producing suction at the discharge end to extend the tertiary air combustion to the discharge end. The results are discussed in Section 5.4.

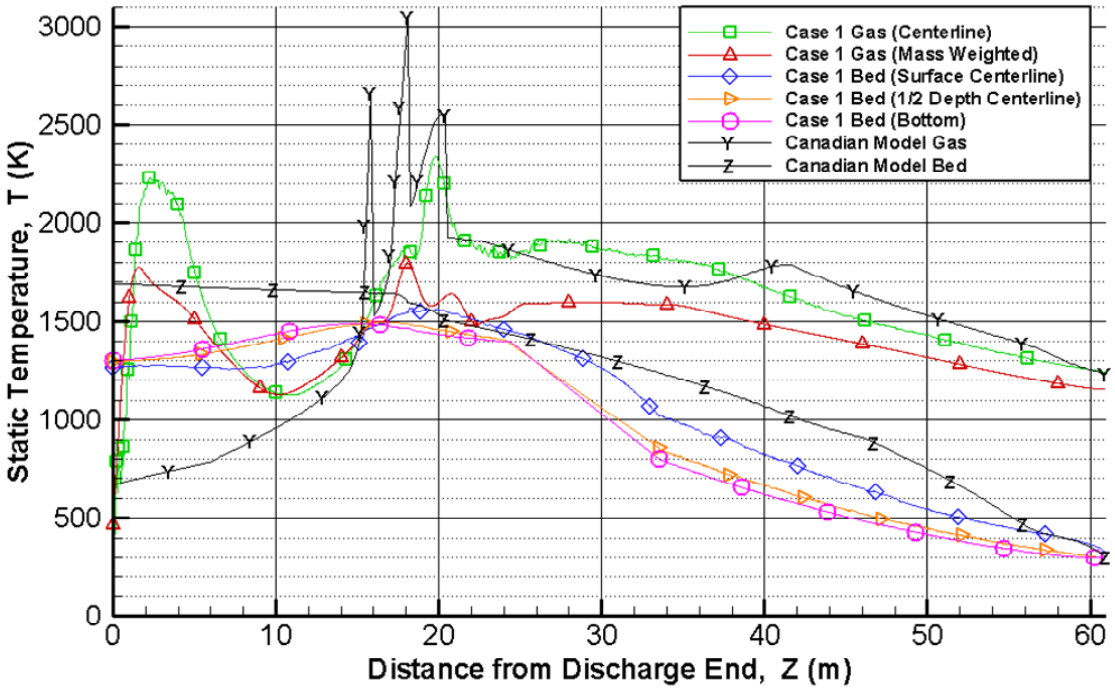

Figure 5.6 Central line static temperatures for gas and coke bed for Case 1 including mass flow weighted gas temperature

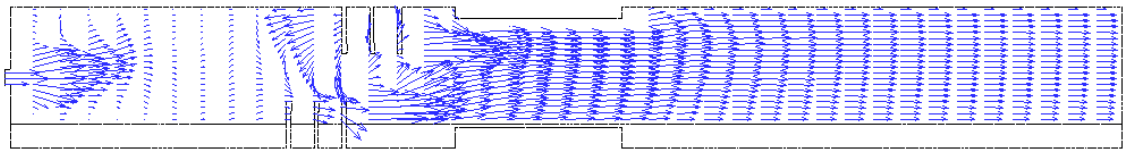

(a) Vertical mid-plane at X = 0

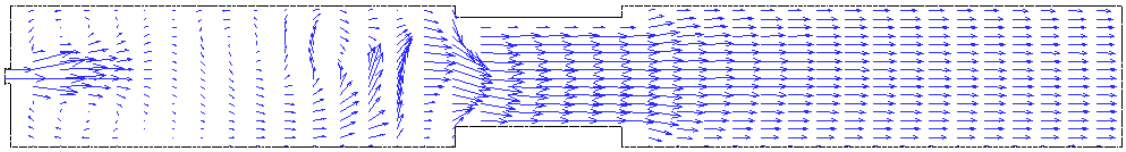

(b) Horizontal mid-plane at Y = 0

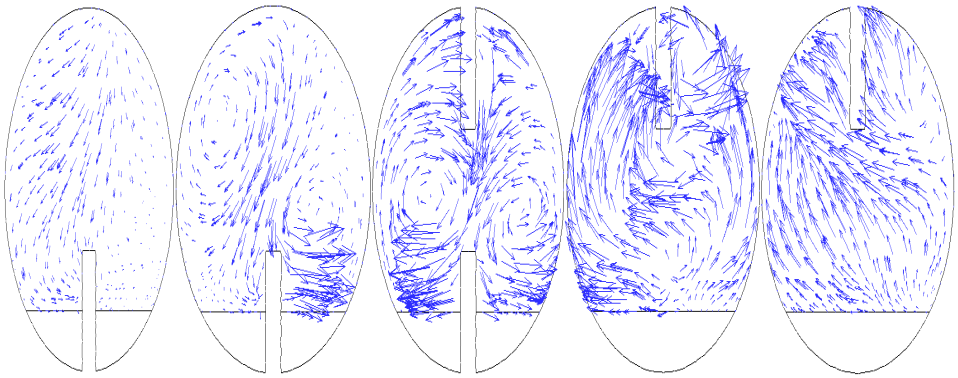

(c) Five tertiary air injection cross-sections

Figure 5.7 Velocity profiles for Case 1

5.2 Various Rotational Angles

Case 1 was conducted with the tertiary air injection plane perpendicular to the coke bed surface as shown in Figure 3.6a. Note that the coke bed generally tilts approximately 15 degrees counterclockwise due to rotation. For convenience and easy reading, Figure 3.6 is plotted with a horizontal coke bed surface. Since the kiln is rotating, the relative positions of the tertiary air injectors with respect to the coke bed surface continuously changes. The result of thermal-flow fields and combustion pattern due to the change of the tertiary air injection positions are compared at five different positions: 0 (Case 5), 45 (Case 6), 90 (Case 9), 135 (Case 10), and 180 (Case 11) degrees, respectively. In this group of simulation, a specific interest is focused on whether the tertiary air injection would disturb the coke bed, kick off coke particles, and result in increased attrition and reduced production. Since the detailed thermo-flow and combustion fields have been analyzed and discussed in Case 1, to shorten the computational time, the conjugate conduction calculation through the coke bed and combustion of coke on the coke bed are not included. Figure 5.8a, vertical plane view of X = 0 for Case 5, shows a temperature field similar to the baseline case (Case 1), except the temperature is lower without including coke fines combustion. Cool air streams can be seen downstream of each injector. In Figure 5.8b (45°) and Figure 5.8c (90°), the temperature range is similar to Case 5, and these two positions produce similar temperature distributions. Since there is no tertiary injection on this plane, no cool air streams are observed.

Regions of hot combustion are seen across the entire kiln in the tertiary air injection area. Due to release of volatile matters from the coke bed, the major combustion region is still located downstream of the tertiary air injections and near the lower part of the kiln. No obvious improvement of combustion is seen on the upper part of the kiln when the tertiary air is injected

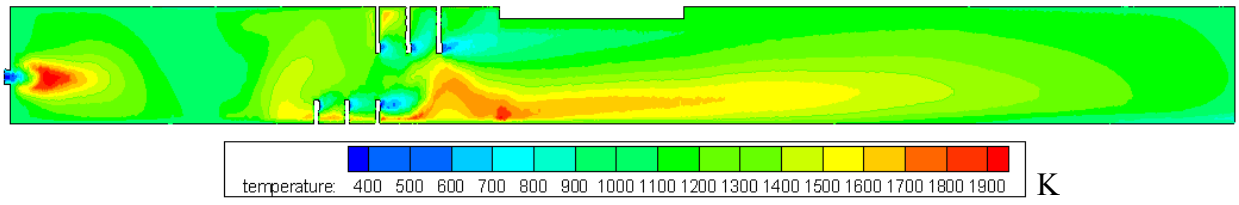

(a) Case 5 (0°)

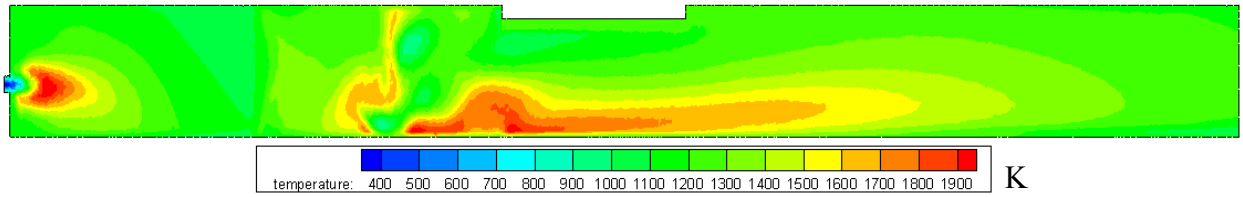

(b) Case 6 (45°)

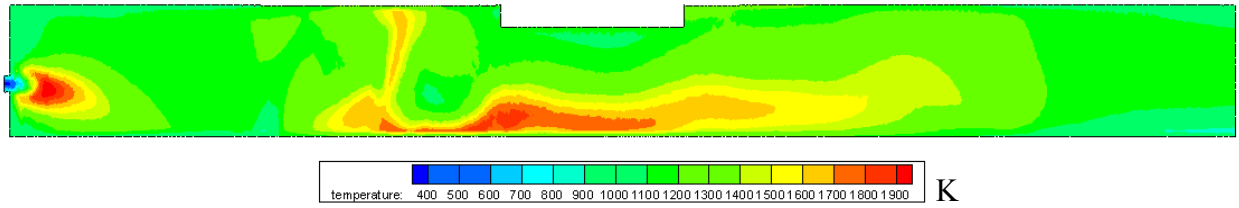

(c) Case 9 (90°)

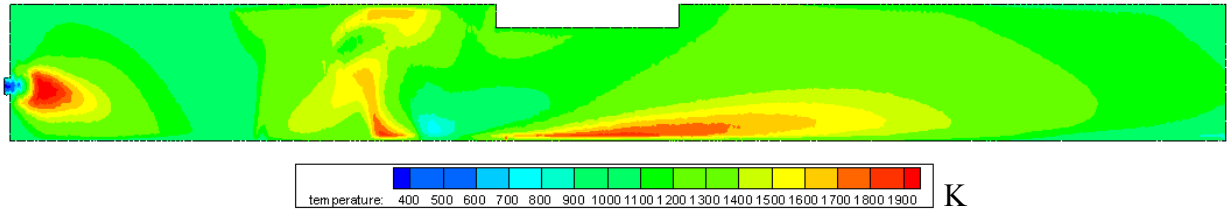

(d) Case 10 (135°)

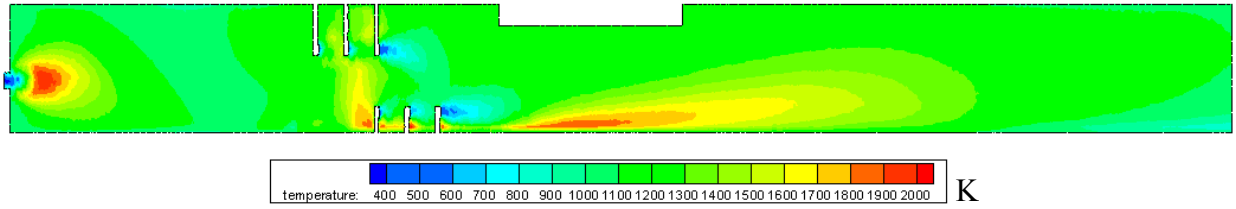

(e) Case 11 (180°)

Figure 5.8 Temperature contours on the vertical plane X = 0 for various rotational angles off from the vertical plane. The cool region between the natural gas combustion flame and the tertiary air injection region is about 100 K hotter than Case 5. The effectiveness of combustion for the tertiary air injection at position 135° in Figure 5.8d is significantly reduced from a similar position at 45° (Figure 5.8b). Due to the switching of downstream and upstream locations of the upper and lower injectors, this combustion reduction seems to be solely caused by the effect of

the flow field. The combustion is suppressed when the lower injectors are located downstream of the upper injectors. This observation is confirmed by the results of Case 11 shown in Figure 5.8e, which occurs when the injectors are rotated 180° off from the baseline location shown in Figure 5.8a.

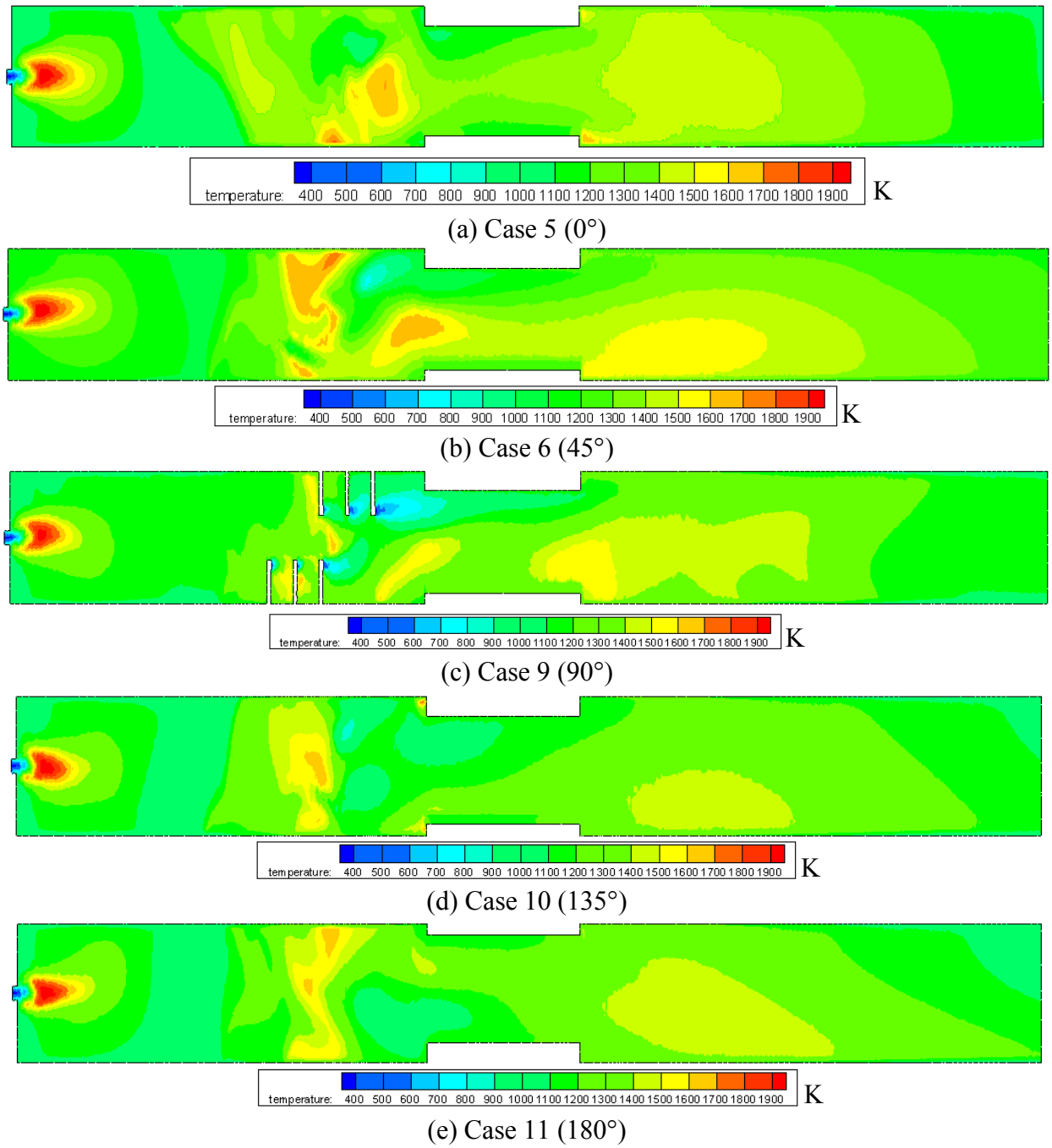

(a) Case 5 (0°)

(b) Case 6 (45°)

(c) Case 9 (90°)

(d) Case 10 (135°)

(e) Case 11 (180°)

Figure 5.9 Temperature contours on the horizontal mid-plane Y = 0 for various rotational angles

Figure 5.9 shows that the temperature contours on the horizontal mid-plane (Y = 0). The relatively lower temperature distribution when compared with the vertical temperature distribution in Figure 5.8 indicates that the combustion is weaker on the mid-plane of the kiln. Case 6 (45°), in Figure 5.9b, shows more combustion than other cases; while Case 9 (90°), in Figure 5.9c, shows the lowest combustion activity on the mid-plane. Combination of the temperature contours on the vertical mid-plane in Figure 5.8, and the horizontal mid-plane in Figure 5.9 clearly indicates most of the combustion taking place near the lower part of the kiln near the coke bed.

As stated earlier, the off-center turning angles (± 15°) of injectors D1, D2, U1, and U2 are made to direct the air streams away from hitting the downstream injectors. During rotation, two of these injectors will periodically blow air towards the coke bed. This will kick the coke dusts off from the coke bed surface and result in coke attrition and loss of product yields. In addition, tertiary air injections exert impacts on the coke bed surface temperature distribution. Although tertiary air provides oxygen to combust the volatiles, it also provides the cooling effect if it is directly blowing towards the bed surface. For example, the snapshot temperature contour in Case 10 (135°), in Figure 5.10e, shows a cool area between the third injector (U3) and the tumbler, which is evidence of the cooling effect of the off-enter air jet blowing from D1. Again, the coke bed surface temperature between natural gas flame and tertiary inlet zone for Case 9, Figure 5.10c, is 100 K higher than other four cases. Recall that the calculation of Cases 5-11 are conducted without including the coke bed, so temperature distribution on the coke bed surface appears to be stripes rather than the bell shape as shown in Figure 5.2c. Comparison among Figures 5.2 a, b, c with Figures 5.8a, 5.9a, and 5.10a shows the effect of conjugate coke bed heat transfer on the coke bed temperature.

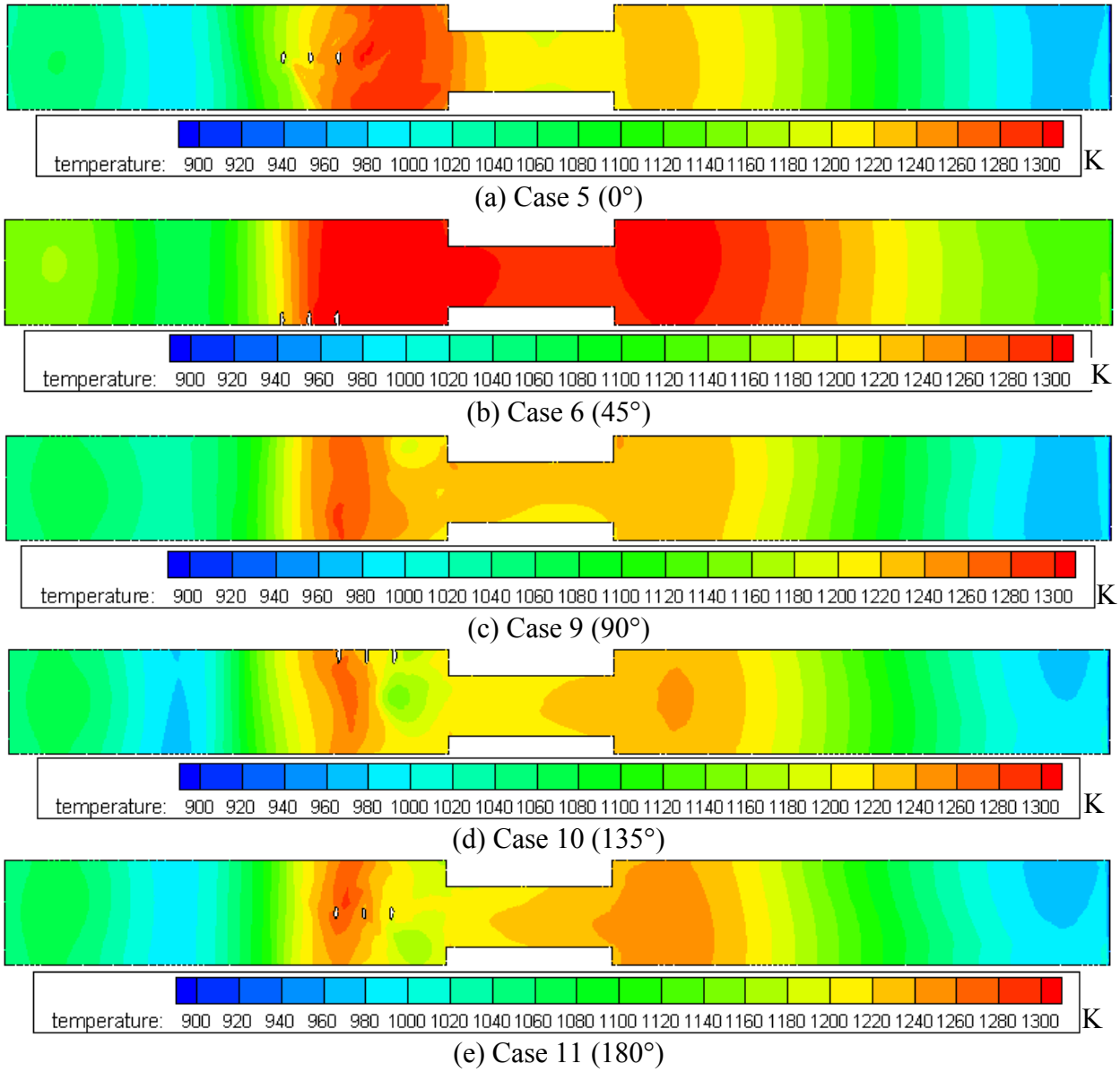

Figure 5.10 Temperature contours of horizontal plane Y = – 0.9144 for various rotational angles

Figure 5.11 shows the temperature distribution at each tertiary air injection cross-section. The evolution of the temperature distribution at each tertiary injection location can be observed by looking at the same location with the rotational sequence. The cold air streams are evident in these sequential cross-sectional temperature contours. In Cases 10 (135°) and Case 11 (180°), the effect of cold stream prevails downstream of the injectors and results in the reduced combustion shown in Figure 5.8 d & e.

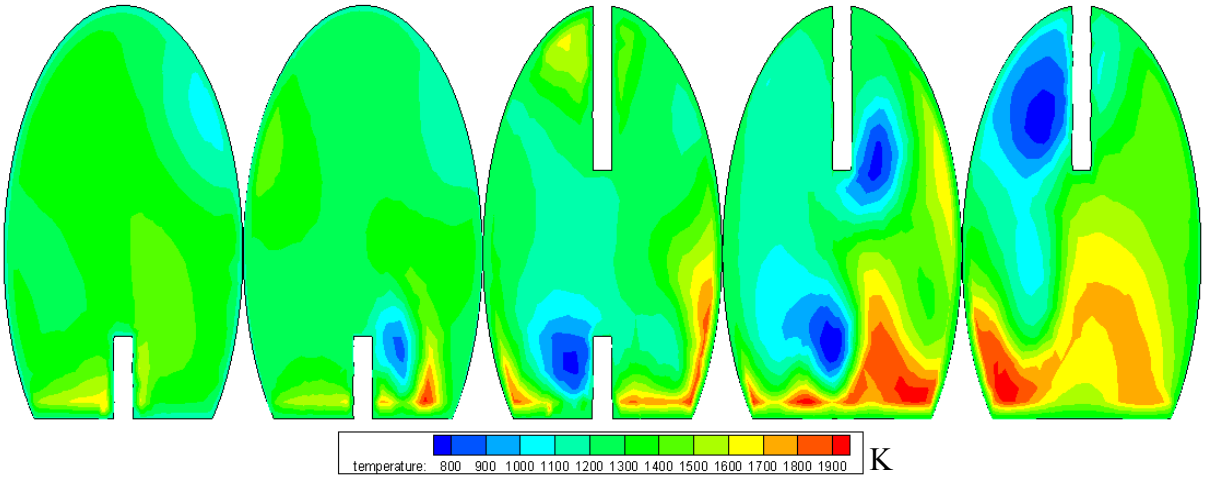

(a) Case 5 (0°)

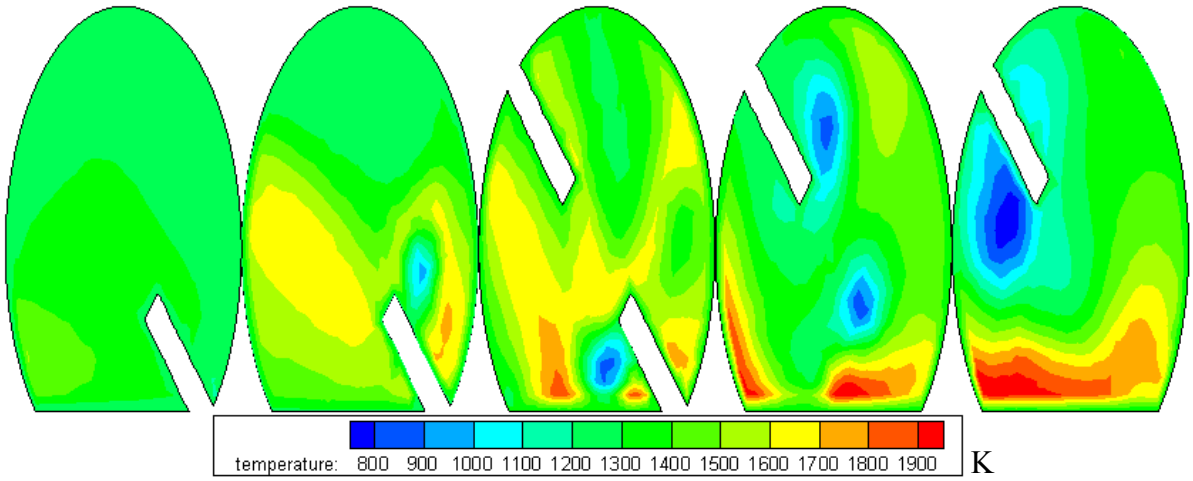

(b) Case 6 (45°)

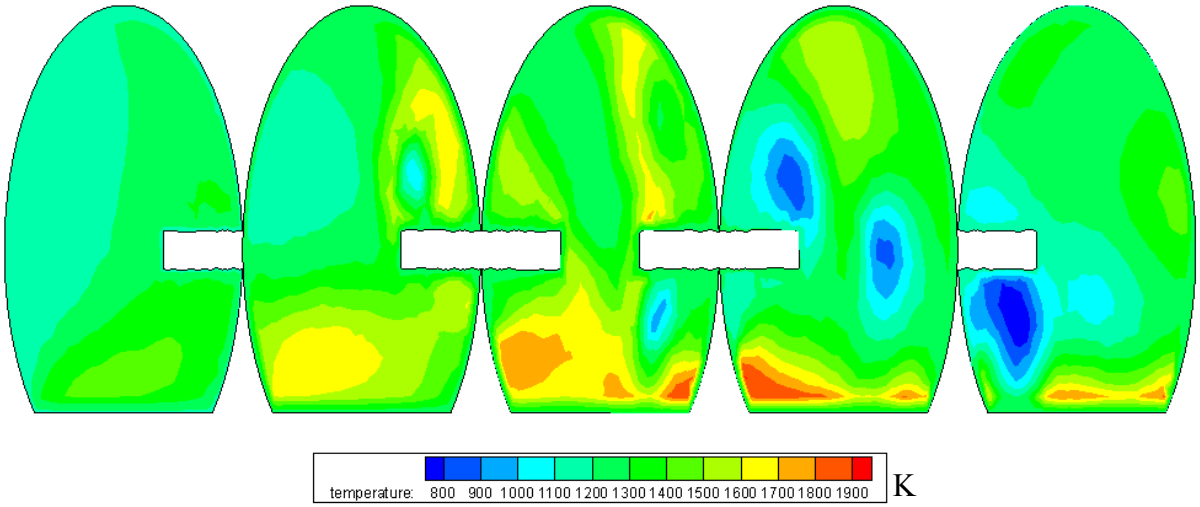

(c) Case 9 (90°)

Figure 5.11 Temperature contours at each tertiary air injection location for various rotational angles

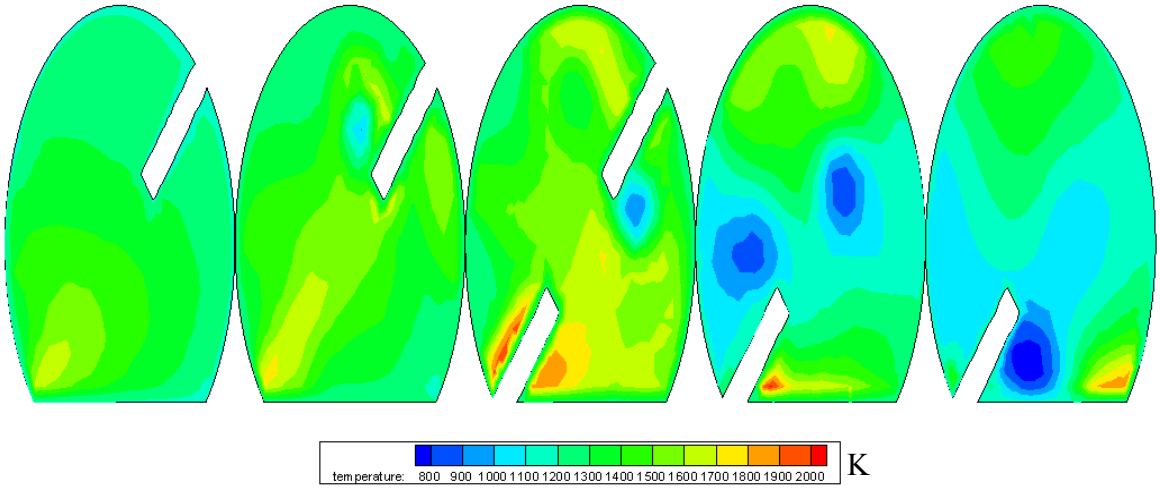

(d) Case 10 (135°)

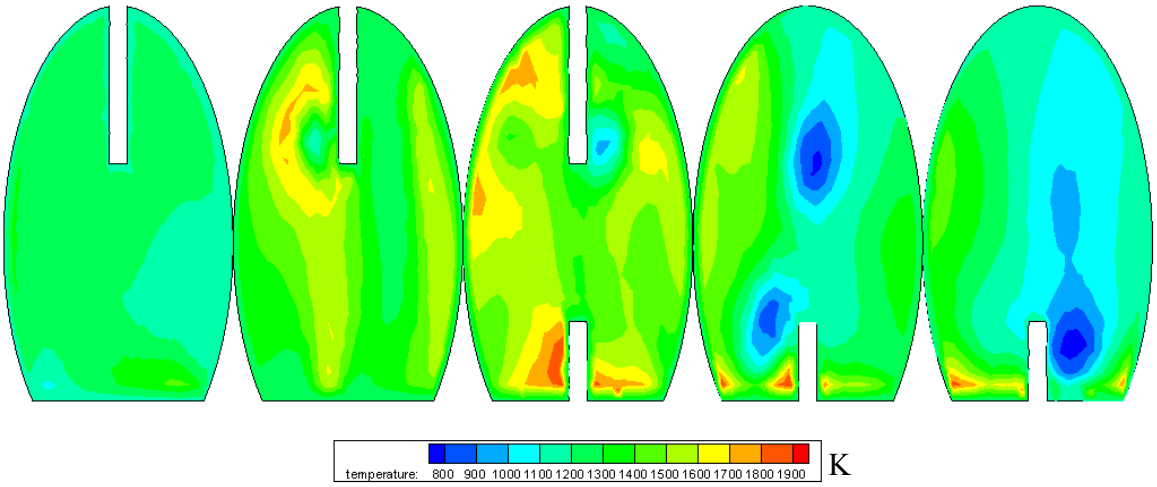

(e) Case 11 (180°)

Figure 5.11 (cont.)

Since Figures 5.8 and 5.9 only show selected planes for comparison, what position produces the best or worst combustion performance is not clear. Mass flow weighted calculations of temperature by integrating over the cross-section at selected axial location are shown in Figure 5.12a for five rotational cases. As expected, the temperature distribution near the discharge end shows negligible difference for all other rotational positions except at 45° rotational angle. The hot regions of tertiary air combustion vary depending on the tertiary air injection position. In a real situation, all the cases will occur in one rotation; the average value of these five cases (lumped value) in Figure 5.12b gives a better description of the averaged temperature

distribution along the kiln. Due to natural gas combustion, the peak temperature of the lumped gas is 1,400 K at around Z = 2 m location. At the tertiary air injection zone, peak combustion temperature occurs at Z = 18 m with highest temperature at about 1,370 K. Bed surface temperature of Case 6 (45°) is approximately 200 K higher than the other four positions as shown in Figures 5.13 and 5.10. Because better combustion and the higher gas temperature of Case 6 (45°) has successfully heat up the coke bed, Case 6 is the best among the five studied rotating locations.

Mass flow weighted calculations of temperature and species mass fractions by integrating over the cross-section at the gas exit plane are shown in Table 5.2. Generally speaking, the cases showing higher temperature, higher CO_2, lower O_2, and lower volatiles are cases of better combustion. However, the data shown in Table 5.2 do not provide a clear picture on which case is the best because the data show Case 9 (90°) has the highest CO_2 production and least residual of O_2, while Case 6 (45°) reaches the highest temperature and Case 5 (0°) has the minimum unburned volatiles. Irrespective of the indecisiveness in determining which case is the best, it is relatively certain that Cases 10 and 11 (135° and 180°) do not perform as well as other cases. In a real situation, all the cases would occur in one rotation. The average values of these five cases in Table 5.2 would give a better description of the averaged overall performance of each rotation. It needs to be noted that the simulation does not model the phenomena of flow disturbance on the coke bed surface when the tertiary jets impingement on the coke bed surface and kick off the coke particles into the gas stream.

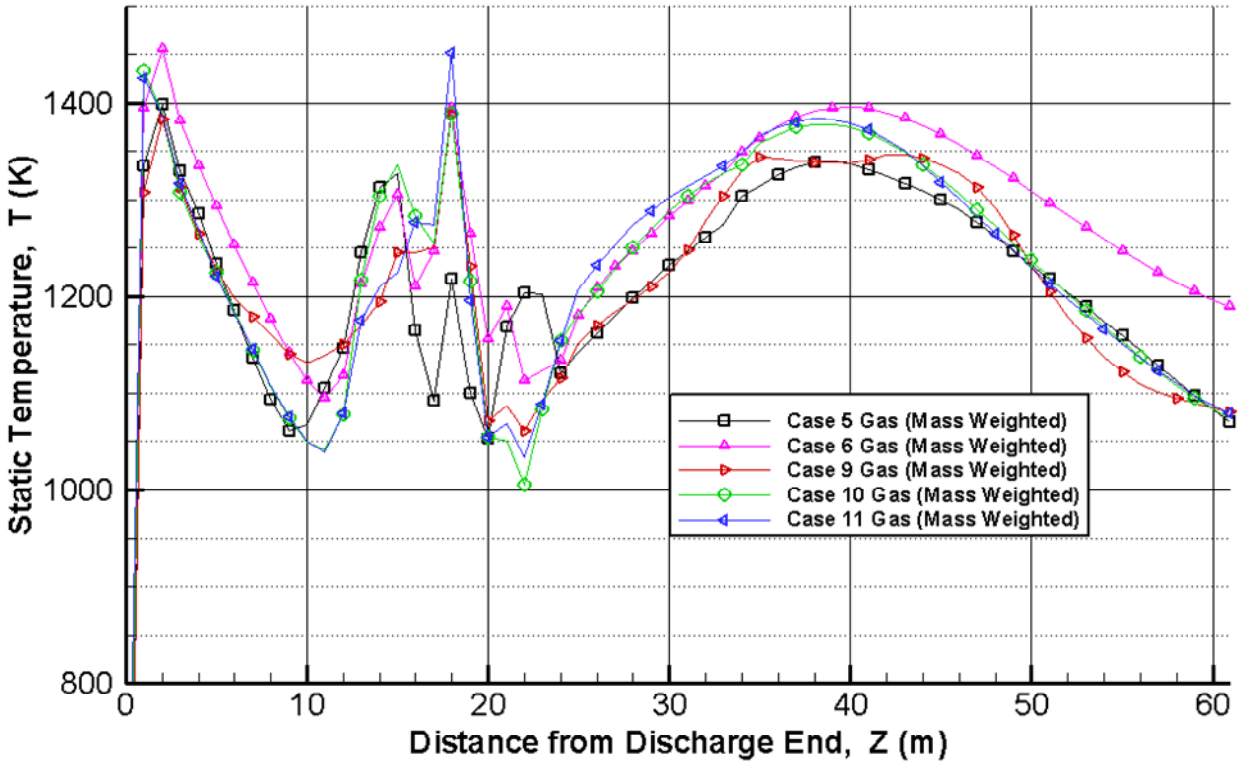

(a) Mass flow weighted average temperature for each rotational angle

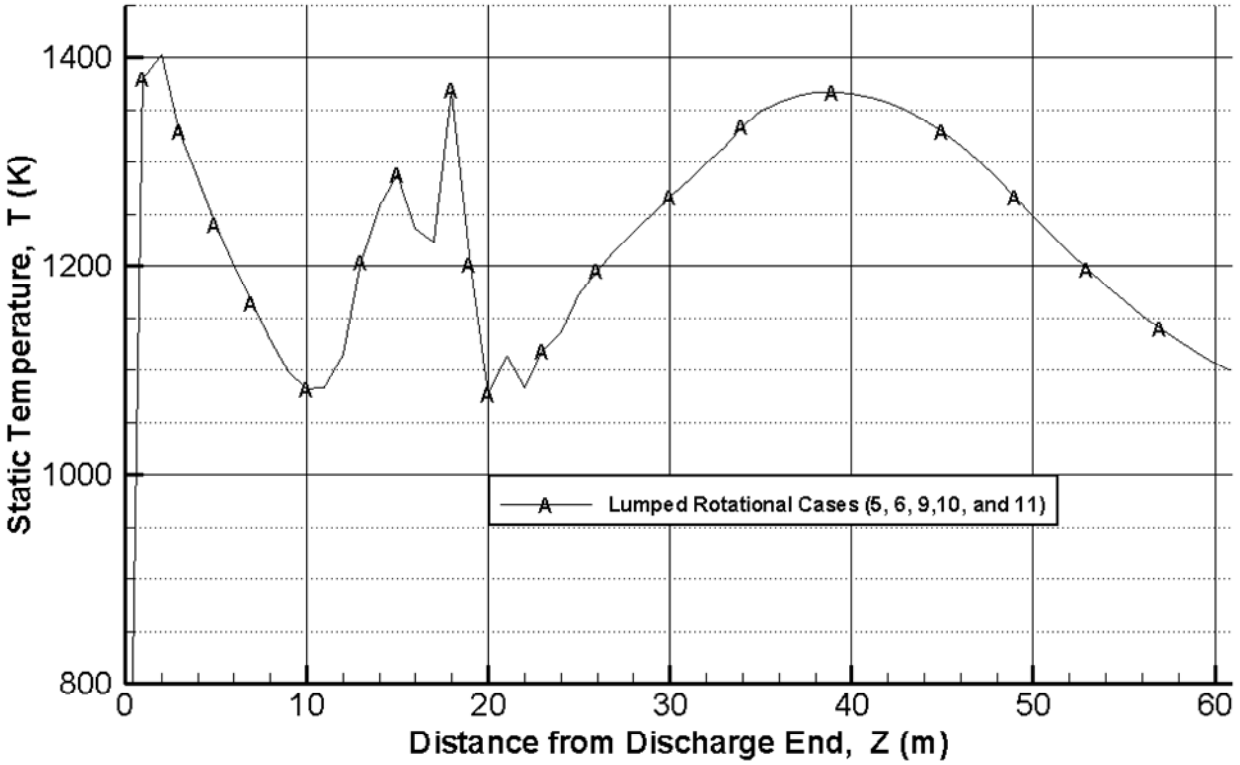

(b) Lumped gas temperature for rotational cases

Figure 5.12 Mass flow weighted average and lumped gas static temperature for various rotational angles

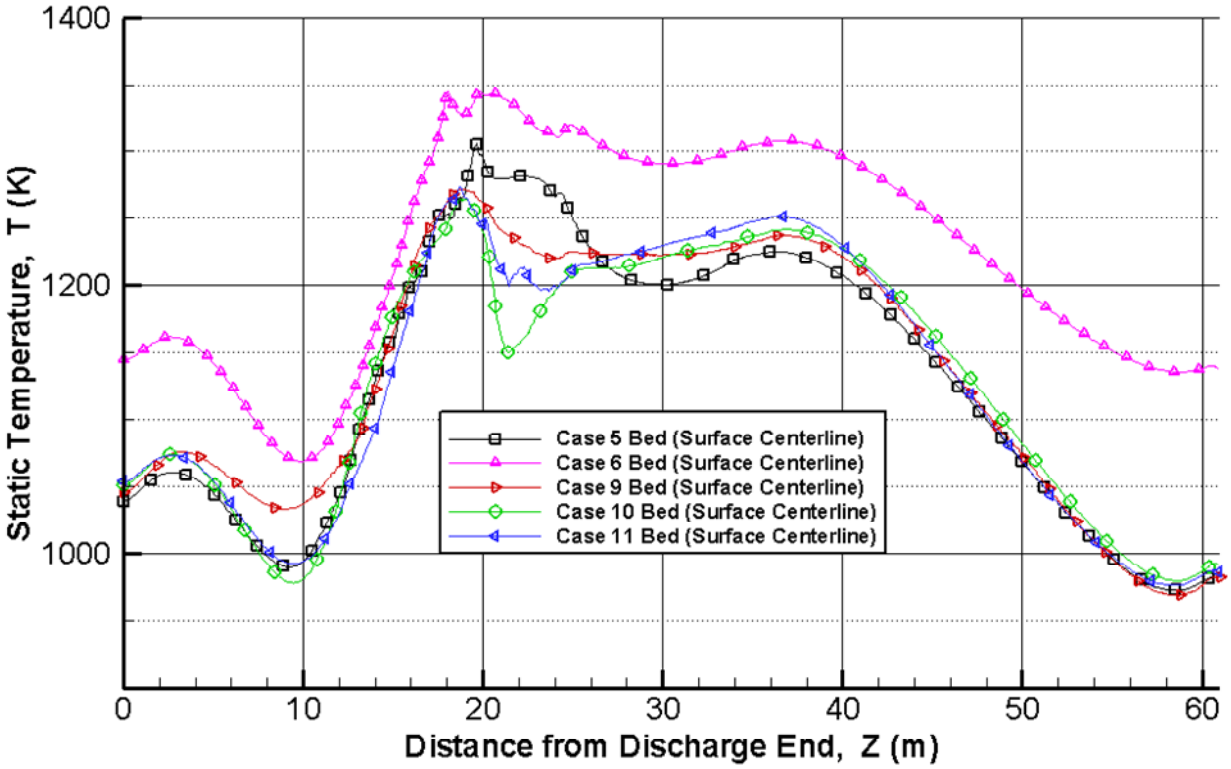

Figure 5.13 Bed surface centerline static temperature for various rotational angles

Table 5.2 Mass flow weighted average values at the feed end for each rotational angle

Rotational Angle	Temperature (K)	CO_2 Mass Fraction	O_2 Mass Fraction	Volatiles Mass Fraction
0° (Case 5)	1070.44	0.1351	0.0495	3.00×10^{-05}
45° (Case 6)	1189.49	0.1427	0.0398	47.08×10^{-05}
90° (Case 9)	1080.11	0.1494	0.0311	3.84×10^{-05}
135° (Case 10)	1073.81	0.1413	0.0418	17.49×10^{-05}
180° (Case 11)	1078.75	0.1433	0.0393	33.84×10^{-05}
Total Average	1098.52	0.1423	0.0403	21.05×10^{-05}

Figures 5.14 and 15 show the streamwise (Z-direction) velocity profiles on the vertical and horizontal mid-planes, respectively. At the tumbler region, the higher velocity flow shifts from top to bottom from Case 5 to Case 11, following the position change of the tertiary air injections. Similar to Figure 5.7, recirculation exists between the main inlet combustion flame and the tertiary air zone. The stagnant zones inhibit hot natural gas flame from moving further downstream.

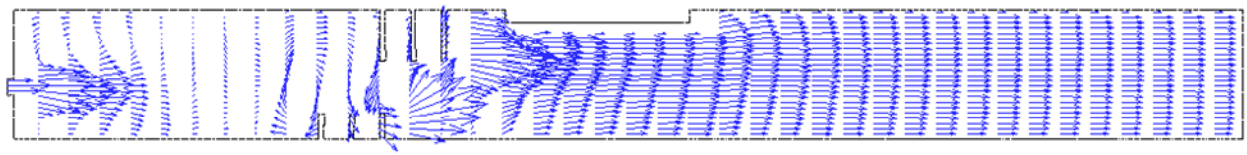

(a) Case 5 (0°)

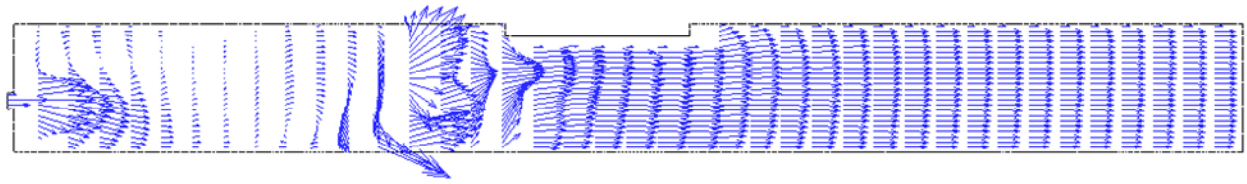

(b) Case 6 (45°)

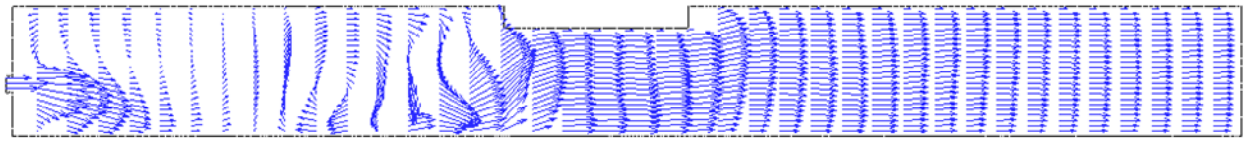

(c) Case 9 (90°)

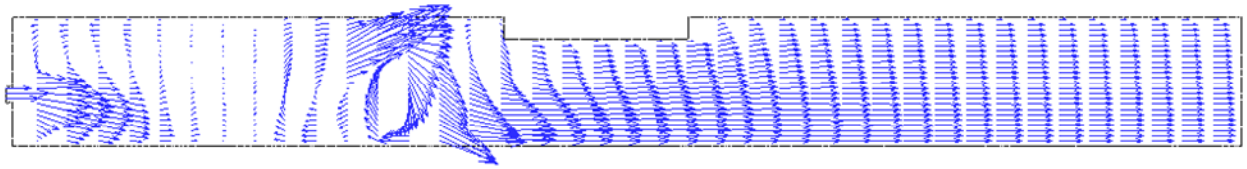

(d) Case 10 (135°)

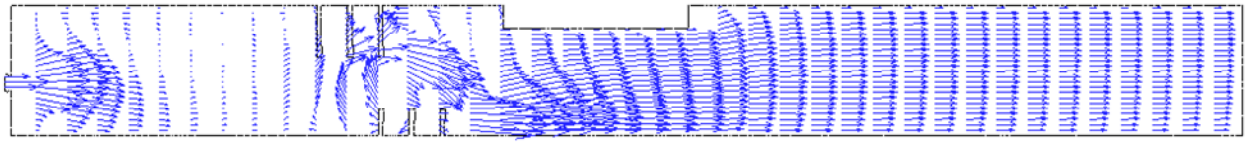

(e) Case 11 (180°)

Figure 5.14 Streamwise velocity profiles on the vertical plane X = 0 for various rotational angles

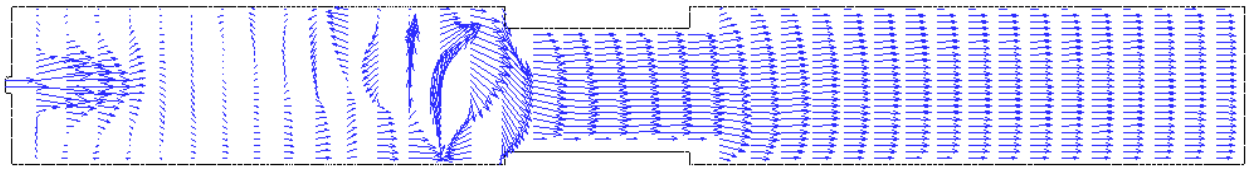

(a) Case 5 (0°)

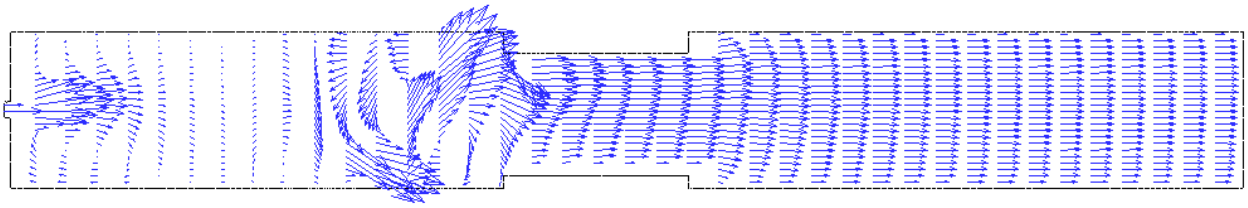

(b) Case 6 (45°)

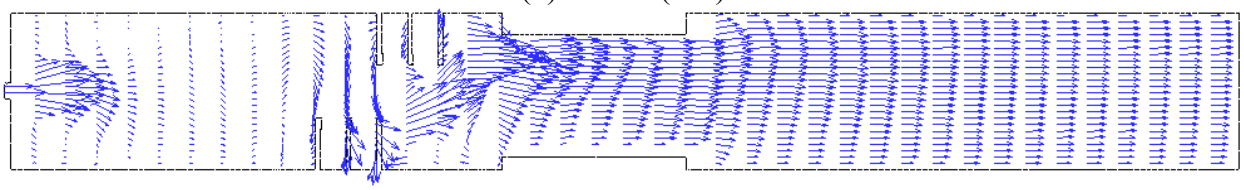

(c) Case 9 (90°)

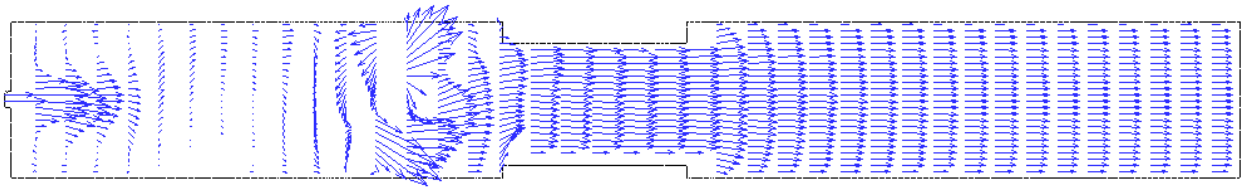

(d) Case 10 (135°)

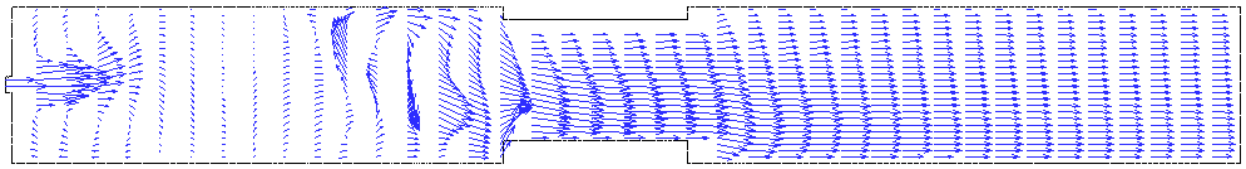

(e) Case 11 (180°)

Figure 5.15 Streamwise velocity profiles on the horizontal plane Y = 0 for various rotational angles

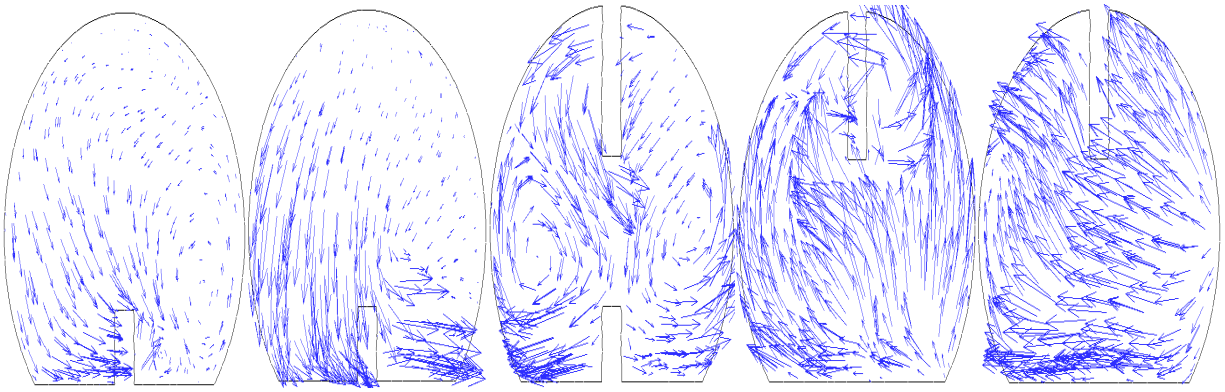

(a) Case 5 (0°)

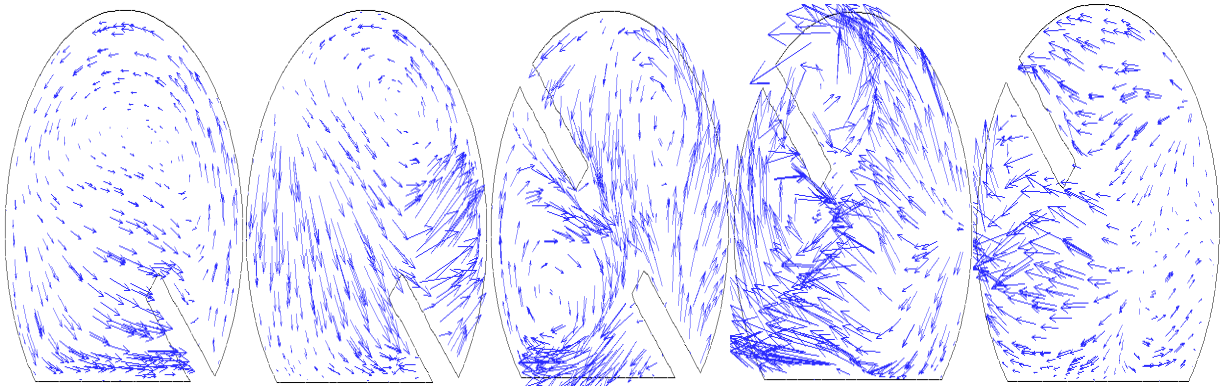

(b) Case 6 (45°)

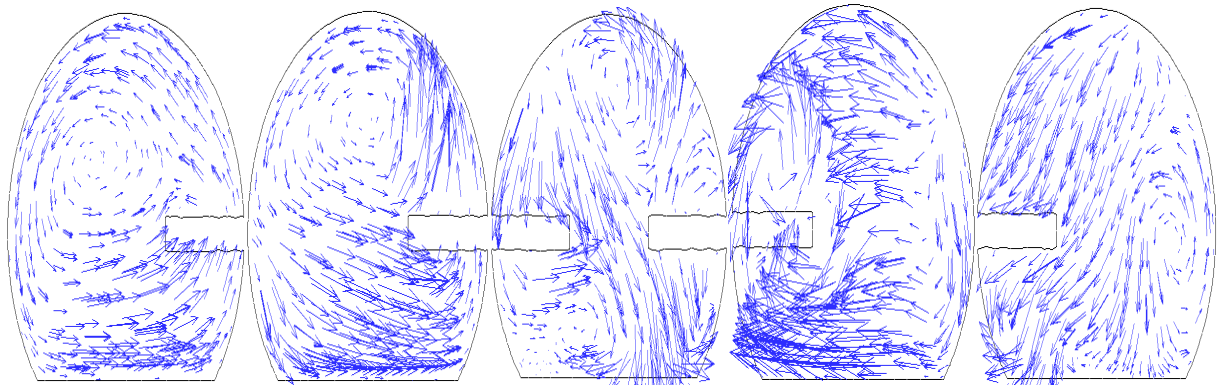

(c) Case 9 (90°)

Figure 5.16 Velocity profiles at each tertiary air injection location for various rotational angles

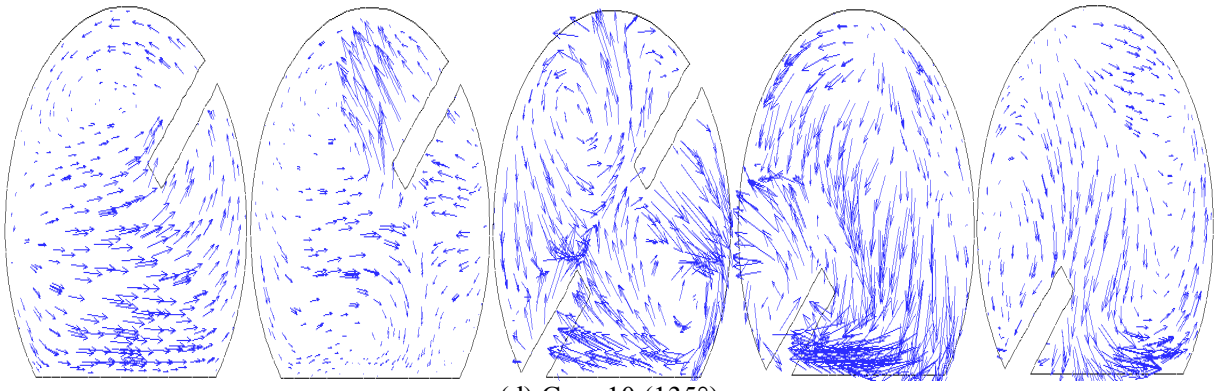

(d) Case 10 (135°)

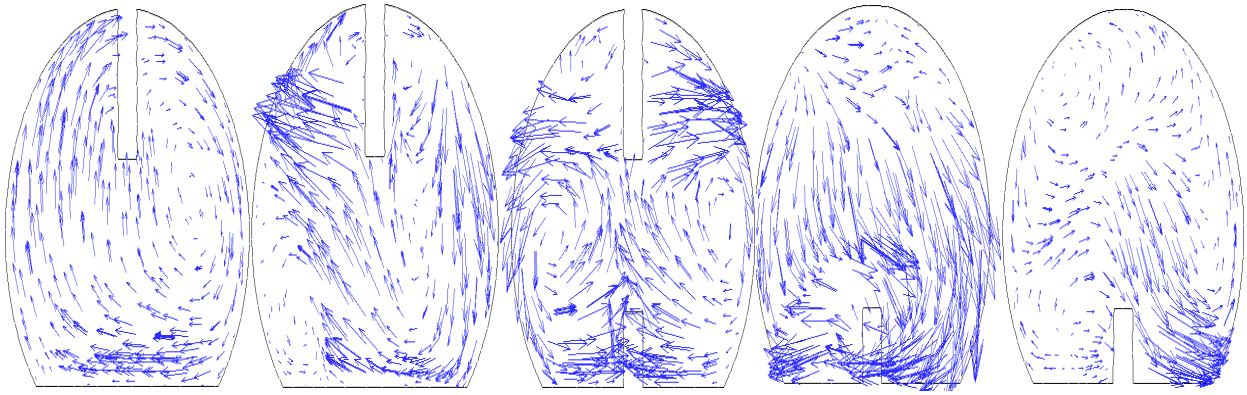

(e) Case 11 (180°)

Figure 5.16 (cont.)

5.3 Various Tertiary Air Injection Angles

This section investigates the effect of tertiary air off-center injection angles on volatiles combustion and coke bed heating. Since the condition when the rotational angle is 45° delivers the best coke bed heating results (Case 6), the effect of tertiary injection angles are conducted with the rotational angle being fixed at 45°. Two new cases are added for comparison: Case 7 turning ± 30° and Case 8 turning ± 45°. Injectors D1 and U1 are turned clockwise and injectors D2 and U2 are turned counterclockwise. The injection angle of Case 6 maintains at ± 15°. In this group's simulations of Cases 6, 7 and 8, the coke bed is removed from the computational domain and only two types of reactions natural gas and volatile matters with air are considered. The carbon combustion from the coke dusts is not included in simulation.

Figures 5.17, 18, and 19 show the temperature contours on the vertical mid-plane (X = 0), the horizontal mid-plane (Y = 0), and the coke bed surface, respectively. It is a surprise to see the effect of the injection angle on combustion, and heating of coke bed is more pronounced than expected. The signature of reduced combustion can be seen in all figures when the injection angle is increased from 15° to 30° and continuous to 45°. The cool spot seen in Figure 5.19b at the one o'clock direction from the U2 injector clearly shows the cool spot is a result of the cold air being injected from U2 injector. This cool spot gets cooler as the injection angle increases from 30° to 45°, as shown in Figure 5.19c. The cooling effect prevails in the tertiary air injection region and downstream region. Generally speaking, the coke bed temperature downstream of the tertiary air injection location decreases 150 K for each injection angle turning 15° off center. For Case 8 (45° injection), the coke bed temperature downstream of the tertiary air injection location is about 250 ~ 300 K cooler than in Case 6 (15° injection). Since the simulation of Cases 6, 7, and 8 are under a controlled condition with the only change being made by the injection angle, it can be concluded those cool regions on the coke bed surface in the calcining zone are the result of cold air being injected towards the bed surface. In addition to this undesired cooling effect, which will reduce the calcined coke quality, larger off-center injection angles will greatly reduce calcined coke quality and increase entrainment rates of coke fines, resulting in a reduction of product yields. The temperature contours in multiple cross-sections in Figure 5.20 further reinforce the previous observation that larger tertiary air injection angles will significantly change the temperature distribution and the effective combustion location.

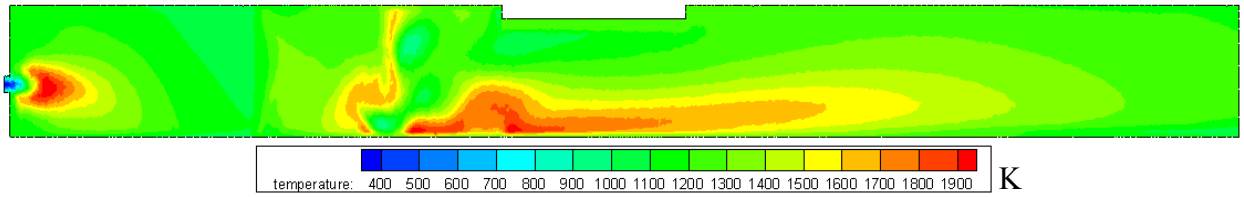

(a) Case 6 (15° injection angle)

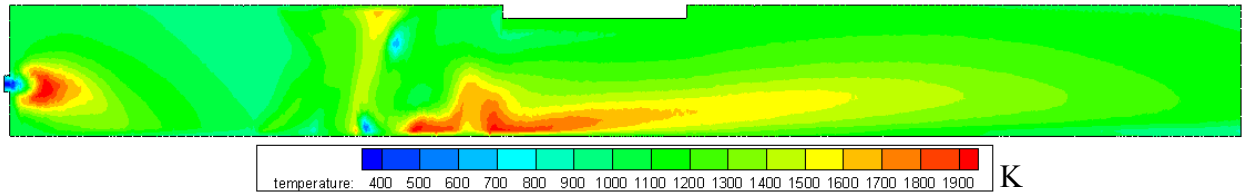

(b) Case 7 (30° injection angle)

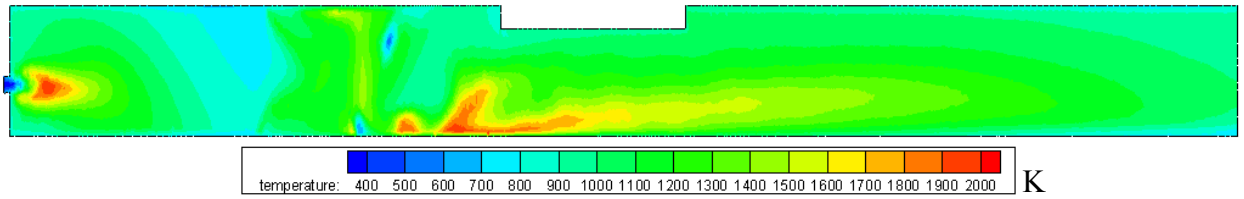

(c) Case 8 (45° injection angle)

Figure 5.17 Temperature contours on the vertical mid-plane X = 0 for various tertiary air injection angles

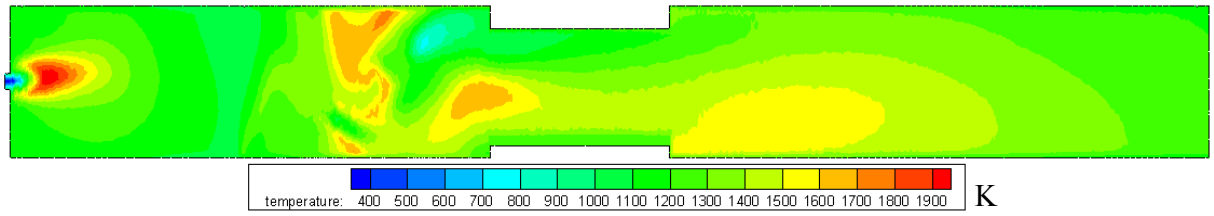

(a) Case 6 (15° injection angle)

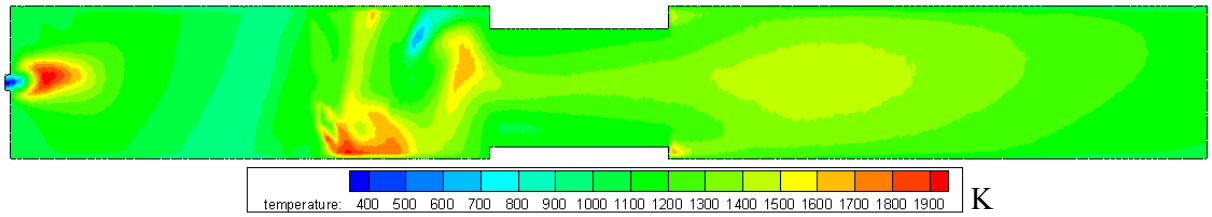

(b) Case 7 (30° injection angle)

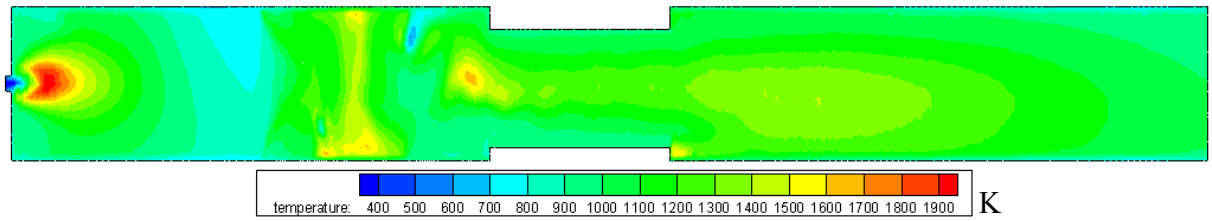

(c) Case 8 (45° injection angle)

Figure 5.18 Temperature contours on the horizontal mid-plane Y = 0 for various tertiary air injection angles

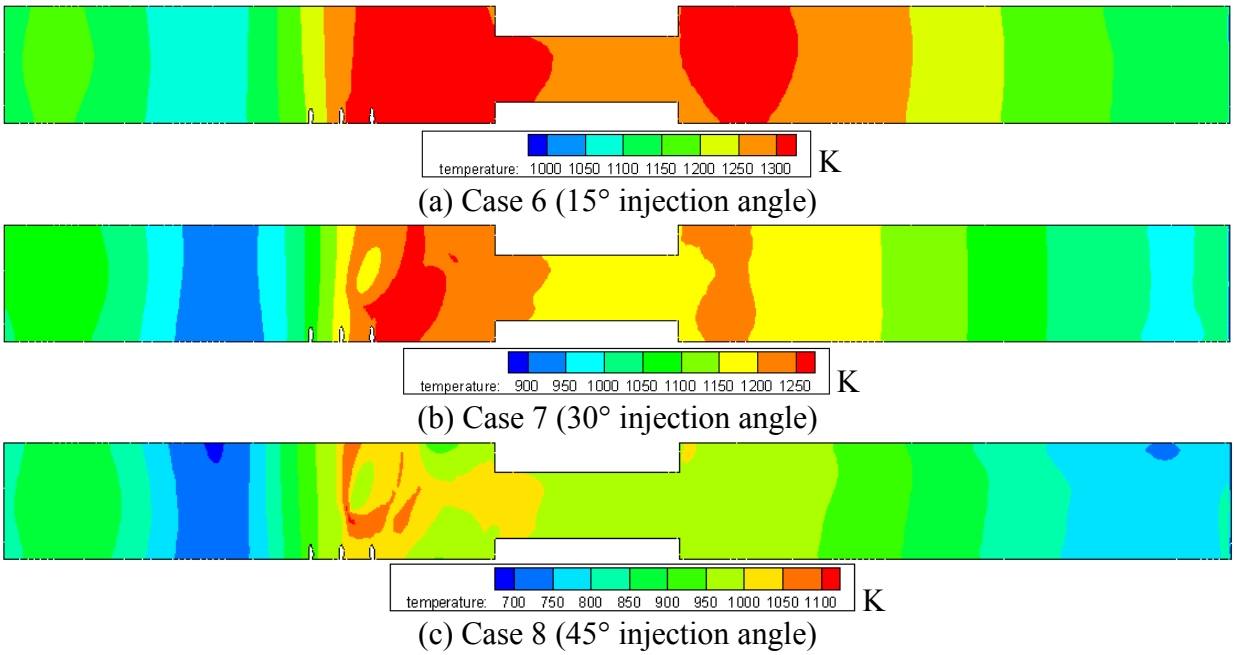

Figure 5.19 Temperature contours on the coke bed surface plane Y = – 0.9144 for various tertiary air injection angles

The mass flow weighted gas temperature in Figure 5.21 shows Case 6 (15°) is about 100 K higher than other two cases along the kiln. The coke bed centerline temperature distributions shown in Figure 5.22 clearly shows the coke bed surface temperature for Case 7 (30° injection) is 100 K lower than Case 6 (15° injection), and Case 8 (45° injection) is 300 K lower than Case 6.

As shown in the velocity vector plots in Figure 5.23 and Figure 5.24, when the tertiary air injection angle increases from 15 degrees to 45 degrees, gas flow from tertiary air inlets hit the bed surface and the kiln wall more directly. The results show that the existing tertiary air injection angle at ±15° is the optimum design. No change is needed.

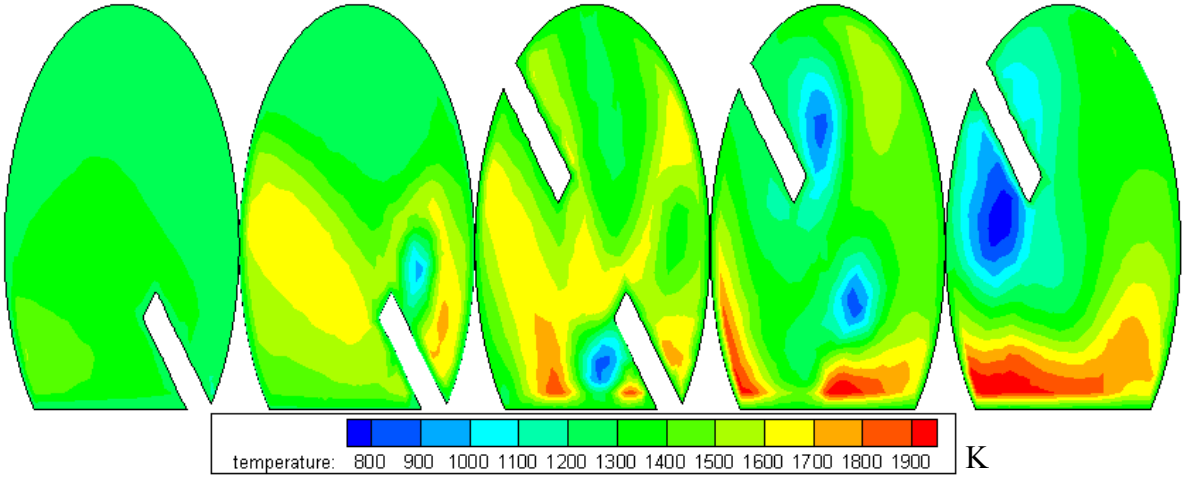

(a) Case 6 (15° injection angle)

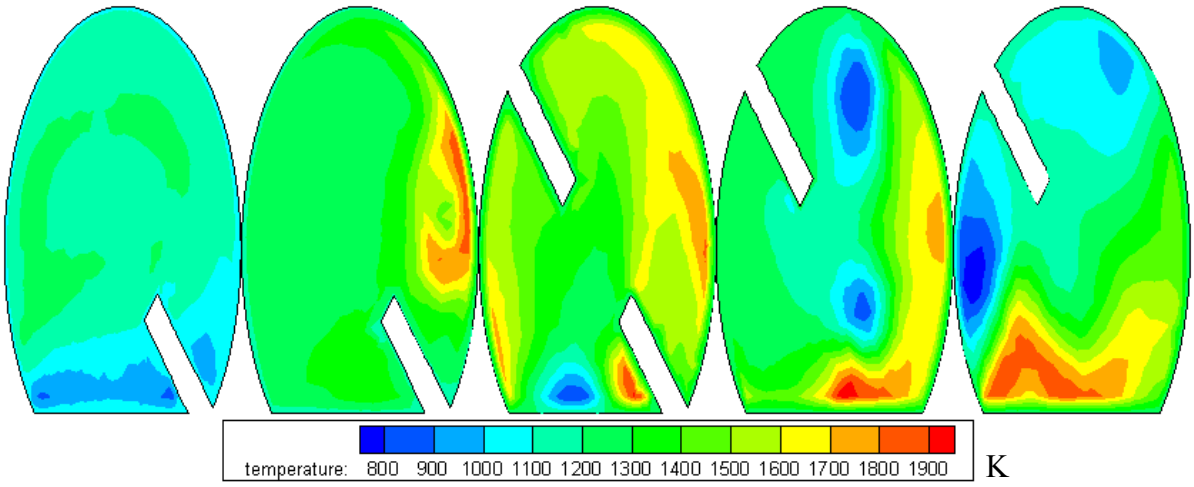

(b) Case 7 (30° injection angle)

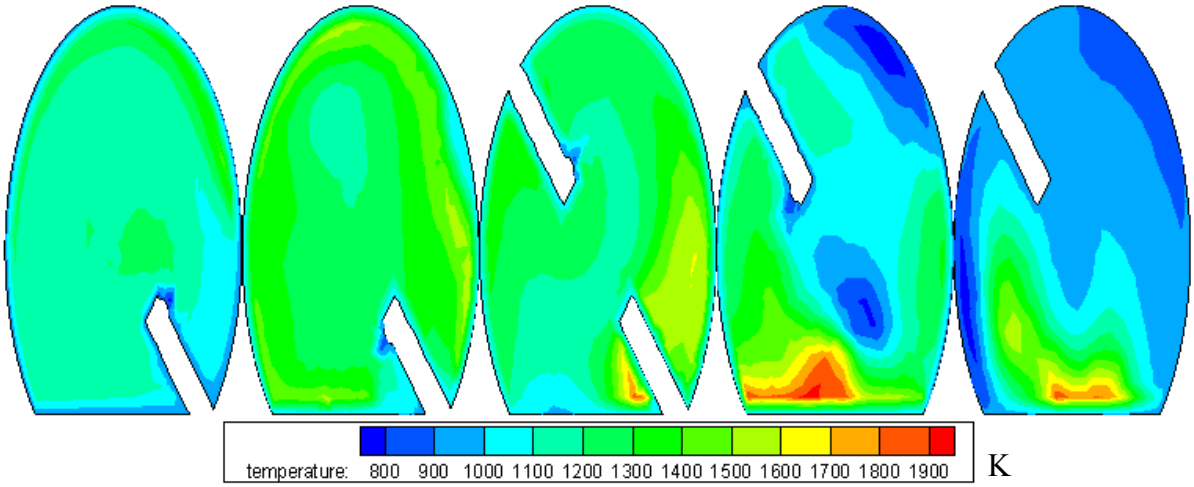

(c) Case 8 (45° injection angle)

Figure 5.20 Temperature contours at each tertiary air Injection location for various tertiary air injection angles

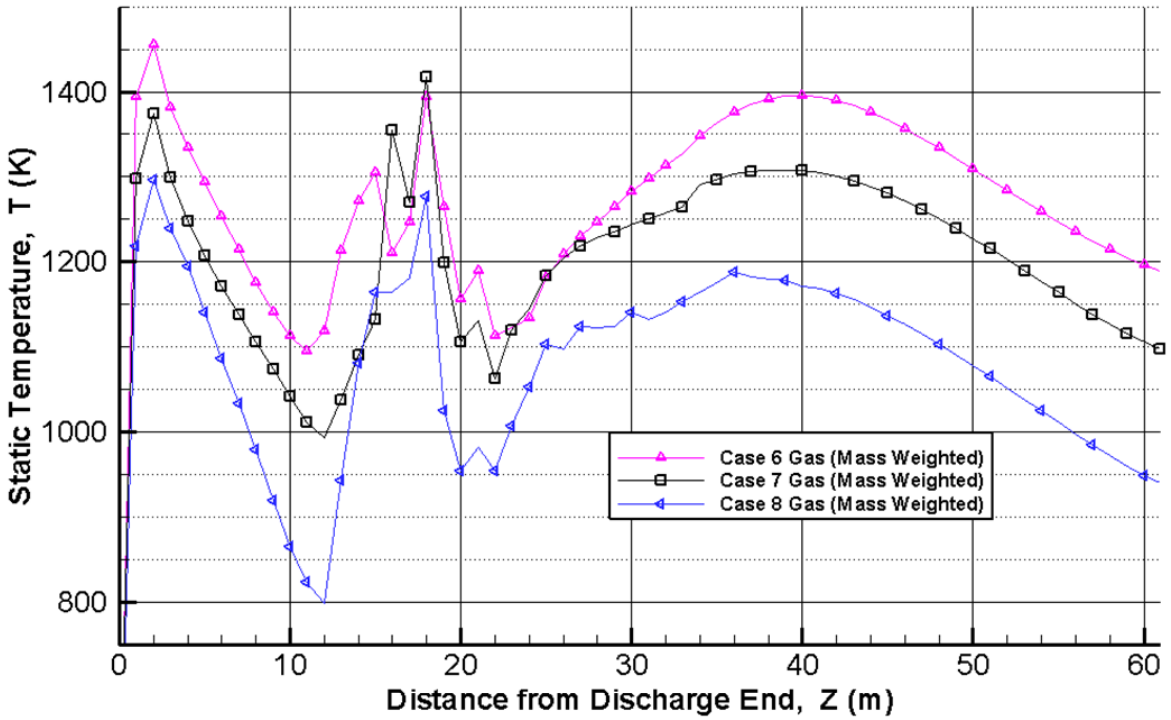

Figure 5.21 Mass flow weighted gas static temperature for various tertiary air injection angles

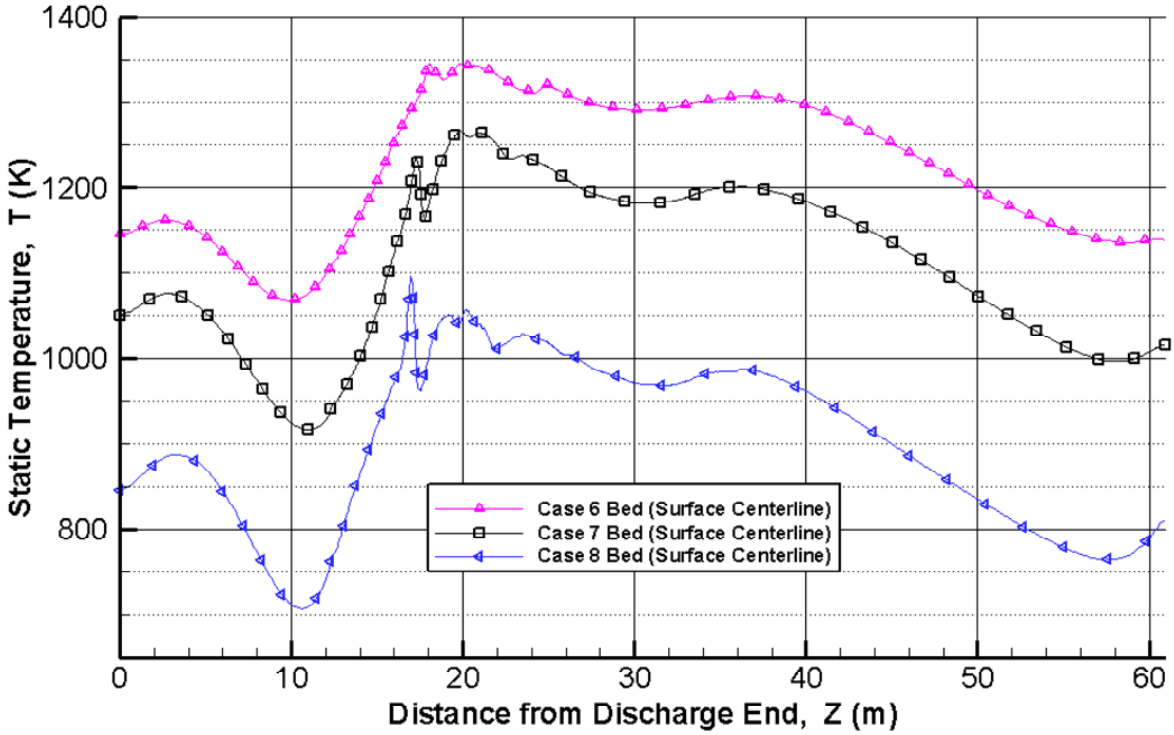

Figure 5.22 Coke bed surface centerline static temperature for various tertiary air injection angles

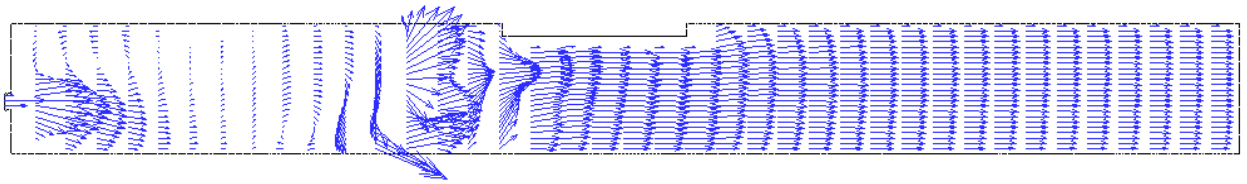

(a) Case 6 (15° injection angle)

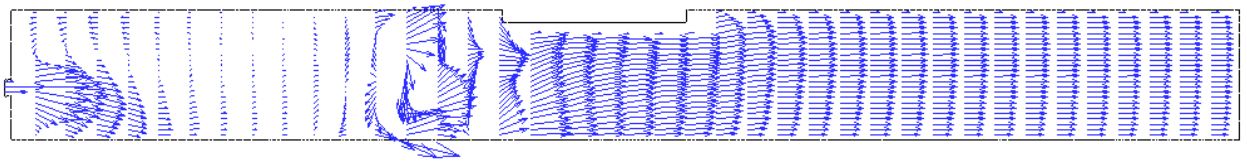

(b) Case 7 (30° injection angle)

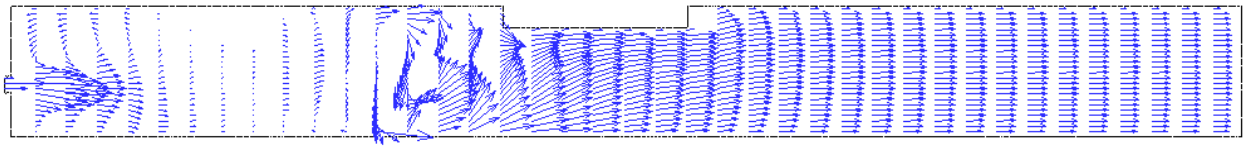

(c) Case 8 (45° injection angle)

Figure 5.23 Streamwise velocity profiles on the vertical mid-plane X = 0 for various tertiary air injection angles

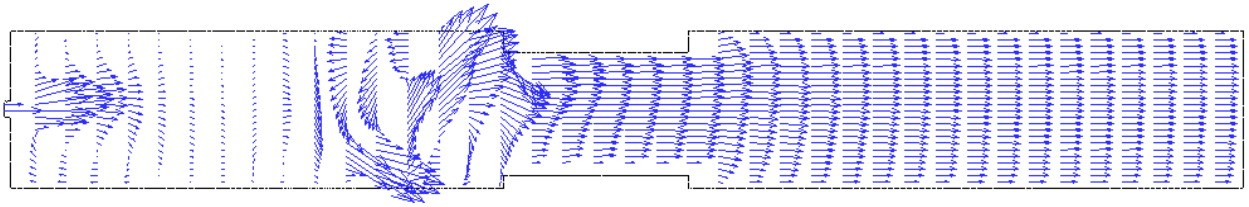

(a) Case 6 (15° injection angle)

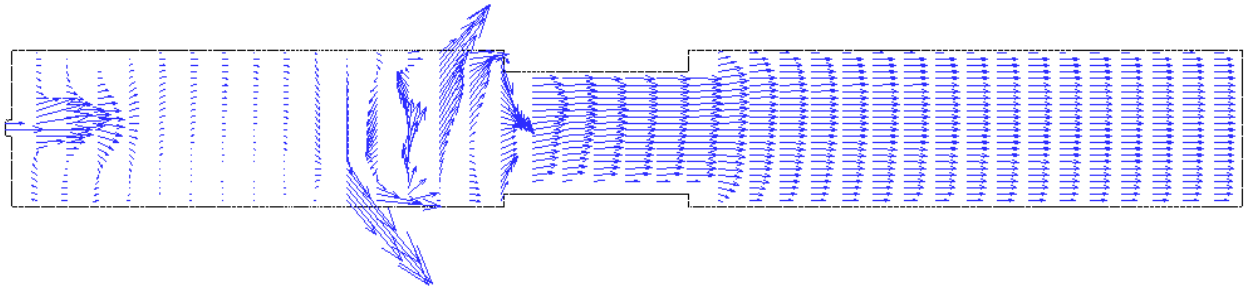

(b) Case 7 (30° injection angle)

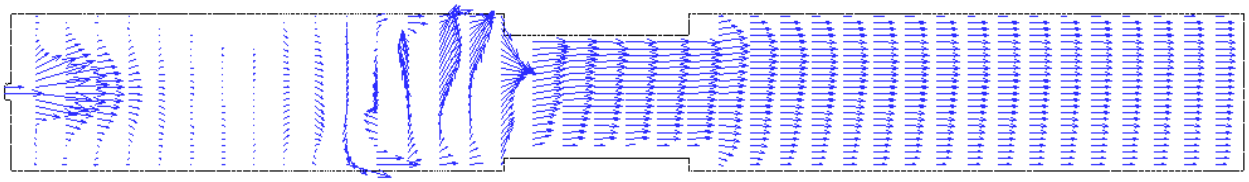

(c) Case 8 (45° injection angle)

Figure 5.24 Streamwise velocity profiles of the horizontal mid-plane Y = 0 for various tertiary air injection angles

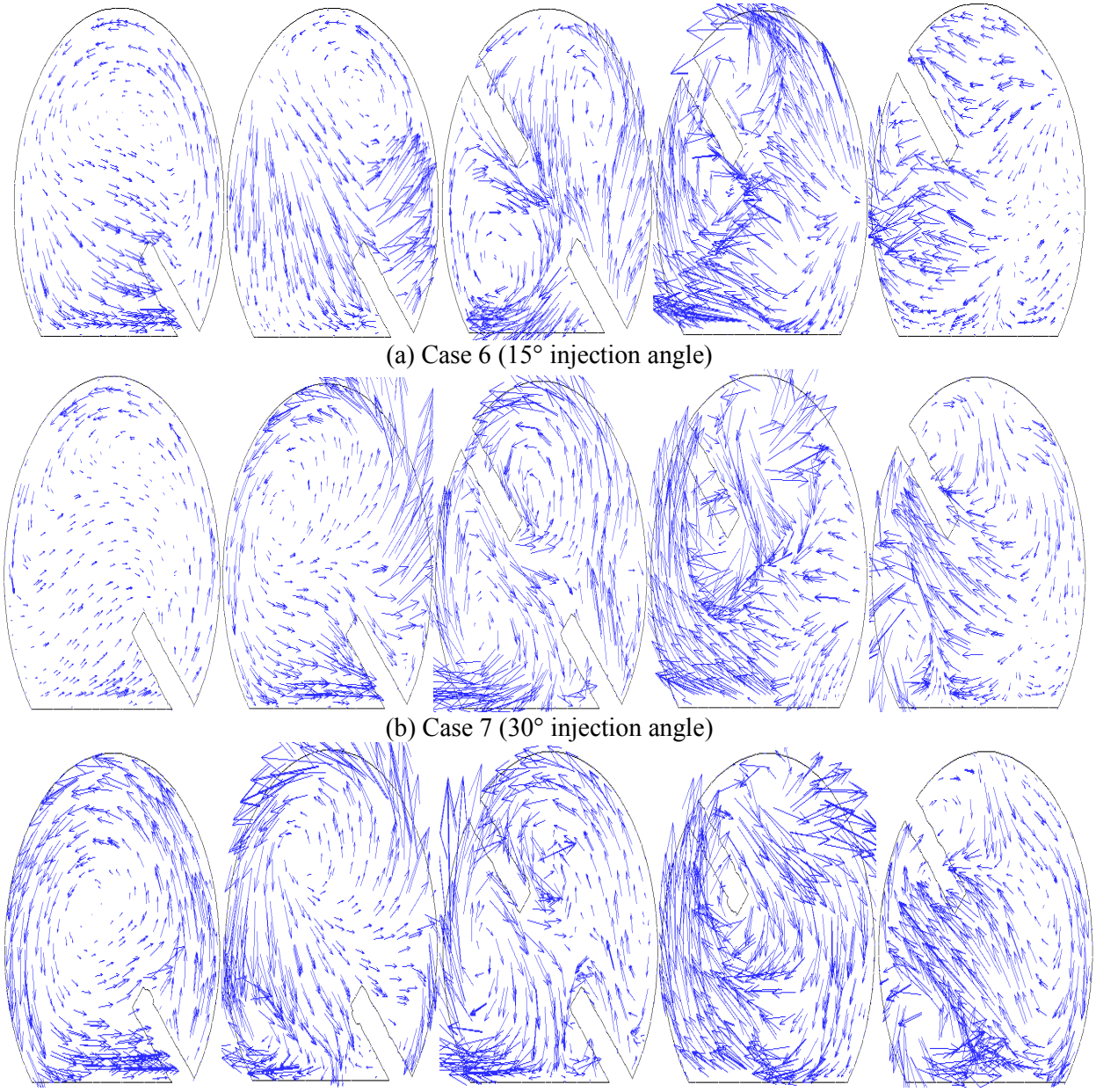

(a) Case 6 (15° injection angle)

(b) Case 7 (30° injection angle)

(c) Case 8 (45° injection angle)

Figure 5.25 Velocity profiles at each tertiary air injection location for various tertiary air injection angles

5.4 Discharge End Flow Control

To reduce or eliminate natural gas consumption in the discharge end, alternative flow controls are examined to seek the possibility of utilizing energy provided by volatiles and coke combustion. In previous cases, a recirculation zone with an almost stagnant flow has blocked the volatiles and tertiary air from moving towards the discharge end. Therefore, it is thought that if air extraction is applied at the discharge end, the volatiles combustion may move upstream toward the discharge end, or at least some hot gas can be sucked toward the discharge end. Based on this reasoning, in Case 2, a constant negative pressure of 10,000 Pascal is applied to the main air inlet at the discharge end and the rest of the settings remain unchanged; i.e. conjugate heat transfer through the coke bed is considered including the rotation effect. In Case 3, the tertiary air injectors U1 and D1 are turned 165 degrees redirecting towards the discharge end; thus, the tertiary air in Case 3 is injected toward both the feed end (D2, D3, U2 and U3) and the discharge end (D1 and U1).

In Figure 5.26b, the suction at the main inlet changes the flow field inside the kiln. A portion of the hot combustion gas is drawn toward the discharge end. The reaction in the calcining zone is less vigorous and the highest temperature is 100 K lower than Case 1. In Figure 5.26c, the reaction at the calcining zone of Case 3 is even less than Case 2. In this vertical plane view, the highest temperature of Case 3 is 600 K less than Case 1. Figure 5.27b shows that the highest gas temperature of Case 2 is 300 K lower than Case 1, and on the horizontal mid-plane view Case 3 is 600 K lower than Case 1. Apparently, sufficient volatiles are not available for combustion near the discharge end, so suction does not help much in Case 2. When the tertiary air is partially injected upstream, it actually cools the gas and coke bed in the absence of combustion. Note, the above results are the consequence of modeling employed by not

specifying the volatiles source term in the calcined coke region near the discharge end (but the coke source layer exists in the calcined coke region).

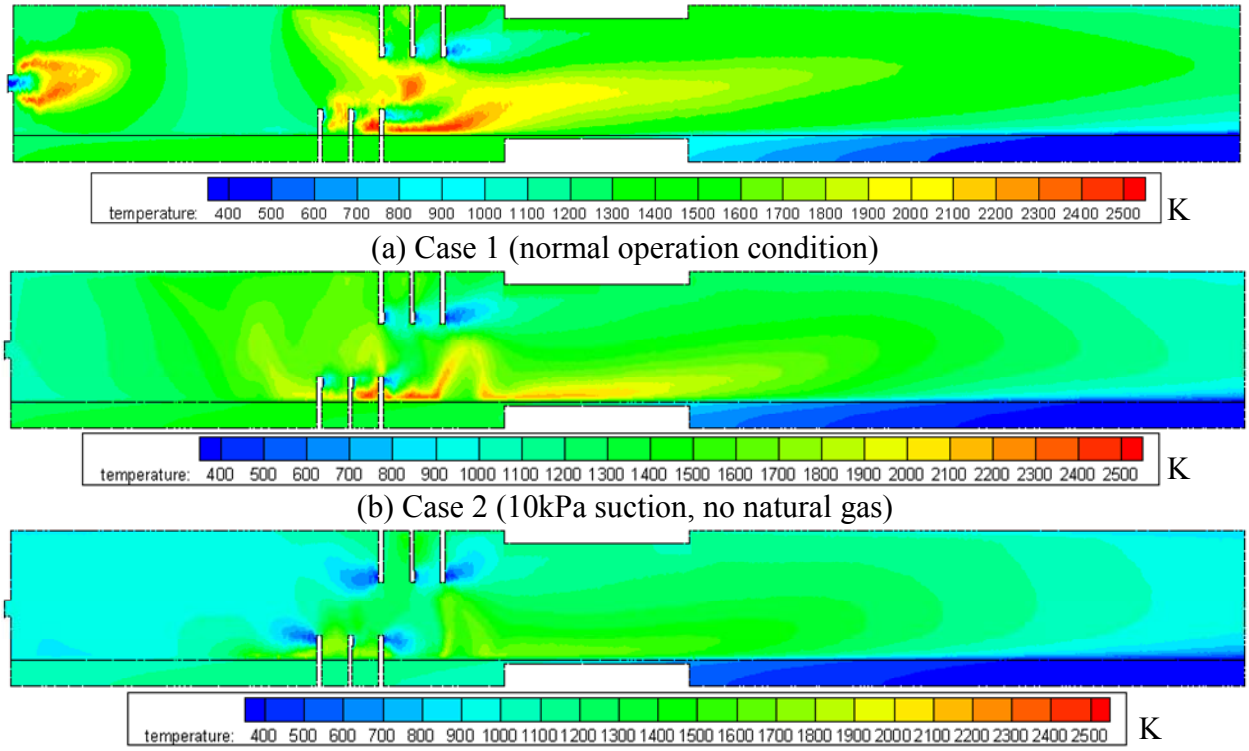

Figure 5.26 Temperature contours on the vertical mid-plane X = 0 for various discharge end flow control cases

Figure 5.28b shows that the coke bed surface temperature of Case 2 is maintained at 1,400 K for a fairly large section and reduces to 1,100 K at the discharge end. But the maximum temperature for Case 2 is 200 K lower than Case 1. Figure 5.28c shows that the coke bed surface temperature of Case 3 is 400 K colder in the calcining zone and compared to case 1, 300 K colder at the discharge end.

The cross-sectional views of the temperature distributions in Figure 5.29 clearly reinforce that discharge end air extraction reduces the combustion downstream of the tertiary air region and increases temperature upstream of the tertiary air region; but the gas temperature is cooled when two tertiary injectors are turned toward an upstream direction. Figure 5.29a shows that in

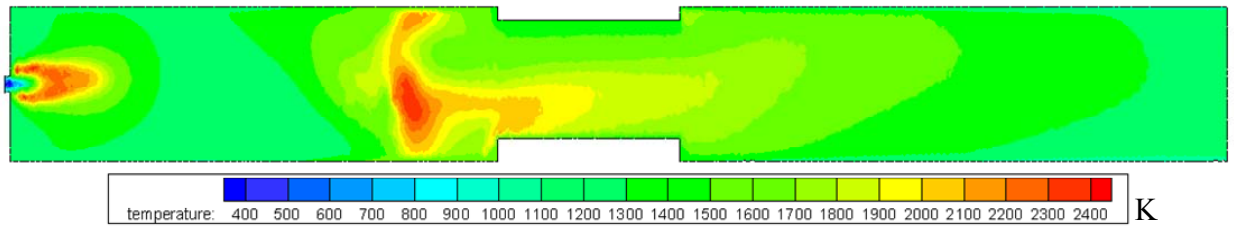

(a) Case 1 (normal operation condition)

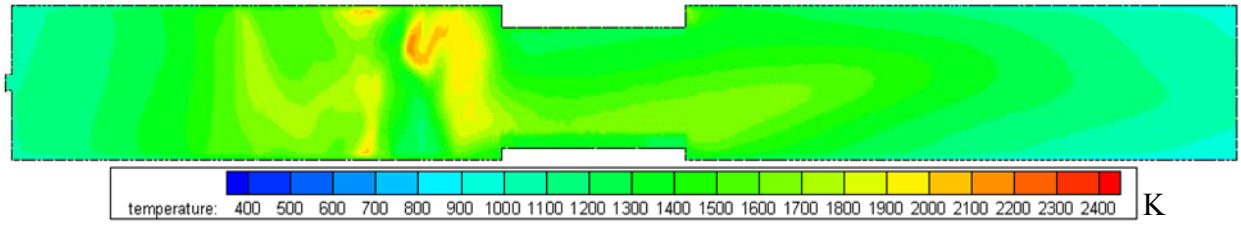

(b) Case 2 (10kPa suction, no natural gas)

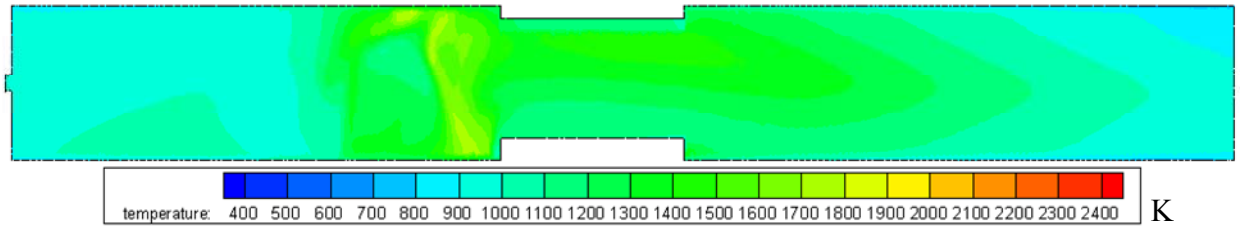

(c) Case 3 (10kPa suction, no natural gas, 2 upstream injectors)

Figure 5.27 Temperature contours on the horizontal mid-plane Y = 0 for various discharge end flow control cases

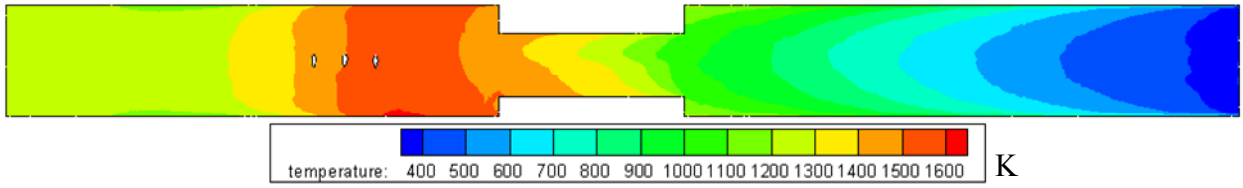

(a) Case 1 (normal operation condition)

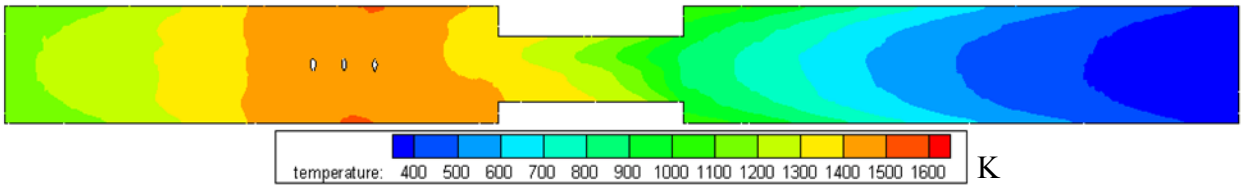

(b) Case 2 (10kPa suction, no natural gas)

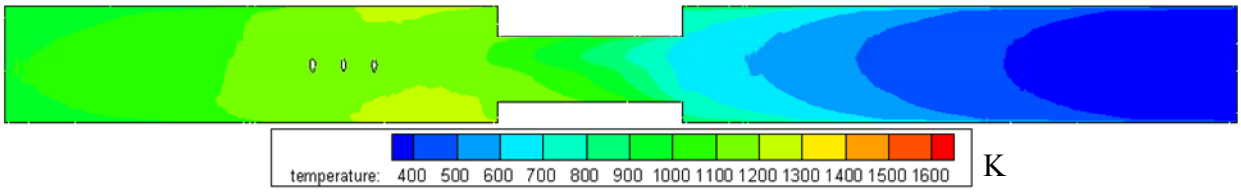

(c) Case 3 (10kPa suction, no natural gas, 2 upstream injectors)

Figure 5.28 Temperature contours of the coke bed surface on the horizontal plane at Y = – 0.9144 for various discharge end flow control cases

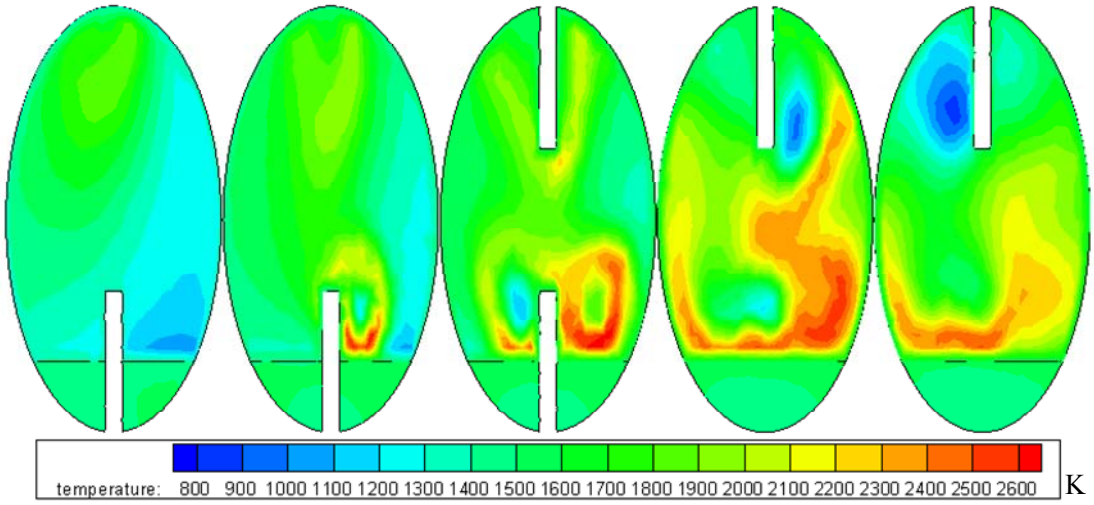

(a) Case 1 (normal operation condition)

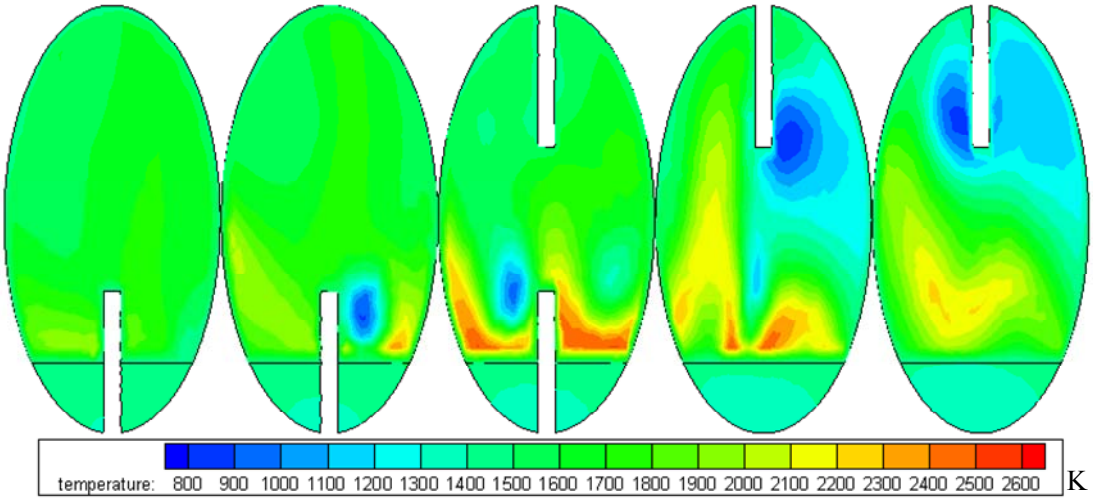

(b) Case 2 (10kPa suction, no natural gas)

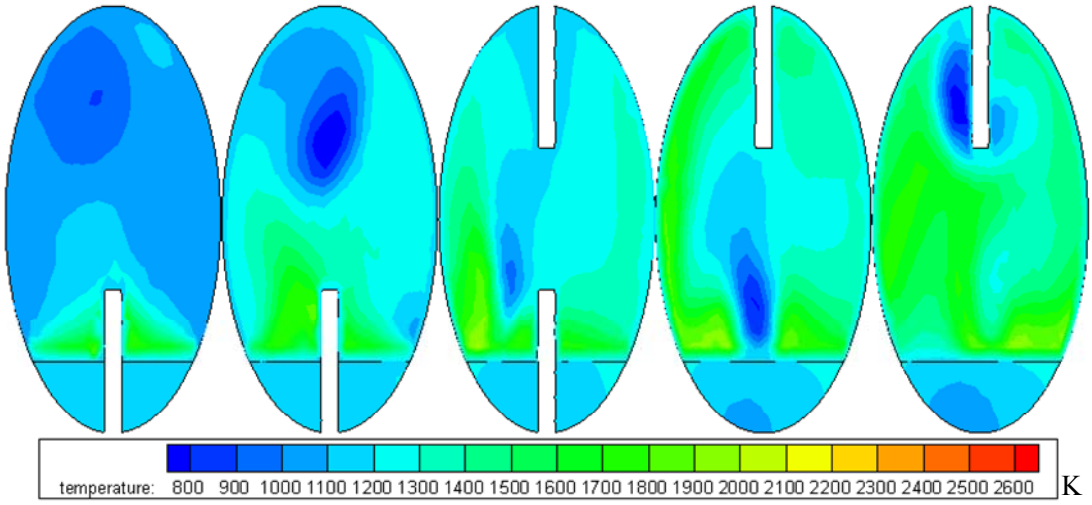

(c) Case 3 (10kPa suction, no natural gas, 2 upstream injectors)

Figure 5.29 Cross-sectional temperature contours at each tertiary air injection location for various discharge end flow control cases

the tertiary air injection location cross-section views the coke bed temperature is shifting between 1,400 K and 1,500 K. Case 2 coke bed temperature starts at 1,300 K and rises to 1,400 K. The coke bed temperature of Case 3 is only at 1,100 K.

A comparison of the mass flow weighted gas temperature distributions of three cases is shown in Figure 5.30. Case 2 seems successful in increasing the gas temperature between 8 to 16 meters from 1,125 K to 1,450 K. The coke bed surface temperature of Case 2 is also successfully raised about 100 K (see Figure 5.31) between 5 and 15 meters from the discharge end, but the temperature decreases approximately 100 K in the rest of the downstream location. Apparently the hot air is extracted out resulting in a net loss of energy; however, the extracted hot gas can be looped back into the downstream location to conserve energy. To recover this lost energy, Case 13 is conducted by returning the extracted hot gas downstream and re-injecting it into the kiln at Z = 35.05 m. For simplicity, the coke fines combustion is not included in Case 13. In Figure 5.34 the mass weighted average gas and bed surface centerline static temperatures of Case 13 are compared with Case 5 which does not employ air extraction or coke fines combustion. The suction at the discharge end successfully increases the temperature between Z = 7 to 15 m by 100 K. However, the returned combustion gas causes a temperature reduction of approximately 100 K in the region of flow re-injection. Depending on the characteristics of the petcoke, reduction of 100 K in the heat-up region could or could not affect the product quality. Another potential adverse impact of this returning-gas approach is the high velocity (around 50 m/s) of the re-injected flow could cause undesired coke fines entrainments and reduced productivity. The facility requirements for extracting and re-injecting this high temperature (970K), low density (35 kg/m^3) combustion gas at this high velocity could be expensive. Case 3 is a clear loser, so it is not discussed.

Discharge end air extraction has completely changed the flow pattern near the discharge end as shown in Figures 5.35, 5.36, and 5.37. In the tumbler region for Case 2 and Case 3, Figure 5.35, a small clockwise gas circulation is formed that pushes the combustion flame from U3 tertiary air injector upwards. Discharge end air extraction and reverse tertiary air injection induce recirculation (Figures 5.35c and 5.36c) and inhibit an effective transport of hot gas from the tertiary combustion zone to the discharge end.

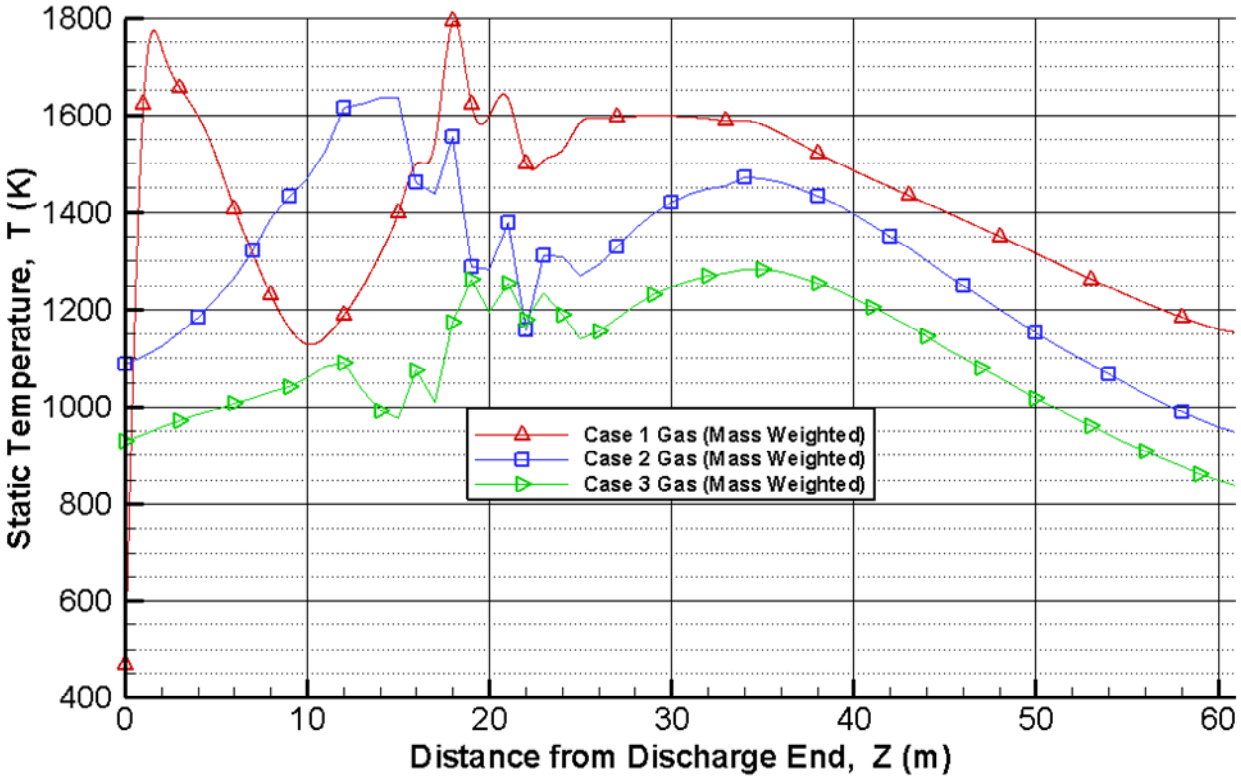

Figure 5.30 Mass flow weighted gas static temperature for various discharge end flow control cases

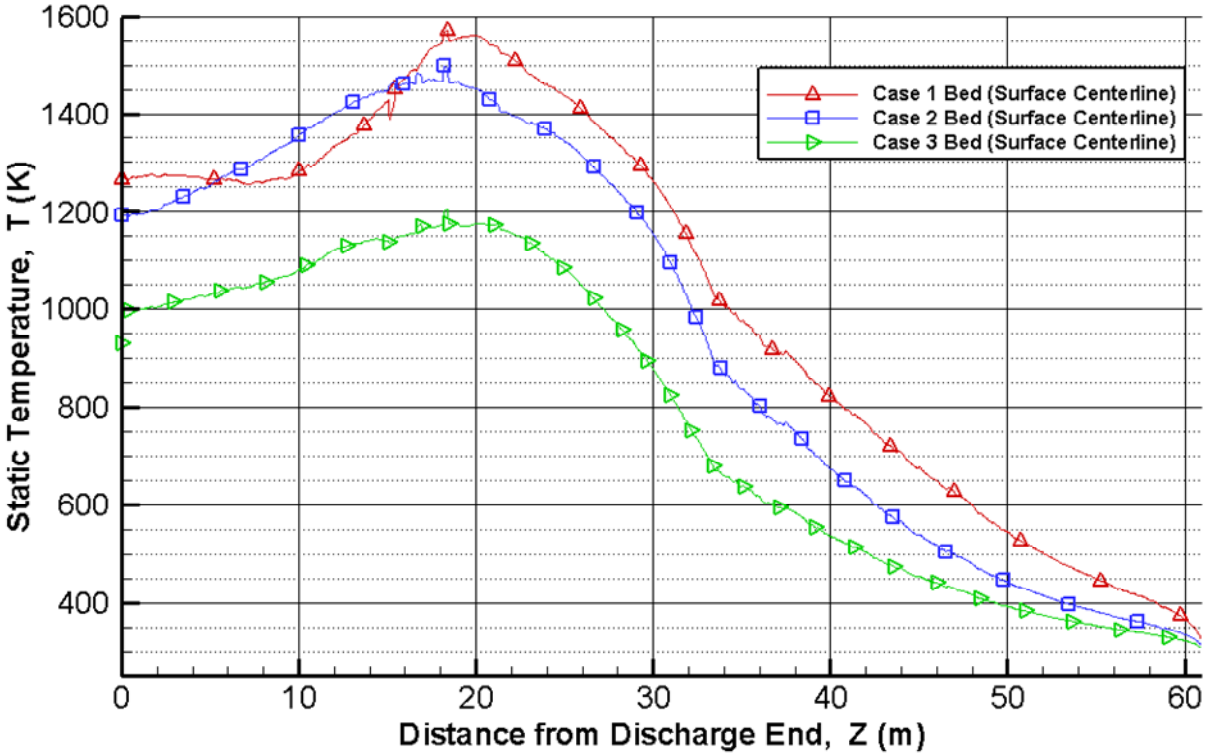

Figure 5.31 Coke bed surface centerline static temperature for various discharge end flow control cases

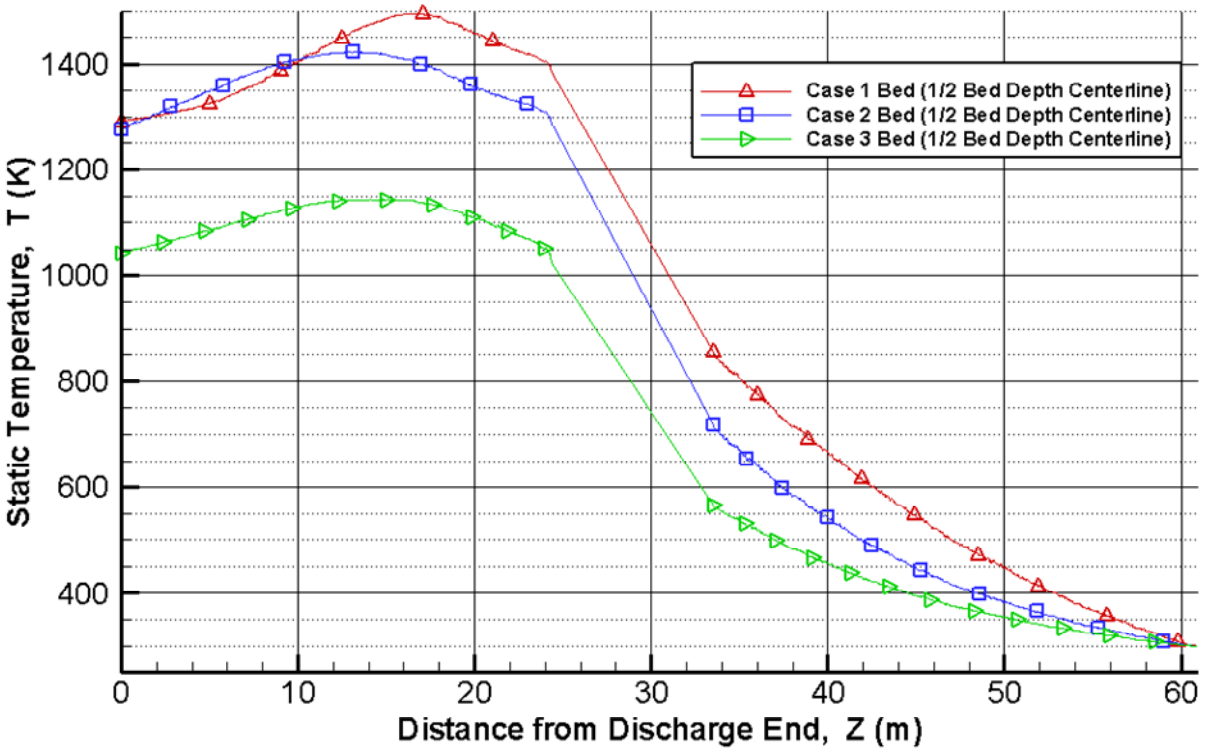

Figure 5.32 Centerline static temperature ½ coke bed depth for various discharge end flow control cases

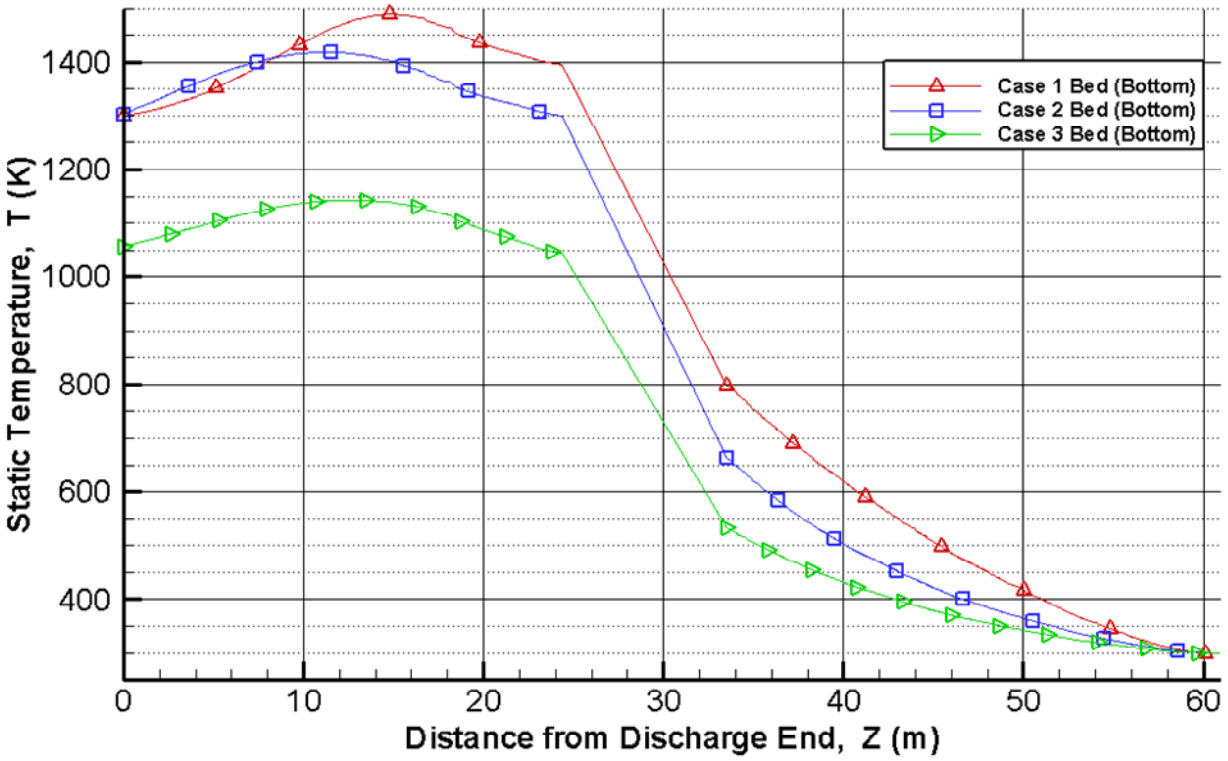

Figure 5.33 Coke bed bottom static temperature for various discharge end flow control cases

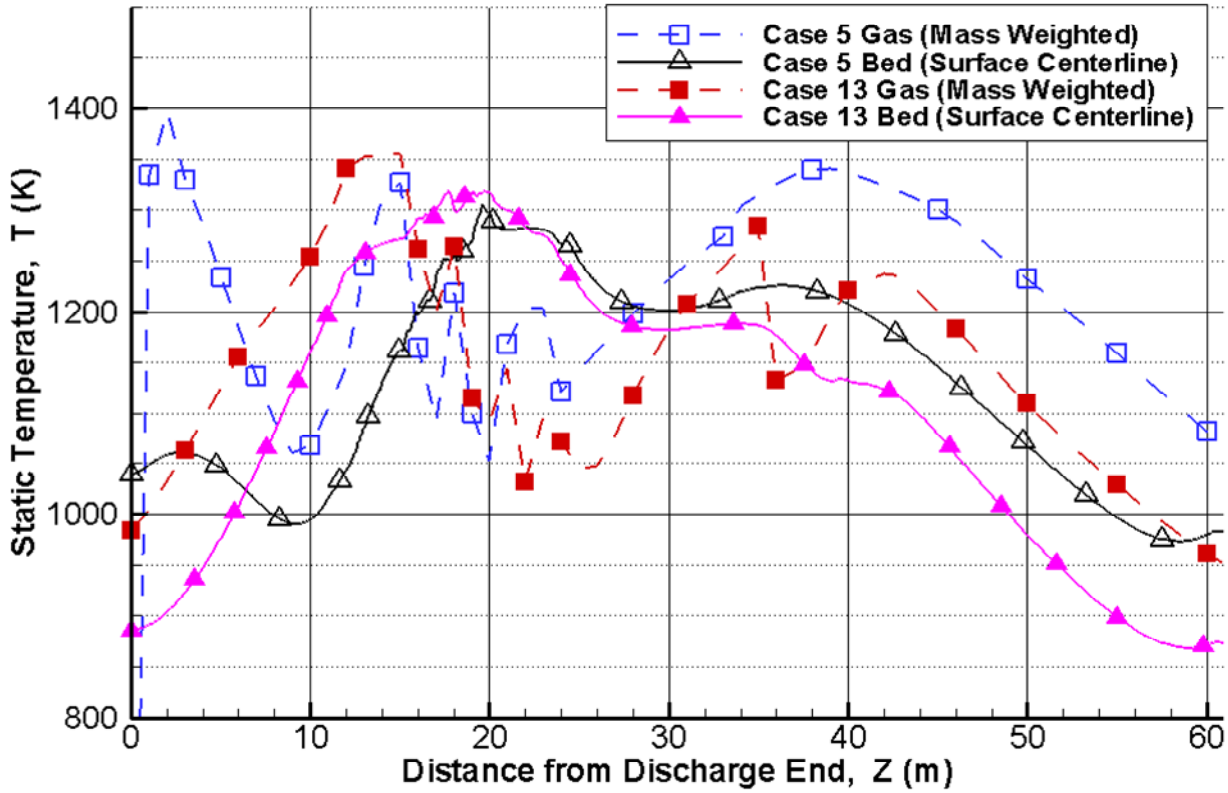

Figure 5.34 Static temperature for the effect of suction with re-feed

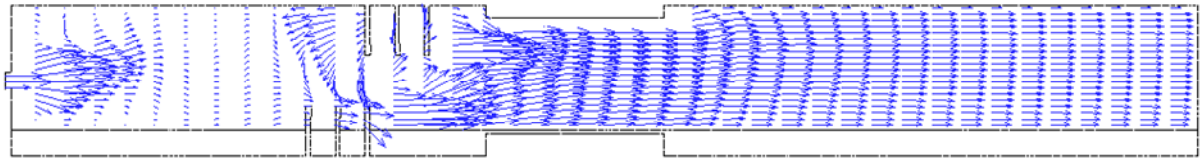

(a) Case 1 (normal operation condition)

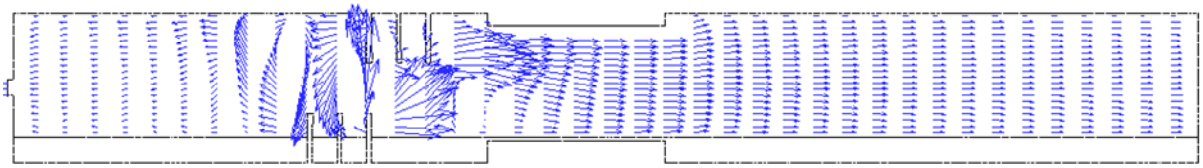

(b) Case 2 (10kPa suction, no natural gas)

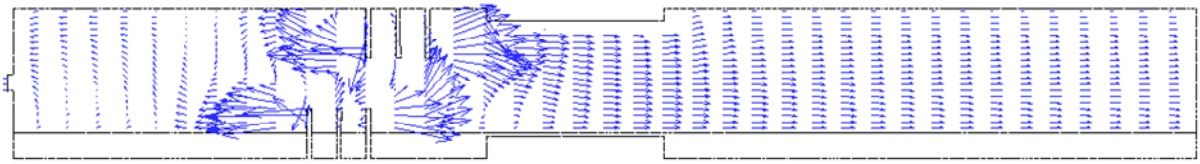

(c) Case 3 (10kPa suction, no natural gas, 2 upstream injectors)

Figure 5.35 Streamwise velocity profiles of vertical mid-plane at X = 0 for various discharge end flow control cases

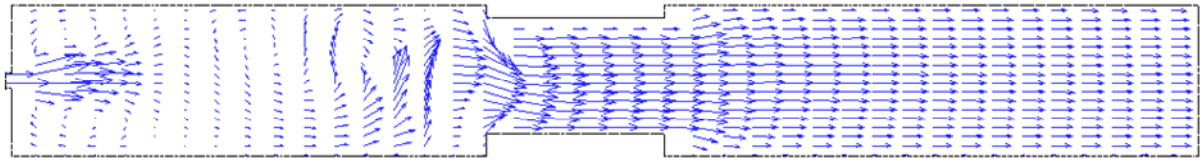

(a) Case 1 (normal operation condition)

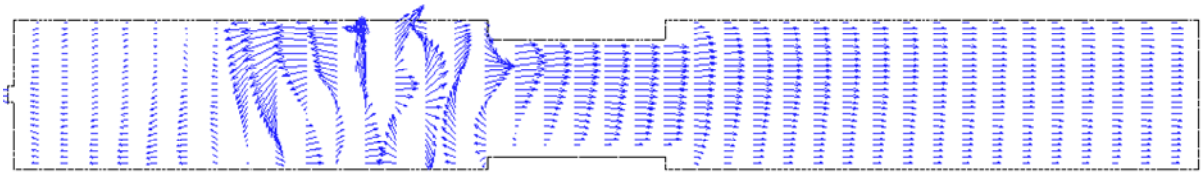

(b) Case 2 (10kPa suction, no natural gas)

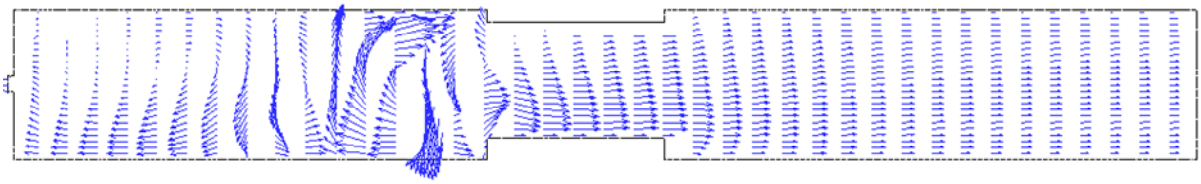

(c) Case 3 (10kPa suction, no natural gas, 2 upstream injectors)

Figure 5.36 Streamwise velocity profiles of horizontal mid-plane at Y = 0 for various discharge end flow control cases

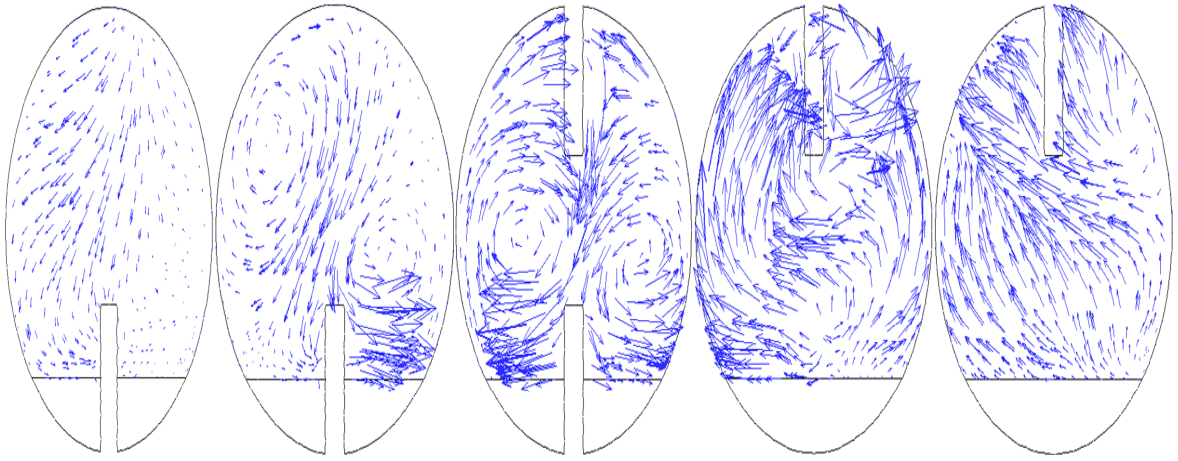

(a) Case 1 (normal operation condition)

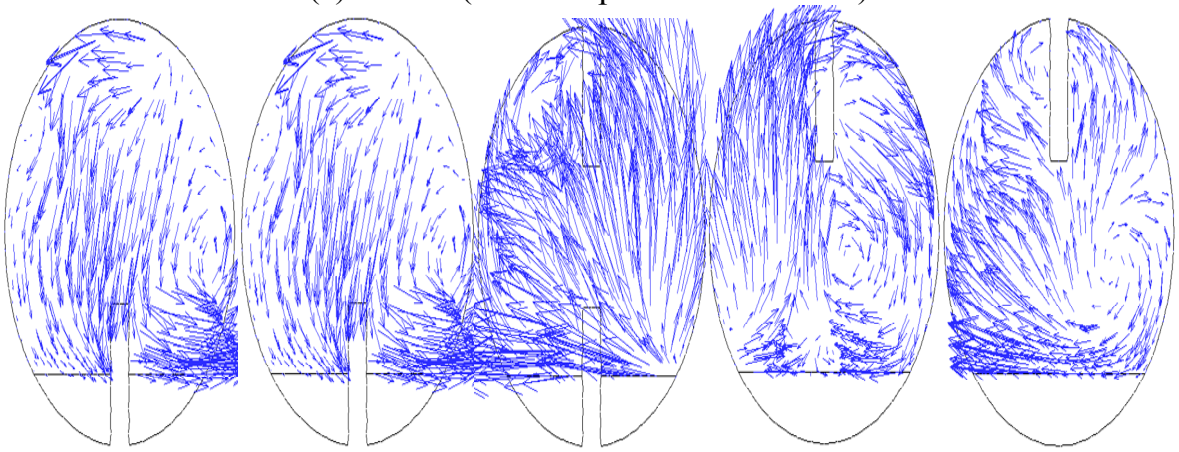

(b) Case 2 (10kPa suction, no natural gas)

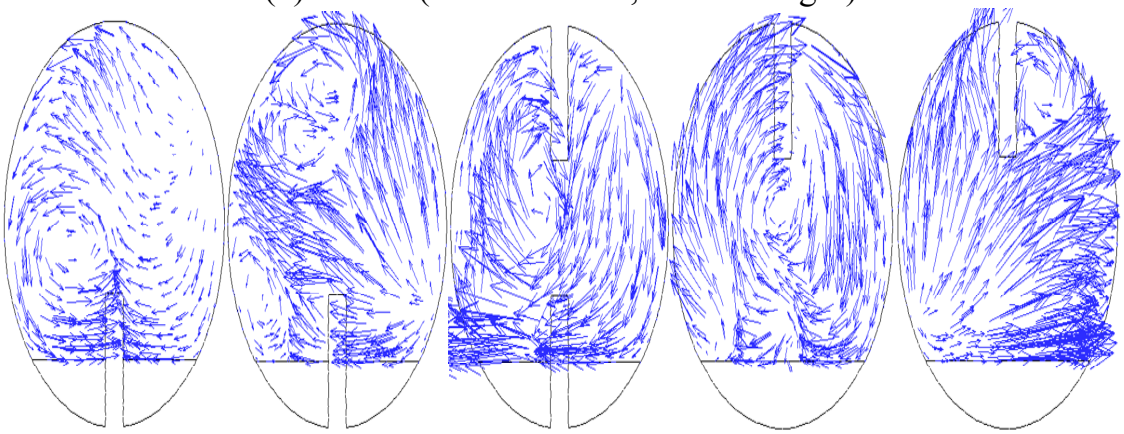

(c) Case 3 (10kPa suction, no natural gas, 2 upstream injectors)

Figure 5.37 Cross-sectional velocity profiles at each tertiary air injection location for various discharge end flow control cases

5.5 Coke Fines Combustion and Various Coke Bed Devolatilization Conditions

During modeling, where the devolatilization process starts or where the coke starts to burn is uncertain. This section investigates the sensitivity of the results to the model variations. In this set of simulations, the coke bed is removed from the computational domain. Cases 4 and 5 have the same domain except Case 5 does not have coke combustion. Case 12 is similar to Case 5 but with a shortened devolatilization zone (only between 19.8 and 36.6 m). Therefore, comparison of Cases 4 and 5 indicates the impact of coke fines combustion; while the comparison of Cases 5 and 12 indicates the effect of devolatilization location and length.

The results show that coke fine combustion is a very important mechanism in the calcining kiln. Figure 5.38a shows the highest temperature in Case 4 is 3,200 K, which is about 1,300 K higher than Case 5 without coke combustion and is 700 K higher than the baseline case. The baseline case allows heat transfer through the coke bed, so the gas temperature is lower than in Case 4, which does not include the coke bed. This high temperature in Case 4 is apparently achieved by the combustion of coke fines. The shortened devolatilization zone in Case 12 emits the same total amount of volatile matter as Case 5 but in a shorter distance. A shorter devolatilization zone causes a cold region at the tertiary air injection zone because no volatiles source term is assigned in the tertiary air zone. Both Figures 5.39 and 5.40 support what has been shown in Figure 5.38; Case 4 has the highest temperature and more vigorous combustion than Cases 5 and 12. With the combustion of coke, the flame temperature is much higher than the combustion of solely volatiles with the air, as shown in Figure 5.41. Coke combustion shows a significant boost to the temperature field in Figures 5.42 and 5.43. The significant reduction of temperature from Case 5 to Case 12, as shown in Figure 5.42, provides surprising evidence showing the sensitivity of modeling the location for releasing volatiles. It is important to ensure

that the devolatilization process will continue into the tertiary air injection region; otherwise, the volatiles would be swept away with less effective combustion.

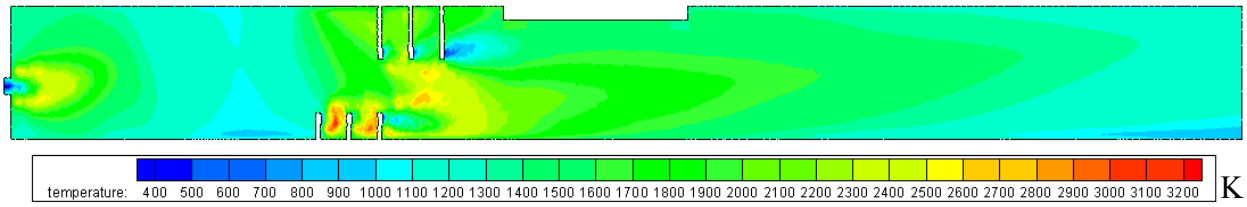

(a) Case 4 (regular devolatile zone, with coke combustion)

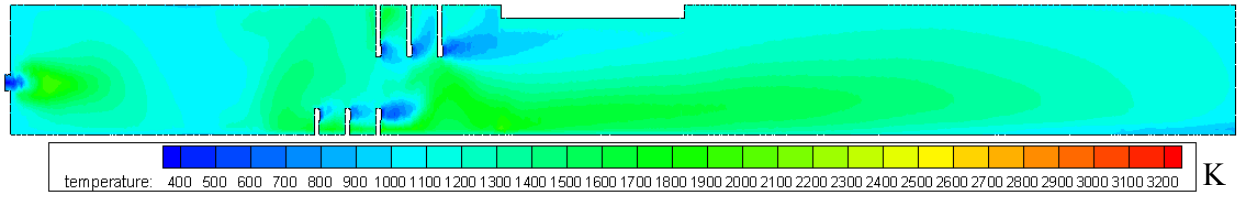

(b) Case 5 (regular devolatile zone, no coke combustion)

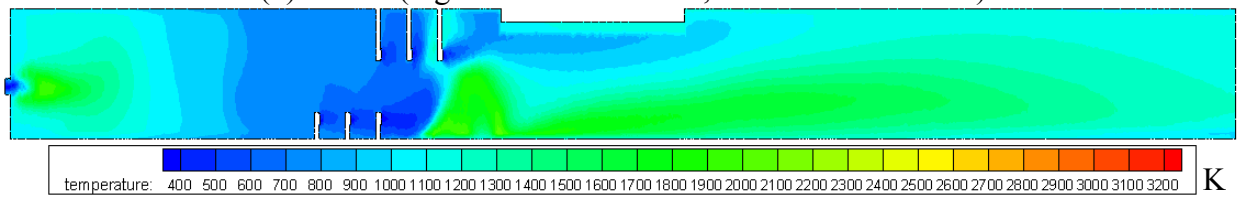

(c) Case 12 (shortened devolatile zone, no coke combustion)

Figure 5.38 Temperature contours on the vertical mid-plane at X = 0 for conditions with coke burning, without coke burning and with a shortened devolatilization zone

Gas temperature affects the flow field between the main inlet combustion flame and the tertiary air injection zone in Figure 5.44. In this region, Case 5 has a clockwise circulation while Case 4 and Case 12 have counterclockwise circulations. The clockwise circulation above the coke bed surface before the tumbler zone in Case 12 lifts the flame. This phenomenon can also be observed in Figure 5.38c. In Figure 5.45, both Cases 5 and 12 have circulations occurring before the tumbler; this circulation is not presented in Case 4. The combustion pattern is therefore affected by the flow field and demonstrates different temperature contours.

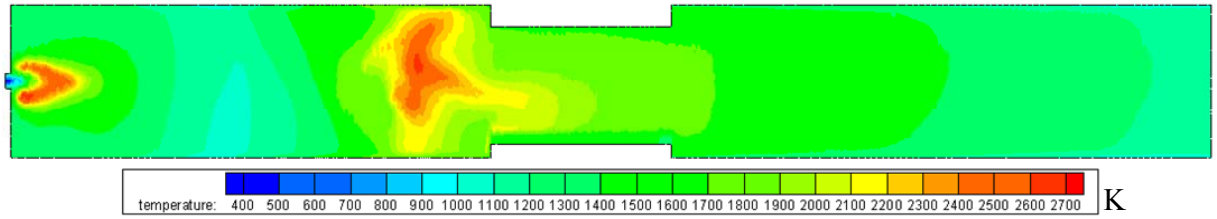

(a) Case 4 (regular devolatile zone, with coke combustion)

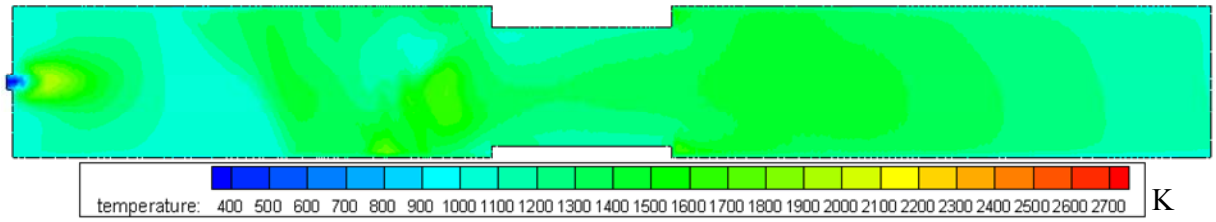

(b) Case 5 (regular devolatile zone, no coke combustion)

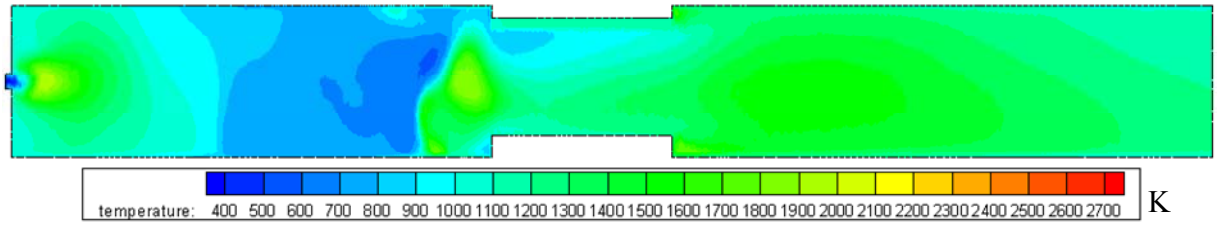

(c) Case 12 (shortened devolatile zone, no coke combustion)

Figure 5.39 Temperature contours on the horizontal mid-plane at Y = 0 for conditions with coke burning, without coke burning and with a shortened devolatilization zone

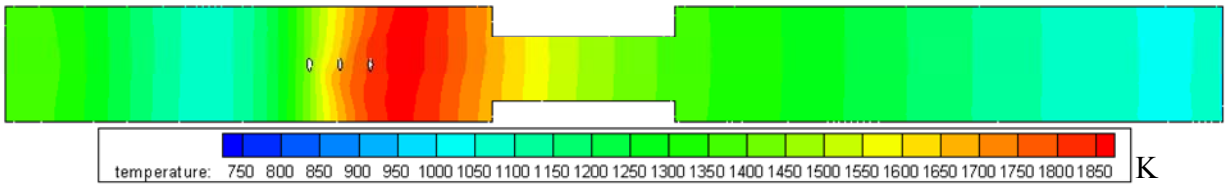

(a) Case 4 (regular devolatile zone, with coke combustion)

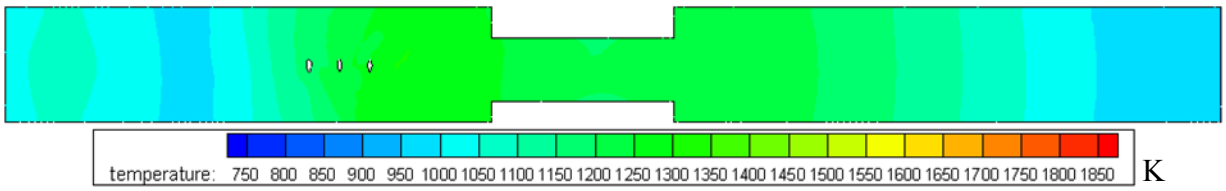

(b) Case 5 (regular devolatile zone, no coke combustion)

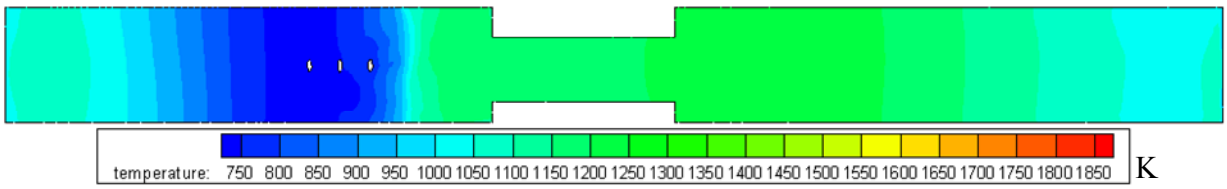

(c) Case 12 (shortened devolatile zone, no coke combustion)

Figure 5.40 Temperature contours on coke bed surface on the horizontal mid-plane at Y = –0.9144 for conditions with coke burning, without coke burning and with a shortened devolatilization zone

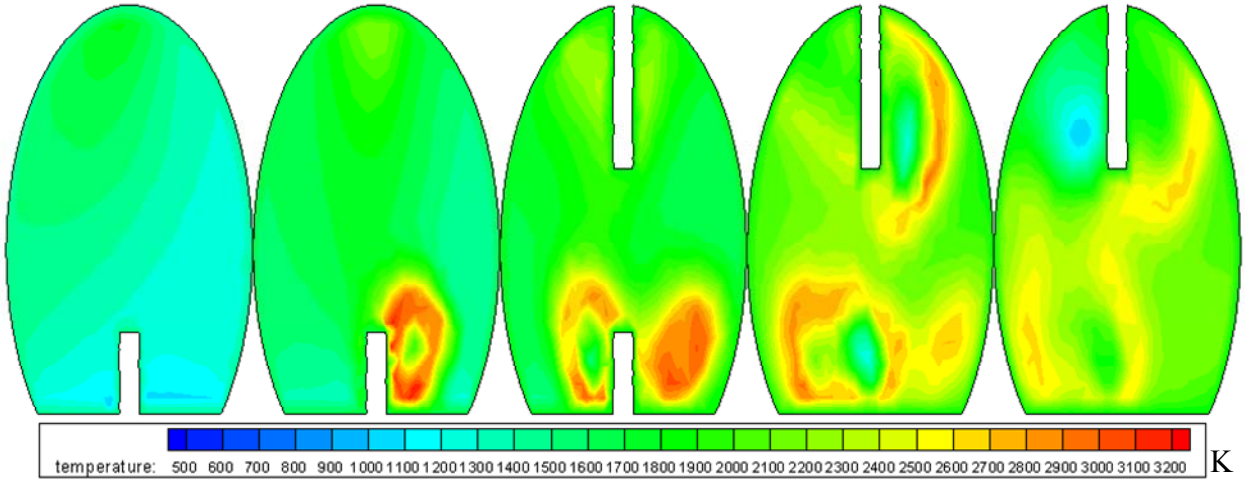

(a) Case 4 (regular devolatile zone, with coke combustion)

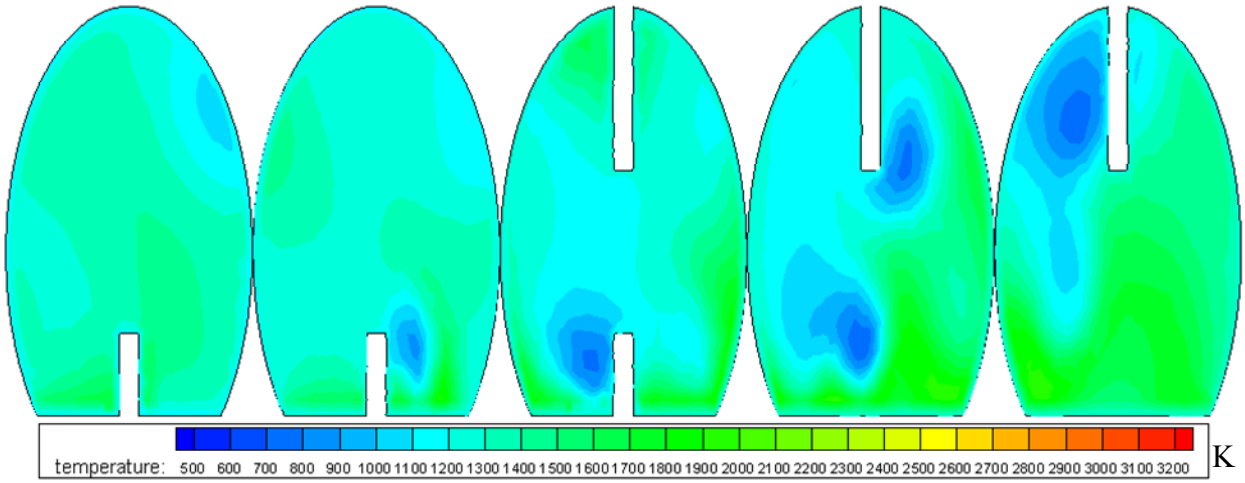

(b) Case 5 (regular devolatile zone, no coke combustion)

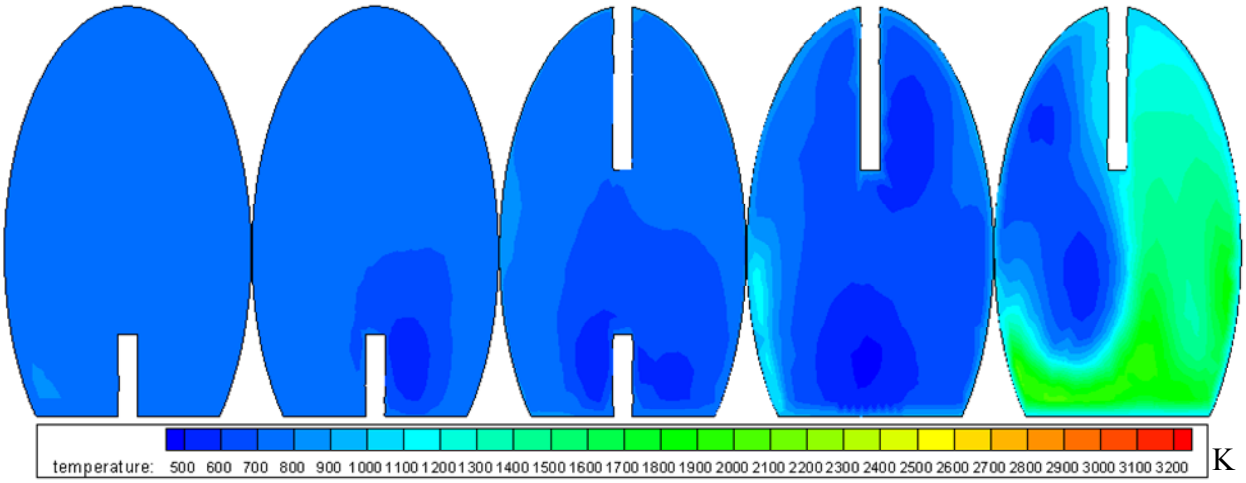

(c) Case 12 (shortened devolatile zone, no coke combustion)

Figure 5.41 Cross-sectional temperature contours at each tertiary air injection location for conditions with coke burning, without coke burning and with a shortened devolatilization zone

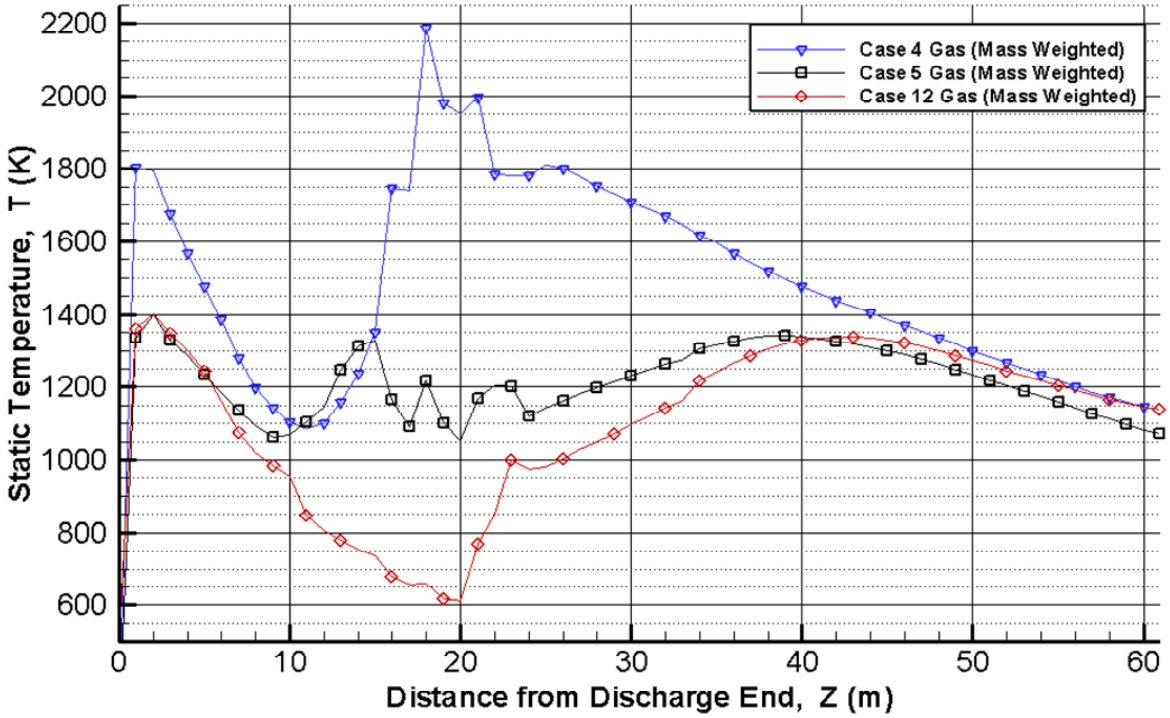

Figure 5.42 Mass flow weighted gas static temperature for conditions with coke burning, without coke burning and with a shortened devolatilization zone

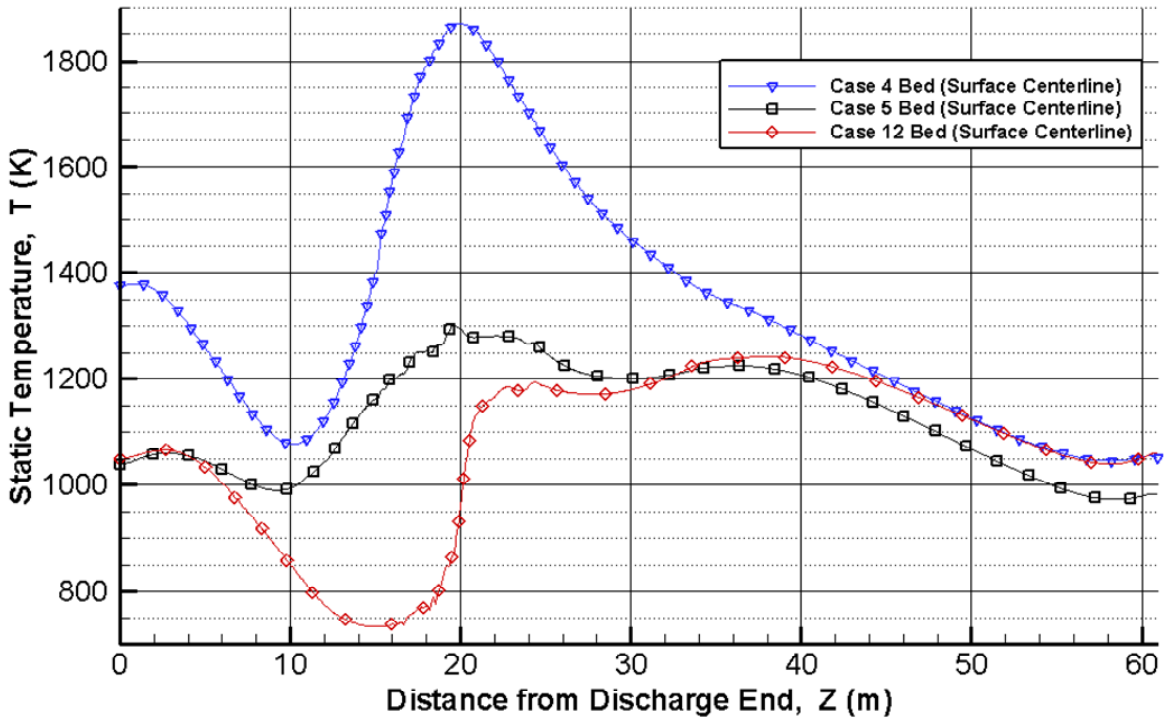

Figure 5.43 Coke bed surface centerline static temperature for conditions with coke burning, without coke burning and with a shortened devolatilization zone

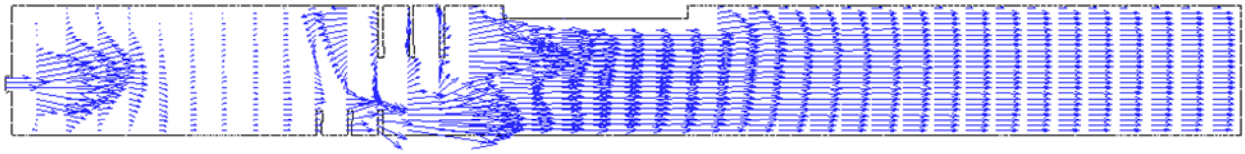

(a) Case 4 (regular devolatile zone, with coke combustion)

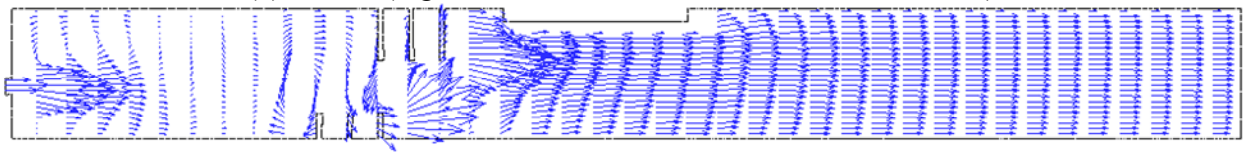

(b) Case 5 (regular devolatile zone, no coke combustion)

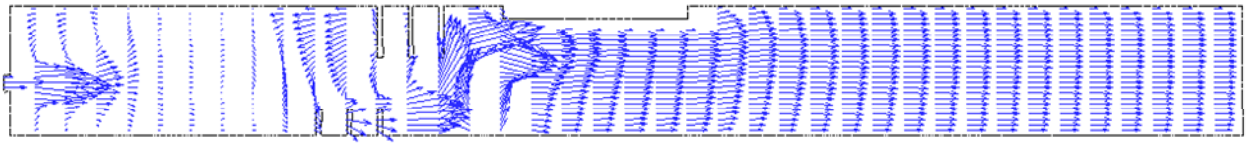

(c) Case 12 (shortened devolatile zone, no coke combustion)

Figure 5.44 Streamwise velocity profiles on the vertical mid-plane at X = 0 for conditions with coke burning, without coke burning and with a shortened devolatilization zone

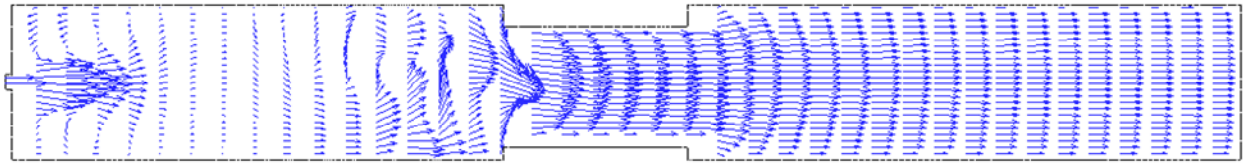

(a) Case 4 (regular devolatile zone, with coke combustion)

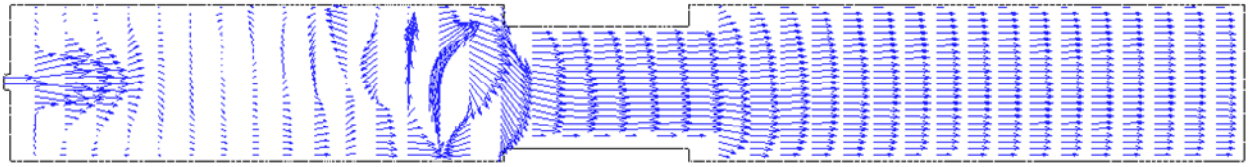

(b) Case 5 (regular devolatile zone, no coke combustion)

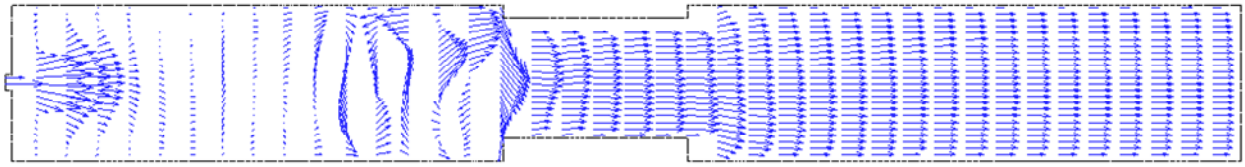

(c) Case 12 (shortened devolatile zone, no coke combustion)

Figure 5.45 Streamwise velocity profiles of the horizontal mid-plane at Y = 0 for conditions with coke burning, without coke burning and with a shortened devolatilization zone

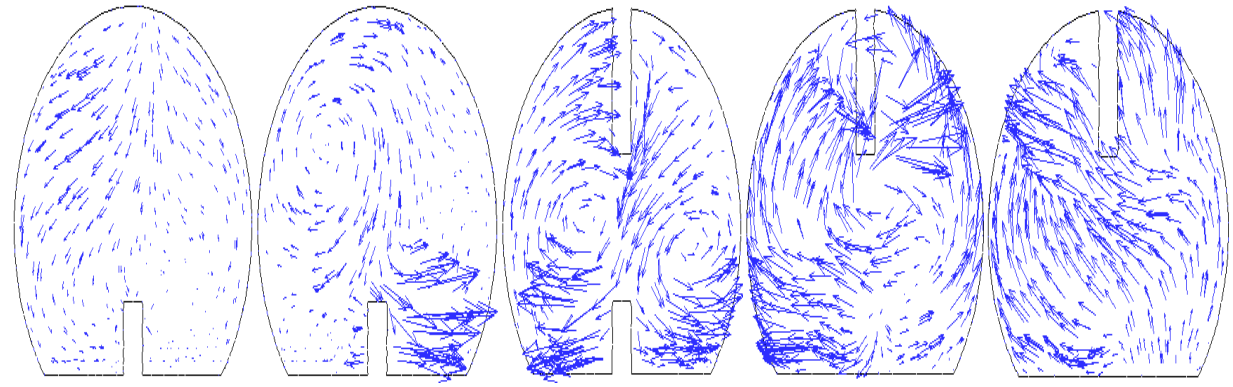

(a) Case 4 (regular devolatile zone, with coke combustion)

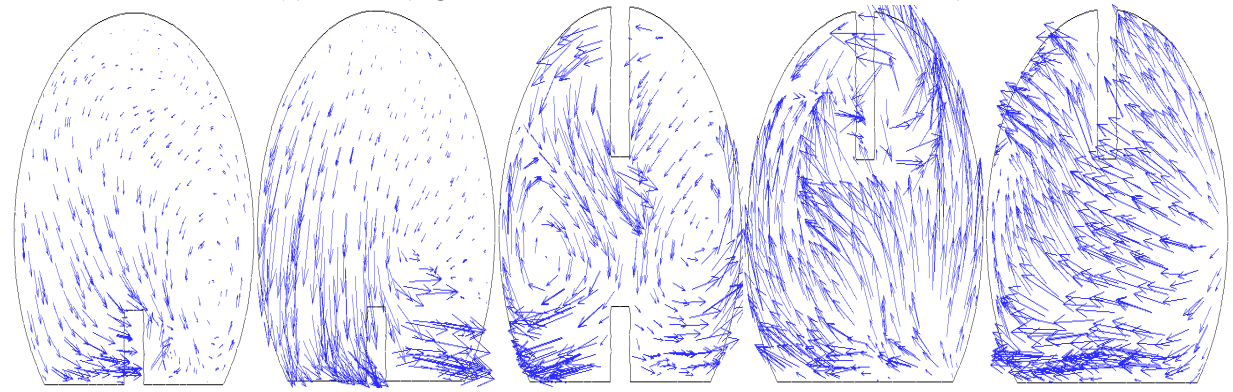

(b) Case 5 (regular devolatile zone, no coke combustion)

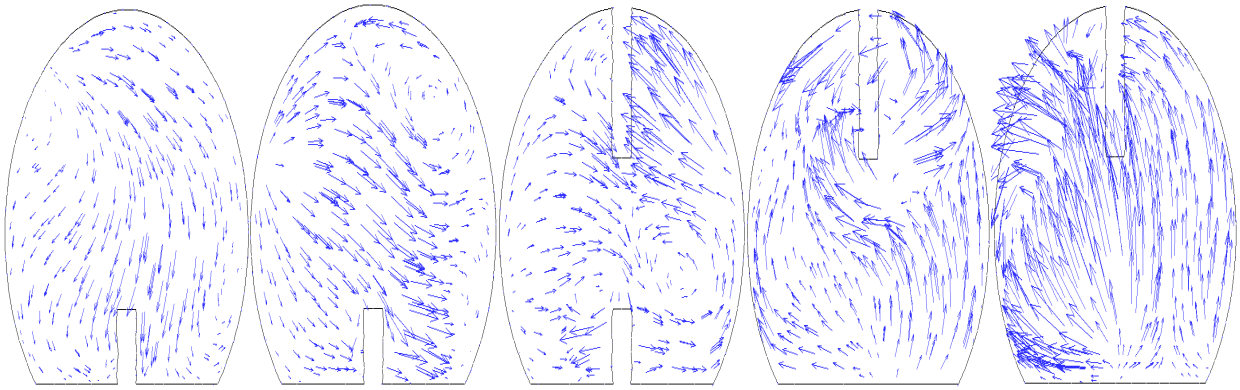

(c) Case 12 (shortened devolatile zone, no coke combustion)

Figure 5.46 Cross-sectional velocity profiles at each tertiary air injection location for conditions with coke burning, without coke burning and with a shortened devolatilization zone

5.6 Various Coke Bed Properties

Simulations in 2-D are carried out to study the impact of coke bed properties on the solutions. The geometry of the 2-D domain is shown in Figure 5.47. The corresponding 2-D case numbers and simulation conditions are listed in Table 5.3. Figure 5.48 shows for the same thermal conductivity and moving speed, coke bed temperature reduces as the heat capacity increases. The specific heat used in this study is 850 J/kg-K. Similarly, for the same heat capacity, coke bed temperature reduces as the thermal conductivity increases. The thermal conductivity of the coke bed varies depending on the size of the petcoke particles and the amount of gas trapped inside the coke bed (i.e. the characteristics of a granular flow), along with the effect of the tumblers. The effective thermal conductivity of the coke bed will be greater than the thermal conductivity of the coke itself; therefore, the effective thermal conductivity in this study is set to be 100 W/m-K. Bed temperature always decreases as the bed axial moving (sliding) speed increases. The coke resident time inside the kiln used in the 3-D studies is 1.65 hour, and coke bed axial moving velocity is 0.01 m/s (0.0328 ft/s).

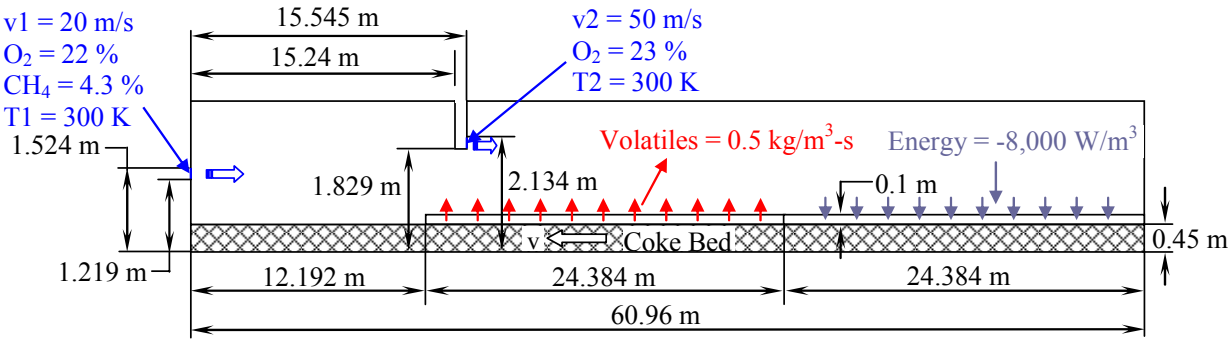

Figure 5.47 Schematic of 2-D simulation domain

Table 5.3 2-D case number and descriptions

2D Case Number	Case Descriptions
Case A	Bed thermal conductivity = 140 W/m-K, bed specific heat = 100 J/kg-K, and bed sliding velocity = 0.005 m/s
Case B	Bed thermal conductivity = 140 W/m-K, bed specific heat = 710 J/kg-K, and bed sliding velocity = 0.005 m/s
Case C	Bed thermal conductivity = 140 W/m-K, bed specific heat = 2,000 J/kg-K, and bed sliding velocity = 0.005 m/s
Case D	Bed thermal conductivity = 140 W/m-K, bed specific heat = 710 J/kg-K, and bed sliding velocity = 0.05 m/s
Case E	Bed thermal conductivity = 1.7 W/m-K, bed specific heat = 100 J/kg-K, and bed sliding velocity = 0.005 m/s
Case F	Bed thermal conductivity = 1.7 W/m-K, bed specific heat = 2,000 J/kg-K, and bed sliding velocity = 0.005 m/s

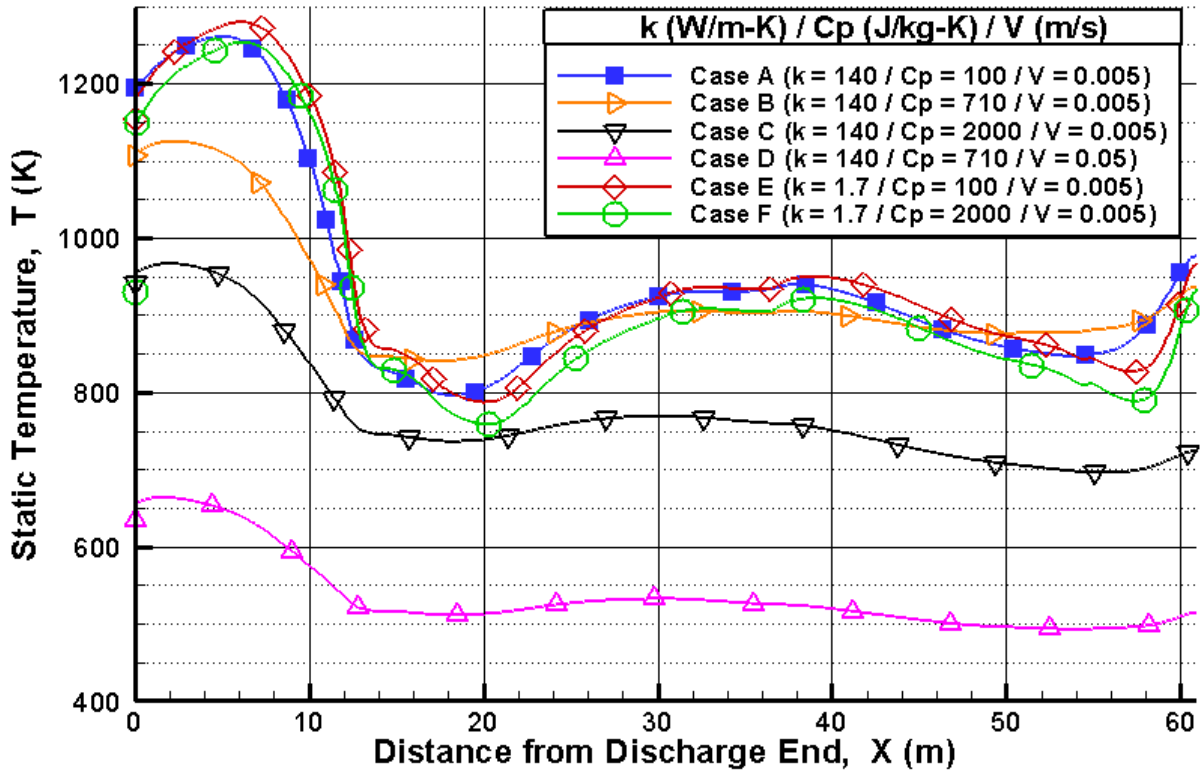

Figure 5.48 2-D coke bed temperature distributions for various bed properties (thermal conductivity/specific heat/bed moving velocity)

CHAPTER SIX

CONCLUSIONS

In this study, the computational simulation of petroleum coke calcination inside a rotary kiln has been conducted using the commercial code FLUENT. The simulations were conducted with different operating conditions and assumptions. The results provide comprehensive information concerning the thermal-flow behavior and combustion inside an industrial rotary kiln. The results show that for the baseline case the peak gas temperature reaches around 1,800 K (2,780 °F) at Z = 18 m in the calcining zone; the lowest gas temperature locates about 1,130 K (1,574 °F) at Z = 10 m between the calcined coke zone and calcining zone; and the exhaust gas temperature at the feed end is approximately 1,150 K (1,610 °F). The discharged calcined coke temperature is approximately at 1,300 K (1,880 °F). The highest coke bed surface temperature is 1,570 K (1,366 °F) occuring at Z = 18.4 m. The typical coke bed temperature difference between surface and bottom varies between 32 to 200 K (90 to 392 °F). For most of the part, the coke surface temperature is higher than the bottom temperature, but between Z = 0 and 17 m, the coke bottom is hotter than the surface. About 14.22 % of the volatiles (0.776 % of the total mass of gas) are not burned inside the kiln and are carried into the pyroscrubber.

Effects of Rotational Angles

Due to the different tertiary air injection angles, the gas temperatures slightly vary for each rotational angle. The 45° rotational angle case shows a better calcination with 100 K higher bed surface temperature at the discharge end compared to the rest of rotational angles. Without including the coke fines combustion and the coke bed, the lumped gas temperature for the

rotational cases shows a peak temperature of 1,400 K (2,060 °F) at the Z = 5 m due to natural gas combustion; the lowest temperature is around 1,075 K (1,475 °F) at two locations, Z = 10 and 20 m respectively. The exhaust gas temperature is approximately 1,100K (1,520 °F).

Effects of Tertiary Air Injection Angles

The case with 15° injection angle provides the best calcining condition: its bed surface temperature is 100 K higher than the case of 30° injection angle, and is 300 K higher than the case of 45° injection angle which shows an adverse cooling effect on the bed surface. Both 30° and 45° injections angles show increased flow disturbance on coke bed surface, which could increase coke fines entrainment and attrition rate. The current 15° injection angle is the optimum design; no change is needed.

Effects of Discharge End Flow Control

Employing gas extraction at the discharge end successfully draws the hot combustion gas from the tertiary air zone towards the discharge end without burning natural gas. The coke bed temperature between 6 and 21 m from the discharge end is successfully raised from 10 to 100 K, but discharge end temperature is reduced 150 K without burning natural gas. The extracted gas at 1,000 K (1,340 °F) is too low to be returned to the kiln, but it could be used to preheat the tertiary air.

Effects of Devolatilization Conditions

Coke fines combustion results in a much higher combustion temperature inside the kiln. An accurate modeling of the devolatilization location has a pronounced effect on the simulated temperature distribution.

Recommended Future Investigations

Based on the present studies, the following studies are recommended to improve calcination performance and conserve energy:

1. Develop and incorporate a coke fines entrainment model to predict the effect of the flow field on coke fines entrainment rates.
2. Include kiln wall (refractory bricks and steel shell) into the computational domain and apply convection outside the kiln.
3. Compare the effect of different turbulence and combustion models on the results.
4. Include variable property values of coke as a function of temperature.
5. Incorporate devolatilization and gasification models to simulate the volatiles releasing rate, reaction rate, and gasification phenomena inside the kiln.
6. Incorporate with the granular flow study and investigate the effectiveness of the tumblers (lifters) and wall effect on the thermal flow pattern.
7. Conduct experiments to improve the performance of the tumblers.

APPENDIX A

APPLICATION OF FLUENT CODE

In this study generalized eddy dissipation chemistry model with standard k - ε turbulence model is used to analyze the petroleum coke calcining system.

Step 1: Grids

1. Read the grid file

   FILE → READ → CASE

   After importing the grid file, FLUENT will report the number of cells that have been read, along with numbers of boundary faces with their zone identifiers.

2. Check the grid

   GRID → CHECK

   The grid check lists the minimum and maximum X, Y and Z values from the grid, and reports on a number of other grid features that are checked. Any errors in the grid would be reported at this time.

3. Scale the grid

   Since this grid was created in units of feet, the SCALE GRID panel will be used to scale the grid into meters.

   GRID → SCALE

   a. Under UNIT CONVERSION, select FT from the drop-down list to confirm that the GRID WAS CREATED IN FEET.

   b. Click on SCALE.

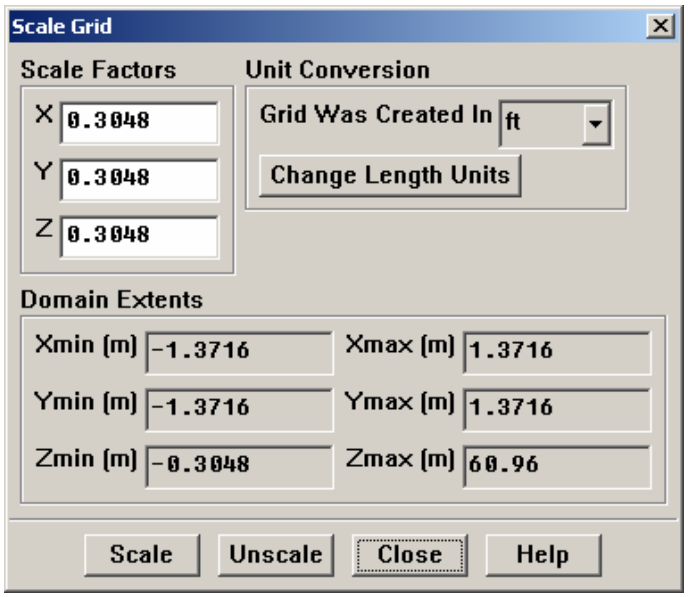

4. Display the grid

   DISPLAY → GRID

Step 2: Models

1. Define the domain space as 3-D, and choose segregated solver.

   DEFINE → MODELS → SOLVER

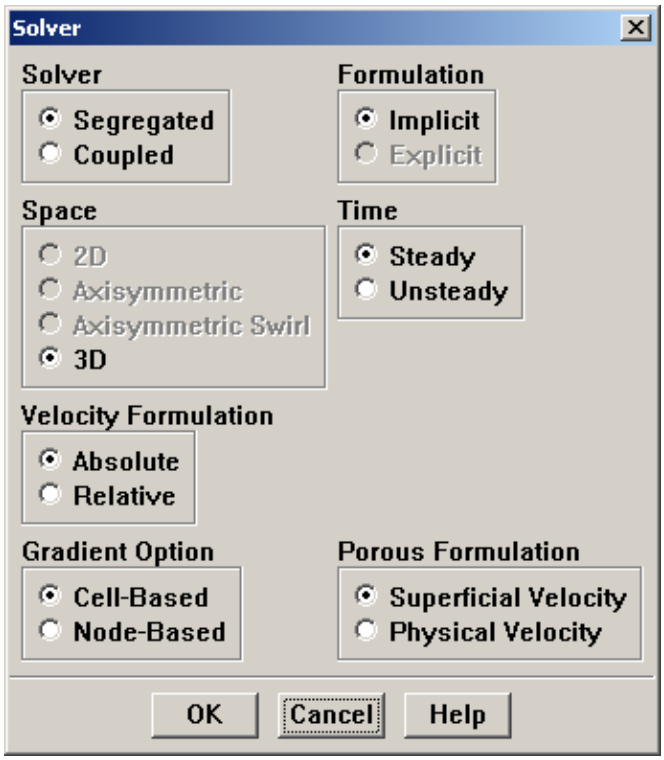

2. Enable heat transfer by activating the energy equation

   DEFINE → MODELS → ENERGY

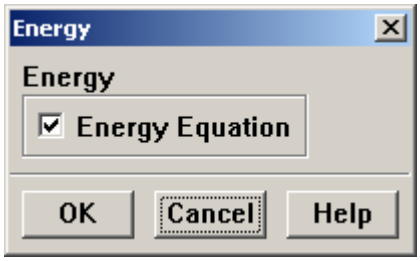

3. Enable the k – ε turbulence model

   DEFINE → MODELS → VISCOUS

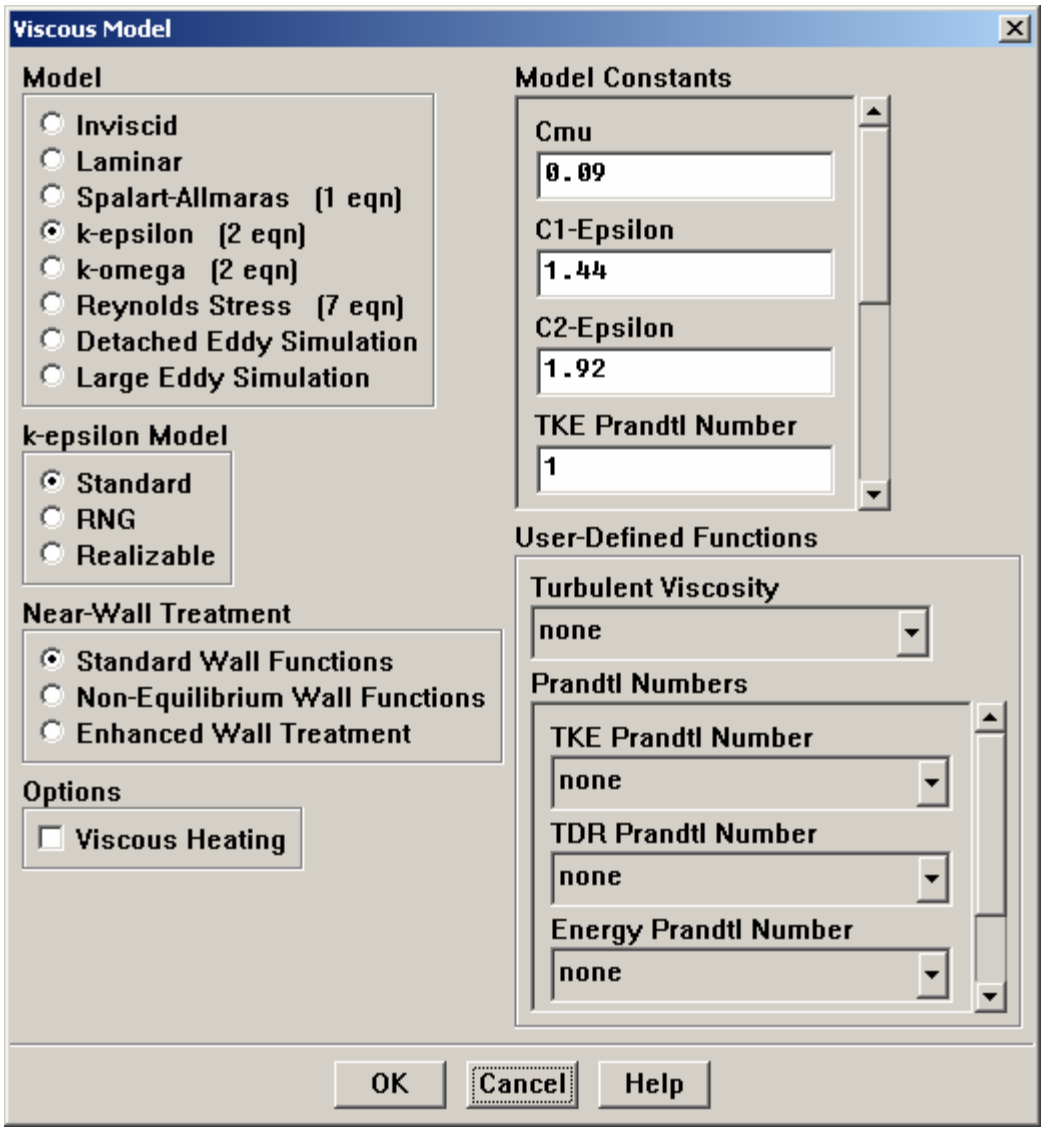

4. Enable P1 radiation model

   DEFINE → MODELS → RADIATION

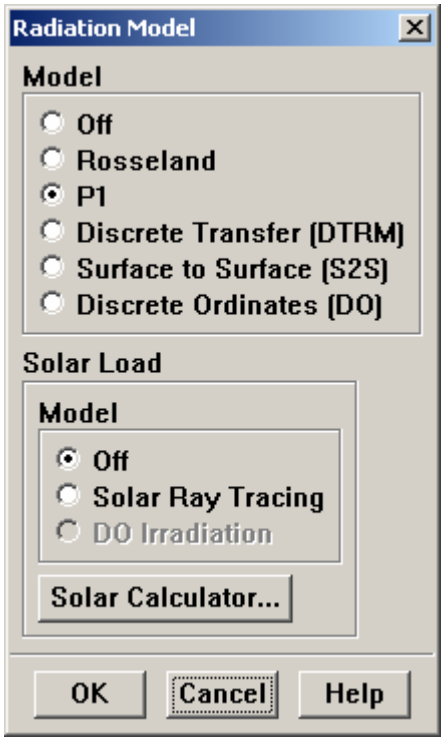

5. Enable chemical species transport and reaction

   DEFINE → MODELS → SPECIES

   a. Select SPECIES TRANSPORT under MODEL.

   b. Select VOLUMETRIC under REACTIONS.

   c. Choose COAL-MV-VOLATILES-AIR in the MIXTURE MATERIAL drop-down list. By selecting one of the pre-defined mixtures, the complete description of the reacting system including chemical species and their physical and thermodynamic properties are accessed.

   d. Select the EDDY-DISSIPATION option under TURBULENCE-CHEMISTRY INTERACTION. The eddy-dissipation model computes the rate of reaction under the

assumption that chemical kinetics are fast compared to the rate at which reactants are mixed by turbulent fluctuations (eddies).

e. Click OK.

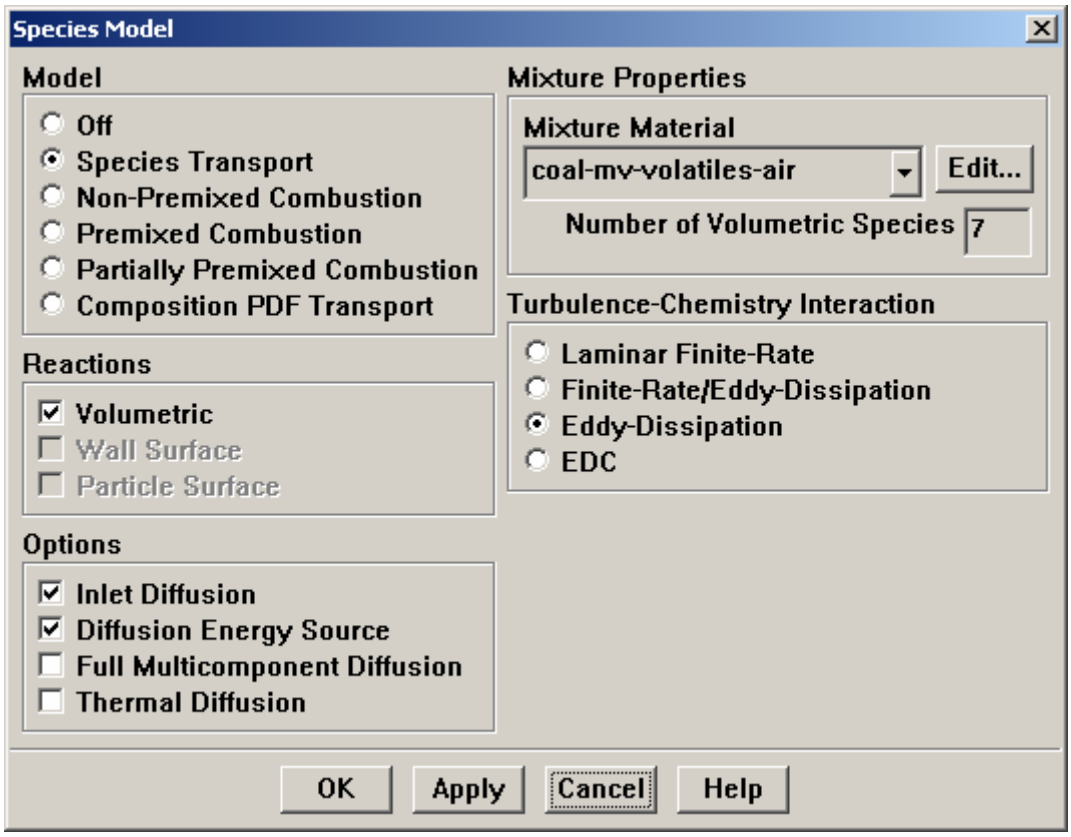

Step 3: Materials and Reactions

DEFINE → MATERIALS

1. The MATERIALS panel shows the mixture material, COAL-MV-VOLATILES-AIR, which was enabled in the SPECIES MODEL panel.

   Set ABSORPTION COEFFICIENT to 0.2 m^{-1}.

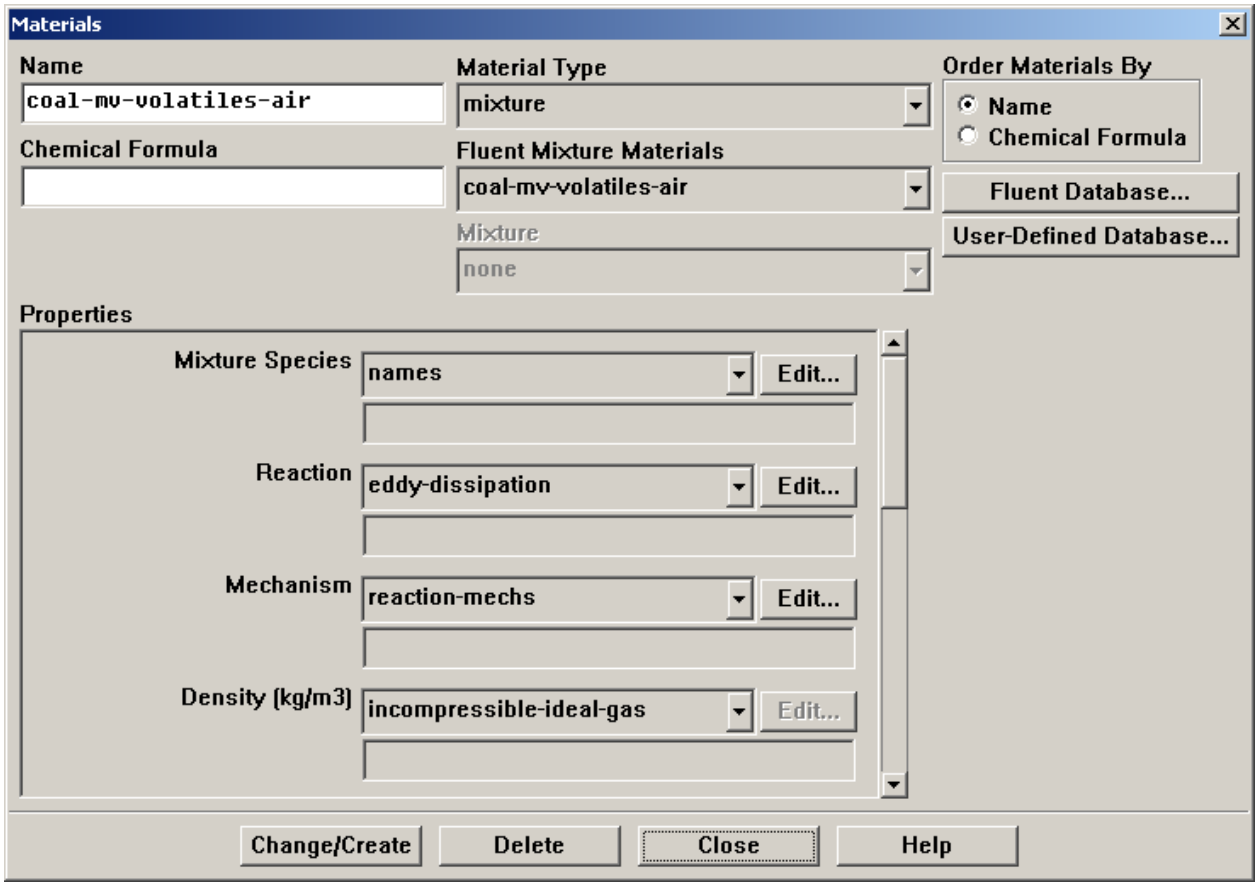

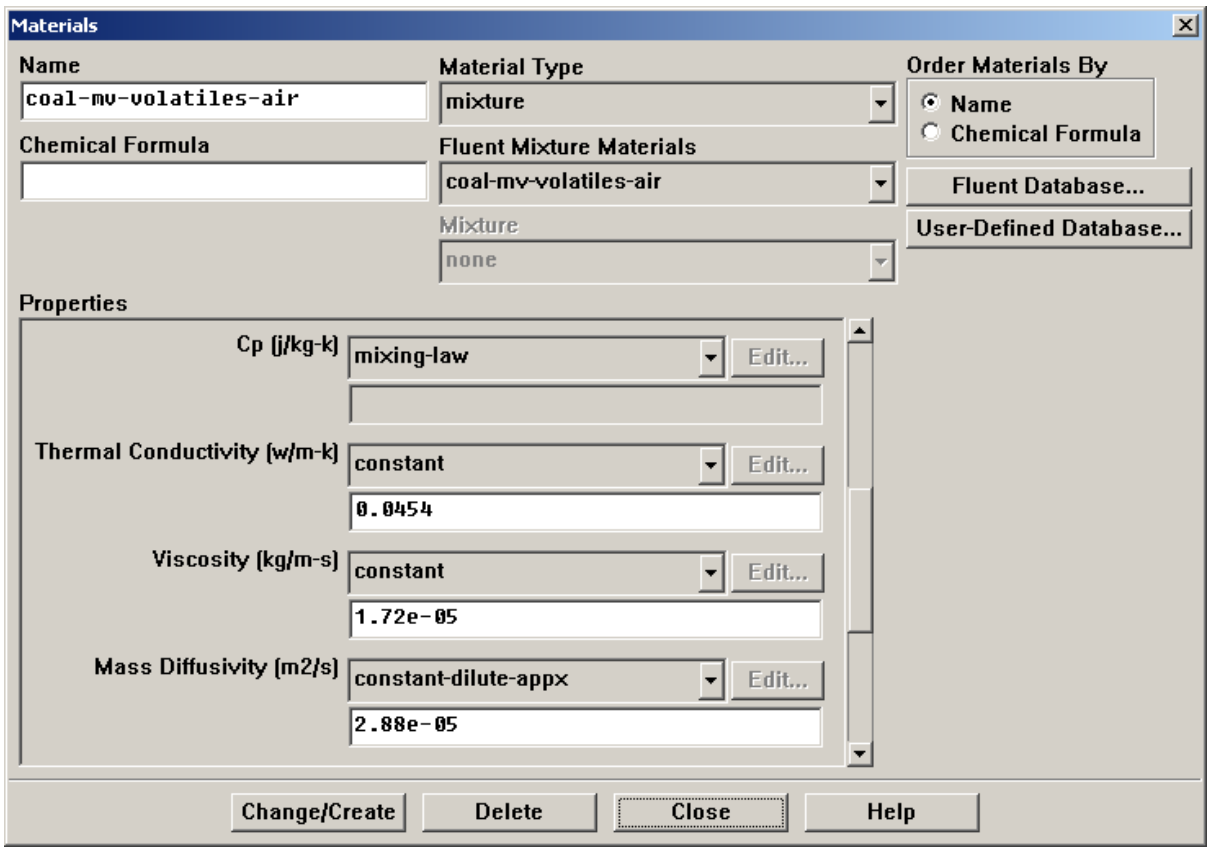
Materials
Name
coal-mv-volatiles-air
Material Type
mixture
Order Materials By
Name
Chemical Formula
Chemical Formula
Fluent Mixture Materials
coal-mv-volatiles-air
Fluent Database...
User-Defined Database...
Mixture
none
Properties
Cp (j/kg-k)
mixing-law
Edit...
Thermal Conductivity (w/m-k)
constant
0.0454
Viscosity (kg/m-s)
constant
1.72e-05
Mass Diffusivity (m2/s)
constant-dilute-appx
2.88e-05
Change/Create
Delete
Close
Help

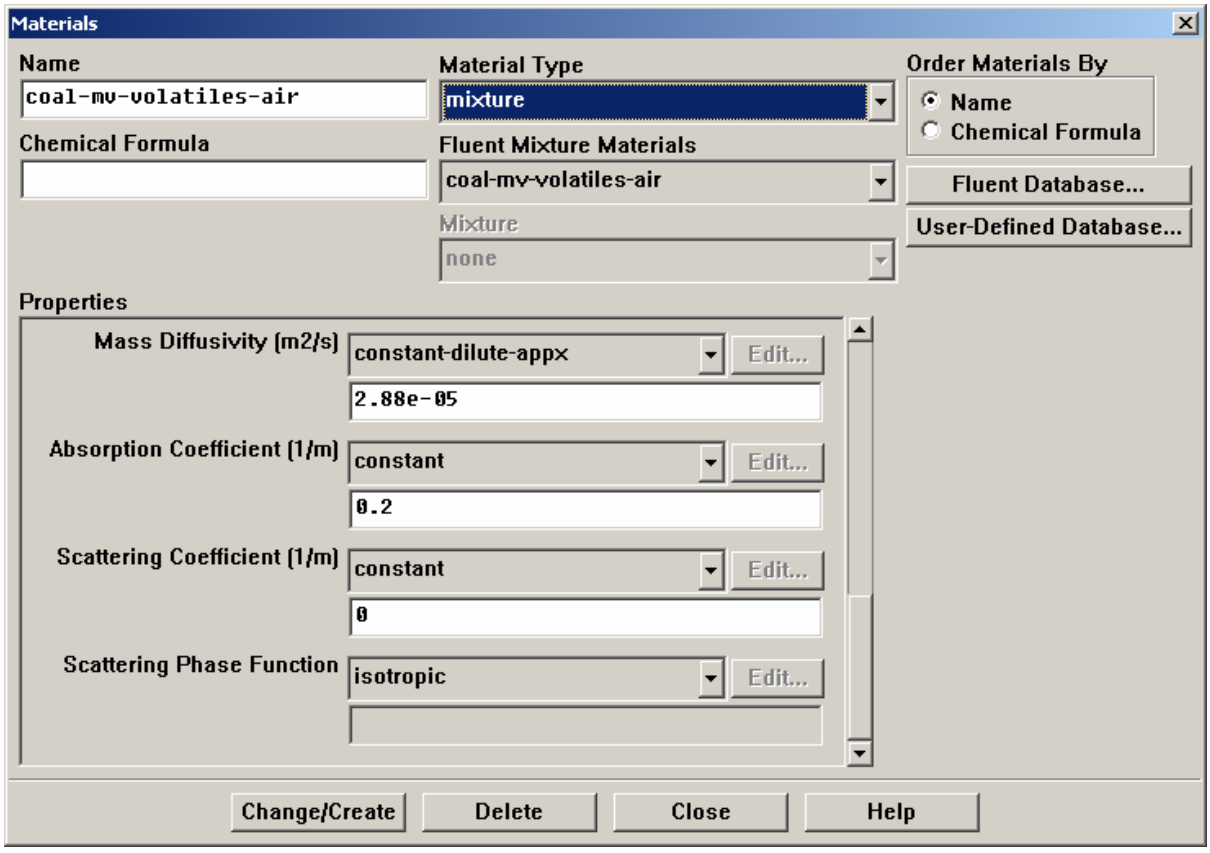
Materials
Name
coal-mv-volatiles-air
Material Type
mixture
Order Materials By
Name
Chemical Formula
Chemical Formula
Fluent Mixture Materials
coal-mv-volatiles-air
Fluent Database...
User-Defined Database...
Mixture
none
Properties
Mass Diffusivity (m2/s)
constant-dilute-appx
Edit...
2.88e-05
Absorption Coefficient (1/m)
constant
0.2
Scattering Coefficient (1/m)
constant
0
Scattering Phase Function
isotropic
Change/Create
Delete
Close
Help

2. Add other fluid species into the computational domain.

   From FLUENT DATABASE, in the MATERIAL TYPE drop-down list, choose FLUID.

   Select METHANE, CARBON, and click COPY.

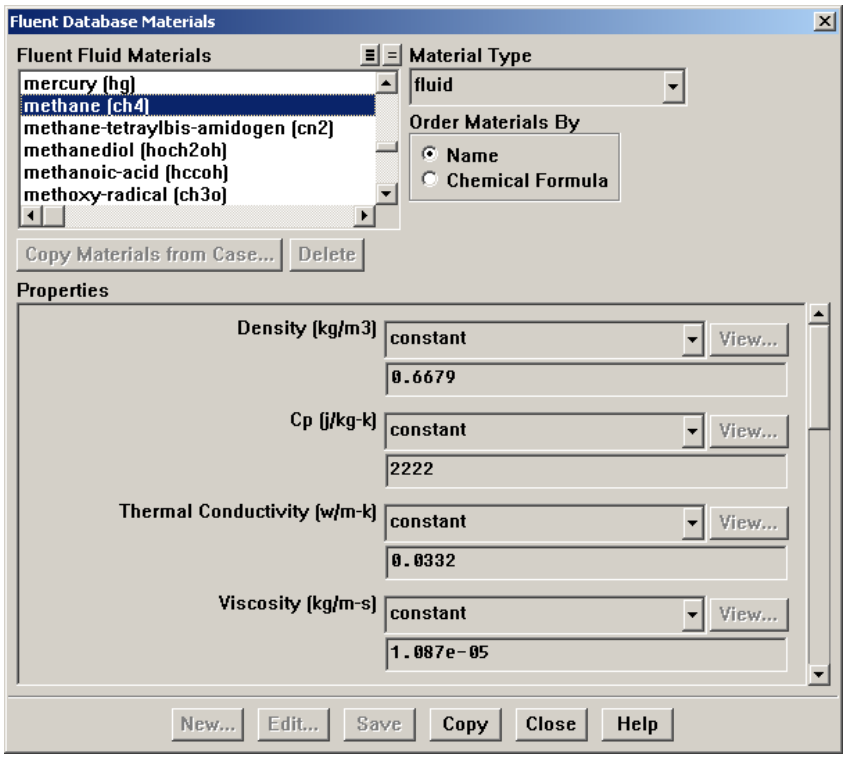

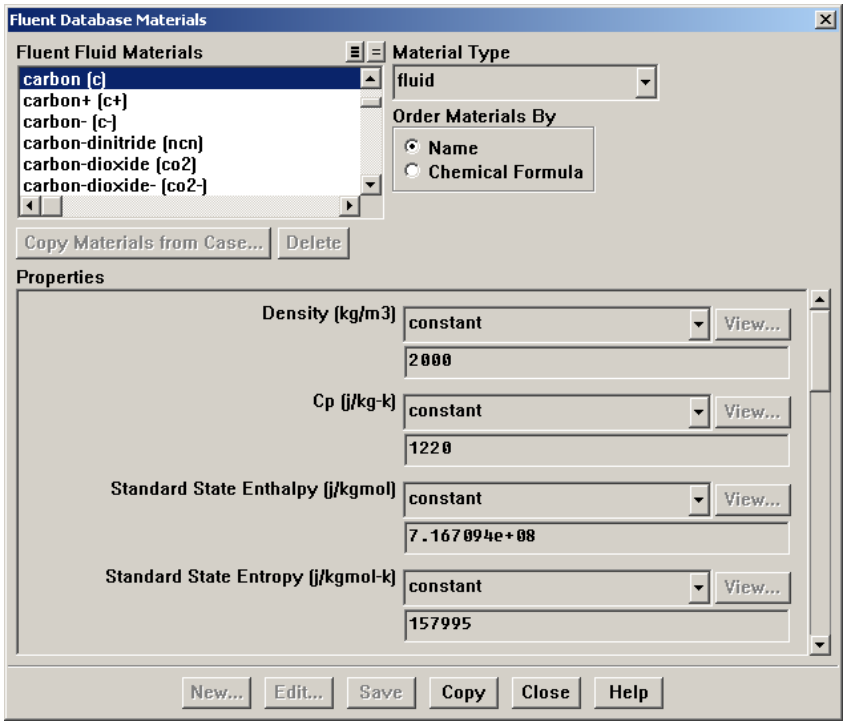

3. In the MATERIALS panel, choose FLUID from the MATERIAL TYPE drop-down list.
    a. Select CARBON, change the REFERENCE TEMPERATURE to 1,200 K and the ABSOPTION COEFFICIENT to 0.2 m^{-1}.
    b. Select COAL-MV-VOLATILES and change the REFERENCE TEMPERATURE to 1,200 K.
    c. Select AIR and change the ABSOPTION COEFFICIENT to 0.2 m^{-1}.

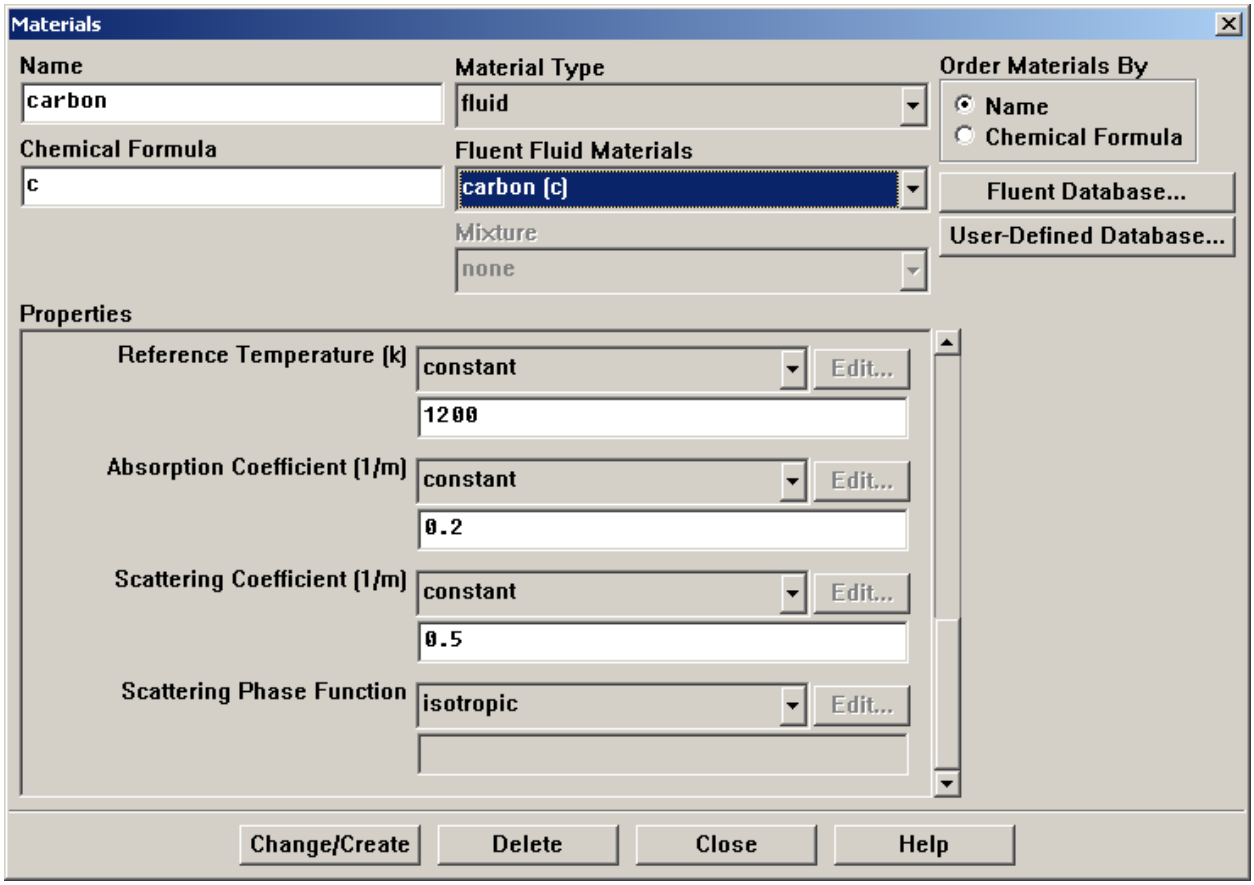

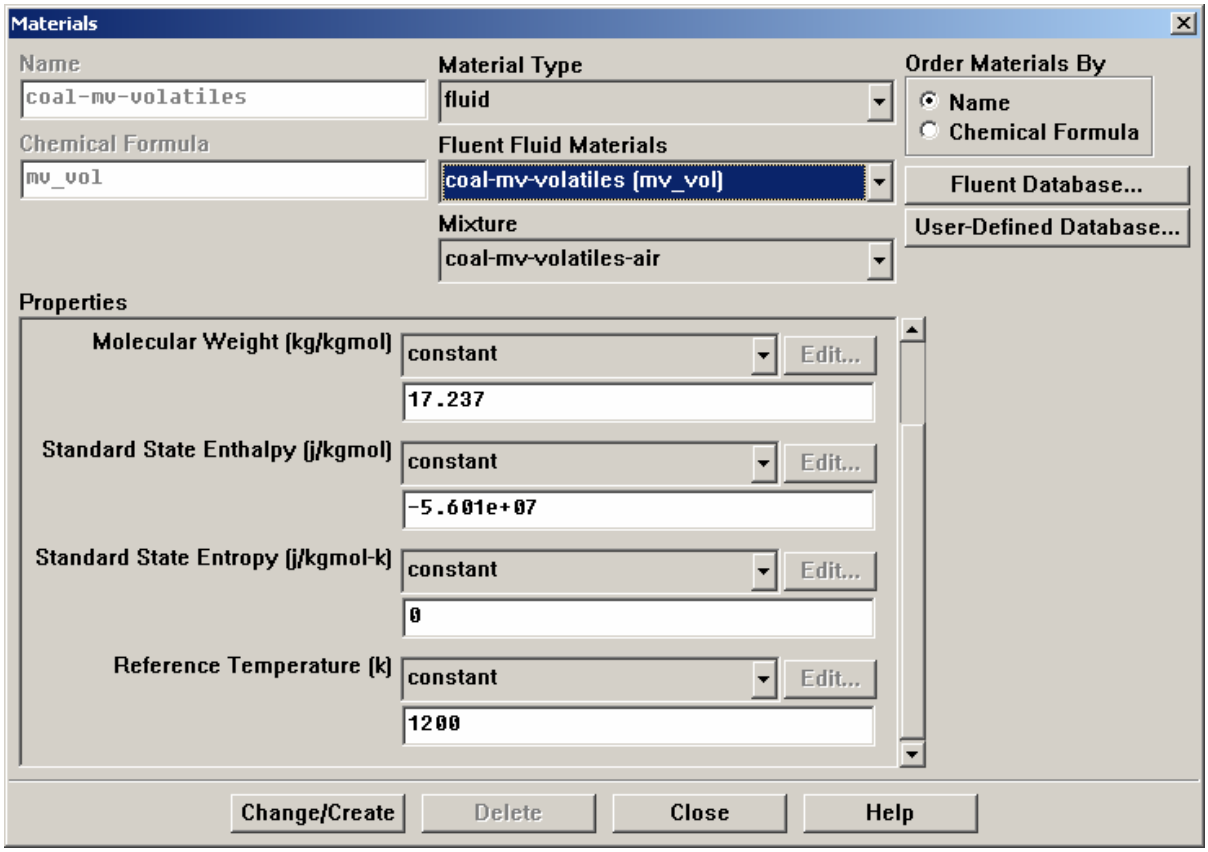
Materials
Name
coal-mv-volatiles
Material Type
fluid
Order Materials By
Name
Chemical Formula
Chemical Formula
mv_vol
Fluent Fluid Materials
coal-mv-volatiles (mv_vol)
Fluent Database...
Mixture
coal-mv-volatiles-air
User-Defined Database...
Properties
Molecular Weight (kg/kgmol)
constant
Edit...
17.237
Standard State Enthalpy (j/kgmol)
constant
Edit...
-5.601e+07
Standard State Entropy (j/kgmol-k)
constant
Edit...
0
Reference Temperature (k)
constant
Edit...
1200
Change/Create
Delete
Close
Help

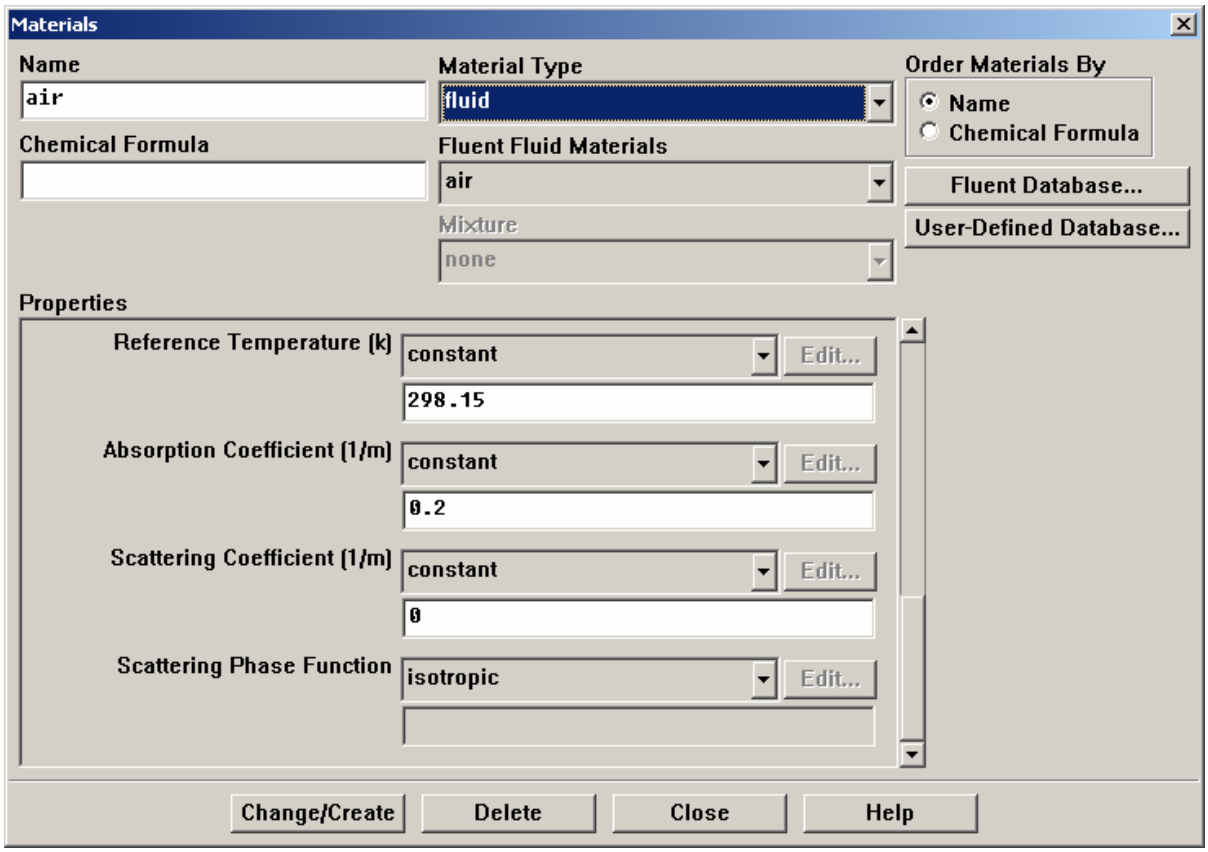
Materials
Name
air
Material Type
fluid
Order Materials By
Name
Chemical Formula
Chemical Formula
Fluent Fluid Materials
air
Fluent Database...
Mixture
none
User-Defined Database...
Properties
Reference Temperature (k)
constant
Edit...
298.15
Absorption Coefficient (1/m)
constant
Edit...
0.2
Scattering Coefficient (1/m)
constant
Edit...
0
Scattering Phase Function
isotropic
Edit...
Change/Create
Delete
Close
Help

4. In the MATERIALS panel, choose SOLID from the MATERIAL TYPE drop-down list. Change the NAME to COKE-BED-CARBON, CHEMICAL FORMULA to C-CARBON, and enter new material properties as DENSITY = 2,000 kg/m^3, c_p = 850 J/kg-K, and THERMAL CONDUCTIVITY = 100 W/m-K.

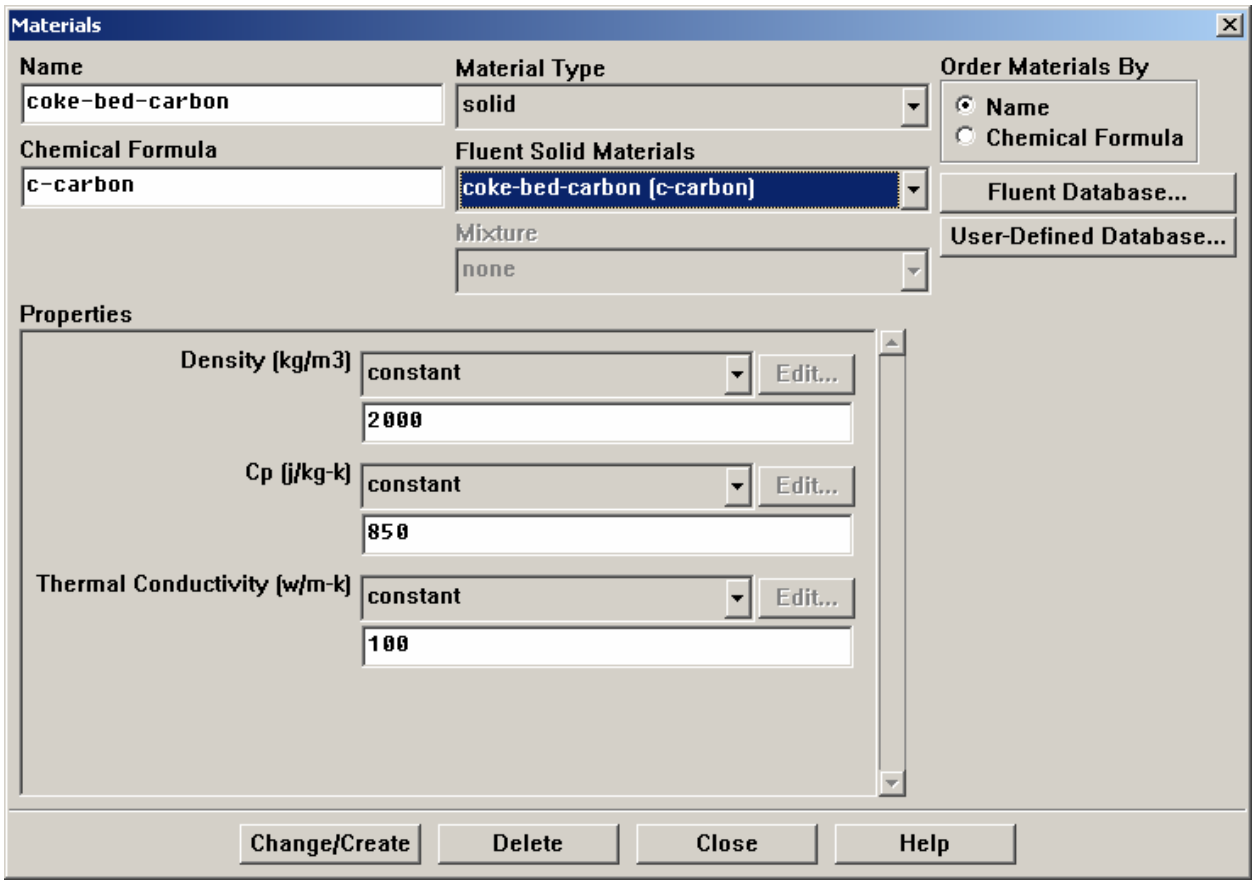

5. In the MATERIALS panel, choose MIXTURE from the MATERIAL TYPE drop-down list. Under PROPERTIES, click EDIT for MIXTURE SPECIES. Add all AVAILABLE MATERIALS into SELECTED SPECIES. Note: Make sure N_2 is the last species in the list.

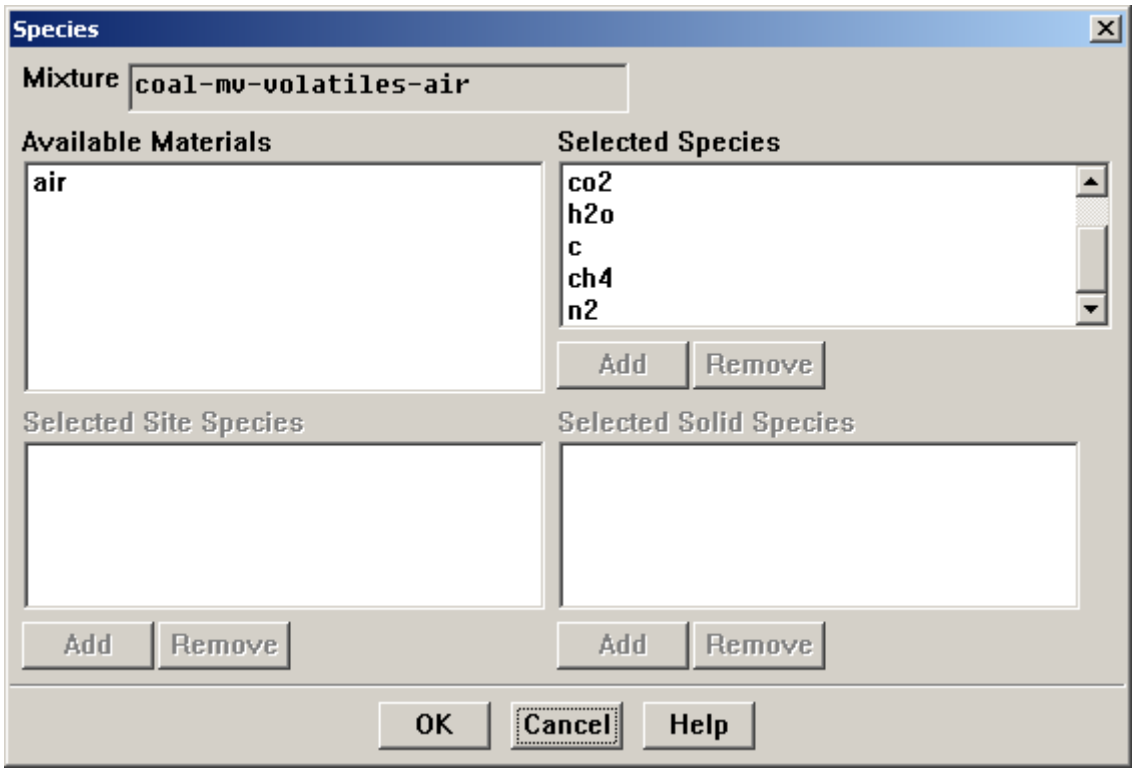

6. In the MATERIALS panel, choose MIXTURE from the MATERIAL TYPE drop-down list. Under PROPERTIES, click EDIT for REACTION.
   a. Increase TOTAL NUMBER OF REACTIONS to 3. Rename the first reaction in REACTION NAME box to VOLATILE COMBUSTION.
   b. Change ID to 2 and rename the second reaction in REACTION NAME box to METHANE COMBUSTION. Enter 2 for both NUMBER OF REACTANTS and PRODUCTS. For reactants, choose CH_4, O_2 and change O_2 STOICH. COEFFICEINT to 2. For products, choose CO_2, H_2O and change H_2O STOICH. COEFFICEINT to 2.

c. Change ID to 3 and rename the second reaction in REACTION NAME box to CARBON COMBUSTION. Enter 2 for NUMBER OF REACTANTS and 1 for NUMBER OF PRODUCTS. For reactants, choose C and O_2. For products, choose CO_2.

d. Click OK and click CHANGE/CREATE.

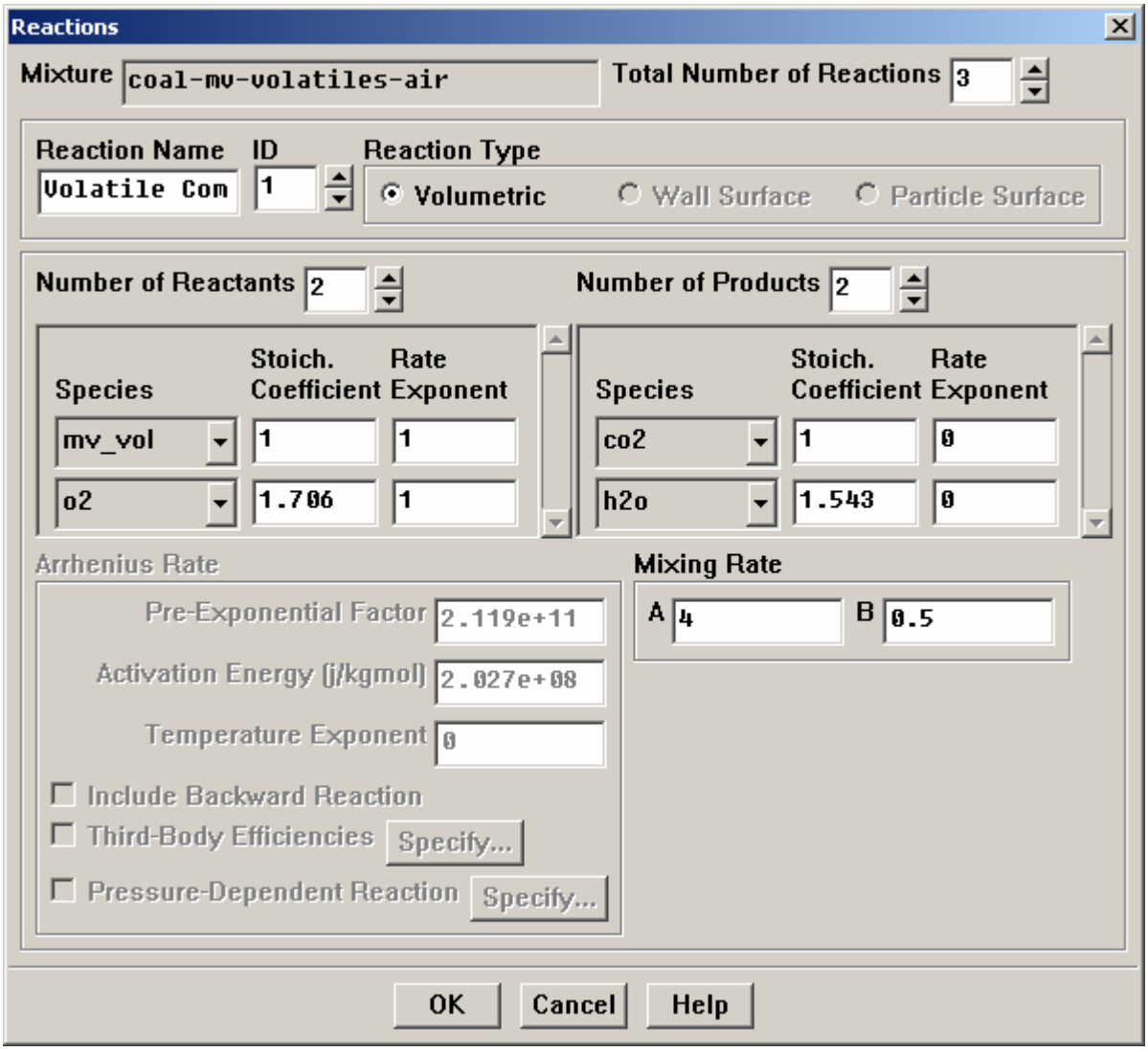

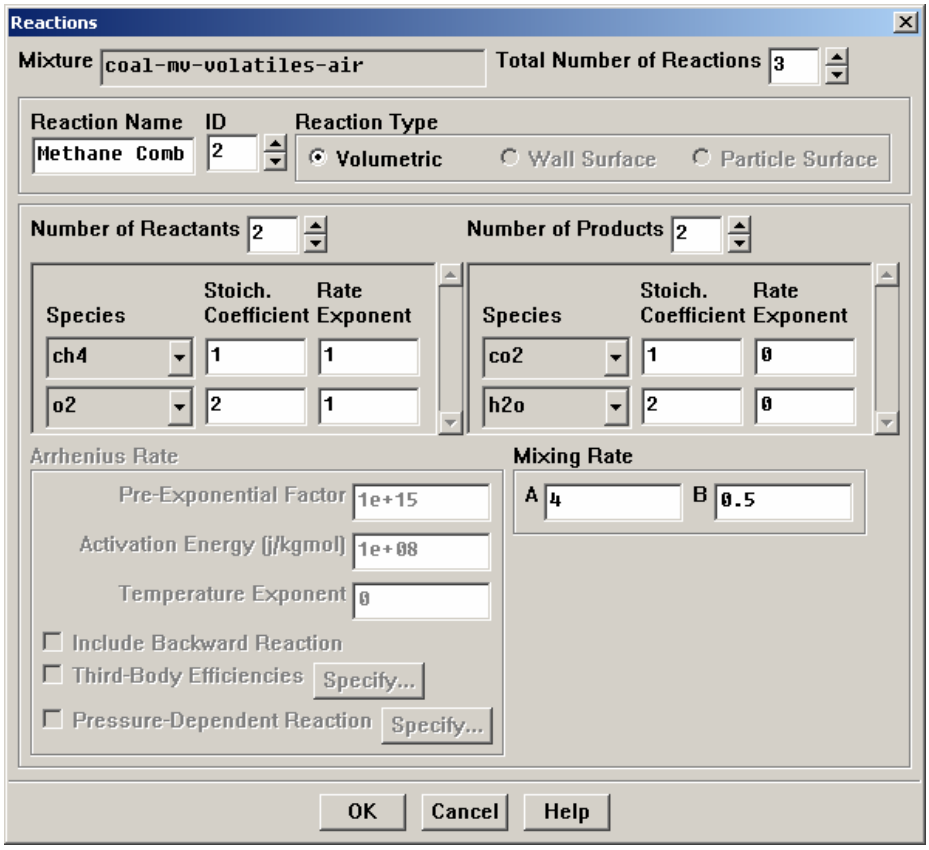
Reactions
Mixture
coal-mv-volatiles-air
Total Number of Reactions
3
Reaction Name
Methane Comb
ID
2
Reaction Type
Volumetric
Wall Surface
Particle Surface
Number of Reactants
2
Number of Products
2
Species
Stoich. Coefficient
Rate Exponent
ch4
1
1
o2
2
1
co2
1
0
h2o
2
0
Arrhenius Rate
Pre-Exponential Factor
1e+15
Activation Energy (j/kgmol)
1e+08
Temperature Exponent
0
Include Backward Reaction
Third-Body Efficiencies
Specify...
Pressure-Dependent Reaction
Specify...
Mixing Rate
A
4
B
0.5
OK
Cancel
Help

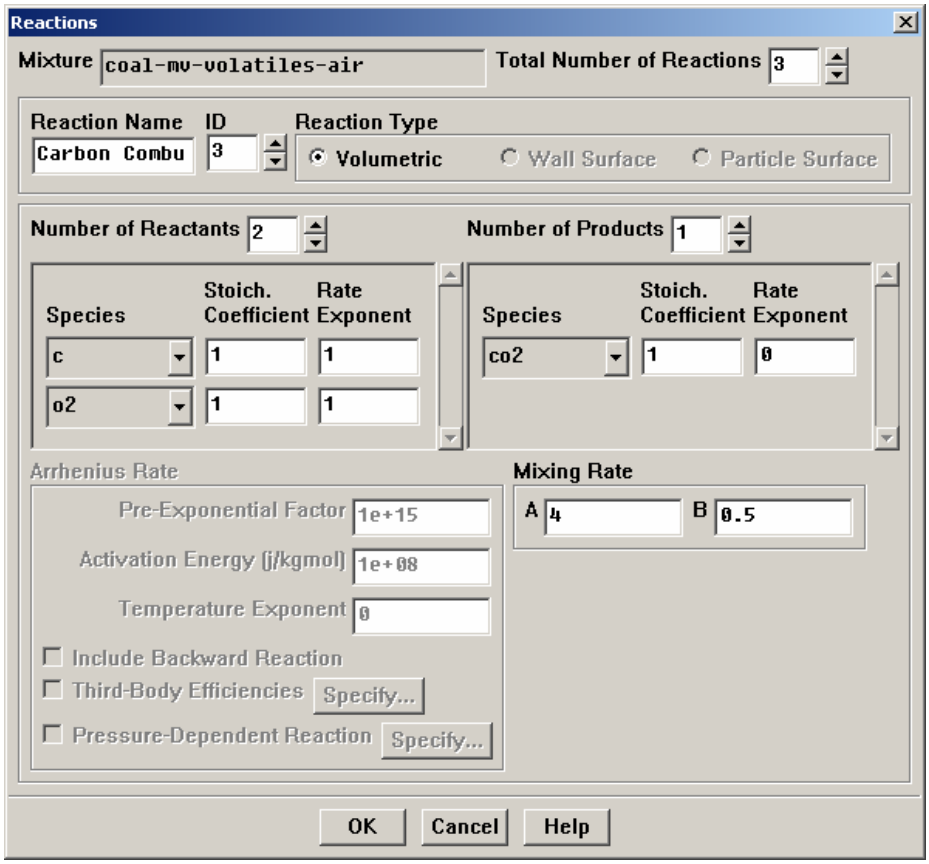
Reactions
Mixture
coal-mv-volatiles-air
Total Number of Reactions
3
Reaction Name
Carbon Combu
ID
3
Reaction Type
Volumetric
Wall Surface
Particle Surface
Number of Reactants
2
Number of Products
1
Species
Stoich. Coefficient
Rate Exponent
c
1
1
o2
1
1
co2
1
0
Arrhenius Rate
Pre-Exponential Factor
1e+15
Activation Energy (j/kgmol)
1e+08
Temperature Exponent
0
Include Backward Reaction
Third-Body Efficiencies
Specify...
Pressure-Dependent Reaction
Specify...
Mixing Rate
A
4
B
0.5
OK
Cancel
Help

Step 4: Interface Coupling

DEFINE → GRID INTERFACES

1. In the INTERFACE ZONE 1 window, select BED_CALCINED_LOWER, and select BED_CALCINED_UPPER in the INTERFACE ZONE 2. Check COUPLED under INTERFACE TYPE. Name it as BED_CALCINED in GRID INTERFACE box. Click CREATE.
2. Repeat 1 for BED_CALCINING and BED_HEATUP.

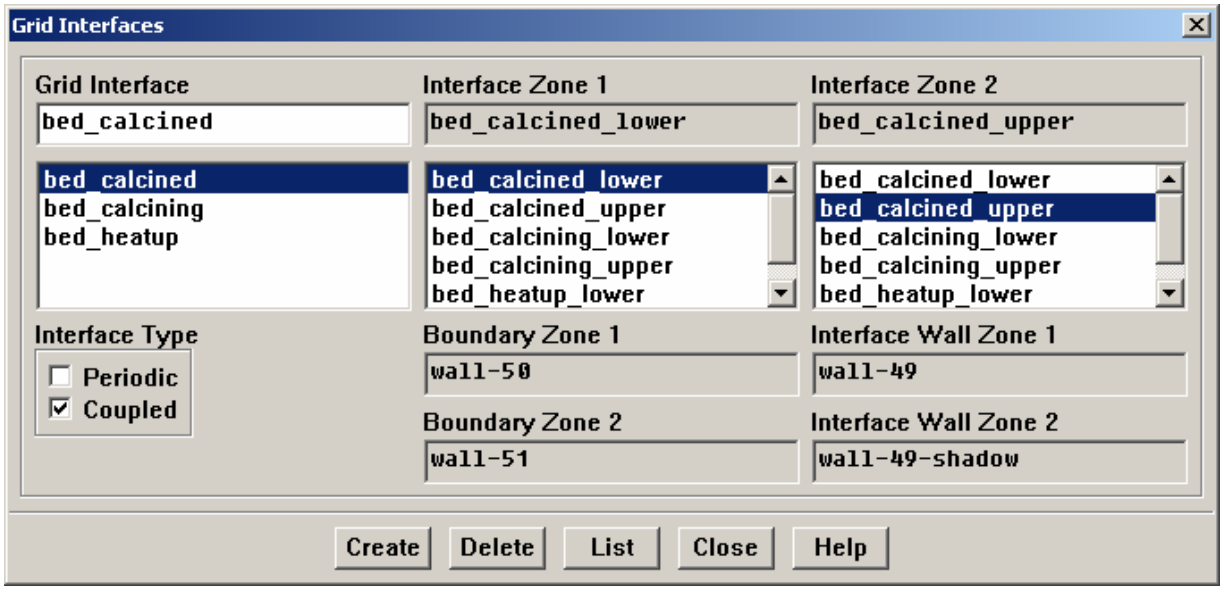

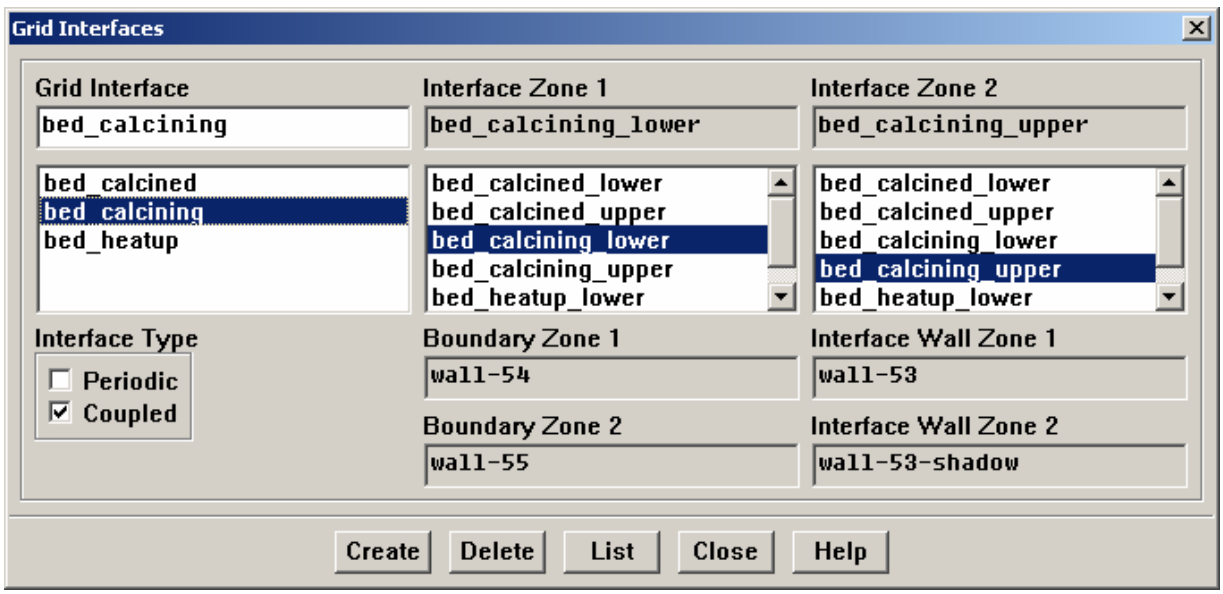

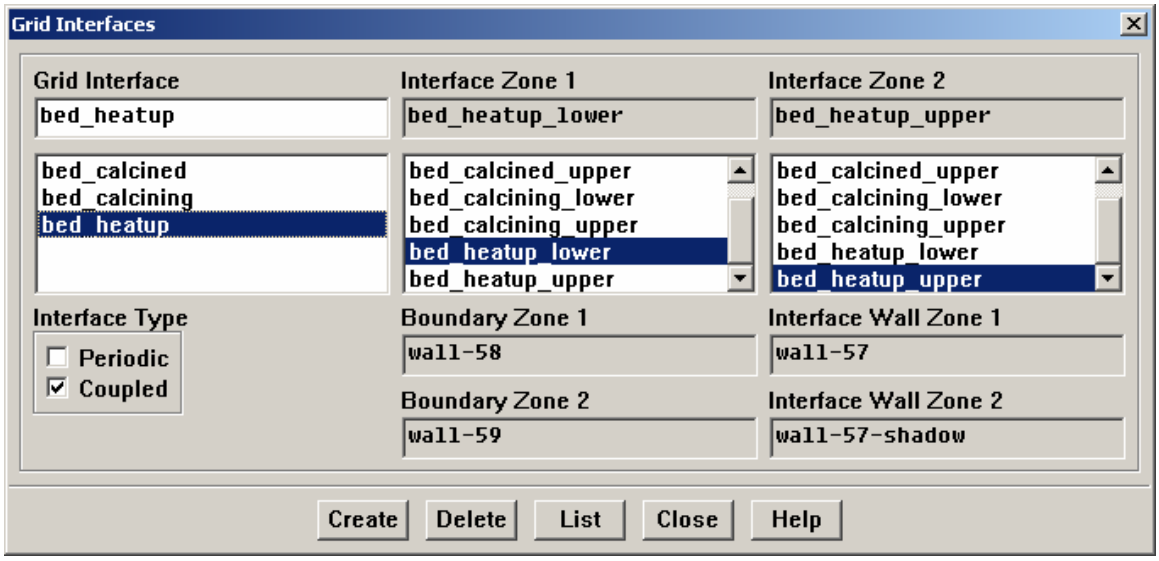

Step 5: Boundary Conditions

DEFINE → BOUNDARY CONDITIONS

1. Select BED_CALCINED_ZONE under ZONE. Change MOTION TYPE to MOVING REFERENCE FRAME and set Z = – 0.01 under TRANSLATIONAL VELOCITY box.
2. Repeat for BED_CALCINING_ZONE and BED_HEATUP_ZONE.

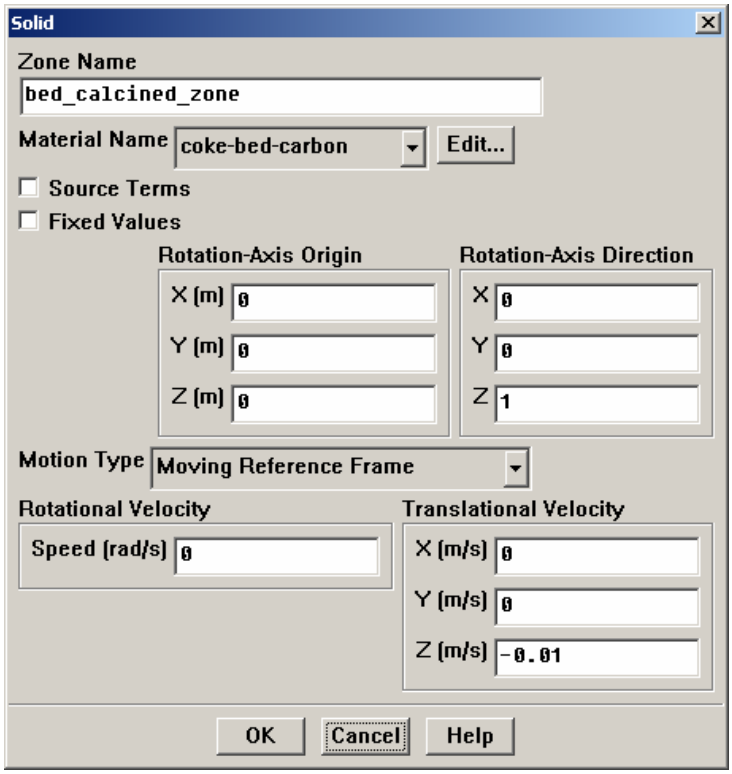

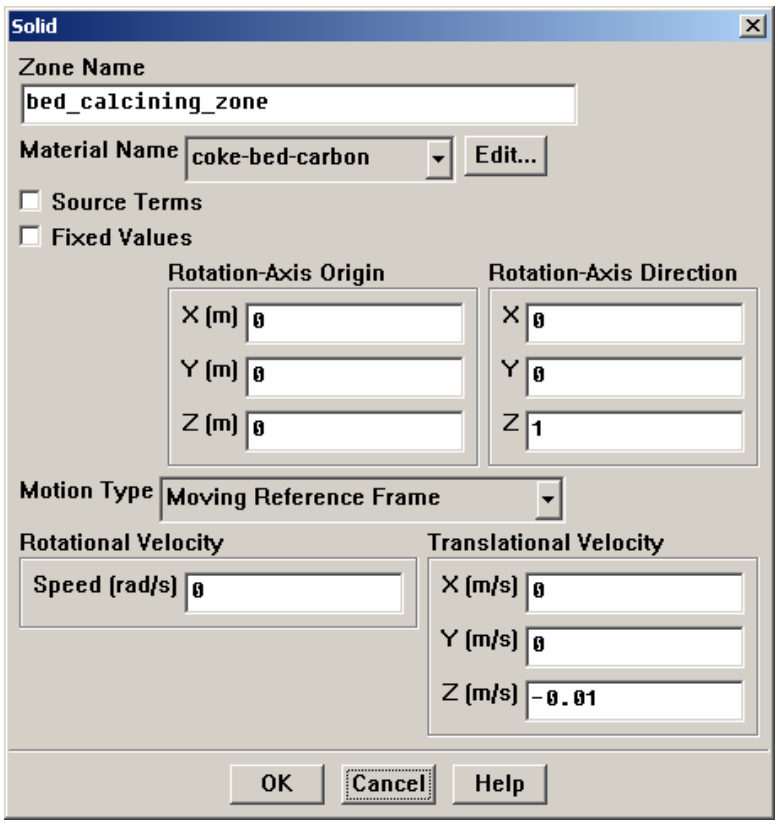
Solid
Zone Name
bed_calcining_zone
Material Name
coke-bed-carbon
Edit...
Source Terms
Fixed Values
Rotation-Axis Origin
X (m) 0
Y (m) 0
Z (m) 0
Rotation-Axis Direction
X 0
Y 0
Z 1
Motion Type
Moving Reference Frame
Rotational Velocity
Speed (rad/s) 0
Translational Velocity
X (m/s) 0
Y (m/s) 0
Z (m/s) -0.01
OK
Cancel
Help

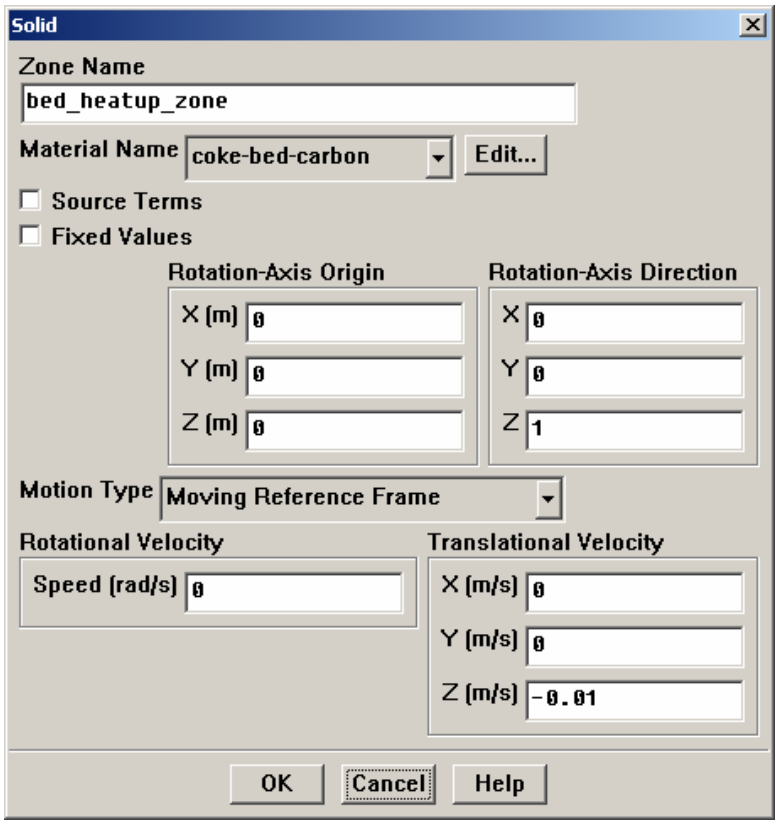
Solid
Zone Name
bed_heatup_zone
Material Name
coke-bed-carbon
Edit...
Source Terms
Fixed Values
Rotation-Axis Origin
X (m) 0
Y (m) 0
Z (m) 0
Rotation-Axis Direction
X 0
Y 0
Z 1
Motion Type
Moving Reference Frame
Rotational Velocity
Speed (rad/s) 0
Translational Velocity
X (m/s) 0
Y (m/s) 0
Z (m/s) -0.01
OK
Cancel
Help

3. Select COKE_FEEDEND under ZONE. Set constant TEMPERATURE at 300 K.

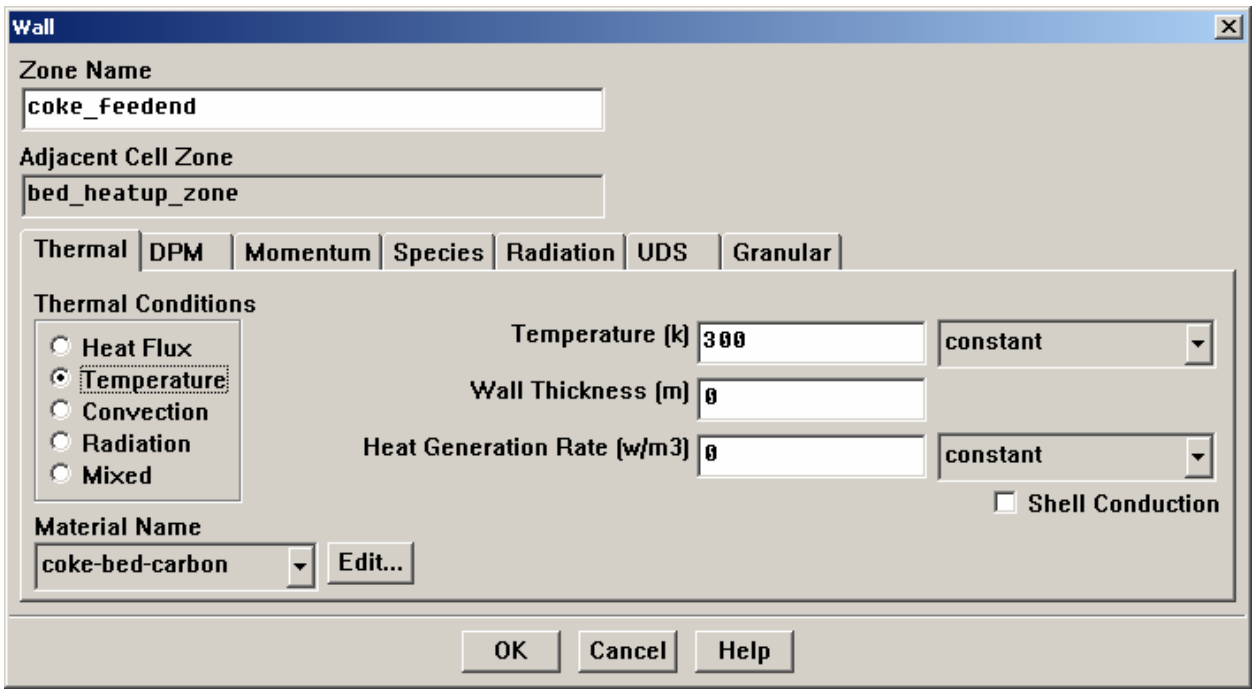

4. Select GAS_BURNCOKE_ZONE under ZONE. Enable SOURCE TERMS. Under SOURCE TERMS tab set MASS and C to CONSTANT (0.0505 kg/m^3-s)

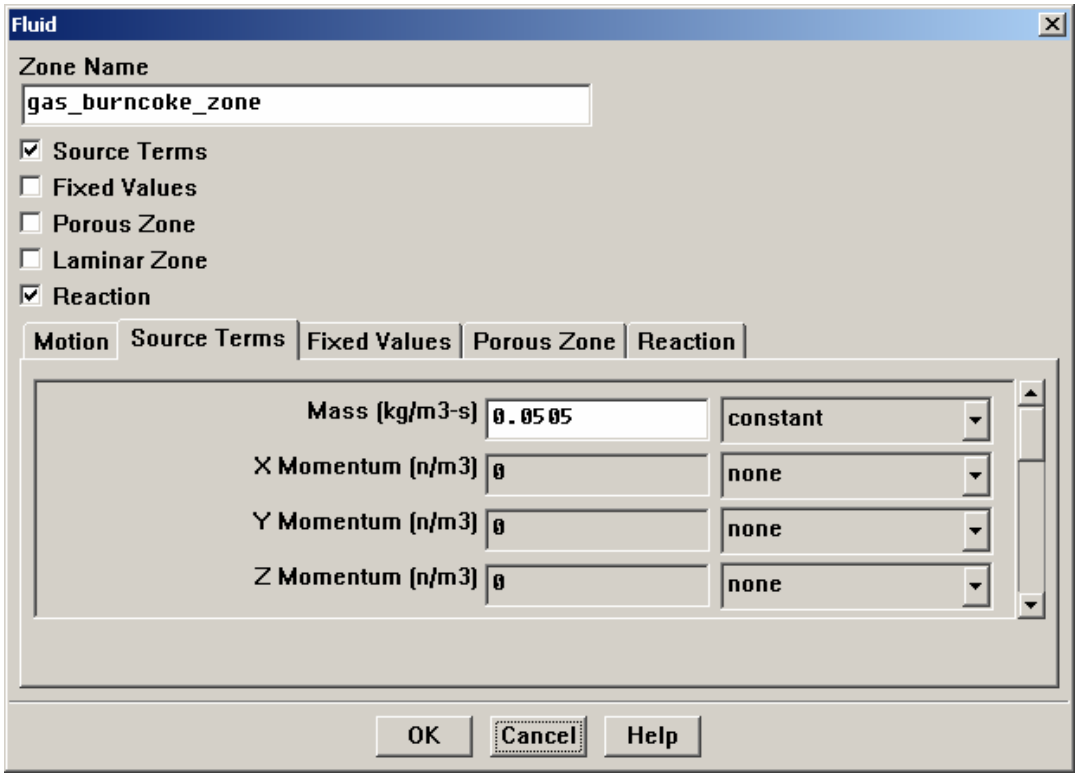

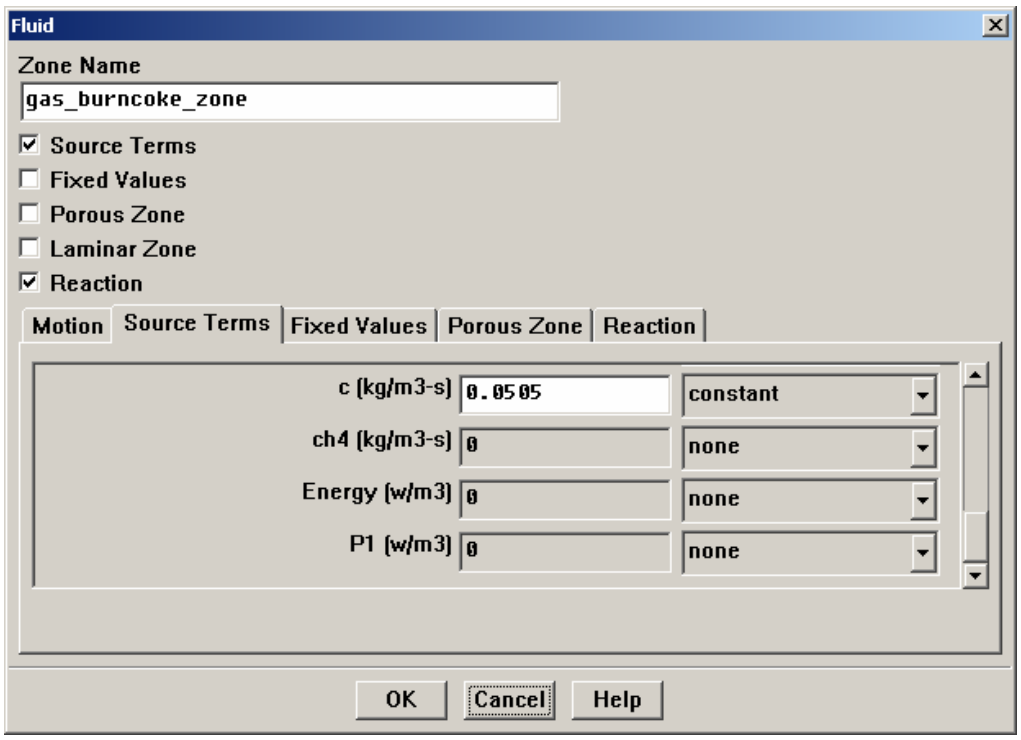

5. Select GAS_VOLATILE_ZONE under ZONE. Enable SOURCE TERMS. Under SOURCE TERMS tab set MASS to CONSTANT (0.2039 kg/m^3-s), MV_VOL to CONSTANT (0.1534 kg/m^3-s), and C to CONSTANT (0.0505 kg/m^3-s).

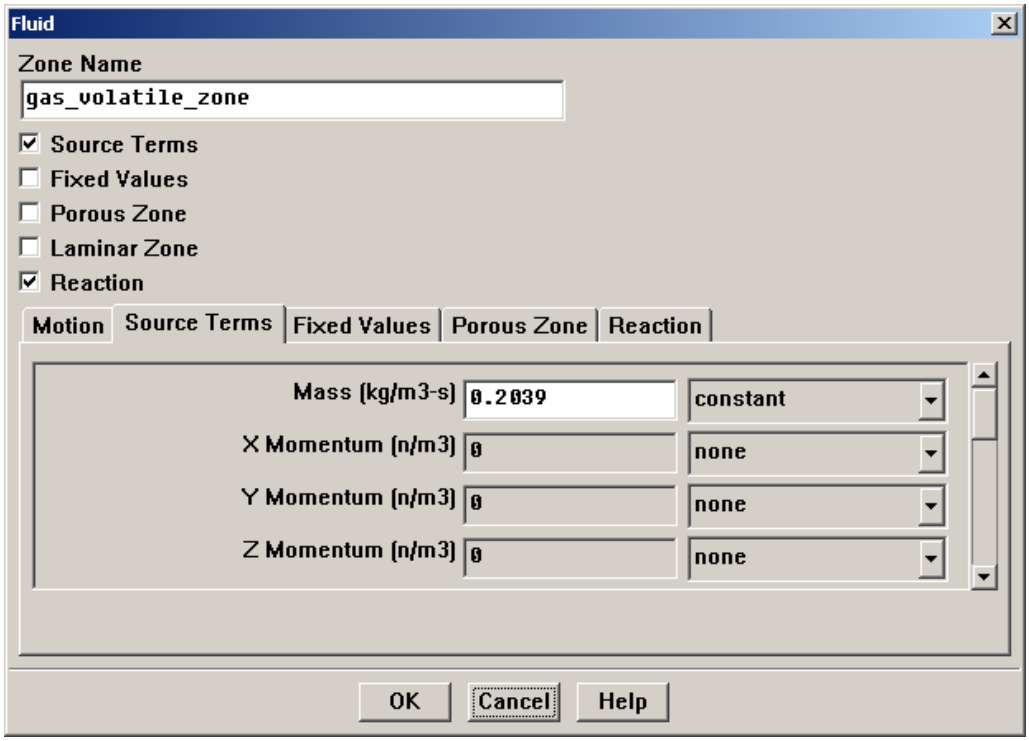

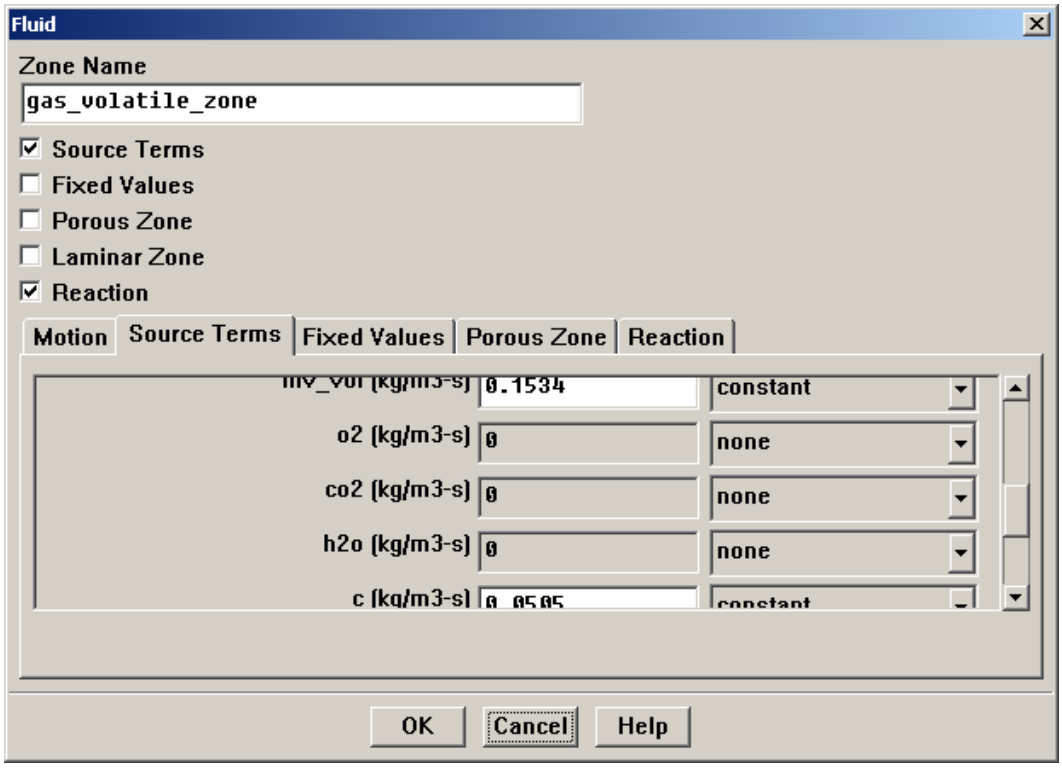

6. Select GAS_VAPOR_ZONE under ZONE. Enable SOURCE TERMS. Under SOURCE TERMS tab set ENERGY to CONSTANT (–346,989.3 W/m^3).

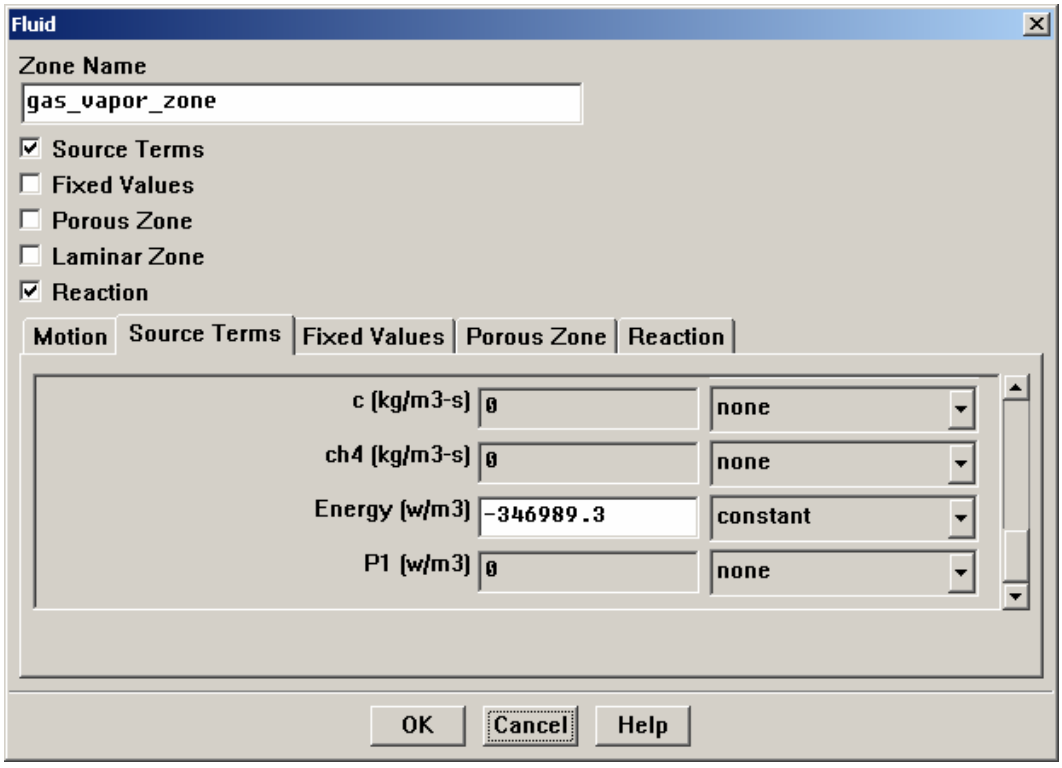

7. Select INLET_MAIN under ZONE. Enter VELOCITY MAGNITUDE = 20 m/s, TEMPERATURE = 300 K. Under SPECIES MASS FRACTIONS, enter 0.22 for O_2 and 0.043 for CH_4.

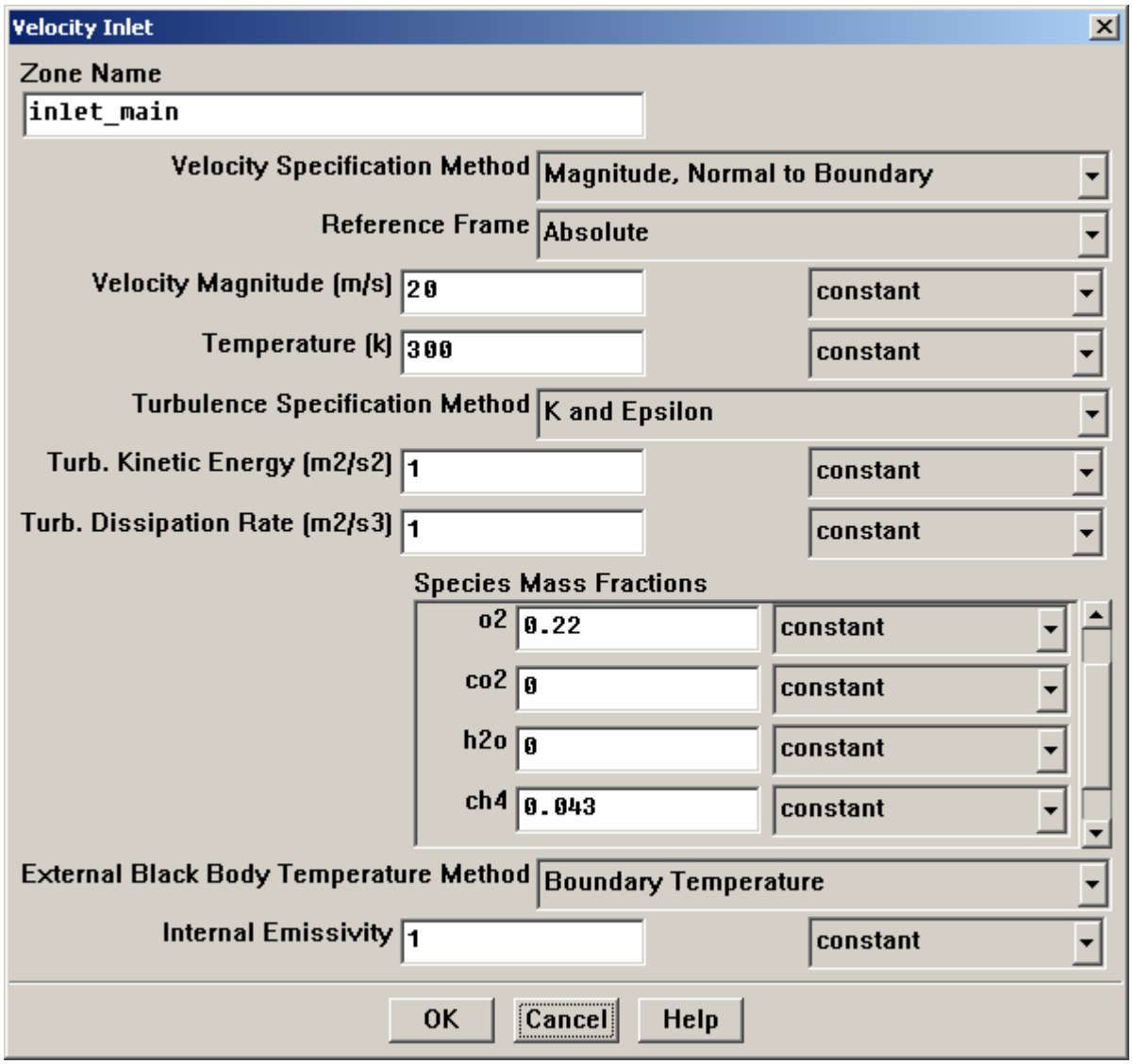

8. Select INLET_TERTIARY under ZONE. Enter VELOCITY MAGNITUDE = 50 m/s, TEMPERATURE = 300 K. Under SPECIES MASS FRACTIONS, enter 0.23 for O_2.

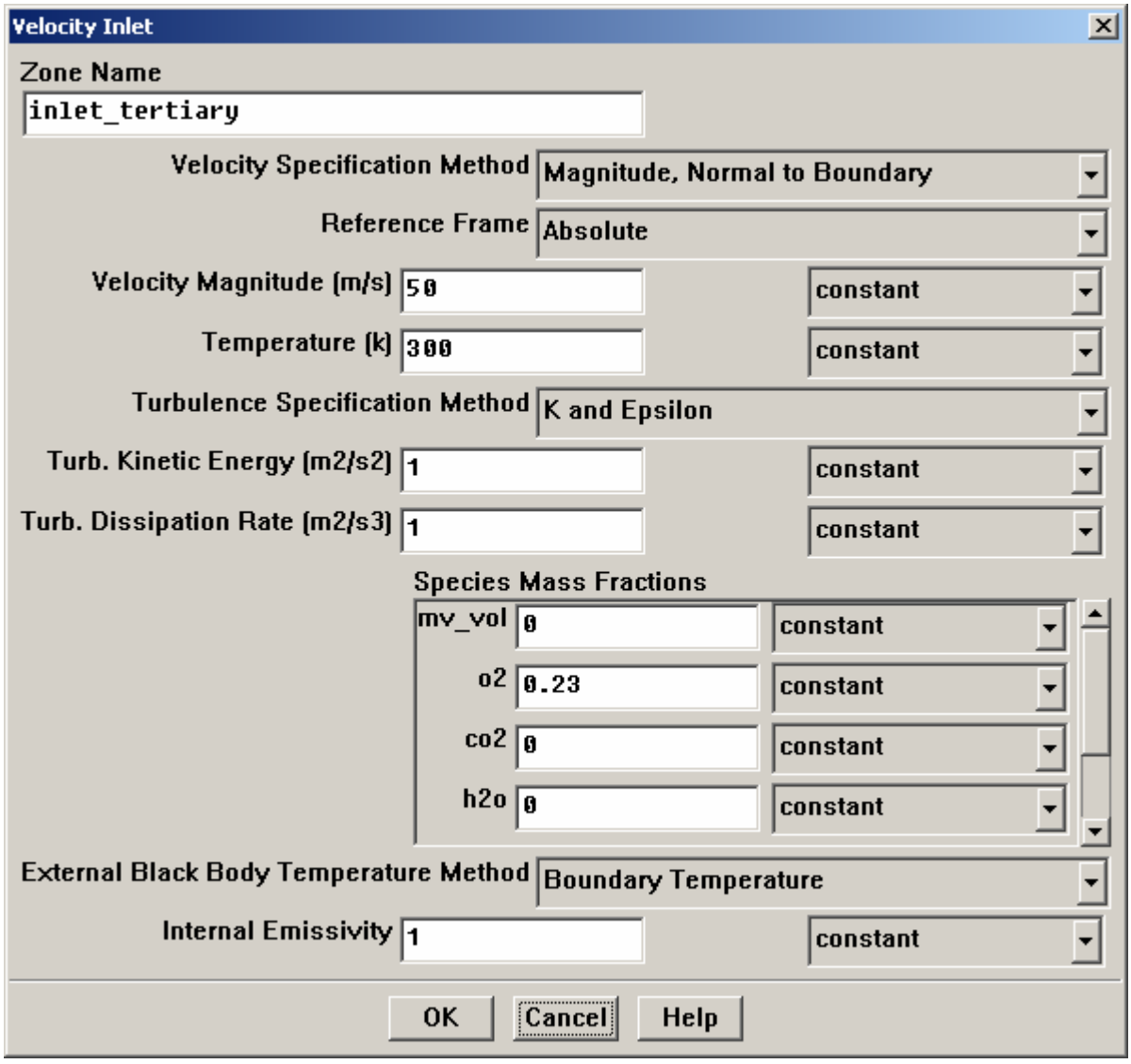

9. Select OUTLET_GAS under ZONE. Enter GAUGE PRESSURE = 0 Pascal, TEMPERATURE = 300 K.

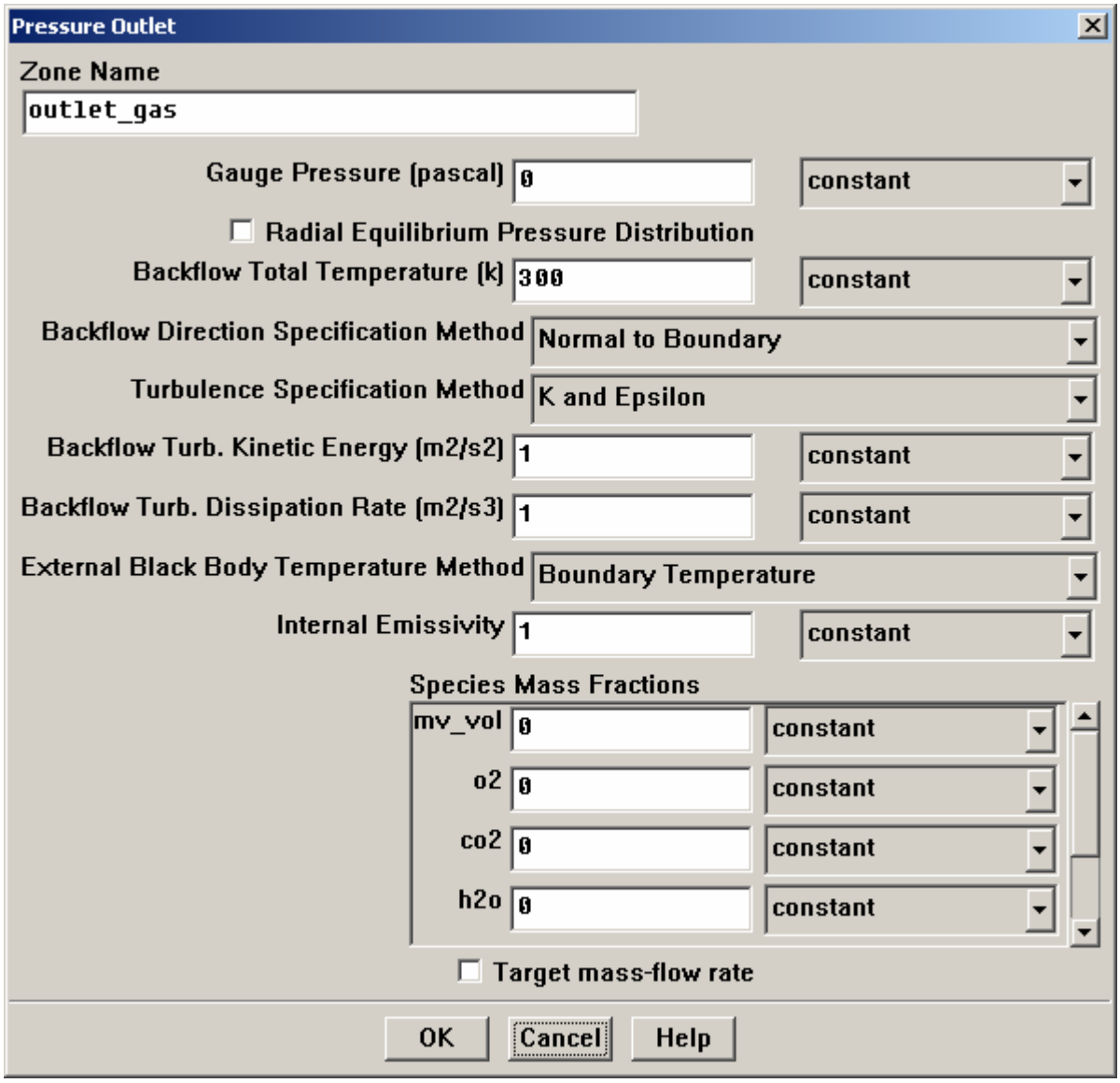

10. Select OUTLET_VAPOR under ZONE. Enter GAUGE PRESSURE = 0 Pascal, TEMPERATURE = 300 K.

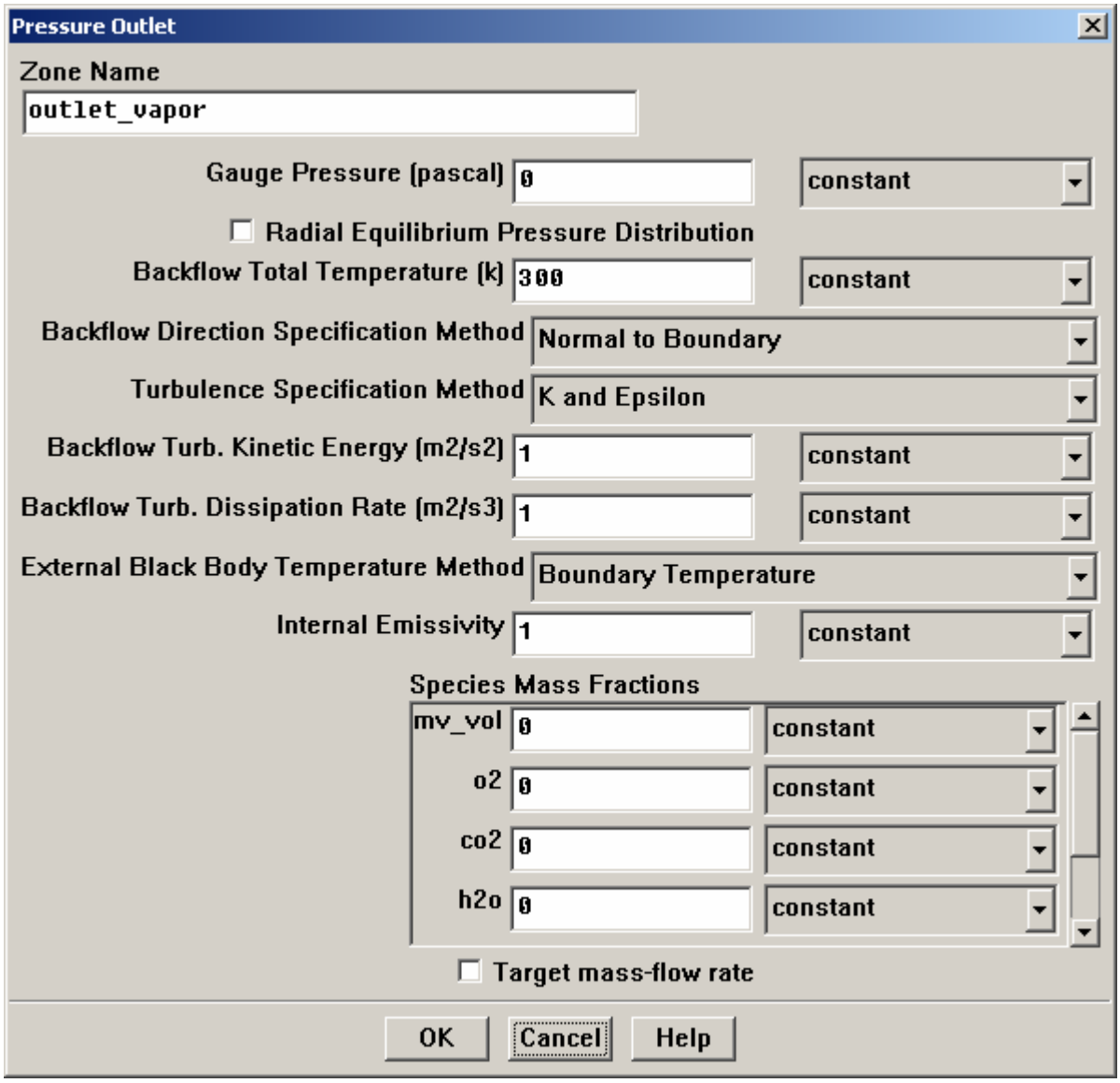

11. Select WALL_GAS_CALCINED_ZONE under ZONE. Under MOMENTUM tab select MOVING WALL for WALL MOTION. Choose ROTATIONAL and ABSOLUTE under MOTION. Set SPEED to 0.133 rad/s and ROTATION-AXIS is Z-axis.

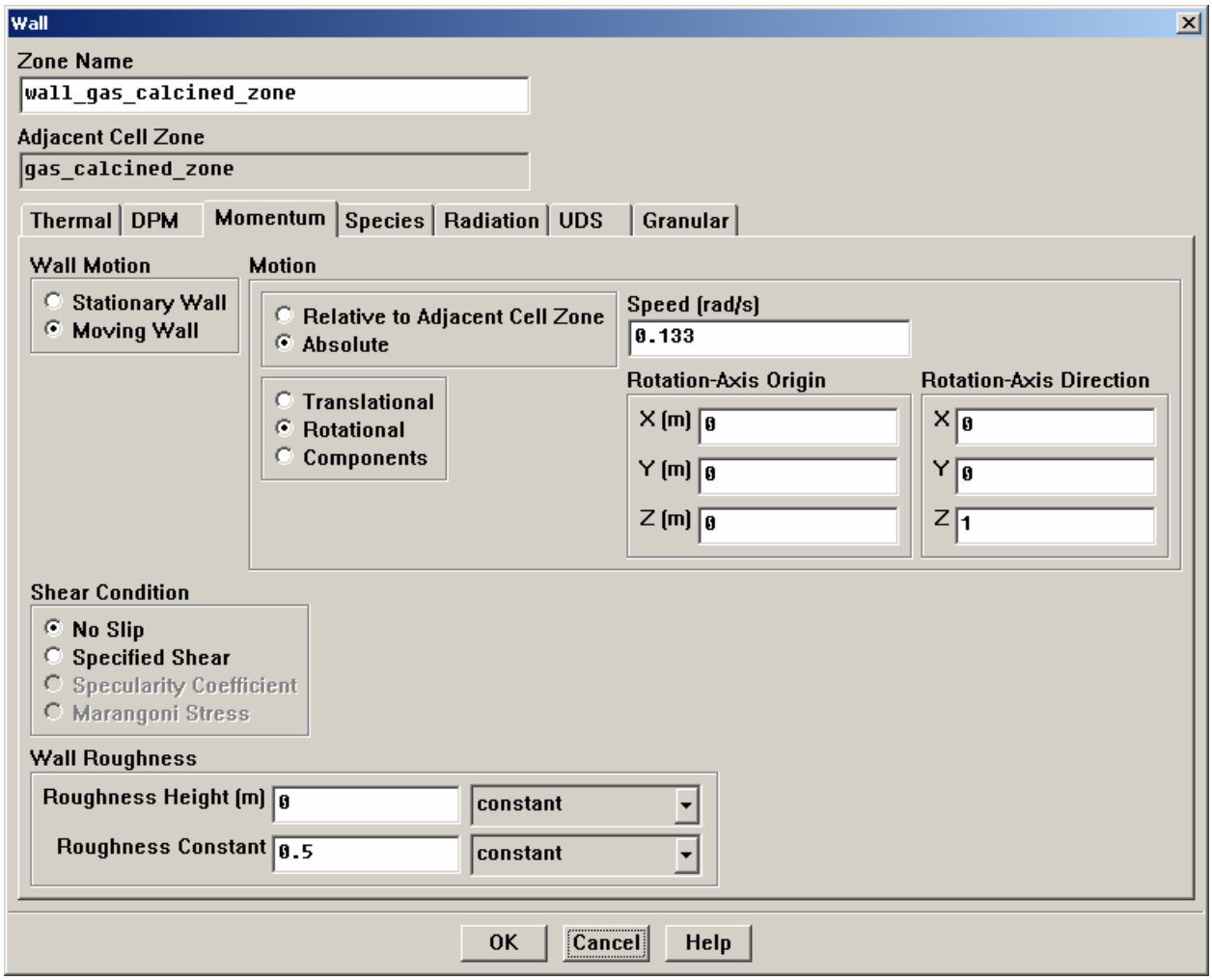

12. Repeat the above step for WALL_GAS_CALCINING_ZONE, WALL_GAS_HEATUP_ZONE, WALL_GAS_BURNCOKE, WALL_GAS_VOLATILE_ZONE, and WALL_GAS_VAPOR_ZONE.

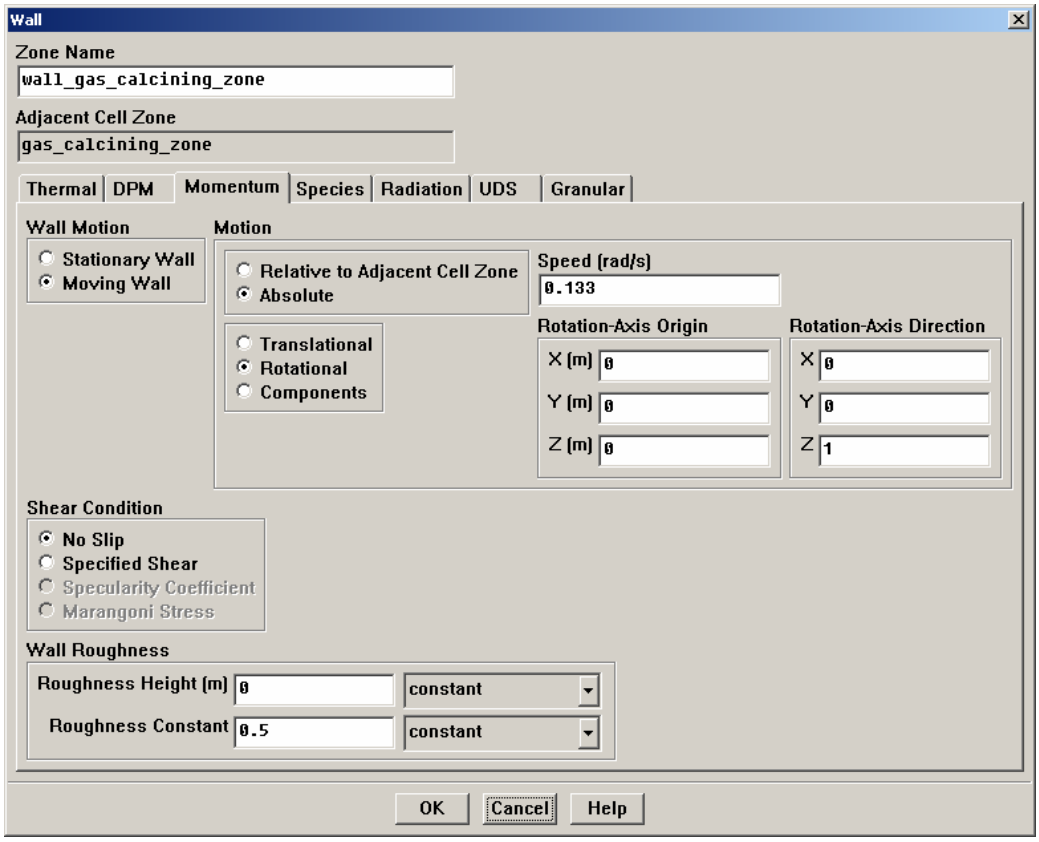
Wall
Zone Name
wall_gas_calcining_zone
Adjacent Cell Zone
gas_calcining_zone
Thermal
DPM
Momentum
Species
Radiation
UDS
Granular
Wall Motion
Stationary Wall
Moving Wall
Motion
Relative to Adjacent Cell Zone
Absolute
Speed (rad/s)
0.133
Translational
Rotational
Components
Rotation-Axis Origin
X (m) 0
Y (m) 0
Z (m) 0
Rotation-Axis Direction
X 0
Y 0
Z 1
Shear Condition
No Slip
Specified Shear
Specularity Coefficient
Marangoni Stress
Wall Roughness
Roughness Height (m) 0
constant
Roughness Constant 0.5
constant
OK
Cancel
Help

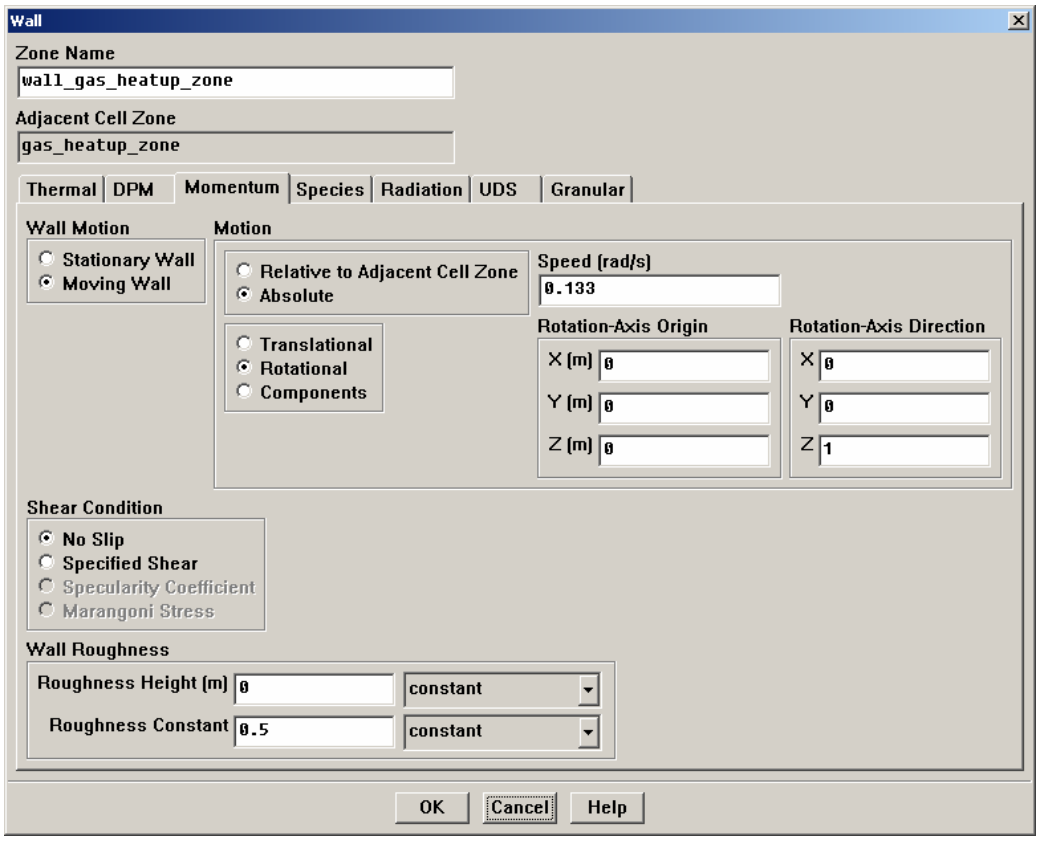
Wall
Zone Name
wall_gas_heatup_zone
Adjacent Cell Zone
gas_heatup_zone
Thermal
DPM
Momentum
Species
Radiation
UDS
Granular
Wall Motion
Stationary Wall
Moving Wall
Motion
Relative to Adjacent Cell Zone
Absolute
Speed (rad/s)
0.133
Translational
Rotational
Components
Rotation-Axis Origin
X (m) 0
Y (m) 0
Z (m) 0
Rotation-Axis Direction
X 0
Y 0
Z 1
Shear Condition
No Slip
Specified Shear
Specularity Coefficient
Marangoni Stress
Wall Roughness
Roughness Height (m) 0
constant
Roughness Constant 0.5
constant
OK
Cancel
Help

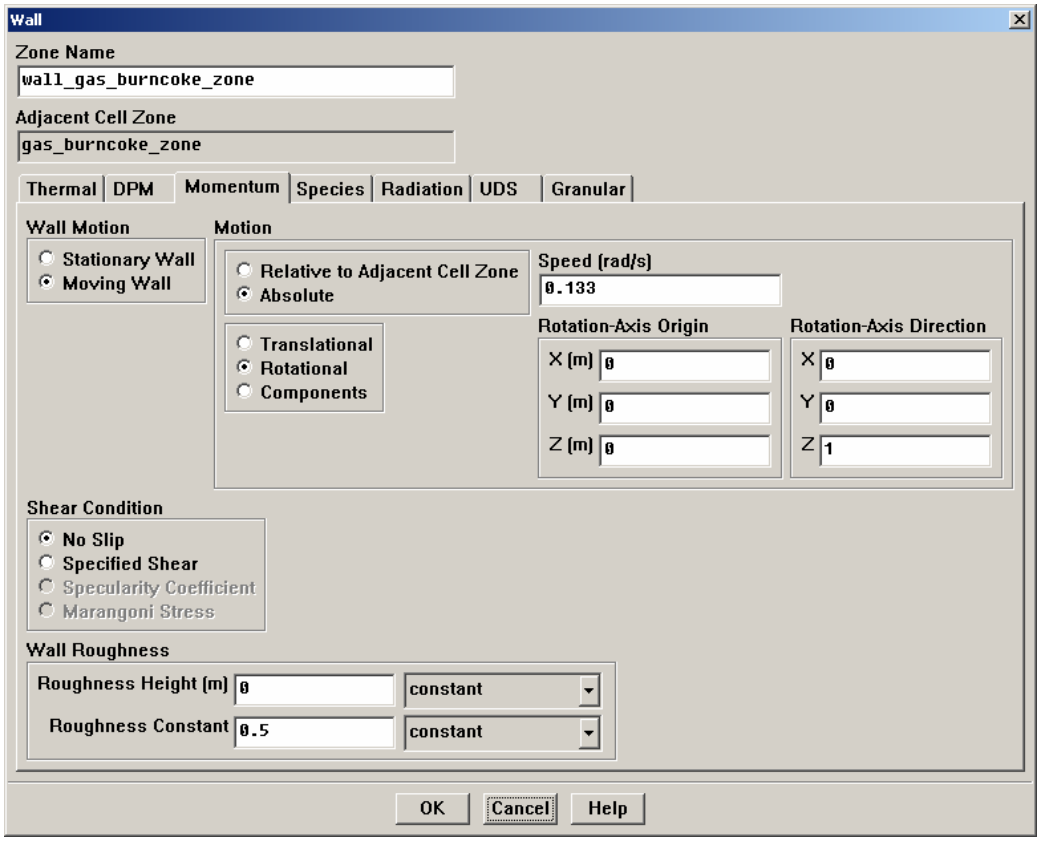
Wall
Zone Name
wall_gas_burncoke_zone
Adjacent Cell Zone
gas_burncoke_zone
Thermal
DPM
Momentum
Species
Radiation
UDS
Granular
Wall Motion
Stationary Wall
Moving Wall
Motion
Relative to Adjacent Cell Zone
Absolute
Speed (rad/s)
0.133
Translational
Rotational
Components
Rotation-Axis Origin
X (m) 0
Y (m) 0
Z (m) 0
Rotation-Axis Direction
X 0
Y 0
Z 1
Shear Condition
No Slip
Specified Shear
Specularity Coefficient
Marangoni Stress
Wall Roughness
Roughness Height (m) 0
constant
Roughness Constant 0.5
constant
OK
Cancel
Help

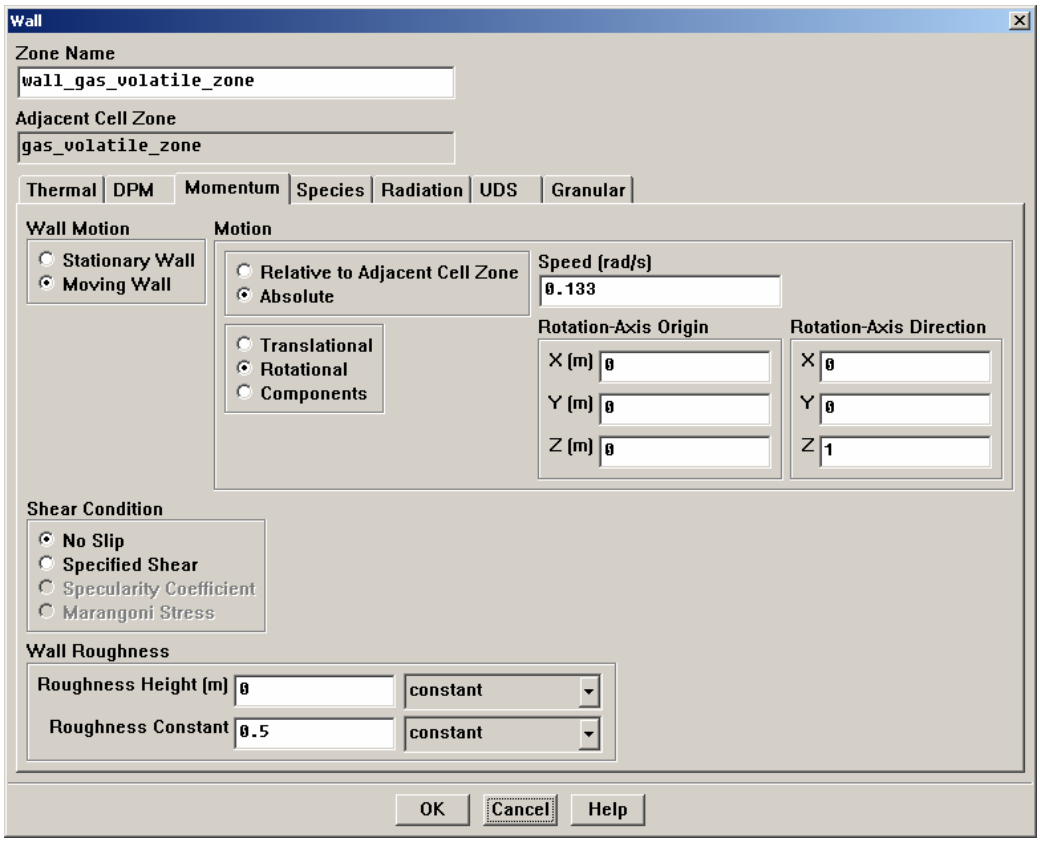
Wall
Zone Name
wall_gas_volatile_zone
Adjacent Cell Zone
gas_volatile_zone
Thermal
DPM
Momentum
Species
Radiation
UDS
Granular
Wall Motion
Stationary Wall
Moving Wall
Motion
Relative to Adjacent Cell Zone
Absolute
Speed (rad/s)
0.133
Translational
Rotational
Components
Rotation-Axis Origin
X (m) 0
Y (m) 0
Z (m) 0
Rotation-Axis Direction
X 0
Y 0
Z 1
Shear Condition
No Slip
Specified Shear
Specularity Coefficient
Marangoni Stress
Wall Roughness
Roughness Height (m) 0
constant
Roughness Constant 0.5
constant
OK
Cancel
Help

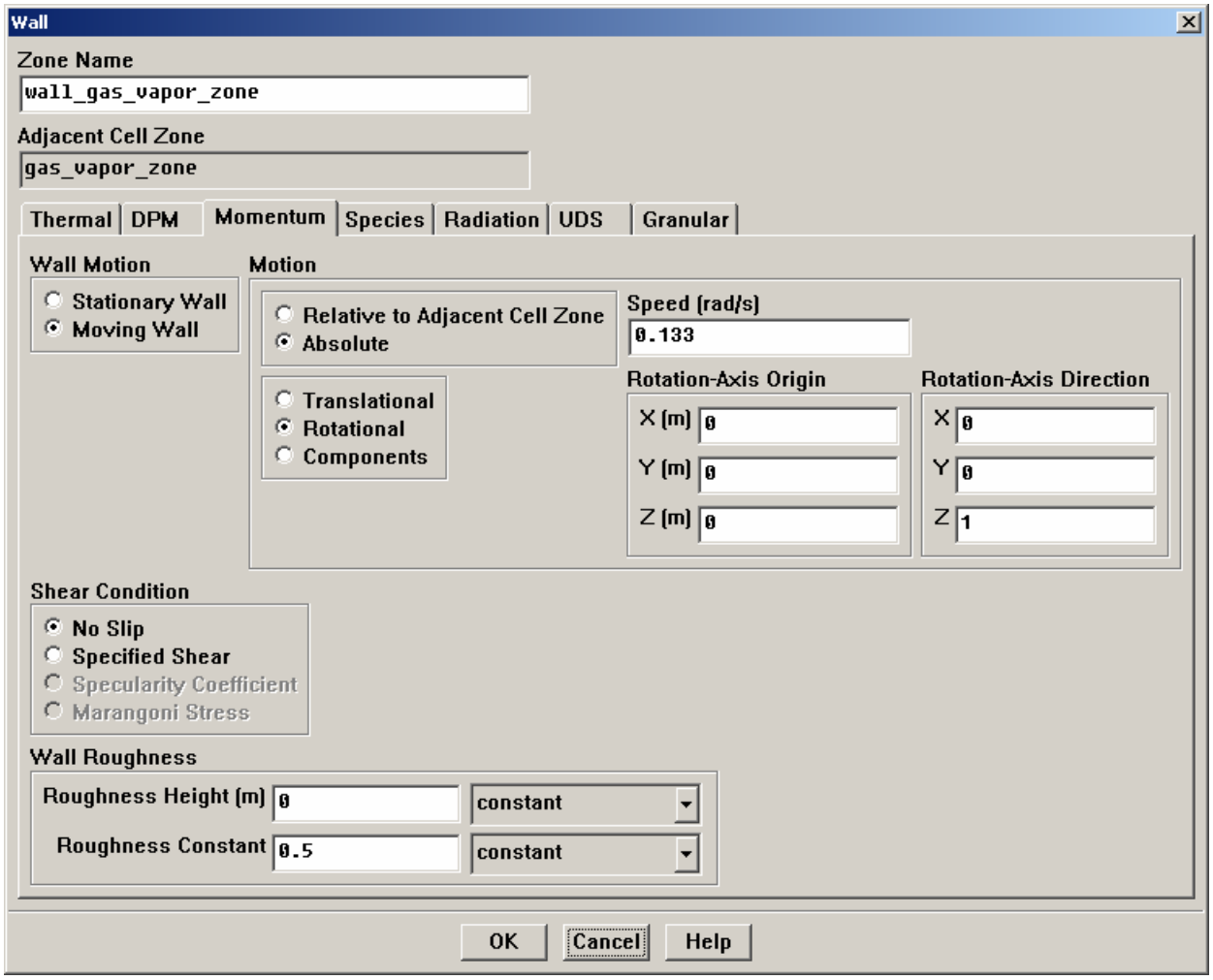

Step 6: Solution Initialization

SOLVE → INITIALIZE → INITIALIZE

1. Initialize the field variables. Choose ALL-ZONES from COMPUTE FROM drop-down list. Use all other default values. Click INIT.
2. Set under-relaxation factors.

   SOLVE → CONTROLS → SOLUTION

   a. Select all under EQUATIONS.

   b. For UNDER-RELAXATION FACTORS, set PRESSURE to 0.3, MOMENTUM to 0.7, and all other variables to 0.8.

c. Under DISCRETIZATION, set PRESSURE to SECOND ORDER and all others to SECOND ORDER UPWIND.

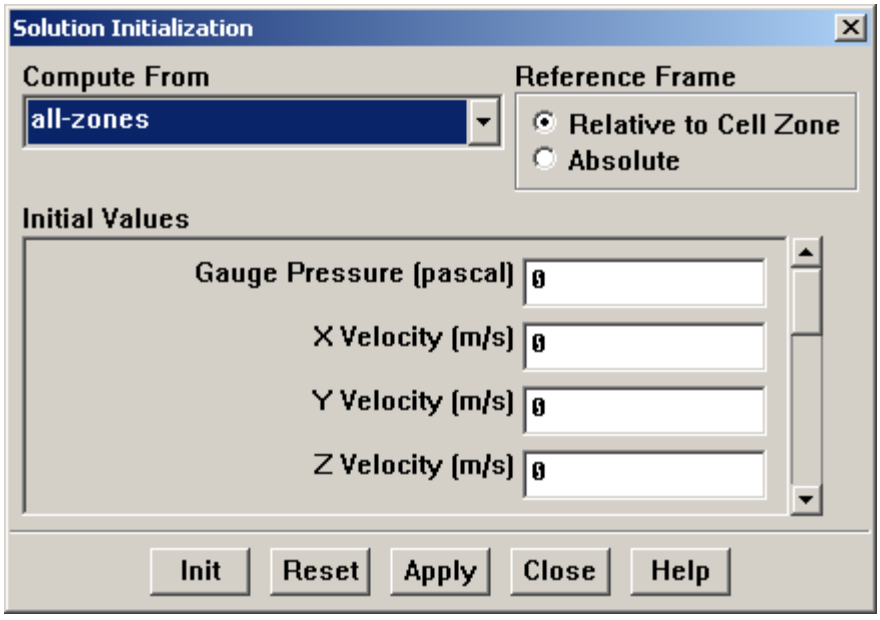

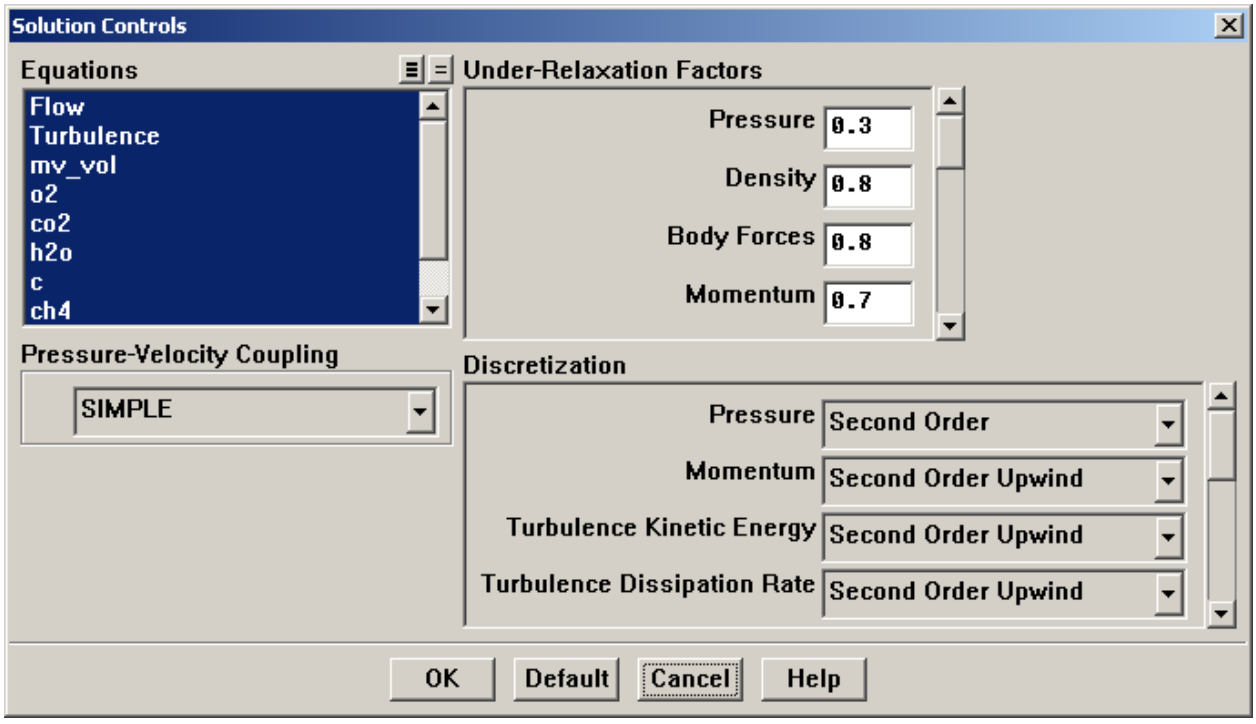

3. Turn on residual plotting during calculation.

   SOLVE → MONITORS → RESIDUAL

   Under OPTIONS, check PLOT. Keep all default CONVERGENCE CRITERION.

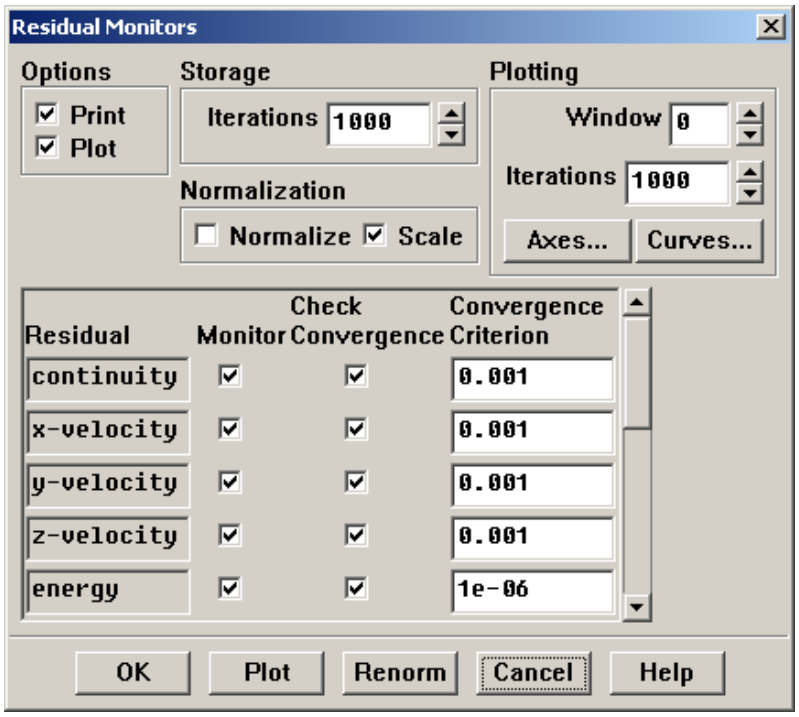

4. Start the calculation by requesting 5000 iterations.

   SOLVE → ITERATE

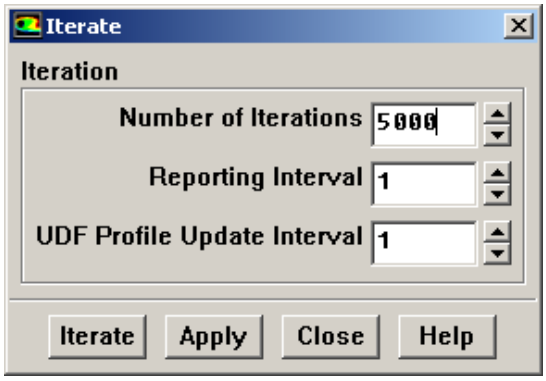

Step 7: Post-processing

Review the solution by examining graphical displays of the results, performing surface integrations, and making energy balance.

APPENDIX B

CALCULATIONS OF INPUT DATA

Coke Bed Calculations:

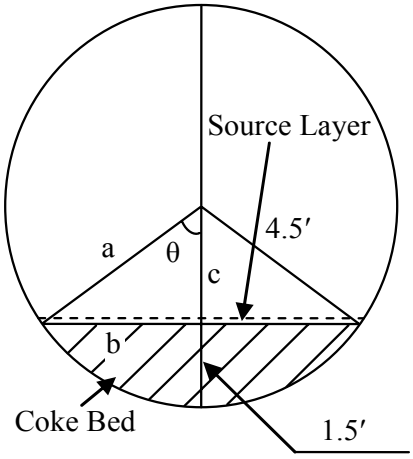

$$\theta = \arccos\theta = \text{arc}\frac{c}{a} = \text{arc}\frac{4.5\text{ ft} - 1.5\text{ ft}}{4.5\text{ ft}} = \text{arc}0.66667 = 48.2°$$

$$b = \sqrt{a^2 - c^2} = \sqrt{(4.5\text{ ft})^2 - (3\text{ ft})^2} = 3.354\text{ ft}$$

$$A_{bed} = \pi R^2 \frac{2\theta}{360} - \frac{1}{2}2bc = \pi \times (4.5\text{ ft})^2 \frac{2 \times 48.2}{360} - 3.354\text{ ft} \times 3\text{ ft}$$
$$= 17.035\text{ ft}^2 - 10.062\text{ ft}^2 = 6.973\text{ ft}^2$$

1. Heat sink source layer volume:

$$V_{heat\ sink} = 0.3\text{ ft} \times (3.354\text{ ft} \times 2) \times 80\text{ ft} = 160.99\text{ ft}^3 = 4.56\text{ m}^3$$

2. Volatiles source layer volume:

$$V_{volatiles} = 0.3\text{ ft} \times (3.354\text{ ft} \times 2) \times 80\text{ ft} = 160.99\text{ ft}^3 = 4.56\text{ m}^3$$

3. Coke fines source layer volume:

$$V_{coke\ fines} = 0.3\text{ ft} \times (3.354\text{ ft} \times 2) \times 120\text{ ft} = 241.49\text{ ft}^3 = 6.84\text{ m}^3$$

4. The volume for the entire coke bed is:

$$V_{bed} = A_{bed} \times L = 6.973\,ft^2 \times 200\,ft = 1394.6\,ft^3 = 39.49\,m^3$$

Calculations of Material Feed Rates:

1. Green coke feed rate = 73855 lbm/hr (Value taken from Canadian model)

$$73855\,\text{lbm/hr} = \frac{73855\,\text{lbm} \times 0.4535924\,\text{kg/lbm}}{1\,\text{hr} \times 3600\,\text{s/hr}} = 9.3\,\text{kg/s}$$

2. Assume moisture content is 6 % of total green coke mass:

   Moisture feed rate = $9.3\,\text{kg/s} \times 0.06 = 0.558\,\text{kg/s}$

3. Assume 8 % volatiles (7.52 % of total green coke mass) is contained within the petcoke after the moisture is driven off:

   Volatiles feed rate = $9.3\,\text{kg/s} \times 0.94 \times 0.08 = 0.6994\,\text{kg/s}$

4. Assume 4.3 % (3.72 % of total green coke mass) coke is burned after moisture and volatiles are driven off:

   Coke fines feed rate = $9.3\,\text{kg/s} \times (1 - 0.06 - 0.94 \times 0.08) \times 0.043 = 0.3456\,\text{kg/s}$

5. Coke bed moving/sliding velocity and resident time:

   Assume petcoke density is 1,400 kg/m^3

$$\text{volume feed rate} = \frac{\text{mass feed rate}}{\rho} = \frac{9.3\,\text{kg/s}}{1400\,\text{kg/m}^3} = 0.00665\,\text{m}^3/\text{s}$$

   The total resident time equals to the time to fill up the entire coke bed:

$$t = \frac{V_{bed}}{\text{volume feed rate}} = \frac{39.49\,\text{m}^3}{0.00665\,\text{m}^3/\text{s}} = 5938\,\text{s} = 99\,\text{minutes}$$

$$v = \frac{60.96\,\text{m}}{5938\,\text{s}} = 0.01\,\text{m/s}$$

6. Rotational velocity is 1.27 rpm (Value taken from Canadian model)

Calculations of Source Term Releasing Rates:

1. Heat sink energy absorption rate:

   Latent energy absorption rate = $\frac{1.582\times10^{6}\ \text{W}}{4.56\ \text{m}^3} = 347\ \text{kW/m}^3$

2. Volatiles releasing rate:

   Volatiles releasing rate = $\frac{0.6994\ \text{kg/s}}{4.56\ \text{m}^3} = 0.1534\ \text{kg/m}^3\text{ - s}$

3. Coke fines releasing rate:

   Coke fines releasing rate = $\frac{0.3456\ \text{kg/s}}{6.84\ \text{m}^3} = 0.0505\text{kg/m}^3\text{ - s}$

Energy Calculations:

1. Energy needed to heat up moisture from 20 to 100 °C:

   $\dot{E}_1 = C\dot{m}\Delta T = 4.186\ \text{J/g - °C}\times 0.558\ \text{kg/s}\times(100\ \text{°C} - 20\ \text{°C}) = 186863\ \text{J/s}$

2. Latent heat to vaporize water:

   $\dot{E}_2 = 2.5\times10^{6}\ \text{J/kg}\times 0.558\ \text{kg/s} = 1.395\times10^{6}\ \text{J/s}$

3. Total energy needed:

   $\dot{E} = \dot{E}_1 + \dot{E}_2 = 0.187\times10^{6}\ \text{J/s} + 1.395\times10^{6}\ \text{J/s} = 1.582\times10^{6}\ \text{W}$

4. Energy required to heat up dry coke from 20 to 1,400 °C:

   $\dot{E}_3 = C\dot{m}\Delta T = 0.85\ \text{kJ/kg - K}\times 9.3\ \text{kg/s}\times(1400\ \text{°C} - 20\ \text{°C}) = 10909\ \text{kJ/s}$

5. Energy required to heat up petcoke from 20 to 1,400 °C (minimum energy required to calcine petcoke):

   $\dot{E} = \dot{E}_1 + \dot{E}_2 + \dot{E}_3 = 187\ \text{kJ/s} + 1395\ \text{kJ/s} + 10909\ \text{kJ/s} = 12491\ \text{kJ/s}$

6. Energy from burning volatiles:

$$mv\_vol + 1.706O2 \rightarrow CO2 + 1.543H_2O + E$$

$$\frac{-5.601\times10^{7}\ \text{J/kgmol}}{17.237\ \text{kg/kgmol}} + 0 = \frac{-3.935324\times10^{8}\ \text{J/kgmol}}{44\ \text{kg/kgmol}}$$

$$+1.543\times\frac{-2.41820\times10^{8}\ \text{J/kgmol}}{18.015\ \text{kg/kgmol}} + E$$

$$E = -3.25\times10^{6}\ \text{J/kg} + 8.94\times10^{6}\ \text{J/kg} + 2.071\times10^{7}\ \text{J/kg} = 2.640\times10^{7}\ \text{J/kg}$$

$$\dot{E}_{\text{volatiles}} = 26400\ \text{kJ/kg}\times0.6994\ \text{kg/s} = 18464\ \text{kJ/s}$$

7. Energy from burning coke fines:

$$C + O2 \rightarrow CO2 + E$$

$$\frac{7.167094\times10^{8}\ \text{J/kgmol}}{12\text{kg/kgmol}} + 0 = \frac{-3.935324\times10^{8}\ \text{J/kgmol}}{44\text{kg/kgmol}} + E$$

$$E = 5.973\times10^{7}\ \text{J/kg} + 8.94\times10^{6}\ \text{J/kg} = 6.867\times10^{7}\ \text{J/kg}$$

$$\dot{E}_{\text{coke fines}} = 68670\ \text{kJ/kg}\times0.3456\ \text{kg/s} = 23732\ \text{kJ/s}$$

Gas Feed Rates:

1. Main air inlet injection velocity and flow rate = 20 m/s (65.62 ft/s),

   Mass flow rate is 3.28 lbm/s (95.7 % is air, 4.3 % is natural gas),

   Air density at the standard state is 0.0752 lbm/ft^3,

$$\dot{Q}_{\text{main}} = \frac{3.28\ \text{lbm/s}\times0.957}{0.0752\ \text{lbm/ft}^3} = 2504.49\ \text{SCFM}$$

2. Natural gas supplying rate:

$$\dot{Q}_{\text{main}} = 3.28\ \text{lbm/s}\times0.043\times3600 = 507.74\ \text{lbm/hr} = 202.93\ \text{SCFM}$$

3. Tertiary air inlet injection velocity and total flow rate = 50 m/s (164.04 ft/s),

   Mass flow rate is 22.91 lbm/s,

$$\dot{Q}_{\text{main}} = \frac{22.91\ \text{lbm/s}}{0.0752\ \text{lbm/ft}^3} = 18279.26\ \text{SCFM}$$

APPENDIX C

GLOBAL ENERGY BALANCE ANALYSIS

Since no measurements have been made in the kiln and no gas analysis has been made at the gas exit (petcoke feeding end) of the kiln to compare with the CFD results in this study, a global energy balance analysis is performed. The approach is based on the steam and electricity generated in Chalmette (Norco) plant to back calculate the energy that is obtained in the pyroscrubber. Based on the results from the Canadian and the present studies, different combinations of entrained coke fines and unburned volatiles are selected to match the energy burned in the pyroscrubber.

From the Canadian Model:

Green coke feed rate: 9.3 kg/s

5.2 % moisture

0.15 % impurities

10.2 % volatile matters (4.09 % burned in kiln, 6.11 % unburned goes into pyroscrubber)

3.72 % coke burned in kiln

9.12 % coke goes into pyroscrubber

Yield: 71.61 % (mass)

From CII Engineer:

Typical yield: average 78 % (75 - 82 %)

Generated electricity: 15-16 MW by 150,000 lbm/hr steam (900 psig and 900 °F) at the Chalmette plant and 180,000 lbm/hr steam (1,300 psig and 900 °F) at the Norco plant

Typical steam turbine efficiency: 35 %

Typical boiler efficiency: 85 %

For Current Studies:

Green coke feed rate: 9.3 kg/s

6 % moisture

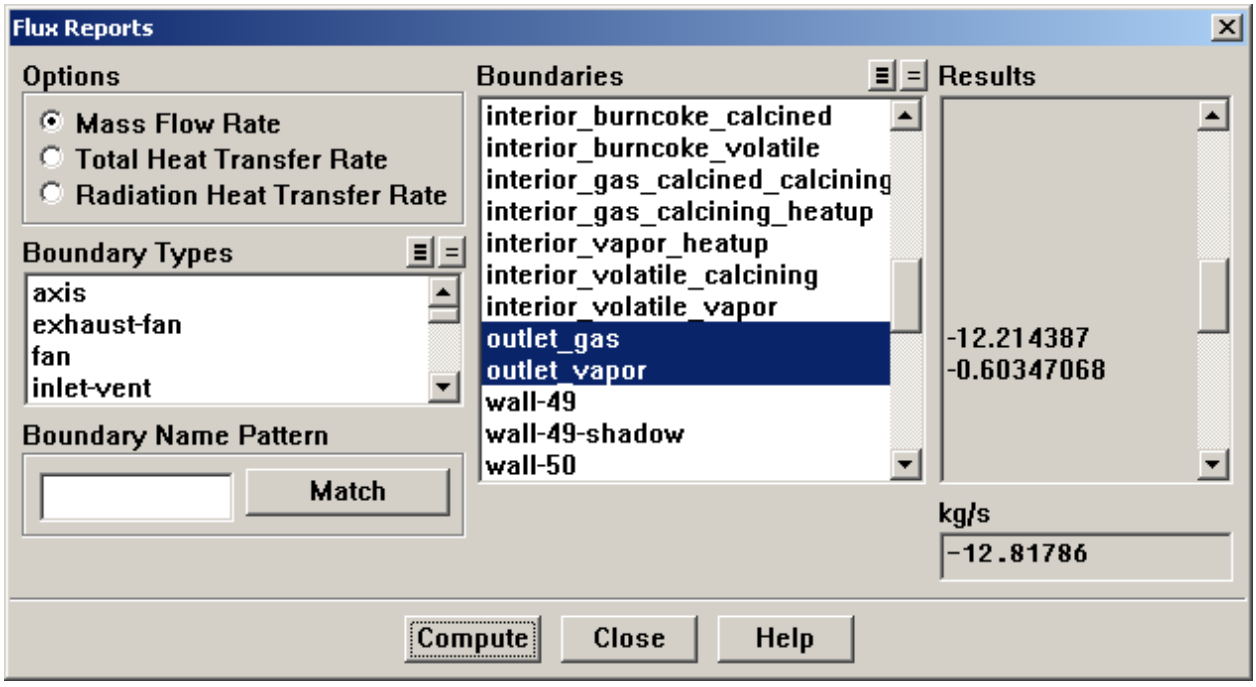

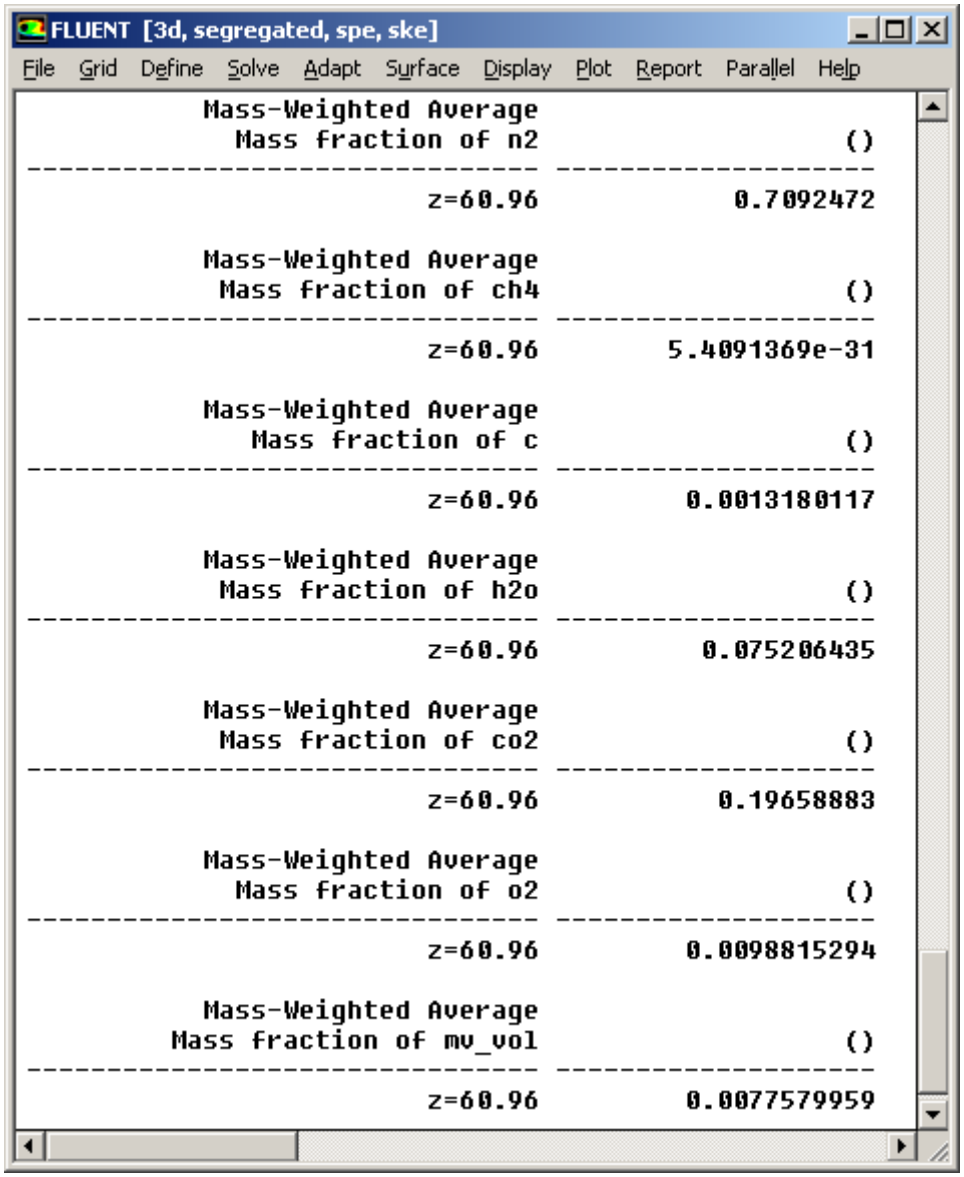

Unburned volatiles:

$$12.81786\text{kg/s} \times 0.0077579959 = 0.0994\text{kg/s}$$

$$\frac{0.0994\text{kg/s}}{9.3\text{kg/s}} = 1.07\%$$

7.52 % volatile matters (6.45 % burned in kiln, 1.07 % unburned goes into pyroscrubber)

$$12.81786\text{kg/s} \times 0.0013180117 = 0.0169\text{kg/s}$$

$$\frac{0.0169\text{kg/s}}{9.3\text{kg/s}} = 0.18\%$$

3.72 % coke lost (3.54 % burned in kiln, 0.18 % unburned goes into pryoscrubber)

FLUENT Material Properties:

Standard state enthalpy (J/kgmol)

C = 7.167094 x 10^8

medium heating value coal volatiles (mv_vol) = –5.601 x 10^7

O_2 = 0

CO_2 = –3.935324 x 10^8

H_2O = –2.41820 x 10^8

Molecular weights (kg/kgmol)

C = 12

medium heating value coal volatiles (mv_vol) = 17.237

O_2 = 32

CO_2 = 44

H_2O = 18.015

$$C + O2 \rightarrow CO2 + E$$

$$\frac{7.167094\times10^8\,\text{J/kgmol}}{12\text{kg/kgmol}} + 0 = \frac{-3.935324\times10^8\,\text{J/kgmol}}{44\text{kg/kgmol}} + E$$

$$E = 5.973\times10^7\,\text{J/kg} + 8.94\times10^6\,\text{J/kg} = 6.867\times10^7\,\text{J/kg}$$

$$mv\_vol + 1.706O2 \rightarrow CO2 + 1.543H_2O + E$$

$$\frac{-5.601\times10^7\,\text{J/kgmol}}{17.237\,\text{kg/kgmol}} + 0 = \frac{-3.935324\times10^8\,\text{J/kgmol}}{44\,\text{kg/kgmol}} + 1.543\times\frac{-2.41820\times10^8\,\text{J/kgmol}}{18.015\,\text{kg/kgmol}} + E$$

$$E = -3.25\times10^6\,\text{J/kg} + 8.94\times10^6\,\text{J/kg} + 2.071\times10^7\,\text{J/kg} = 2.640\times10^7\,\text{J/kg}$$

Case I (Upper Limit of Coke Feed):

All steam energy is generated from burning volatiles. This result will provide an upper limit when no coke fines are entrained out of the kiln and entering into the pyroscrubber.

The required green coke feed rate to achieve this goal is:

$$\frac{15\times10^{6}\,\text{J/s}}{35\%\times85\%\times2.64\times10^{7}\,\text{J/kg}\times6.11\%}=31.258\,\text{kg/s}$$

As expected, the result is much higher than the petcoke feed rate (9.3 kg/s).

Case II (Lower Limit of Coke Feed, Assuming 9.12% Entrainment Rate):

All steam energy is generated from burning entrained coke fines at 9.12% of the total coke feed mass. This result will provide a lower limit when all volatiles are burned in the kiln and no unburned volatiles escapes into the pyroscrubber.

The required green coke feed rate to achieve this goal is:

$$\frac{15\times10^{6}\,\text{J/s}}{35\%\times85\%\times6.867\times10^{7}\,\text{J/kg}\times9.12\%}=8.051\,\text{kg/s}$$

This coke feed rate is less than the actual feed rate at 9.3kg/s. This means the coke fines entrainment at 9.12 % is overestimated.

Case III (The required coke entrainment rate to power 15MW without volatiles.):

A raw petcoke feed rate of 9.3 kg/s used in this study with a coke fines entrainment rate of 7.89% will have sufficient energy to generate 15 MW electricity with 85 % efficiency for boiler and 35 % efficiency for steam turbine (i.e. an overall efficiency of 29.75 % for the steam power plant).

Case IV (The required coke entrainment rate to power 15MW with 1.07% unburned volatiles escaping to the pyroscrubber.):

A raw petcoke feed rate of 9.3 kg/s used in this study with an coke fines entrainment rate of 7.48% and 1.07 % unburned volatiles escaped to the pyroscrubber will have sufficient energy to generate 15 MW electricity with 85 % efficiency for boiler and 35 % efficiency for steam turbine (i.e. an overall efficiency of 29.75 % for the steam power plant).

$$\frac{15\times10^{6}\,\text{J/s}}{35\%\times85\%\times9.3\,\text{kg/s}} = 6.867\times10^{7}\,\text{J/kg}\times\text{X}\% + 2.64\times10^{7}\,\text{J/kg}\times1.07\%$$

$$\text{X}\% = 7.48\%$$

This global energy balance analysis shows that the CFD results with 0.18% coke fines being entrained into the pyroscrubber does not provide sufficient energy to generate 15MW power. Therefore, an appropriate model for more accurately calculating the coke fines entrainment rate is important for improve the current prediction model.

REFERENCES

[1] Allred, V. D., "Rotary Hearth Calcining of Petroleum Coke," Light Metals, 1971, pp. 313-329.

[2] Anderson, J. D. Jr, "Computational Fluid Dynamics, the basics with application," McGraw-Hill Inc., 1995.

[3] Bagdoyan, E. A., and Gootzait, E., "Refiners Calcine Coke," Hydrocarbon Processing, September 1985, pp.85-90.

[4] Brooks, D. G., "Mathematical Simulation of a Rotary Coke Calciner," Light Metals, 1989, pp. 461-469.

[5] Burmeister, L. C., "Convective Heat Transfer," John Wiley & Sons Inc., 1983.

[6] CII Carbon L.L.C., "Canadian Rotary Coke Calciner Modeling," 2004.

[7] Ellis, P. J., and Paul, C. A., "Tutorial: Petroleum Coke Calcining and Uses of Calcined Petroleum Coke," AIChE 2000 Spring National Meeting, Third International Conference on Refining Processes, Session T9005, March 2000.

[8] FLUENT 6.1 User's Guide, February 2003.

[9] Incropera, F. P., and DeWitt, D. P., "Introduction to Heat Transfer," 4th Edition, John Wiley & Sons Inc., 1996.

[10] Kaiser Aluminum, "The Use of Refractory Tumblers in Coke Calcination," Kaiser Aluminum brochure, circa 1983.

[11] Munson, Young, and Okiishi, "Fundamentals of Fluid Mechanics," 3rd Edition, John Wiley & Sons Inc., 1998.

[12] Merrill, Jr., and Lavaun, S., "Particulate Emissions from A M-W Rotary Hearth Calciner," Light Metals, 1978.

[13] Patankar, S.V., "Numerical Heat Transfer and Fluid Flow," McGraw-Hill Inc., Hemisphere, 1980.

[14] Siegel, R., and Howell, J. R., "Thermal Radiation Heat Transfer," Hemisphere Publishing Corporation, Washington D.C., 1992.

[15] Tennekes, H., and Lumley, J. L., "A First Course in Turbulence," The Massachusetts Institute of Technology, 1972.

[16] Thomas, L. C., "Heat Transfer," 2nd edition, Capstone Publishing Corporation., 2000.

[17] Turns, Stephen R., "An Introduction to Combustion," 2nd Edition, McGraw-Hill Inc., 2000.

[18] Van Wylen, G. J., Sonntag, R. E., "Fundamentals of Classical Thermodynamics," 3rd Edition, John Wiley & Sons Inc., 1986.

[19] White, Frank, "Viscous Flow," 2nd edition, McGraw-Hill Inc., 1991.

[20] Zhao, L. and Wang, T., "Investigation of Potential Benefits of Using Bricks of Higher Thermal Capacity and Conductivity in a Calcining Kiln, -- A Rotational Transient Conduction Study," ECCC Report 2007-01, Energy Conversion and Conservation Center, University of New Orleans, submitted to CII Carbon, LLC, April 2007.

VITA

Zexuan Zhang was born in Shanghai, People's Republic of China. He came to the United States in 1998. He received his B.S. degree from the University of New Orleans in 2003 and joined the M.S. program in Mechanical Engineering at the University of New Orleans in fall 2004.